Comparison of human and mouse AKR1C enzymes: implications for modeling human cancer

Pedro Veliça

A thesis submitted to
The University of Birmingham
for the degree of

DOCTOR OF PHILOSOPHY

School of Biosciences
College of Life and Environmental Sciences
The University of Birmingham
April 2010

Abstract

Human aldo-keto reductases (AKR) of the 1C subfamily have been implicated in the progression of prostate, breast and endometrial carcinomas as well as leukaemias due to their ability to modify key signaling molecules: steroid hormones and prostaglandins (PGs). In leukaemia, the AKR1C3 isoform has been identified as a novel therapeutic target since its PGD_2 reductase activity prevents cell differentiation. Mice are ideal organisms for *in vivo* studies, using knock-out or over-expression strains. However, no mouse models for AKR1C enzymes have been generated to date since the functional conservation of these enzymes between human and mice is yet to be described. This study compared and characterised the phylogeny, substrate preference and tissue expression profile of the four human (AKR1C1,-1C2, -1C3 and -1C4) and the eight mouse (AKR1C6, -1C12, -1C13, -1C14, -1C18, -1C19, -1C20 and -1C21) isoforms. Despite being orthologues, AKR1C enzymes of mouse and humans have undergone significant divergence in number and sequence which was reflected in different substrate preference and tissue distribution. Mouse AKR1C isoforms lacked the PGD_2 reductase activity but AKR1C6 was able to reduce PGE_2 instead, an activity absent amongst human isoforms. Reduction of the key steroids androstenedione, 5α-dihydrotestosterone, progesterone and estrone was performed by 4 of the murine isoforms. However, unlike humans, no AKR1C isoforms were detected in murine prostate, testes, uterus and haemopoietic progenitors. This study exposes significant lack of phylogenetic and functional conservation between human and murine AKR1C enzymes. Therefore, it is concluded that mice are not suitable to model the role of AKR1C in human carcinomas and leukemia.

Additionally, the role of PGD_2 in adult muscle differentiation was investigated using the mouse myoblast cell line C2C12. PGD_2, but not PGE_2 or $PGF_{2\alpha}$, inhibited myotube formation in a dose dependent manner. Exposure to PGD_2 disrupted the expression of myogenic regulators (MyoD and myogenin) during differentiation and suppressed cell fusion, α-actin expression and creatine kinase activity. Inhibition of myogenesis was independent of PGD_2 surface receptors DP1 and DP2 and activation of the peroxisome proliferator-activated receptor γ (PPARγ) suggesting a new form of signaling is involved. This discovery has implications in the interplay between inflammation, where high levels of PGD_2 are secreted, and adult muscle regeneration, two processes that are intimately related.

Dedicated to my parents, Paula Bicho and Cristóvão Veliça.

Ó mar salgado, quanto do teu sal
São lágrimas de Portugal!
Por te cruzarmos, quantas mães choraram,
Quantos filhos em vão rezaram!
Quantas noivas ficaram por casar
Para que fosses nosso, ó mar!

Fernando Pessoa

TABLE OF CONTENTS

List of figures

List of tables

List of abbreviations

15d-PGJ_2	15-deoxy-$\Delta^{12,14}$-PGJ_2
5α-DHT	5α-dihydrotestosterone
AA	arachidonic acid
AC	adenylyl cyclase
ADP	adenosine diphosphate
AF	activating function
AKR	aldo-keto reductase
AKR1CL	AKR1C-like
ALL	acute lymphoblastic leukaemia
AML	acute myeloid leukaemia
AMP	adenosine monophosphate
AP-1	activator protein 1
AR	androgen receptor
ATM	ataxia telangiectasia mutated
ATP	adenosine triphosphate
ATRA	all-*trans* retinoic acid
BABP	bile acid-binding protein
BEZ	bezafibrate
BGH	bovine growth hormone
BRUCE	BIR ubiquitin-conjugating enzyme
BSA	bovine serum albumin
cAMP	cyclic adenosine monophosphate
CAR	constitutive androstane receptor
CBG	corticosteroid-binding globulin
cDNA	complementary DNA
CK	creatine kinase
CLL	chronic lymphoblastic leukaemia
CML	chronic myeloid leukaemia
CMV	cytomegalovirus
COX	cyclooxygenase
cPGES	cytosolic PGE synthase
$cPLA_2$	cytosolic phospholipase A_2
CRTH2	chemoattractant receptor homologous molecule expressed in Th2
CSF	cerebrospinal fluid
CYP	cytochrome P450
DAG	diacylglycerol
DBD	DNA-binding domain
DHEA	dehydroepiandrosterone
DMEM	Dulbecco’s modified Eagle's medium
DMSO	dimethyl sulfoxide

DNA	deoxyribonucleic acid
dNTP	deoxyribonucleotide
DOC	deoxycorticosterone
DTT	dithiothreitol
EDTA	ethylenediaminetetraacetic acid
EET	epoxyeicosatrienoic acid
ELISA	enzyme-linked immunosorbent assay
EMT	epithelial-to-mesenchymal transition
EPO	erythropoietin
ER	estrogen receptor
FACS	fluorescence assisted cell sorter
FBS	foetal bovine serum
FI	fusion index
FITC	fluorescein isothiocyanate
FPLC	fast protein liquid chromatography
GAPDH	glyceraldehyde 3-phosphate dehydrogenase
GFP	green fluorescent protein
GPCR	G-protein-coupled receptor
GR	glucorticoid receptor
GSH	glutathione
HETE	hydroxyeicosatetraenoic acid
HIF	hypoxia inducible factor
HPC	haemopoietic progenitor cell
H-PGDS	heamopoietic-PGD synthase
HRP	horse-radish peroxidase
HS	horse serum
HSD	hydroxysteroid dehydrogenase
HSP	heat shock protein
IKK	IκB kinase
IL-1	interleukin-1
INF-γ	interferon-γ
iNOS	inducible NO synthase
IP3	inositol trisphosphate
IPTG	isopropyl β-D-1-thiogalactopyranoside
IRES	internal ribosome entry site
IsoP	isoprostane
LB	Luria Bertani
LBD	ligand-binding domain
LIF	leukaemia inhibitory factor
LOX	lipoxygenases
L-PGDS	lipocalin-PGD synthase
LPS	lipopolysaccharide
mESC	murine embryonic stem cell
miRNA	micro RNA

MPA	medroxyprogesterone acetate
mPGES	membrane-bound PGES
MR	mineralocorticoid receptor
MRF	myogenic regulatory factor
MSCV	murine stem cell virus
Myf-5	myogenic factor 5
MyoD	myogenic differentiation
NAD^+	β-Nicotinamide adenine dinucleotide
NADH	β-Nicotinamide adenine dinucleotide reduced
$NADP^+$	β-Nicotinamide adenine dinucleotide phosphate
NADPH	β-Nicotinamide adenine dinucleotide phosphate, reduced
NCBI	National Center for Biotechnology Information
NES	nuclear export signal
NFATC2	nuclear factor of activated T cells, isoform C2
NF-κB	nuclear factor-κB
Ni-NTA	nickel-nitrilotriacetic acid
NLS	nuclear localization signal
NOR1	nuclear orphan receptor 1
NR	nuclear receptor
Nrf2	NF-E2 related factors
NSAID	non-steroidal anti-inflammatory drug
NTD	N-terminal domain
ORF	open reading frame
PAGE	polyacrylamide gel electrophoresis
PBL	peripheral blood leukocytes
PBS	phosphate buffer saline
PCR	polymerase chain reaction
PE	phycoerythrin
PG	prostaglandin
PGDS	PGD synthase
PGES	PGE synthase
PGFS	PGF synthase
PGIS	PGI synthase
PGK	phosphoglycerate kinase
PGT	prostaglandin transporter
PKC	protein kinase C
PLC	phospholipase C
PML	promyelocytic leukaemia
PPAR	peroxisome proliferator-activated receptor
PQ	9,10- phenanthrenequinone
PR	progesterone receptor
PXR	pregnane X receptor
QRT-PCR	quantitative real time PCR
RAR	retinoic acid receptors

RNA	ribonucleic acid
RORα	RAR-related orphan receptor α
ROS	reactive oxygen species
RPMI	Roswell Park Memorial Institute
RT-PCR	reverse transcriptase PCR
RXR	retinoid X receptor
SCF	stem cell factor
SDR	short-chain dehydrogenase/reductase
SDS	sodium dodecyl sulfate
SF1	steroidogenic factor 1
SHBG	steroid hormone-binding globulin
shRNA	short-hairpin RNA
STAT	signal transducer and activator of transcription
SUMO	small ubiquitin-like modifier
T3	triiodothyronine
TLC	thin layer chromatography
TNFα	tumour necrosis factor-α
TPO	thrombopoietin
TR	thyroid hormone receptor
tTS	tetracycline-responsive transcription silencer
TXA_2	thromboxane A_2
TXAS	TXA synthase
UV	ultra-violet
VDR	vitamin D receptor
VSMC	vascular smooth muscle cells

CHAPTER ONE: Introduction

1.1 A short introduction to aldo-keto reductases in leukaemia

In 1994, Bunce and colleagues identified indomethacin as a potentiator of differentiation of HL60 cells, a model of myeloid leukaemia (Bunce et al., 1994). Indomethacin is a non-steroidal anti-inflammatory (NSAID) drug that acts by blocking cyclooxygenase (COX) activity and suppressing the synthesis of prostanoids. However, the authors could not provide evidence that COX was the molecular target that promoted HL60 differentiation and other targets of indomethacin were sought (Bunce et al., 1996). This led to the identification of an enzyme with 3α-hydroxysteroid dehydrogenase activity belonging to the aldo-keto reductase (AKR) superfamily as the molecular target of indomethacin (Bunce et al., 1996, Mills et al., 1998). Subsequently, other known inhibitors of this enzyme were shown to potentiated HL60 differentiation.

The enzyme was later identified as AKR1C3, one of four closely related human aldo-keto reductases and found to be expressed in leukaemic cell lines and primary leukaemic cells from patients (Birtwistle et al., 2008). Whilst inhibition of AKR1C3 resulted in enhanced HL60 cell sensitivity to differentiation stimuli, over-expression yielded more resistant cells, confirming AKR1C3 as a suppressor of cell differentiation and a novel therapeutic target in acute myeloid leukaemia (AML) (Desmond et al., 2003). The anti-differentiation effects of AKR1C3 were shown to rely on its ability to catalyse the reduction of prostaglandin (PG) D_2 to 11β-$PGF_{2\alpha}$, thus preventing the spontaneous generation of 15-deoxy-$\Delta^{12,14}$-PGJ_2 (15d-PGJ_2) a reactive molecule with anti-tumour effects (Khanim et al., 2009, Desmond et al., 2003).

Later it was shown that the combination of medroxyprogesterone acetate (MPA), also an AKR1C3 inhibitor, and bezafibrate, a lipid-lowering drug, was active in promoting differentiation or apoptosis of multiple primary leukaemic cells confirming the therapeutic advantage of targeting this enzyme (Hayden et al., 2009, Tiziani et al., 2009, Khanim et al., 2009, Fenton et al., 2003). This therapeutic approach has since then been used in a small scale clinical trial and shown to be efficient against AML in elderly and relapsed patients (Murray et al., 2010).

The research project presented in this thesis originates from the need to understand the role of AKR1C3 in normal physiology: how the enzyme functions in the context of a whole organism and how it is involved in leukaemogenesis. Most studies elucidating the function of AKR1C3 derive from isolated primary or immortalised cell lines. Therefore, the objective of this study was to interrogate the function of AKR1C3 in mice, a commonly used model for mammalian physiology that can be genetically manipulated. The use of total and conditional knock-out mouse strains for the homologue of human AKR1C3 would be a key tool to understand the biology of the enzyme. Thus, the objectives of the study were:

A) Identification and characterisation of the AKR1C3 homologue (PGD_2 11β-ketoreductase) in mice.

B) Generation of transgenic mouse strains (knock-out; inducible knock-down) to ascertain the physiological role of AKR1C3 in a whole organism.

C) Facilitate the study of the role of AKR1C3 in the homeostasis of several organs, particularly in haematological tissues.

What follows is an introduction to the enzymes of the AKR superfamily, their known substrates and roles in human disease. Also, an overview of the synthesis and signaling by steroid hormones and prostaglandins is presented.

1.2 The aldo-keto reductase superfamily

1.2.1 Overview

The AKRs are a large superfamily of enzymes present in bacteria, fungi, protozoans, plants and animals. AKRs are small (approximately 320 amino-acid residues in size), usually monomeric, share a common tertiary structure and catalyse the reversible reduction of carbonyl groups to hydroxyl groups using NADH or NADPH as a co-factor (Figure 1) (Jez et al., 1997a). Despite these common features, AKRs metabolise a wide variety of substrates including sugars, steroids, prostaglandins, aldehydes and isoflavonoids and are therefore involved in a myriad of biological processes (Jez et al., 1997a, Seery et al., 1998, Jez and Penning, 2001, Hyndman et al., 2003).

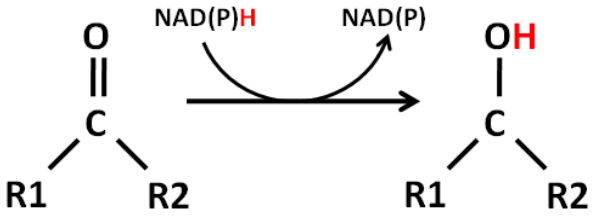

Figure 1 - AKRs reduce carbonyl groups to hydroxyl groups.

Currently there are over 150 proteins attributed to the AKR superfamily, subdivided into 15 families according to their phylogeny. A comprehensive database of known AKR proteins is available at the AKR homepage (http://www.med.upenn.edu/akr/) (Hyndman et al., 2003). The AKR homepage database includes the amino-acid sequences of the known members and their respective enzymatic activities, available crystal structures, the rules of the nomenclature system, phylograms of the superfamily and other useful resources. Furthermore, the website contains instructions for the assignment of new sequences to the superfamily.

1.2.2 Tertiary structure of AKR enzymes

AKRs are widely distributed across the kingdoms of life but have a conserved three-dimensional structure (Jez et al., 1997a). Upon folding, AKRs adopt a $(\alpha/\beta)_8$-barrel structure, as determined by X-ray crystallography (El-Kabbani et al., 1998, Hoog et al., 1994, Lovering

et al., 2004). Figure 2 shows an example, the AKR1C3 $(\alpha/\beta)_8$-barrel fold. This structure is composed of eight parallel β-strands alternating with eight α-helices running anti-parallelly, thus forming the structure of a barrel that encloses the catalytic pocket. Also, the structure contains three flexible protruding loops which vary greatly in sequence and size amongst the AKR superfamily (see alignment in Figure 4)

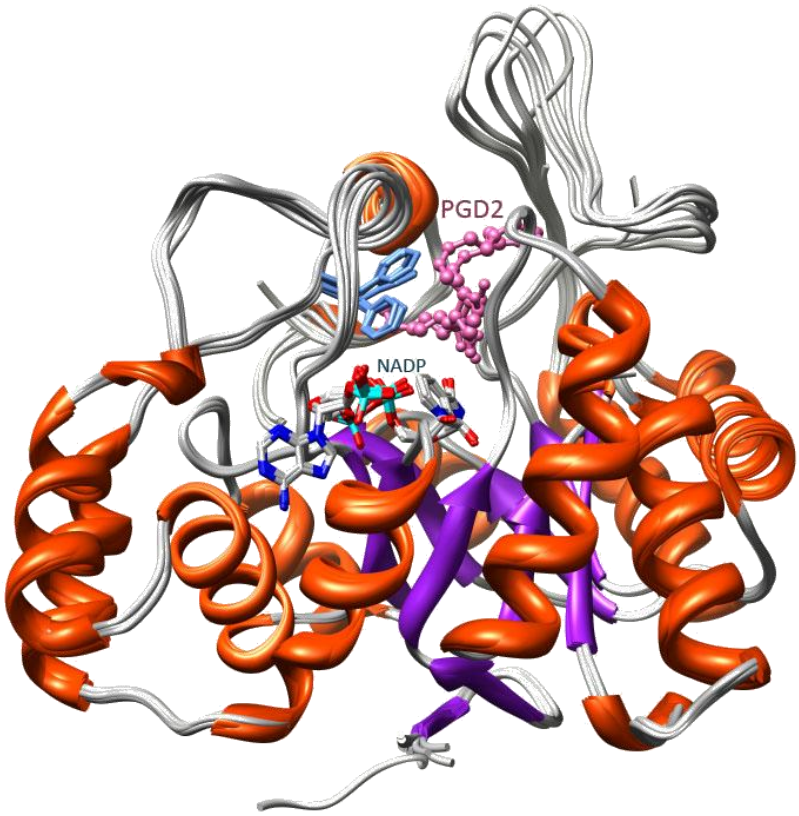

Figure 2 - Tertiary structure of an aldo-keto reductase.

Aldo-keto reductases (AKRs) have a conserved tertiary structure. This crystal structure was obtained from the super-imposition of several crystal structures obtained for AKR1C3 in complex with PGD_2 and $NADP^+$. Eight β-strands alternate (purple) with eight α-helixes (red) forming a barrel-like structure referred to as $(\alpha/\beta)_8$-barrel fold. The barrel encloses a wide catalytic pocket where conserved residues (*blue*) bind to the cofactor NAD(P)H and substrate to perform the reaction. The three protruding loops on top of the structure (A-, B- and C-loop) are flexible and are believed to be responsible for substrate recognition (created by Dr J Ride and Dr N Davies, University of Birmingham, UK)

The crystal structures obtained in previous studies revealed a spatial conservation of four catalytic residues inside the pocket: Asp50, Tyr55, Lys84 and His117 (Jez et al., 1997a). These residues interact with NAD(P)H and substrate (

Figure 3) and Tyr55 acts as the proton donor for the reduction reaction (Petrash et al., 1994). Due to the conservation of these residues it is believed that the catalytic mechanism is strictly conserved across the AKR superfamily.

Substrate specificity in AKRs is thought to be determined by the size and sequence of the three protruding loops (Jez et al., 1997a). However, each AKR can usually accommodate several types of molecules in their catalytic pocket hence their substrate promiscuity. It is likely that AKRs evolved from a common multifunctional ancestor and, after gene duplication and divergence, substrate specialization occurred by modification of the protruding loops whilst maintaining the $(\alpha/\beta)_8$-barrel structure and the general catalytic mechanism.

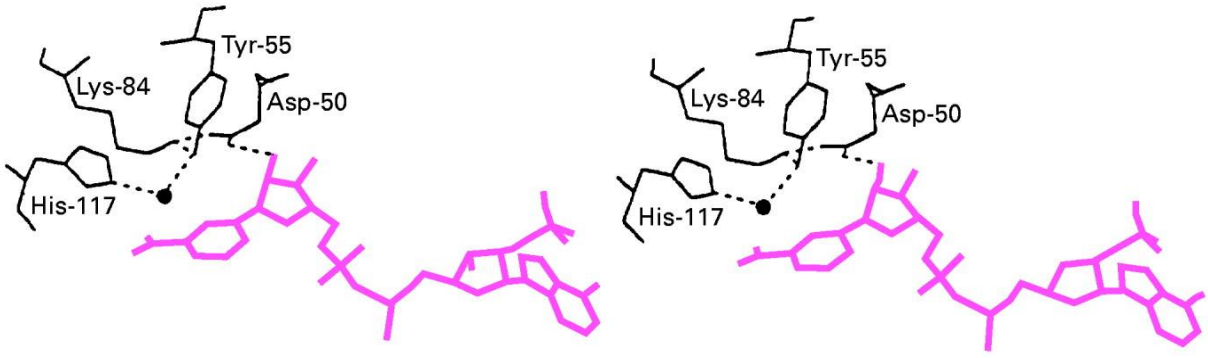

Figure 3 - The AKR active site.

The three-dimensional structures of all AKRs retain the same spatial relationship between the active-site residues (Asp50, Tyr55, Lys84 and His117), the nicotinamide cofactor (shown in pink) and a water molecule, as shown in this stereo-view of the rat liver 3α-HSD/AKR1C9•NADP+ binary-complex active site (Jez et al., 1997a).

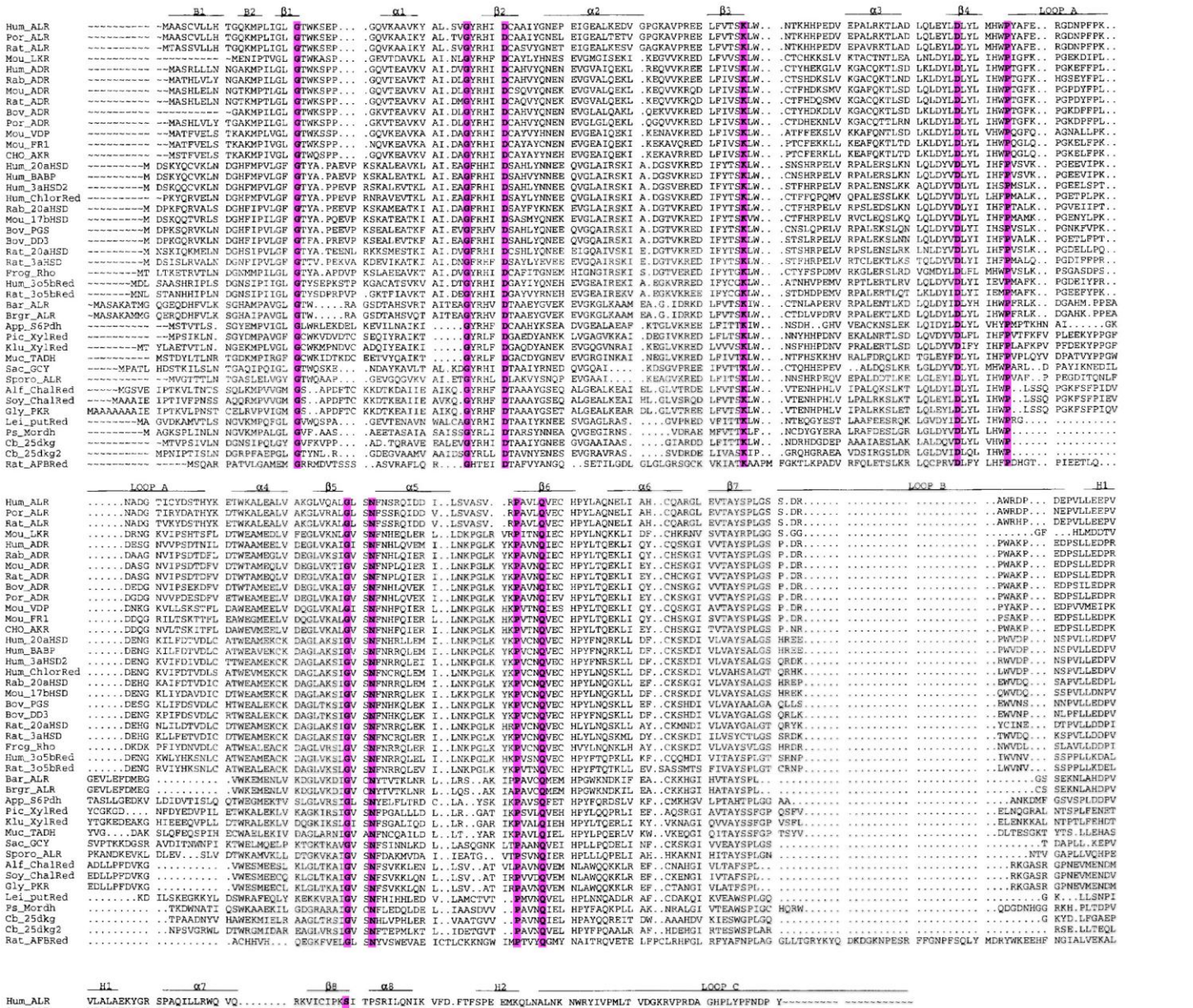

Figure 4 - Multiple sequence alignment of several members of the AKR superfamily.

(opposite page) Multiple sequence alignment showing the location of α-helices, β-strands and the three protruding loops. B1, B2, H1 and H2 are β-sheets and α-helices not forming the core of the $(\alpha/\beta)_8$-barrel structure. Invariant residues are highlighted in pink (Jez et al., 1997a).

1.2.3 Nomenclature and organization of the superfamily

Initially, AKR enzymes were named after their enzymatic activity. However, due to their broad substrate preference this nomenclature system became somewhat confusing. For instance, one AKR was known as dihydrodiol dehydrogenase 2, bile acid-binding protein and 3α-hydroxysteroid dehydrogenase type III while another related AKR was known as dihydrodiol dehydrogenase 1 and 20α (3α)-hydroxysteroid dehydrogenase. Furthermore, enzymes of other superfamilies, such as the short-chain dehydrogenase/reductases (SDR), showed overlapping activities with members of the AKR superfamily. Therefore, in 1997 a unified and systematic nomenclature system based on amino-acid sequence identity was adopted for the AKR superfamily (Jez et al., 1997b). All enzymes with a predicted $(\alpha/\beta)_8$-fold have the root name "AKR", for aldo-keto reductase, followed by an Arabic numeral (1, 2, 3…) designating the family, a letter (A, B, C…) designating the subfamily and an Arabic numeral designating a unique sequence (Figure 5).

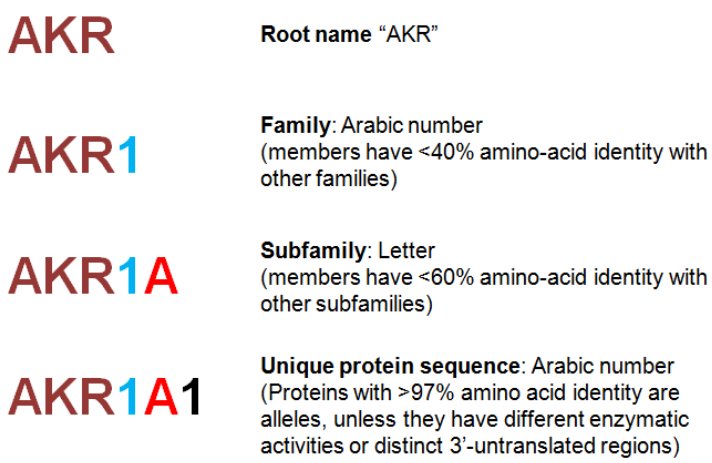

Figure 5 - Nomenclature system of the AKR superfamily.

Delineation of families and subfamilies is based on the amino-acid sequence identity of the proteins. Enzymes with >40% amino-acid identity are grouped in the same family. Currently, the sequence alignment has determined a total of 15 AKR families (AKR1-AKR15). Families can be further divided into subfamilies that group enzymes sharing >60% amino-acid identity. Presently, 11 of the 15 families are divided into multiple subfamilies. When the nomenclature was adopted the individual numbers were attributed arbitrarily amongst the known AKRs (AKR1A1, AKR1A2, and AKR1A3 are the aldehyde reductases from human, pig, and rat, respectively). New additions to a subfamily are numbered chronologically. Any two AKR sequences sharing more than 97% amino-acid identity are considered alleles of the same gene unless they are coded by different genes, in which case the 3'-untranslated region of the mRNA will be different, and/or have different substrate preferences. Members of the AKR2, AKR6 and AKR7 families have been shown to form multimers (Hyndman et al., 2003). For these cases the nomenclature also informs about the stoichiometry of the multimer. For example, AKR7A1 : AKR7A4 (1:3) would designate a tetramer of the composition indicated (Jez et al., 1997b).

1.2.4 The AKR families

A summary of the 15 AKR families is shown on Table 1. Presently, the AKR1 family is the largest, with 49 sequences found exclusively in animals (metazoans) with particular incidence in vertebrates. This family includes six subfamilies including the aldehyde reductases (AKR1A), aldose reductases (AKR1B), hydroxysteroid dehydrogenases (AKR1C, discussed in detail in section 1.3) and the Δ^4-3-ketosteroid-5β-reductases (AKR1D).

Enzymes of the AKR6 and AKR7 families are also present in vertebrates. The AKR6 enzymes are part of the voltage-gated potassium (Kv) channel complexes as β-subunits (Tipparaju et al., 2008). These enzymes associate with the cytosolic portion of the channel and modulate its opening by using NADPH. The AKR7 enzymes are highly conserved in mammals and are responsible for the detoxification of a commonly ingested fungal toxin, aflatoxin (Knight et al., 1999). Both AKR6 and AKR7 enzymes form homo- or heterodimers.

AKR enzymes are also found in plants, yeasts, filamentous fungus and protozoans where they are involved in a variety of synthetic pathways.

Table 1 - Summary of the AKR families

Family	Subfamilies	Number of sequences	Organisms	Function	Notes
AKR1	A	4	human, rat, wild boar, mouse	Aldehyde reductases; metabolism of neurotransmitters; detoxification; osmoregulation	
	B	15	human, rabbit, mouse, rat, chinese hamster, chicken	Conversion of glucose to sorbitol; detoxification; retinoic acid synthesis; PGF synthase ($PGH_2 \rightarrow PGF_2\alpha$) in the adrenal gland	Enzymes coded in a single gene cluster
	C	24	human, rabbit, mouse, rat, bovine, frog, horse, macaque	Hydroxysteroid dehydrogenases (androgens, estrogens, glucocorticoids and progestins); PGF synthase using PGH_2, PGE_2 and PGD_2 as substrate; detoxyification	Enzymes coded in a single gene cluster; implications in regulation of nuclear receptors
	D	3	human, rat, rabbit	Δ^4-3-ketosteroid-5β-reductases; bile acid synthesis and steroid hormone catabolism	Reduce C=C bonds rather than carbonyl groups due to a modified catalytic pocket
	E	2	human, mouse	Reduction of 1,5-anhydro-D-fructose, a glycogen breakdown product, to 1,5-anhydro-D-glucitol	Enzymes coded in the same gene cluster as AKR1C enzymes
	G	1	*C. elegans*	unknown function	
AKR2	A-E	14	Plants, yeasts, filamentous fungi, insects	Sugar metabolism	
AKR3	A-F	13	yeasts, filamentous fungi	Metabolism of arabinose, fucose, galactose and xylose	
AKR4	A-C	24	plants	Oxidation and reduction of a wide variety of substrates; stress-responsive enzymes	
AKR5	A-G	10	bacteria, *Trypanosoma bruce*, *Leishmania major*	Ascorbic acid synthesis in bacteria; PGF synthase ($PGH_2 \rightarrow PGF_{2\alpha}$) in *Trypanosoma* and *Leishmania*	
AKR6	A-C	18	human, rat, rabbit, mouse, *Xenopus laevis*, *Drosophila*, plants	β-subunits of voltage-gated potassium (Kv) channels; regulate the opening of the channel	Catalytic tetrad is not conserved with His117 replaced by an Asn residue
AKR7	A	5	human, rat, mouse	Detoxification of the fungal carcinogen aflatoxin	Expressed in liver, stomach and kidney; form hetero- or homodimers
AKR8-15	12	15	bacteria, yeasts	reduction of carbonyl groups in toxic compounds generated by oxidants and heavy metals; biosynthesis of secondary metabolites	

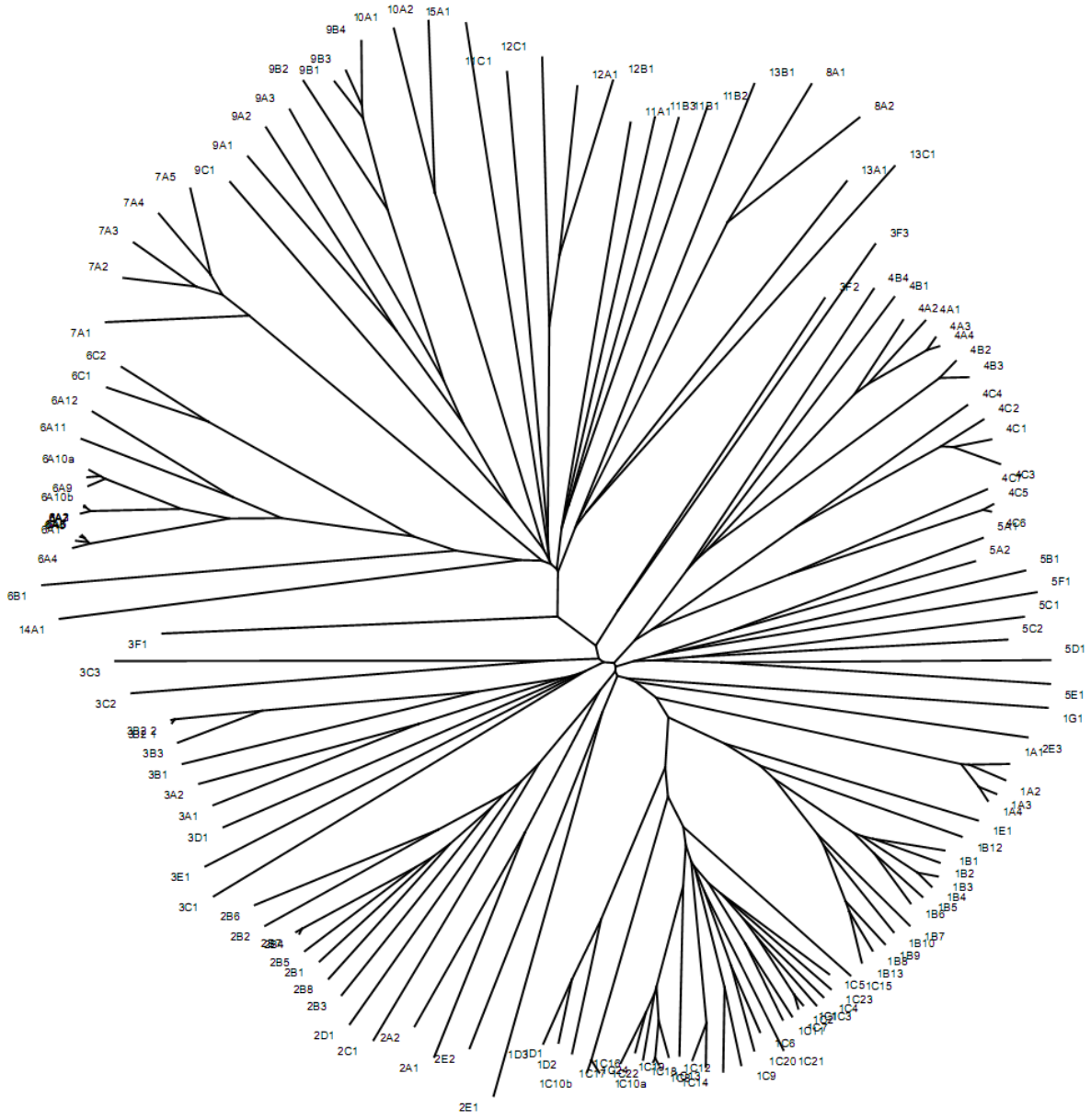

Figure 6 - Unrooted phylogram of all known AKR proteins.

Unrooted phylogram produced from the amino-acid sequence alignment of all known AKR proteins. Family AKR1 (bottom right side of phylogram) groups most of the known AKRs and is subdivided into 6 subfamilies (AKR1A-AKR1G). Phylogram obtained from the AKR homepage (http://www.med.upenn.edu/akr/tree.shtml) (Hyndman et al., 2003).

1.3 AKR1C subfamily

To date, enzymes of the AKR1C subfamily have been described exclusively in vertebrates and, apart from frog AKR1C10, are all found in mammalian species. AKR1C enzymes have been extensively studied for their ability to modify important signaling molecules (steroids and prostaglandins) thus affecting a plethora of processes in normal physiology and disease. Furthermore, AKR1C activity has been implicated in both activation and inactivation of toxic compounds (Jin and Penning, 2007). A detailed description of the subfamily, with particular incidence on the human isoforms, is presented in this section.

1.3.1 AKR1C gene cluster and tissue expression

Currently, 24 sequences have been attributed to the AKR1C subfamily all belonging to vertebrate species (Table 2). In these species, multiple AKR1C-coding genes have been found clustered in a single locus of their respective genomes. Due to the availability of sequenced and annotated genomes, both human and mouse AKR1C gene clusters are well described (Nishizawa et al., 2000, Vergnes et al., 2003).

Figure 7 shows a scale representation of the human AKR1C gene cluster, located on the short arm of chromosome 10. The four AKR1C genes are coded in the same orientation, sit in close proximity, have similar gene organization with identical size and number of exons and high sequence similarity suggesting a recent history of gene duplication. Two additional AKR-coding genes coded in the opposite orientation can be found in this cluster. *AKR1CL1* is coded between *AKR1C3* and *AKR1C4* and slightly overlaps the latter. This gene has an identical exon-intron organization but is considered a pseudogene in the NCBI database. Nevertheless the predicted enzyme coded in this gene has 68% amino-acid identity with the four AKR1C isoforms and would belong to the same subfamily. The *AKR1E2* gene (also known as *AKR1CL2*) codes a protein of the AKR1E subfamily highly expressed in the testis and homologous to murine AKR1E1 (Azuma et al., 2004).

A similar AKR1C-gene cluster has been described in mouse chromosome 13, the syntenic region of the human gene cluster (Vergnes et al., 2003). Like the human locus, the mouse cluster harbors all genes coding for known mouse AKR1C enzymes plus AKR1E1 (mouse AKR1C enzymes detailed in section 1.4). Likewise, the AKR1C enzymes described in Table

2 from rat, bull, macaque and horse are coded in similarly organized gene clusters on their respective genomes. This genomic organization suggests a common ancestral locus in which the number of subsequent gene duplications varied as the different mammalian lineages radiated.

Tissue expression of AKR1C genes

Each human AKR1C gene has a specific tissue distribution. Figure 8 shows two independent measurements of AKR1C expression in human tissues (Penning et al., 2000, Nishizawa et al., 2000). AKR1C1 is present in the heart, liver, adrenal gland, kidney, muscle, peripheral blood lymphocytes (PBL), uterus and testis. AKR1C2 is highly expressed in the liver, kidney and muscle but can also be detected in the heart, adrenal gland, lung and testis. AKR1C3 is the most broadly distributed isoform, being most expressed in the kidney, muscle, mammary gland, prostate, PBLs and uterus and also, but to a lesser extent, in liver, lung, heart, adrenal gland, ovary and testis. Unlike the other isoforms, AKR1C4 expression is fairly restricted, with almost exclusive presence in the liver and some expression in the adrenal gland. The presence of AKR1C enzymes in tissues such as the adrenal gland, mammary gland, prostate, testis, uterus, PBLs and liver is related with their activities towards steroid hormones and prostaglandins or as detoxifying enzymes.

Table 2 - Described members of the AKR1C subfamily (adapted from the AKR homepage)

AKR	Known enzymatic activities	Species	Identity (relative to AKR1C1)
1C1	20α-HSD dihydrodiol dehydrogenase 1	*Homo sapiens*	100%
1C2	3α-HSD type III dihydrodiol dehydrogenase 2 bile acid binding protein	*Homo sapiens*	97%
1C3	3α-HSD type II dihydrodiol dehydrogenase 3 17β-HSD type V PGD_2 11β-ketoreductase PGH_2 9,11-endoperoxide reductase	*Homo sapiens*	87%
1C4	3α-HSD type I dihydrodiol dehydrogenase 4 chlordecone reductase	*Homo sapiens*	82%
1C5	PGE_2 9-ketoreductase 20α-HSD	*Oryctolagus cuniculus*	80%
1C6	Estradiol 17β-HSD 17β-HSD type V	*Mus musculus*	76%
1C7	PGH_2 9,11-endoperoxide reductase PGD_2 11β-ketoreductase	*Bos taurus*	77%
1C8	20α-HSD	*Rattus norvegicus*	68%
1C9	3α-HSD	*Rattus norvegicus*	69%
1C10	rho-crystalline	*Rana temporaria*	60%
1C11	PGH_2 9,11-endoperoxide reductase PGD_2 11β-ketoreductase	*Bos taurus*	78%
1C12	unknown	*Mus musculus*	68%
1C13	unknown	*Mus musculus*	66%
1C14	unknown	*Mus musculus*	68%
1C15	unknown	*Rattus norvegicus*	69%
1C16	unknown	*Rattus norvegicus*	68%
1C17	unknown	*Rattus norvegicus*	67%
1C18	20α-HSD	*Mus musculus*	85%
1C19	3(20α)-HSD	*Mus musculus*	72%
1C20	dihydrodiol dehydrogenase	*Mus musculus*	73%
1C21	17α-HSD	*Mus musculus*	73%
1C23	17β(20α)-HSD	*Equus ferus*	80%
1C24	17β-HSD	*Rattus norvegicus*	68%
1C25	3(20)α-HSD	*Macaca fuscata*	82%

HSD, hydroxysteroid dehydrogenase; PG, prostaglandin; *Homo sapiens*, human; *Oryctolagus cuniculus*, rabbit; *Mus musculus*, mouse; *Bos taurus*, bull; *Rattus norvegicus*, rat; *Equus ferus*, horse; *Macaca fuscata*, macaque; *Rana temporaria*, common frog.

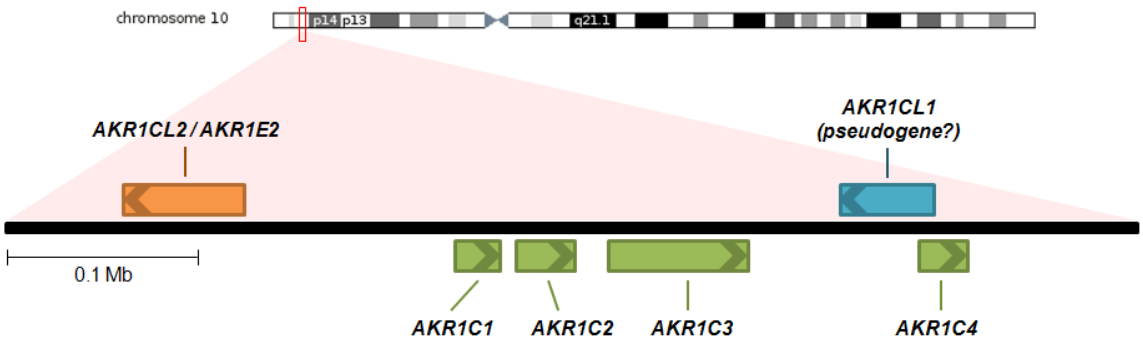

Figure 7 - Structure of the AKR1C gene cluster on human chromosome 10.

The four human AKR1C isoforms, AKR1C1, -1C2, -1C3 and -1C4, are coded in a gene cluster located on the short arm of chromosome 10. The four isoforms are coded in the same orientation and sit in close proximity (green boxes). Two additional AKR genes are coded in the same cluster but in reverse orientation. The protein coded in the *AKR1E2* / *AKR1CL2* gene (orange box) shares less than 60% amino-acid identity with the remaining AKR1C enzymes and belongs to the AKR1E subfamily. The *AKR1CL1* gene (blue box) overlaps *AKR1C4* and is described in the NCBI database as a pseudogene. However, in the Ensembl database *AKR1CL1* is considered a protein-coding gene and the predicted enzyme has 68% amino-acid identity with the remaining human AKR1C isoforms. Diagram is drawn to scale and was based on the genomic map from the Ensembl database (Hubbard et al., 2009).

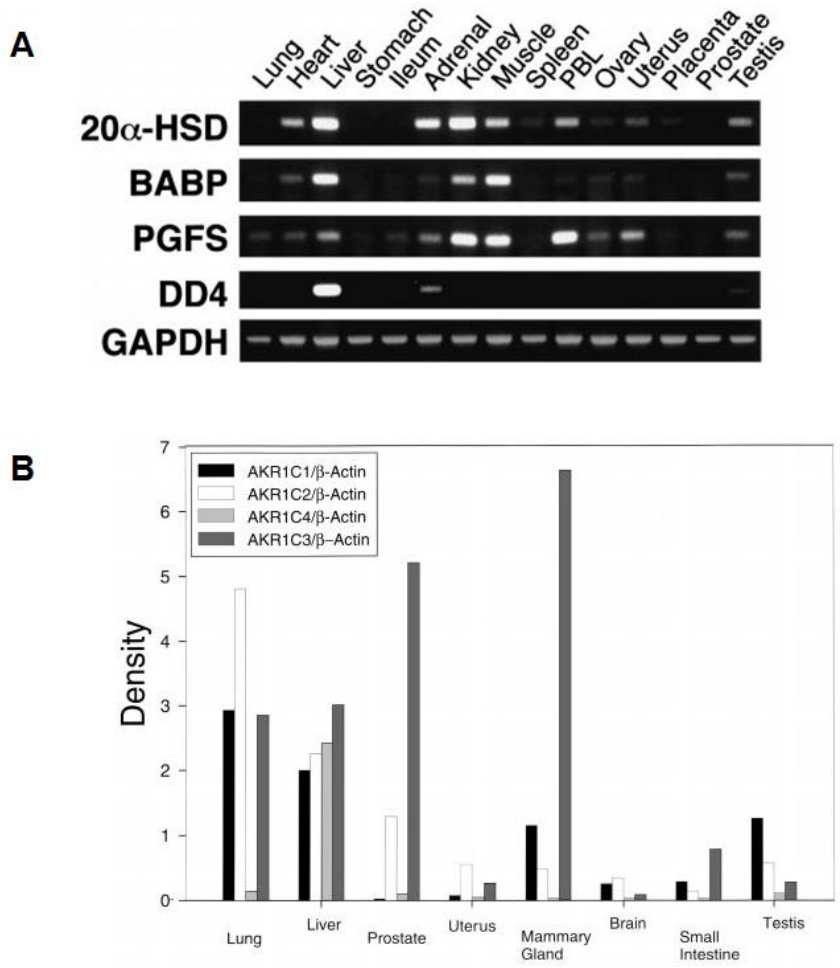

Figure 8 - Tissue-expression pattern of human AKR1C enzymes.

A. Reverse-transcriptase PCR (RT-PCR) measurement of human AKR1C enzymes: AKR1C1 (20α-HSD), AKR1C2 (bile acid binding protein; BABP), AKR1C3 (PGF synthase; PGFS) and AKR1C4 (dihydrodiol dehydrogenase 4; DD4). GAPDH was used as loading control. PBL; peripheral blood lymphocytes. Adapted from (Nishizawa et al., 2000). **B**. Expression of the four AKR1C enzymes was measured in several human tissues using RT-PCR (18 cycles). Products were separated by gel electrophoresis, transferred to nitrocellulose and Southern-blot analysed using cDNA probes. Density of bands was quantified and normalized to β-actin band. Figure taken from (Penning et al., 2000).

1.3.2 Steroid hormone metabolism

AKR1C enzymes were first described because of their hydroxysteroid dehydrogenase (HSD) activities. By reducing specific carbonyl groups, AKR1C enzymes can potentiate or inactivate steroid hormones in a tissue-specific manner and affect their local signaling impact. This modulatory property of AKR1C enzymes is shared with members of the short-chain dehydrogenase/reductase (SDR) family (Mizrachi and Auchus, 2009).

Human AKR1C enzymes have a variety of ketosteroid reductase activities towards steroid hormones such as progesterone, androstenedione, estrone, 5α-dihydrotestosterone (5α-DHT) and deoxycorticosterone (DOC) (Figure 10). AKR1C1 acts predominately as a 20α-HSD but also as a 3β-HSD. AKR1C2 and -1C4 have been described as 3α-HSD while AKR1C3 has both 17β- and 20α-HSD activity (Penning and Drury, 2007, Penning and Byrns, 2009). Similar activities have been described in other non-human AKRs, as described in Table 2. Although AKR1C enzymes can also catalyse oxidation of hydroxysteroids *in vitro* it is believed that *in vivo* they function predominantly as reductases. This is supported by the fact that AKR1C enzymes have 1000-fold higher affinity for NADPH than NAD+ and, when over-expressed in COS-1 cells, perform exclusively ketosteroid reduction (Penning and Byrns, 2009). The physiological implications of these activities are discussed below, after a short introduction to steroidogenesis and steroid signaling.

1.3.2.1 Steroid hormone synthesis pathway

Steroid hormones are lipid-derived endocrine signaling molecules. *De novo* synthesis of steroid hormones occurs mainly in the testis, ovary and adrenal gland and, to a lesser extent, in brain, placenta and adipose tissue. Enzymes involved in steroidogenesis belong to the cytochrome P450 (CYP), SDR and AKR superfamilies (Baker, 2004, Nebert and Russell, 2002, Sanderson, 2006). A scheme of the steroid hormone synthesis pathway is shown in Figure 9. In the initial step, cholesterol, the precursor for all steroid hormones, is converted to pregnenolone by CYP11A, an enzyme bound to the mitochondrial membrane and expressed exclusively in steroidogenic tissues. Pregnenolone is converted to the active steroid progesterone by the 3β-HSD, a membrane-bound enzyme of the SDR superfamily (SDR11E1). Pregnenolone and progesterone form the precursors for all other steroid hormones (Sanderson, 2006).

Unlike the gonads, the adrenal gland is a vital organ and is considered the most important steroidogenic tissue. Steroid 21-hydroxylase (CYP21A1) is exclusively expressed in the adrenal gland and is responsible for the synthesis of glucocorticoids (initiated by the conversion of 17α-OH-progesterone to 11-deoxycortisol) and mineralocorticoids (initiated by the conversion of progesterone to deoxycorticosterone). The active hormones aldosterone and corticosol are then produced by CYP11B2 and CYP11B1, respectively, which are also exclusively expressed in the adrenal gland (Sanderson, 2006).

CYP17A1 has two distinct catalytic sites and has both 17α-hydroxylase activity, converting pregnenolone and progesterone to the respective 17α-OH forms, and a 17,20-lyase activity, converting the 17α-OH steroids to the weak androgens dehydroepiandrosterone (DHEA) and androstenedione. This enzyme is expressed in the adrenal gland, ovaries and testis.

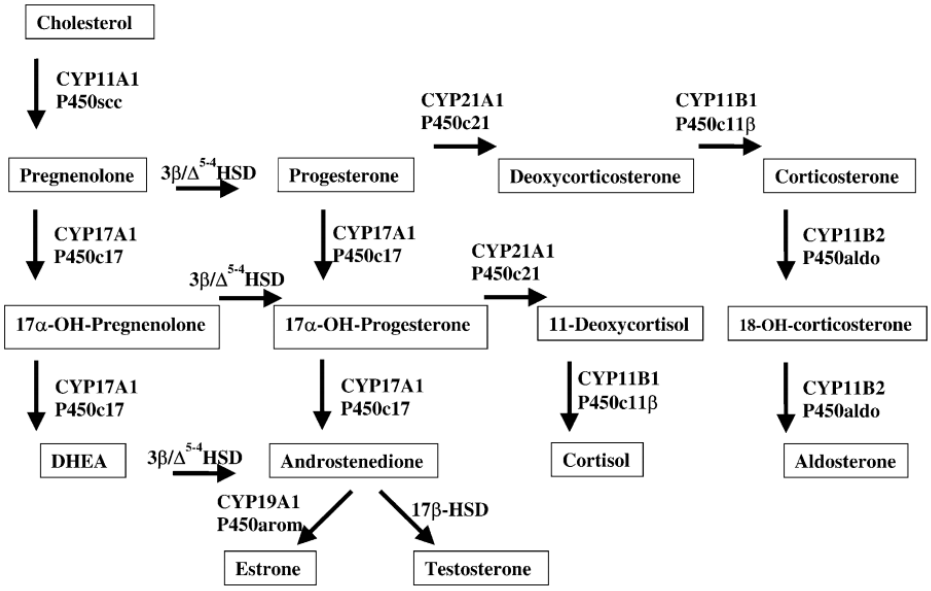

Figure 9 - Enzymes involved in the synthesis of adrenal and sex steroids.

Cholesterol is the precursor of adrenal and sex steroids. Steroid hormone synthesis is carried out by enzymes of the cytochrome P450 (CYP), SDR and AKR superfamilies (Baker, 2004).

In the testis, CYP17A1 catalyses the production of the weak androgens DHEA and androstenedione. Androstenedione is then converted to testosterone, a potent androgen, by enzymes with 17β-HSD activity. Seven types of human 17β-HSD have been described: types 1, 2, 3, 4, 5, 7 and 8 (Luu-The, 2001). Of these, 17β-HSD type 5 is AKR1C3 while the remaining enzymes belong to the SDR family. Both type 3 and type 5 (AKR1C3) are expressed in the testis where they have been implicated in testosterone production (Luu-The, 2001). When released into the blood stream, testosterone reaches the peripheral tissues where it can be further metabolised. For instance, in the prostate, testosterone can be oxidized back to androstenedione by 17β-HSD type 2 or be locally converted to 5α-dihydrotestosterone (5α-DHT), the most potent endogenous androgen, by 5α-reductases (Sanderson, 2006). Both 17β-HSD enzymes act as molecular switches, either reducing or enhancing the potency of testosterone in a tissue-specific manner.

In the ovaries, the aromatase (CYP19arom) converts androstenedione to estrone which is further converted to estradiol by 17β-HSD type 1, 5 (AKR1C3) and 7. Inactivation of estradiol, a potent estrogen, back to estrone is also mediated by 17β-HSD type 2 (Sanderson, 2006). In addition, testosterone can be directly converted to estradiol by aromatase.

Due to their lipophilic nature, steroid hormones are able to cross cellular membranes without the aid of transporters and spread through the body via the bloodstream. In the plasma, steroid hormones are mainly found associated with specific protein carriers such as the steroid hormone-binding globulin (SHBG) for testosterone and 17β-estradiol, or the corticosteroid-binding globulin (CBG) for cortisol and progesterone (Andreassen, 2006). These carriers also assist in the tissue-specific endocytic uptake of steroid hormones. Steroid hormones can reach peripheral organs, enter the cells and interact with steroid hormone receptors to elicit a response. Also, in peripheral tissues, steroid hormones can be activated or inactivated by locally expressed enzymes, such as AKRs.

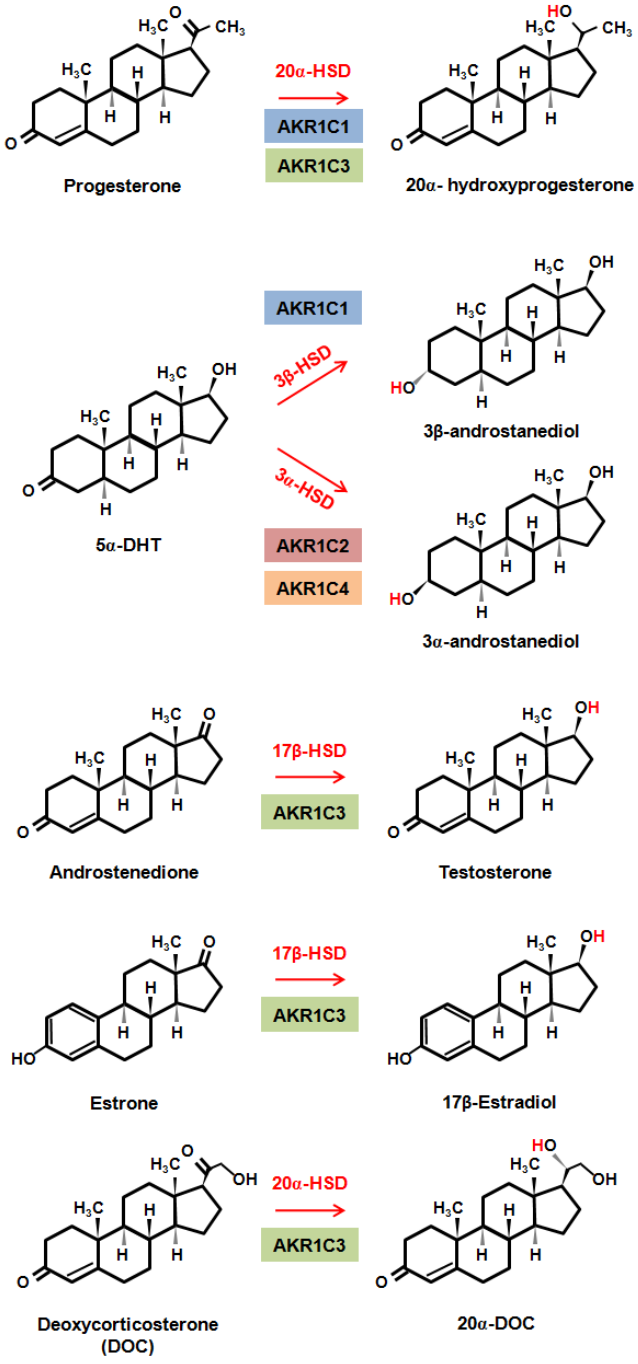

Figure 10 - Steroid hormone reductase activities of human AKR1C enzymes.

Human AKR1C enzymes have multiple hydroxysteroid dehydrogenase (HSD) activities towards several steroid hormones. AKR1C1 is predominantly a 20α-HSD but can also act as a 3β-HSD. Both AKR1C2 and -1C4 have 3α-HSD activity whereas AKR1C3 has 20α- and 17β-HSD activities.

1.3.2.2 Nuclear receptors

Steroid hormones elicit their effects in target tissues by activating steroid hormone receptors. These are intracellular ligand-activated transcription factors that belong to the nuclear receptor (NR) superfamily. Recently, steroid hormones have also been shown to signal via surface receptors of the G protein-coupled receptor family (Levin, 2009).

NRs have only been found in animals (metazoans) where they regulate many processes in embryonic development and adult physiology, such as reproduction, metabolism, differentiation and homeostasis (Escriva et al., 2004). All NRs share a common tertiary structure and are grouped in six subfamilies based on their amino-acid sequence comparison, much like the AKR families (Table 3). Humans have 48 NRs but for almost half of these proteins no naturally occurring ligand is known. These NRs are termed "orphan receptors".

1.3.2.2.1 The NR family

Table 3 shows a list of all known human NRs, their common name, their systematic name (reflecting their phylogeny) and known natural or synthetic ligands. Steroid hormone receptors are highlighted in orange: estrogen receptor (ERα and -β), androgen receptor (AR), progesterone receptor (PR), glucocorticoid receptor (GR) and mineralocorticoid receptor (MR). Retinoic acid receptors are highlighted in blue: RARα, -β and -γ; RORβ and RXRα, -β and -γ. Thyroid hormone receptors are highlighted in pink (TRα and -β). The vitamin D receptor is highlighted in purple (VDR). Peroxisome-proliferator activated receptors that bind fatty acids and eicosanoids like 15d-prostaglandin J_2 and leukotriene are highlighted in green (PPARα, -β and -γ). Other nuclear receptors, such as the pregnane X receptor (PXR) and the constitutive androstane receptor (CAR) are activated by xenobiotics and elicit a detoxification response. For many NRs no natural or synthetic ligand is known.

1.3.2.2.2 Mechanisms of nuclear receptor transcriptional activation

There are three main mechanisms by which NRs are activated, bind to DNA and modulate transcription (Figure 11). Steroid hormone receptors, AR, ER, PR, GR and MR, are synthesised in an inactive form that is sequestered in the cytoplasm by heat-shock proteins (HSPs). Binding of steroid hormone causes a conformation change in the NR that leads to its dissociation from the HSP complex followed by translocation to the nucleus. In the nucleus,

the receptor binds to the response elements in the target gene promoter as a homodimer and, associated with co-activators, induces gene transcription (Glass and Ogawa, 2006).

Heterodimeric NRs, such as TR, VDR, RAR, LXR and PPARs, are constitutively bound to the response elements in the DNA with their binding partner, RXR. In the absence of ligand, heterodimeric NRs associate with co-repressors that induce tightening of the chromatin structure in the promoter region, suppressing gene transcription. Ligand binding induces a conformation change in the NR leading to dissociation from the co-repressor complex and interaction with co-activator proteins that promotie gene transcription (Glass and Ogawa, 2006).

Several NRs are known to bind to DNA as monomers. Most of these monomeric NRs are "orphan receptors" as no ligand is known to activate them. It is speculated that such NRs can modulate transcription by changes in their expression or by post-translational modification, such as phosphorylation or SUMOylation, induced by other signaling pathways (Glass and Ogawa, 2006). Additionally, some NRs, such as GR, LXR and the PPARs, can repress gene expression in a ligand-dependent manner. This is usually the ligand-dependent transrepression of other transcription factors such as nuclear factor-κB (NF-κB). Unlike other forms of NR-mediated action, ligand-dependent transrepression does not seem to require binding to response elements or dimerization (Glass and Ogawa, 2006, Straus et al., 2000). However, the detailed molecular mechanisms leading to transrepression are still poorly understood.

In conclusion, NRs have a diverse array of functions that depend not only on the type of ligand that can activate them but also in which tissue they are present, which co-activators and co-repressors are expressed in the same cell type, the combined activity of other transcription factors and the presence of enzymes that modify the ligands.

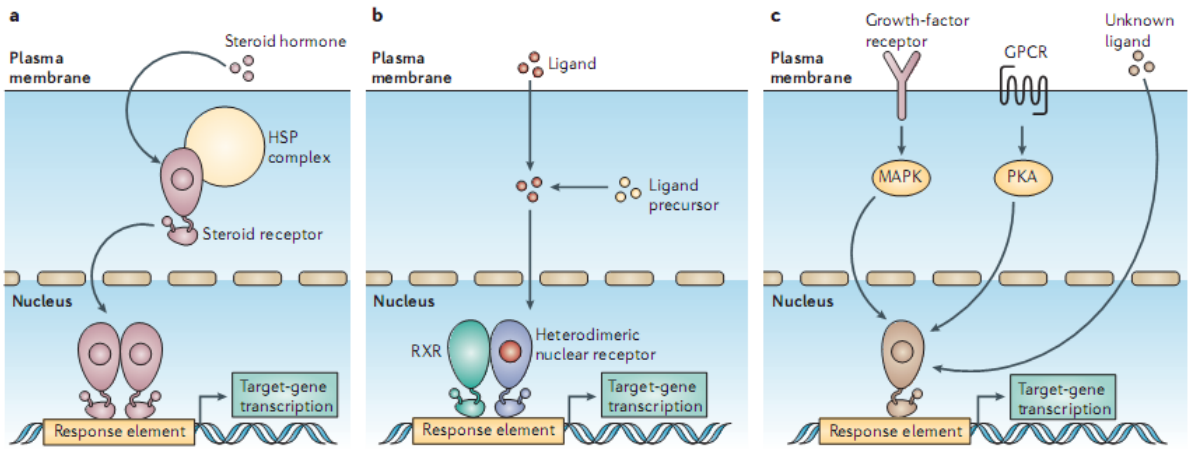

Figure 11 - Mechanism of nuclear receptor DNA binding and transcription activation.

Three main mechanisms by which NRs influence gene transcription. **A**: Steroid hormone receptors are produced in an inactive form and, in the absence of ligand, are sequestered in the cytoplasm by heat-shock proteins (HSPs). Upon ligand binding, the receptor dissociates from the HSP proteins, translocates to the nucleus and binds the response elements in the DNA as a homodimer. **B**: NRs, such as the PPARs, LXR are constitutively bound to the DNA in a heterodimer with RXR. In the absence of ligand, these heterodimers are associated with co-repressors and repress gene transcription. Upon ligand binding the receptor changes conformation and associates with co-activators and promotes gene transcription. **C:** Monomeric NRs are often “orphan receptors” as no ligand is known to activate them. These NRs might modulate transcription by post-translational modifications induced by other signaling pathways (Glass and Ogawa, 2006)

Table 3 - Human nuclear receptors.

Name	Nomenclature	Ligands
TRα	NR1A1	Thyroid hormones
TRβ	NR1A2	Thyroid hormones
RARα	NR1B1	*All-trans* retinoic acid
RARβ	NR1B2	*All-trans* retinoic acid
RARγ	NR1B3	*All-trans* retinoic acid
PPARα	NR1C1	Fatty acids, leukotriene B_4, fibrates
PPARβ	NR1C2	Fatty acids
PPARγ	NR1C3	Fatty acids, 15d-prostaglandin J_2, thiazolidinediones
Rev-erbα	NR1D1	Orphan
Rev-erbβ	NR1D2	Orphan
RORα	NR1F1	Cholesterol, cholesteryl sulfate
RORβ	NR1F2	Retinoic acid
RORγ	NR1F3	Orphan
LXRα	NR1H3	Oxysterols, T0901317, GW3965
LXRβ	NR1H2	Oxysterols, T0901317, GW3965
FXRα	NR1H4	Bile acids, fexaramine
FXRβ	NR1H5	Lanosterol
VDR	NR1I1	Vitamin D, 1,25-dihydroxyvitamin D_3
PXR	NR1I2	Xenobiotics, 16α-cyanopregnenolone
CAR	NR1I3	Xenobiotics, phenobarbital
HNF4α	NR2A1	Orphan
HNF4γ	NR2A2	Orphan
RXRα	NR2B1	9-*cis* retinoic acid, *all-trans* retinoic acid
RXRβ	NR2B2	9-*cis* retinoic acid, *all-trans* retinoic acid
RXRγ	NR2B3	9-*cis* retinoic acid, *all-trans* retinoic acid
TR2	NR2C1	Orphan
TR4	NR2C2	Orphan
TLL	NR2E2	Orphan
PNR	NR2E3	Orphan
COUP-TFI	NR2F1	Orphan
COUP-TFII	NR2F2	Orphan
EAR2	NR2F6	Orphan
ERα	NR3A1	Estradiol-17β, tamoxifen, raloxifene
ERβ	NR3A2	Estradiol-17β, various synthetic compounds
ERRα	NR3B1	Orphan
ERRβ	NR3B2	DES, 4-OH tamoxifen
ERRγ	NR3B3	DES, 4-OH tamoxifen
GR	NR3C1	Cortisol, dexamethasone, RU486
MR	NR3C2	Aldosterone, spirolactone
PR	NR3C3	Progesterone, medroxyprogesterone acetate, RU486
AR	NR3C4	Testosterone, 5α-DHT, flutamide
NGFI-B	NR4A1	Orphan
NURR1	NR4A2	Orphan
NOR1	NR4A3	Orphan
SF1	NR5A1	Orphan
LRH-1	NR5A2	Orphan
GCNF	NR6A1	Orphan
DAX-1	NR0B1	Orphan
SHP	NR0B2	Orphan

Adapted from (Germain et al., 2006)

1.3.2.3 Co-evolution of steroid modifying enzymes and steroid hormone receptors

The colonization of land by animals led to the evolution of new organs and more complex developmental mechanisms. This required the specialization of several high-affinity steroid hormone receptors as well as steroid-activating and -inactivating enzymes in the SDR, CYP and AKR superfamilies that regulate ligand access to the receptors in a tissue-specific and cell-selective manner (Baker, 2004). This form of regulation, known as *pre-receptor regulation*, is important in adult physiology but is often subverted in pathophysiology, such as cancer.

1.3.3 Androgen metabolism and prostate cancer

Prostate cancer is the most common invasive cancer in men, as is breast cancer in women (Risbridger et al., 2010). Prostate cancer is a hormone-dependent tumour in which malignant cells express AR and require androgens to drive proliferation and survival (Mellado et al., 2009) (Figure 12). Estrogens, although much less prevalent than androgens in the male body, also play a role in prostate cancer, through stimulation of ERα and ERβ.

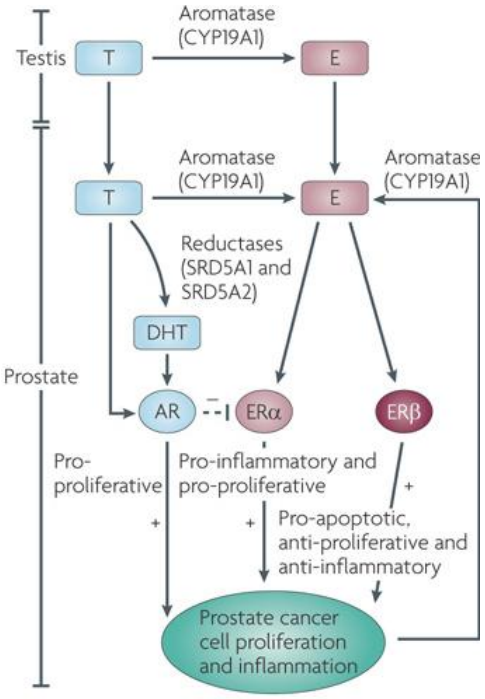

Figure 12 - Hormone interactions in prostate cancer cells.

Androgens (testosterone, T, and 5α-DHT) and estrogens (estradiol, E) have implications in prostate cancer. In the prostate, T can be converted into the potent androgen 5α-DHT by 5α-reductases (SRD5A1 and -5A2) and both stimulate AR that drives cancer proliferation. Aromatase (CYP19A1) can convert T to E that can stimulate both ERα and ERβ in the prostate. However, ERα and ERβ have opposing effects, with the former being pro-proliferative and the latter anti-proliferative. Nevertheless, in the male body the predominant sex steroids and drivers of cancer progression are the androgens. Adapted from (Risbridger et al., 2010).

Initially, all prostate cancer patients are submitted to hormonal therapy, i. e., restriction of either androgen synthesis or AR activation (Risbridger et al., 2010). However, most patients will gradually develop resistance and the cancer progresses even in the absence of androgen signaling.

Despite castration causing a drastic decrease in serum testosterone levels, steroid precursors from the adrenal gland can still be locally activated in the prostate, creating a pro-androgenic environment. One enzyme capable of local androgenesis is the type 5 17β-HSD, AKR1C3 (Mellado et al., 2009, Risbridger et al., 2010).

1.3.3.1 AKR1C enzymes in prostate androgen metabolism

Both AKR1C2 and AKR1C3 are expressed in the prostate and modulate AR activation (Penning and Byrns, 2009, Rizner et al., 2003, Penning et al., 2006) (Figure 13). Some studies have also reported the presence of AKR1C1 in this tissue (Bauman et al., 2006, Ji et al., 2007). AKR1C3, with its 17β-HSD activity, locally converts androstenedione to testosterone which can be further converted to 5α-DHT by the 5α-reductases. Through its 3α-HSD activity, AKR1C2 inactivates 5α-DHT by converting it to the weak androgen 3α-androstanediol (Penning and Byrns, 2009). Due to its unique 3β-HSD activity, AKR1C1 converts 5α-DHT to 3β-androstanediol, an ERβ ligand. Therefore, in the prostate, AKR1C3 activity induces cell proliferation via AR activation whereas AKR1C1 and -1C2 counteract it by catabolizing 5α-DHT. Furthermore, by producing an ERβ ligand, AKR1C1 generates an anti-proliferative stimulus (Figure 12 and Figure 13).

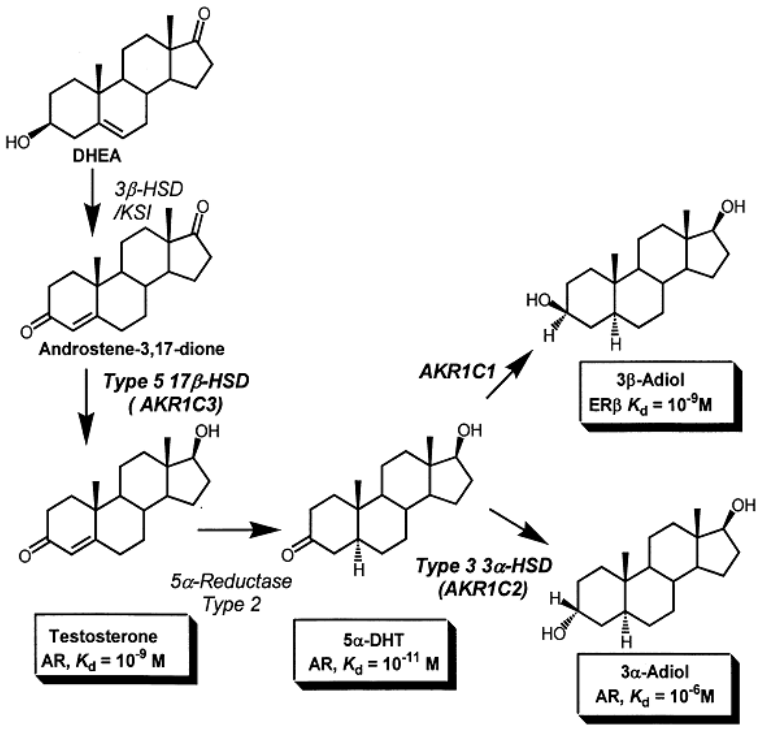

Figure 13 - Role of human AKR1C enzymes in prostate androgen metabolism and pre-receptor regulation.

Prostate or adrenal gland-derived androstenedione is converted to testosterone (potent androgen) by AKR1C3 which is further converted to 5α-DHT (very potent androgen) by 5α-reductases. Subsequently, 5α-DHT can be inactivated by conversion to 3α-androstanediol (weak androgen) by AKR1C2 or 3β-androstanediol (potent estrogen) by AKR1C1 (Penning and Byrns, 2009).

1.3.3.2 AKR1C enzymes in prostate cancer

In a recent study, the gene expression pattern of 33 metastatic androgen-independent prostate cancer samples was compared with that of 22 primary androgen-dependent prostate cancer samples using Affymetrix microarrays (Stanbrough et al., 2006). Besides increased AR expression in the androgen-independent cancers, several enzymes involved in androgen synthesis and catabolism were found upregulated including 5α-reductase and AKR1C3. The over-expression of AKR1C3 in androgen-independent prostate cancer was also confirmed by immunohistochemistry in agreement with previous studies (Fung et al., 2006, Penning et al., 2006). Both AKR1C1 and -1C2, involved in the inactivation of 5α-DHT, were also found upregulated in the androgen-independent tumours. However, the magnitude of amplification of these enzymes (3.1- and 3.4-fold, respectively) was less than that of AKR1C3 (5.3-fold).

The authors concluded that there was an overall increase in enzymes promoting local androgen synthesis.

In another study, paired comparisons were made between primary prostate cancer samples and benign tissue from 13 patients to determine differences in 5α-DHT synthesis and catabolism (Ji et al., 2007, Ji et al., 2003). Expression levels of AKR1C1 and/or AKR1C2 were found to be significantly decreased in 11 out of 13 tumour samples relative to their benign counterparts. In addition, levels of 5α-DHT were increased in all cancer samples by an average magnitude of 42%. Radio-labeled 5α-DHT was predominantly reduced to 3α- or 3β-androstanediol in benign samples. Such catabolism of 5α-DHT was reduced in the tumour samples in a manner that correlated with AKR1C and -1C2 loss. Finally, over-expression of AKR1C1 and AKR1C2, but not AKR1C3, resulted in increased 5α-DHT turn-over and inhibited the 5α-DHT-stimulated proliferation of PC-3 and LAPC-4 cells (prostate cancer cell line). These results suggest that loss of AKR1C1 and -1C2 in prostate cancer promotes cell proliferation by reducing 5α-DHT inactivation.

These and other studies have implicated the human AKR1C enzymes in pre-receptor regulation of AR in prostate cancer. In addition the pro-proliferative activity of AKR1C3 in prostate disease has rendered this enzyme a potential therapeutic target.

1.3.4 Estrogen metabolism and breast cancer

Like prostate cancer, breast cancer is a sex steroid-driven malignancy. Estrogen activation of ERα is the most important stimulus driving proliferation and survival in breast cancer cells (Figure 14) (Risbridger et al., 2010). Estrogens also activate ERβ which counter-acts ERα activity by suppressing cell proliferation. However, expression of ERα in breast cancer is generally higher than ERβ, hence the proliferative outcome (Kurebayashi et al., 2000). Progesterone signaling via PR has both pro- and anti-proliferative actions in breast cancer, although in the long-term, these effects seem to be predominantly inhibitory (Purmonen et al., 2008). Androgen signaling, via AR, also counter-acts the ERα-mediated pro-proliferative signaling. However, in the female body, the levels of estrogens are higher than those of androgens and thus AR activation in breast cancer is reduced.

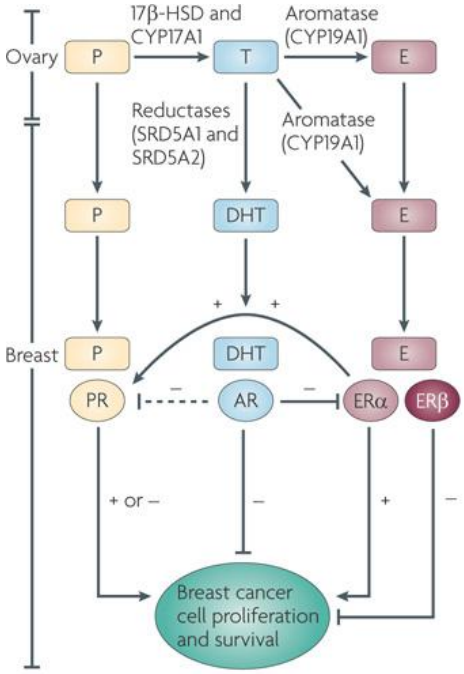

Figure 14 - Hormone interactions in breast cancer cells.

Activation of ERα by estrogens (E) is considered the main proliferative and survival stimulus in breast cancer cells. ERα activation also causes upregulation of PR which can have both pro- and anti-proliferative effects when activated by progesterone. Activation of ERβ has anti-proliferative effects but this receptor is less expressed than ER α in breast cancer cells. Androgens (T, DHT) also play a role in breast cancer via AR activation, an anti-proliferative signal. Some evidence suggests AR activation inhibits PR activity, but this remains uncertain. Figure from (Risbridger et al., 2010)

As with prostate cancer patients, hormone therapy is the first treatment against breast cancer. However, the majority of patients also tend to relapse and develop an estrogen-independent disease, mainly by developing an intra-tumoural estrogen synthesis pathway.

1.3.4.1 AKR1C enzymes in estrogen and progesterone metabolism in breast cancer

AKR1C3 is expressed in normal breast tissue and has consistently been found upregulated in breast cancer samples where it is associated with poor prognosis (Jansson et al., 2006, Lin et al., 2004). The two predominant activities of AKR1C3, 17β-HSD and 20α-HSD, create an advantageous pro-estrogenic environment in the malignant cells that stimulates cell proliferation. Firstly, the concerted activities of AKR1C3 and CYP19 aromatase convert androstenedione to the potent ER ligands estrone and 17β-estradiol (Figure 15). In addition, AKR1C3 can inactivate progesterone to its 20α-hydroxyl form thus preventing PR activation (Penning and Byrns, 2009). Artificial over-expression of AKR1C3 in MCF-7, a breast cancer cell line, resulted in enhanced testosterone and 17β-estradiol production from androstanediol and estrone, respectively, and progesterone inactivation. Furthermore, transfected cells had increased proliferation in response to estrone and 17β-estradiol, strongly implying AKR1C3 in breast cancer development (Byrns et al., 2010).

A paired comparison between 24 breast cancer samples and adjacent normal tissue revealed that AKR1C1 expression was substantially (>5-fold) decreased in 13 of those samples (Ji et al., 2004). In 6 of those 13 samples, AKR1C2 was also substantially down-regulated whereas AKR1C3 levels were unchanged in all samples. The authors speculate that this change in AKR1C expression results in modified progesterone metabolism advantageous for cancer progression.

In addition to breast cancer, de-regulation of AKR1C expression has been observed in other estrogen-driven malignancies as both AKR1C1 and -1C3 were found predominantly over-expressed in endometrial (Rizner et al., 2006) and ovarian cancer samples (Smuc et al., 2009).

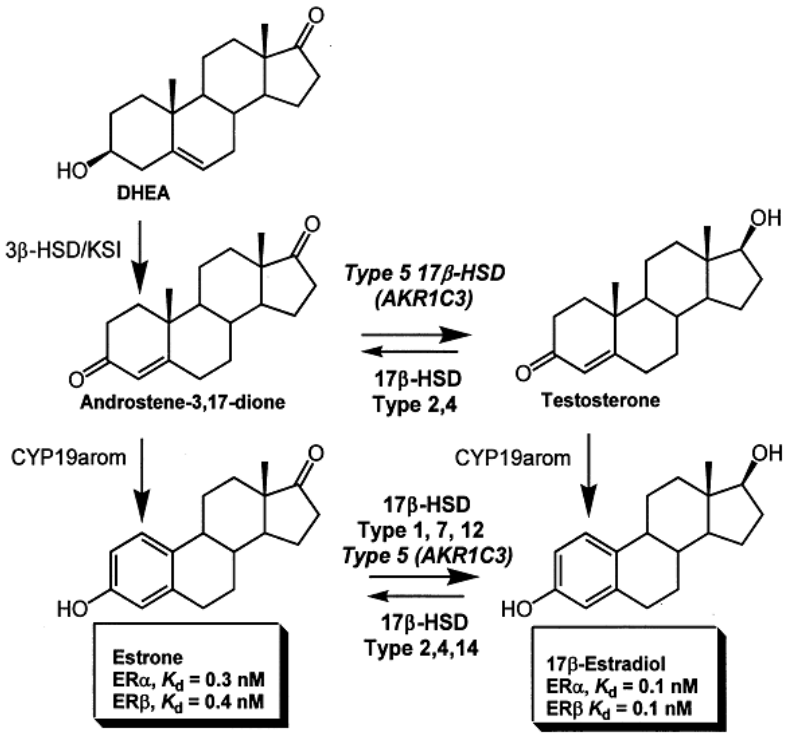

Figure 15 - Role of AKR1C3 in breast estrogen metabolism and pre-receptor regulation.

The combined actions of AKR1C3 and CYP19 aromatase generate a pro-estrogenic environment in the breast. Aromatase converts androstenedione (weak androgen) to estrone (potent estrogen) which is further converted to 17β-estradiol (very potent estrogen) by AKR1C3. Alternatively, androstenedione can be converted to testosterone (potent androgen) by AKR1C3 which is then reduced to 17β-estradiol by aromatase. Figure from (Penning and Byrns, 2009)

1.3.5 Deoxycorticosterone metabolism in the kidney

AKR1C3 also exerts 20α-HSD activity towards deoxycorticosterone (DOC), a potent ligand for the mineralocorticoid receptor (MR). Highly expressed in the renal tubules, MR activity promotes the reabsorption of sodium in the urine affecting the water and salt balance of the body. AKR1C3 converts DOC to 20α-hydroxy-DOC, an inactive mineralocorticoid, thus preventing MR activation (Sharma et al., 2006). Expression of both AKR1C3 and MR was detected in renal duct epithelial cells suggesting a role in pre-receptor regulation. Furthermore, AKR1C3 over-expression has been detected in renal cell carcinoma, papillary urothelial carcinoma, and Wilms' tumour (renal malignancies) (Azzarello et al., 2009).

1.3.6 Prostaglandin metabolism

In addition to steroids, AKR1C enzymes catalyse the ketoreduction of prostaglandins (PGs), lipid-derived signaling molecules involved in a variety of physiological processes such as inflammation, vaso and bronchoconstriction, platelet aggregation, regulation of sleep and cell proliferation (Funk, 2001). Prostaglandins belong to a larger group of molecules known as eicosanoids which are fatty acid-derived and have 20 carbons in their structure (*eicosa*- Greek for twenty). The molecular structures and sub-classes of eicosanoids are shown in

Figure 16.

The prostaglandins, PGE_2, PGD_2, $PGF_{2\alpha}$ and PGI_2 (prostacyclin), together with thromboxane (TXA_2), compose the prostanoids. Prostanoids are characterised by a 5-carbon ring (cyclopentane ring) at the extremity of the structure, and result from the peroxidation and cyclization of the arachidonic acid (AA), a fatty acid derived from membrane phospholipids. The modifications in the cyclopentane ring vary amongst the prostanoids conferring them with different stabilities and signaling properties.

Prostaglandins can not be stored in cells and are synthesised *de novo* in response to external stimuli. The amount and type of prostaglandins produced depends on the enzymatic machinery expressed in a given cell-type and, once released into the extra-cellular space,

these short-lived molecules interact locally with surface receptors of neighbouring cells to elicit autocrine and paracrine signaling effects.

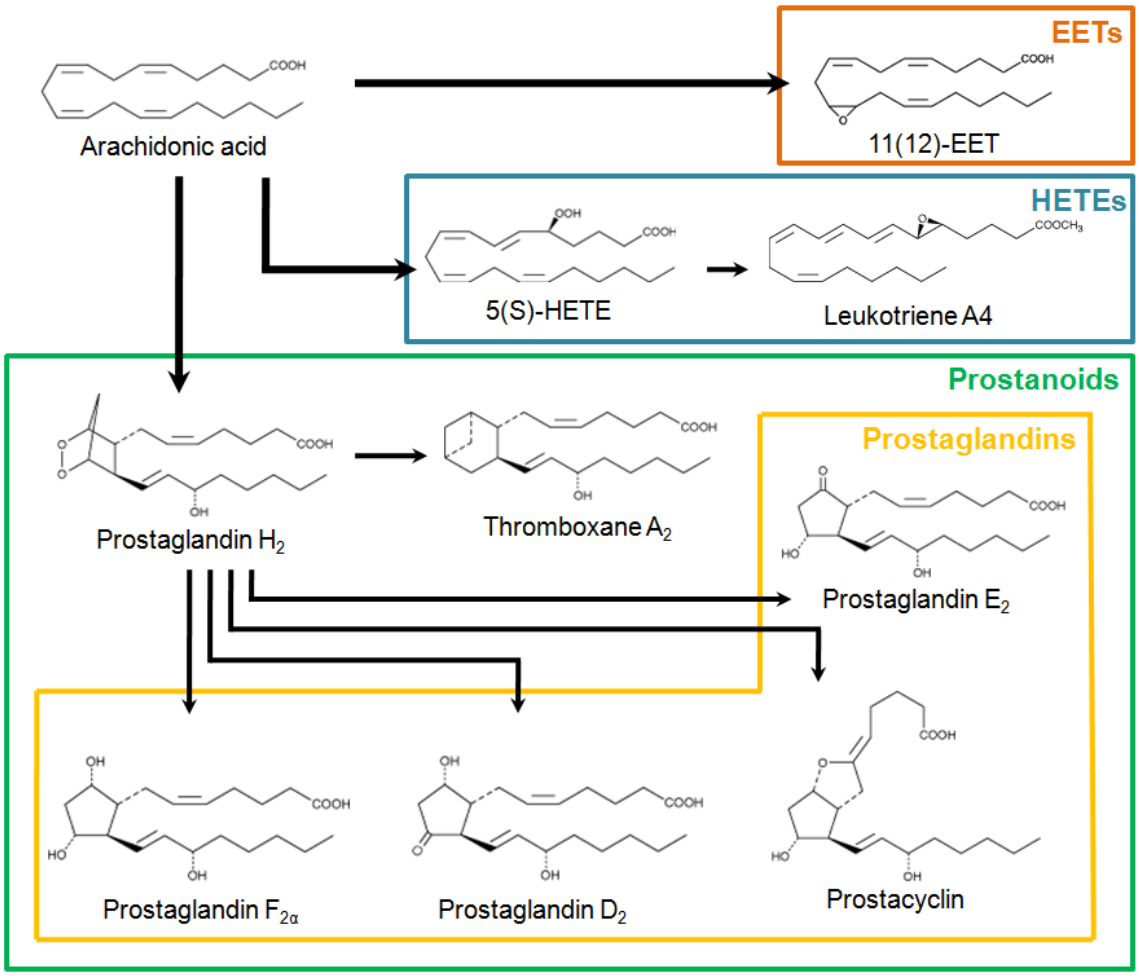

Figure 16 - Molecular structure and classification of the eicosanoids.

All eicosanoids are derived from C20 fatty acid precursors (*eicosa*- Greek for twenty), usually arachidonic acid (AA). Oxygenation of AA is required for the synthesis of epoxyeicosatrienoic acids (EETs) and hydroxyeicosatetraenoic acids (HETEs). Peroxidation and cyclization of AA is required for the synthesis of prostanoids, a class of eicosanoids that includes prostaglandins (PGE_2, $PGF_{2\alpha}$, PGD_2 and prostacyclin) and thromboxane A_2.

1.3.6.1 Prostaglandin synthesis pathway

1.3.6.1.1 Eicosanoid synthesis begins with cPLA$_2$

Eicosanoids are short-lived molecules and can not be stored in cells. Instead, *de novo* eicosanoid synthesis occurs in cells after stimulation by a variety of agents such as cytokines, hormones, growth factors, neurotransmitters, mitogens, mechanical trauma, antigens and endotoxins (Clark et al., 1995, Hirabayashi et al., 2004) (Figure 19). These stimuli induce the translocation of cytosolic phospholipase A_2 (cPLA$_2$) from the cytoplasm to the perinuclear membranes. Once anchored to the lipid bilayer, cPLA$_2$ hydrolyzes the *sn*-2 bond of membrane phospholipids, releasing arachidonic acid (AA), the eicosanoid precursor (Schaloske and Dennis, 2006). Activation of cPLA$_2$ is the rate-limiting step in eicosanoid synthesis and is followed by a cascade of reactions leading to the production of active prostanoids.

1.3.6.1.2 Cyclooxygenases initiate the production of prostanoids

Released AA can be further metabolised by cyclooxygenases (COX), lipoxygenases (LOX) and P450 epoxygenases to generate prostanoids, hydroxyeicosatetraenoic acids (HETEs) or epoxyeicosatrienoic acids (EETs), respectively (

Figure 16). The most well characterised LOX metabolites are the leukotrienes, which promote accumulation of leukocytes during inflammation and their adhesion to vessel endothelial cells (Peters-Golden and Henderson, 2007). Epoxygenase-derived EETs are another class of eicosanoids and have been described as potent regulators of systemic blood pressure (Capdevila et al., 2007).

Mechanism of COX activity

COXs are the rate-limiting enzymes in prostanoid biosynthesis and important clinical targets. Like cPLA$_2$, COXs are membrane-bound enzymes located at the perinuclear membranes and perform the cyclization of AA into prostaglandin H_2 (PGH_2), the unstable prostanoid precursor. This is a two-step reaction consisting of a cyclooxygenation followed by a

peroxidation resulting in the sequential conversion of AA to PGG_2 and PGG_2 to PGH_2, respectively (

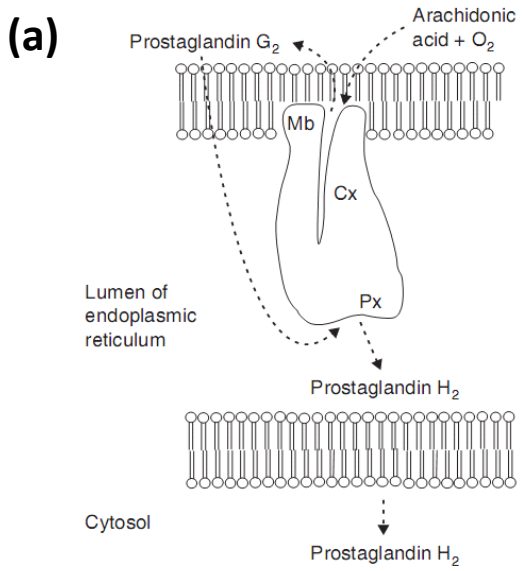

Figure 17). Therefore COX enzymes are bifunctional with two distinct catalytic sites. Nevertheless the two reactions are functionally coupled as the synthesis of PGH_2 in the peroxidation site results in the reactivation of the cyclooxygenase site (Simmons et al., 2004, Chandrasekharan and Simmons, 2004, Dubois et al., 1998).

Constitutive COX and inducible COX

All vertebrates have two COX isoforms, COX-1 and COX-2, coded by two different genes. Despite sharing 60 to 75% amino-acid identity and performing the same reaction, each isoform has a particular physiological function. COX-1 is the constitutive cyclooxygenase and is expressed ubiquitously in tissues at relatively similar levels suggesting it works as a provider of prostanoids for homeostatic regulation (Dubois et al., 1998). It has particular

importance in the protection of gastric mucosa, kidney blood flow and is the only COX expressed in platelets where prostanoids regulate blood clotting (Simon, 1999).

COX-2 expression is normally undetected in most tissues but can be quickly induced by a variety of pro-inflammatory factors such as interleukin-1 (IL-1), tumour necrosis factor-α (TNF-α), interferon-γ (INFγ), lipopolysaccharides (LPS), hormones and even prostanoids (Tanabe and Tohnai, 2002). This upregulation provides the cell with a sudden boost in prostanoid production. The effect is transient since COX-2 mRNA is naturally unstable and is quickly degraded upon termination of stimulus (Wu, 1996, Morita, 2002).

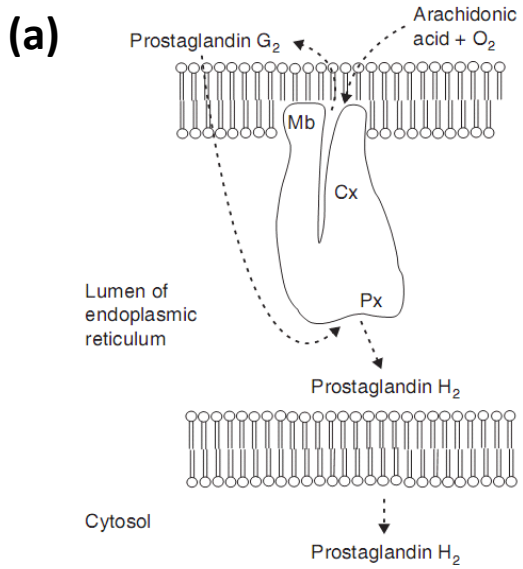

Figure 17 - Catalytic mechanism of cyclooxygenases

A Cross-section of a COX monomer in the lumen of the endoplasmic reticulum. The COX active site (Cx) faces the membrane where the binding (Mb) domain anchors the enzyme. The peroxidation site (Px) faces the lumen of the organelle. **B** COXs perform two consecutive reactions. AA is cyclooxygenated to PGG_2 followed by peroxidation yielding PGH_2. Figure adapted from (Chandrasekharan and Simmons, 2004).

Upregulation of COX-2 is particularly important in inflammation where prostanoid signaling plays a key role (Suleyman et al., 2007). In addition, COX-2 expression is often increased in a variety of tumours including lung (Patel and Chiplunkar, 2007), prostate (Aparicio Gallego et al., 2007), liver (Breinig et al., 2007), cervical (Young et al., 2008) and colon (Eisinger et al., 2007).

COX inhibition with NSAIDs

COXs are inhibited by synthetic molecules known as non-steroidal anti-inflammatory drugs (NSAIDs). These analgesic and anti-inflammatory drugs rely on their eicosanoid-depressing properties to exert function and include acetylsalicylate (aspirin), indomethacin, ibuprofen and acetaminophen (Paracetamol) (Blobaum and Marnett, 2007). However, in addition to their anti-inflammatory actions, NSAIDs have undesired side-effects such as the development of gastric ulcers, kidney malfunction and reduced blood clotting.

Conventional NSAIDs inhibit both COX isoforms. Development of COX-2 specific inhibitors is possible and can be achieved by targeting small differences in the catalytic site. Examples of these COX-2 specific inhibitors are Celecoxib and Rofecoxib (Simon, 1999).

1.3.6.1.3 PGH_2 is converted to the five primary prostanoids

PGH_2 is a highly unstable and short-lived precursor that is quickly converted to one of the five primary prostanoids: PGE_2, PGD_2, $PGF_{2\alpha}$, PGI_2 or TXA_2 (Figure 19). These conversions are catalysed by the PGE synthases (PGES), PGD synthases (PGDS), PGF synthases (PGFS), PGI synthase (PGIS) and TXA synthase (TXAS), respectively.

TXAS, a member of the CYP enzyme family, is highly expressed in platelets, the major site of TXA_2 production (Nakahata, 2008). TXAS null mice have normal haemopoiesis but its platelets fail to aggregate, resulting in prolonged bleeding time (Yu et al., 2004). In agreement, certain mutations in human TXAS are associated with bleeding disorders (Wang and Kulmacz, 2002, Shen and Tai, 1998). PGIS, which is also a CYP enzyme, is most highly expressed in endothelial and smooth muscle cells (Wu and Liou, 2005). PGIS null mice show increased blood pressure due to thicker vascular walls and interstitial fibrosis, especially in the kidneys (Yokoyama et al., 2002).

Three PGE_2 synthases have been described. Two are membrane bound (mPGES-1 and mPGES-2) and one is cytosolic (cPGES). Both mPGES-2 and cPGES are constitutively expressed and produce basal levels of PGE_2 whilst mPGES-1 is induced by pro-inflammatory agents (Park et al., 2006). These enzymes are widely distributed in the tissues and are involved in production of PGE_2 for a variety of physiological processes, particularly inflammation and pain.

$PGF_{2\alpha}$ synthases

Several PGFS have been identified in humans and other animals. However, unlike the other primary prostanoids, $PGF_{2\alpha}$ can be synthesised via reduction of PGH_2, PGE_2 or PGD_2 (in the latter case the product is the stereoisomer 9α,11β-$PGF_{2\alpha}$) (Watanabe, 2002). Most enzymes with PGFS activity are members of the AKR superfamily (Figure 18). This is the case for human AKR1C3, which has both PGH_2 9-,11-endoperoxide and PGD_2 11β-ketoreductase activity (Suzuki-Yamamoto et al., 1999). Similar activities were found in bovine AKR1C7 (lung) and -1C11 (liver) (Suzuki et al., 1999, Watanabe et al., 1985). AKR1B1 from human, AKR1B3 and -1B7 from mouse and AKR5A1 and -5A2 from trypanosome use exclusively PGH_2 as substrate (Kabututu et al., 2009, Kubata et al., 2000) whereas rabbit AKR1C5 is the only described PGE_2 9-ketoreductase (Wintergalen et al., 1995). Recently, an enzyme belonging to the thioredoxin-like superfamily from human and its mouse homologue were shown to have PGFS activity using PGH_2 as substrate (Moriuchi et al., 2008). The PGD_2 11β-ketoreductase activity of AKR1C3 is essential in regulating leukaemic cell survival and is discussed in section 1.3.7.

PGD_2 synthases

There are two PGDS each from a distinct protein family, exemplifying a case of convergent evolution (Urade and Eguchi, 2002). Haemopoietic-type PGDS (H-PGDS) belongs to the glutathione *S*-transferases (GST) family of enzymes and requires glutathione (GSH) as a co-factor. H-PGDS is responsible for PGD_2 synthesis in haemopoietic tissues such as mast cells, antigen presenting cells and Th2 cells (Kanaoka and Urade, 2003). Two studies revealed that H-PGDS knock-out mice have an augmented inflammatory response characterised by high pro-inflammatory cytokine production and lymphocyte proliferation (Rajakariar et al., 2007, Trivedi et al., 2006). H-PGDS was also shown to have protective effects in colon cancer. A mouse strain prone to develop intestinal adenomas, the *Apc* $^{Min/+}$ mice, was crossed with either transgenic or knock-out H-PGDS mice. Overexpression of H-PGDS resulted in ~80% less carcinomas whereas absence of H-PGDS caused a ~50% increase in carcinoma incidence (Park et al., 2007).

Lipocalin-type PGDS (L-PGDS) also known as brain-type PGDS is a member of the lipocalin family. These are secreted proteins such as β-lactoglobulin and plasma retinol-binding protein

that bind and transport small lipophilic ligands. Interestingly, L-PGDS was the first member of the lipocalin family to be recognized as an enzyme. Structurally this activity relies on residue Cys65 as mutations of this amino-acid result in complete loss of PGDS activity (Ragolia et al., 2007). This cysteine residue is not present in other lipocalin proteins. It is also a target for *N*-glycosylation, another unprecedented characteristic of a lipocalin family member (Ragolia et al., 2007). L-PGDS is a small (~ 30 kDa) monomeric enzyme that requires free sulfhydril compounds (β-mercaptoethanol, GSH, dithiothreitol, cysteine or cysteamine) for the reaction. The enzyme is synthesised with an N-terminal signal peptide that targets the protein for secretion. L-PGDS has been found in body fluids such as cerebrospinal fluid (CSF), seminal plasma, blood plasma and ocular fluids. The protein still retains its lipocalin functions and binds with high affinity to small lipophilic molecules such as retinoic acid, bilirubin, biliverdin and thyroid hormone (Urade and Eguchi, 2002). L-PGDS expression can be modulated by steroid hormones since the upstream region of its gene contains thyroid hormone and glucocorticoid response elements (Leone et al., 2002).

Alternatively L-PGDS can be found inside cells. In oligodendrocytes and arachnoid cells of rat brain, L-PGDS has been observed in the ER and perinuclear membranes, co-localizing with COX enzymes. Therefore it is proposed that L-PGDS is a bifunctional protein acting as a lipocalin when secreted and as a prostaglandin synthase when intracellular (Urade and Hayaishi, 2000a, Urade and Eguchi, 2002, Leone et al., 2002). In knock-out studies, mice lacking L-PGDS showed reduced reaction to tactile pain (allodynia) caused by injection of pain producing substances such as PGE_2 and bicuculline. This lack of sensitivity was rescued by co-injection with femtogram amounts of PGD_2 (Eguchi et al., 1999).

Because L-PGDS protein levels are increased in fluids of type 2 diabetic patients (Hirawa et al., 2001), a study was undertaken to elucidate its role in insulin resistance. L-PGDS knock-out mice were shown to have higher glucose intolerance and insulin resistance when fed a high-fat diet. This was accompanied by larger adipocytes, increased nephropathy and aortic thickening when fed a high-fat diet (Ragolia et al., 2003). Also, addition of L-PGDS to the culture media inhibited cell proliferation and induced glucose uptake in rat vascular smooth muscle cells, suggesting a role in sugar metabolism and possibly the development of diabetes (Ragolia et al., 2008, Ragolia et al., 2004).

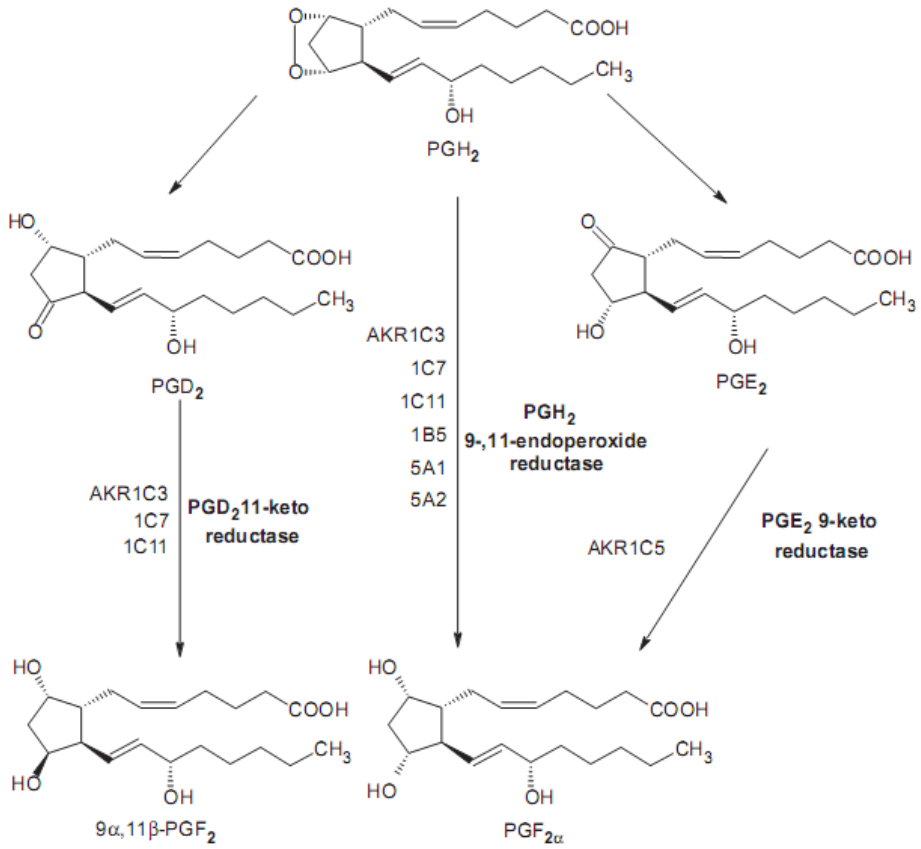

Figure 18 - PGF synthases

Enzymes producing $PGF_{2\alpha}$ or the stereoisomer 9α,11β-$PGF_{2\alpha}$ are considered PGF synthases. Three routes lead to $PGF_{2\alpha}$: 9-,11-endoperoxide reduction of PGH_2; 9-ketoreduction of PGE_2 or 11β-ketoreduction of PGD_2. The names of AKR enzymes with known PGFS activities are shown. Figure from (Kabututu et al., 2009).

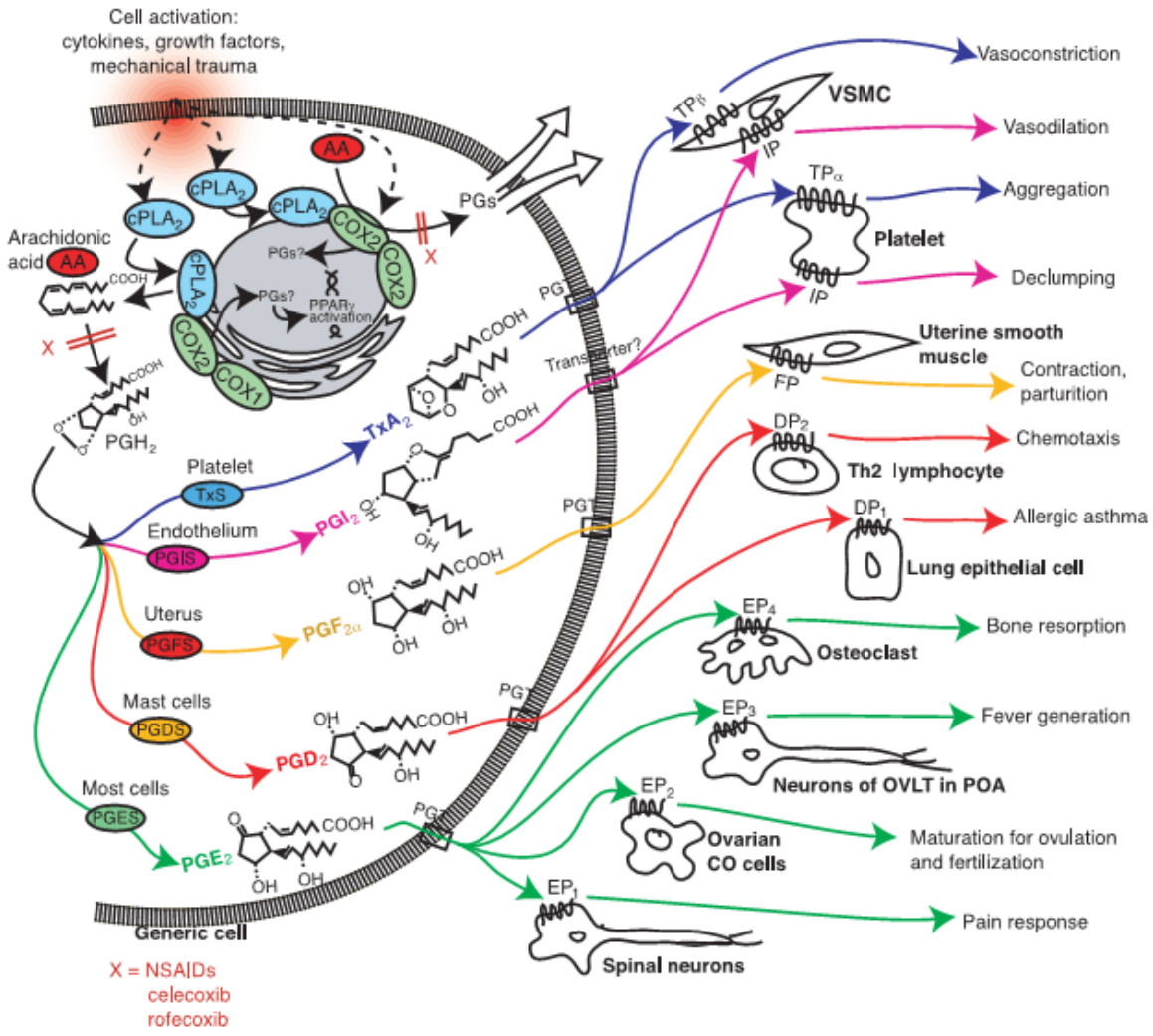

Figure 19 - Prostanoid synthesis and actions.

Prostanoid synthesis is induced by external stimuli such that induce the translocation of cytosolic phospholipase A_2 ($cPLA_2$) from the cytoplasm to the perinuclear membranes, where it catalyses the release of arachidonic acid (AA) from membrane phospholipids. Then, membrane-bound cyclooxygenases (COX-1 or COX-2) perform the cyclization and peroxidation of free AA into PGH_2. COX activity can be blocked by NSAIDs such as aspirin or indomethacin. The terminal synthases PGES, PGDS, PGFS, PGIS and TxS then convert PGH_2 to PGE_2, PGD_2, $PGF_{2\alpha}$, PGI_2 (prostacyclin) or TXA_2 (thromboxane). Newly synthesised prostanoids cross the cell membrane either by diffusion through the lipid bilayer or through the generic prostaglandin transporter (PGT). Prostanoids exert their effects in neighbouring cells via surface G protein-coupled receptors. TXA_2 signals via TP to promote platelet aggregation and smooth-muscle cell constriction while PGI_2 signals via IP to counter-act TXA_2 signaling. $PGF_{2\alpha}$ interacts with FP in uterine smooth muscle cells and induces contraction leading to parturition. PGD_2 exerts multiple effects via DP1, such as activation of lung epithelial cells, and DP2 (CRTH2). PGE_2 signals via four receptors, EP1-EP4, and is involved in a variety of processes such as bone resorption, fever generation, fertilization and pain response. Alternatively, some prostanoids resulting from spontaneous dehydration of PGE_2 and PGD_2 can signal intracellularly by activating nuclear receptors such as PPARγ. Figure from (Funk, 2001).

1.3.6.2 Transport

Once synthesised in the cytosol, prostanoids have to cross the cell membrane to reach the extracellular space and exert signaling effects. Most prostanoids can exit cells by slowly diffusing across the membrane (Schuster, 2002). Nevertheless, active prostaglandin transporters have been described. The rat prostaglandin transporter (PGT) was first characterised in 1995 (Kanai et al., 1995), followed by the human (Lu et al., 1996) and mouse (Pucci et al., 1999) homologues. These transporters bind to the five primary prostanoids with identical affinities and mediate both influx and efflux via a lactate exchange mechanism (Schuster, 2002). Transporters of other protein families have also been shown to transport prostanoids, but unlike PGT, these seem to have less affinity and transport other types of eicosanoids as well (Schuster, 2002).

1.3.6.3 Signaling

Once secreted, prostanoids exert their effects in neighbouring cells by activating surface G-protein-coupled receptors (GPCRs). The end-result of prostanoid signaling depends on which types of receptors are expressed by cells near the site of synthesis (Figure 19). The several prostanoid receptors have a relatively high sequence homology, suggesting a common ancestral prostanoid receptor (Figure 20) (Bos et al., 2004).

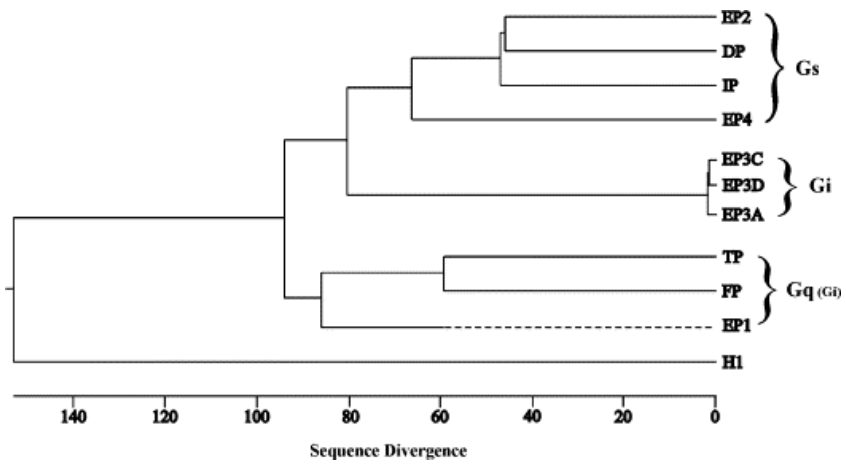

Figure 20 - Phylogenetic tree of primary prostanoid receptors.

The different prostanoid receptors and their associated G-proteins. The histamine H1 receptor is shown as reference. Figure from (Bos et al., 2004).

The receptors are named after their respective prostanoid ligands. TXA_2 binds to TP; PGI_2 binds to IP; $PGF_{2\alpha}$ binds to FP; PGD_2 binds to DP1 and DP2 (also named CRTH2; not shown in phylogram) and PGE_2 binds EP1, EP2, EP3 and EP4. Also, although each receptor has highest affinity for their cognate prostanoids significant cross-reactivity with other prostanoids also occurs (Breyer et al., 2001). Prostanoid receptors can be subdivided into three groups, depending on what type of G-protein they normally associate with. The relaxant receptors EP2, DP1, IP and EP4 activate G_s which stimulates cyclic AMP (cAMP) production to exert signaling. The contractile receptors EP1, TP and FP activate G_q protein that causes an increase in intracellular calcium. The EP3 isoforms signal via G_i proteins resulting in decreased cAMP levels. Nevertheless, the G-protein associated to the receptors may differ according to cell types (Bos et al., 2004).

FP

Levels of $PGF_{2\alpha}$ increase immediately before parturition in gestational tissues, plasma, amnion fluids and urine leading to uterus contraction and consequently to birth. Also, $PGF_{2\alpha}$ levels increase in plasma, urine and lymph causing luteolysis at the end of the oestrous cycle in ruminants (Unezaki et al., 1996). Broncho and vasoconstriction have also been associated with $PGF_{2\alpha}$ signaling (Seibert et al., 1987). The upstream region of the FP gene contains estrogen and progesterone response elements linking yet again $PGF_{2\alpha}$ and reproductive physiology (Abramovitz et al., 1994, Olson et al., 2003). FP-null mice develop normally but, when pregnant, fail to induce parturition at term (Sugimoto et al., 1997).

DP1 and DP2/CRTH2

High levels of PGD_2 can be detected in the cerebrospinal fluid, spleen, bone marrow and during inflammation (Ujihara et al., 1988a, Ujihara et al., 1988b). Functions include mediation of pain perception, induction of sleep, inhibition of platelet aggregation, vasodilation, bronchoconstriction and mediation of inflammation as a chemotractor for Th2 cells, eosinophils and basophils (Kostenis and Ulven, 2006). Tissue resident mast cells release large amounts of PGD_2 upon stimulation (Schratl et al., 2007).

DP1 is expressed in haematological and non-haematological tissues. Activation of DP results in stimulation of adenylyl cyclase (AC) and consequent increase in intracellular cAMP levels

(Figure 21). This induces platelet aggregation, bronchodilation and vasodilation as well as suppressing activation and/or migration of T cells, eosinophils, basophils, dendritic cells and fibroblasts (Kostenis and Ulven, 2006). This suggests that DP1 has an anti-inflammatory role. However, this notion was challenged by the phenotype of the DP1-null mice. When lungs of wild type mice were challenged with an allergen an increase in inflammatory cell infiltration was observed (mainly eosinophils and lymphocytes) accompanied by an increase in inflammatory cytokines (IL-4, IL-13 and IL-5). All these effects were abolished in DP-/- mice suggesting an important role in inducing allergic inflammation (Matsuoka et al., 2000). Indeed, a single-nucleotide polymorphism reducing DP transcription efficiency is associated with lower asthma susceptibility in humans (Oguma et al., 2004).

DP2 was cloned and characterised in 1999. Although still a member of the GPCR superfamily, the receptor had higher sequence homology with the subgroup of chemoattractant receptors than with the other prostanoid receptors (Abe et al., 1999, Xue et al., 2005). DP2 is a promoter of chemotaxis of Th2 cells where it is highly expressed and is also named chemoattractant receptor homologous molecule expressed in Th2 cells (CRTH2). DP2 is otherwise known as CD294, a cell surface marker that allows distinction between Th2 and Th1 cells. High expression of DP2 is found in haematological cells (Th2, eosinophils and basophils) but also in osteoblasts, brain, heart, stomach, adrenal gland and liver (Kostenis and Ulven, 2006). Stimulation of DP2 causes decrease in cAMP (by inhibiting AC) and mobilization of Ca^{2+} from ER stores (Figure 21). The increase of PGD_2 at the inflammatory micro-environment attracts Th2 cells, eosinophils and basophils via DP2. For this reason DP2 has been linked to pro-inflammatory signaling (Kostenis and Ulven, 2006, Nagata and Hirai, 2003). Injection of allergens in mice skin results in increased local PGD_2 production and recruitment of H-PGDS positive cells (lymphocytes, neutrophils, eosinophils and basophils). This effect is abrogated by either H-PGDS or CRTH2 specific inhibitors. Concordantly, DP2 null mice show impaired allergic response to the same stimulus (Satoh et al., 2006). These studies relating PGD_2 and allergy have instigated an interest in the development of new drugs that can block PGD_2 synthesis and/or signaling as a means of treating chronic allergic conditions.

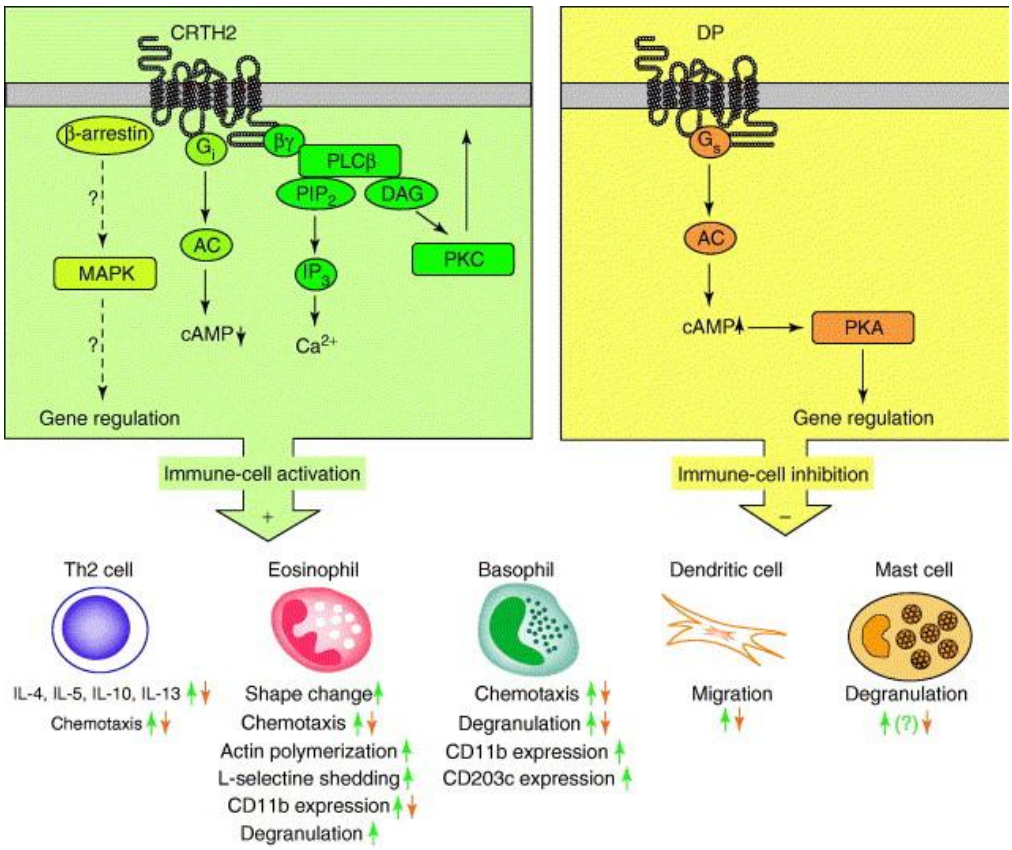

Figure 21 - Downstream signaling of the PGD_2 receptors DP1 and DP2/CRTH2

DP2/CRTH2 inhibits adenylyl cyclase (AC) through G_i proteins; this inhibition leads to a decrease of intracellular cAMP levels. Gi activation also stimulates PLCβ, which generate diacylglycerol (DAG) and inositol trisphosphate (IP3) that mobilizes Ca^{2+} from endoplasmic-reticulum stores. CRTH2 also signals through arrestin proteins in a G-protein-independent fashion. It is possible but not yet proven that arrestin recruitment might also lead to G-protein-independent MAP-kinase activation. Together, activation of various CRTH2 signaling pathways leads to immune-cell activation. The responses of immune cells that are elicited by CRTH2 activation are listed below the individual cells, and the nature of the response is indicated by green arrows. The DP receptor stimulates AC through G_s proteins and increases intracellular cAMP levels which, in immune cells, is generally linked to inhibition of cell functions. The consequences on immune cells of DP activation are indicated by orange arrows. On a cellular level, DP and CRTH2 can be regarded as antagonistic receptors: CRTH2 mediates pro-inflammatory and pro-stimulatory effects and DP limits CRTH2 activation upon exposure to PGD_2. Figure from (Kostenis and Ulven, 2006).

1.3.6.4 Cyclopentenone prostaglandins

In addition to the primary prostanoids, another group of bioactive prostaglandins has important roles in physiology – the cyclopentenone prostaglandins. These prostaglandins result from spontaneous dehydration within the cyclopentane ring of PGE_2 and PGD_2 (Figure 22). In aqueous solution, PGE_2 gives rise to PGA_2 whilst PGD_2 gives rise to the J-series prostaglandins, with 15-deoxy-$\Delta^{12,14}$-PGJ_2 (15d-PGJ_2) as the end product. The non-enzymatic process of PGD_2 dehydration is accelerated by albumin (Straus and Glass, 2001). These prostaglandins are characterised by the presence of α,β-unsaturated carbonyl groups in their structure that contain highly-reactive electrophilic centres. PGA_2 has one electrophilic centre while 15d-PGJ_2 has two. The electrophilic centers react with free sulfhydryl groups of cysteine residues present in glutathione (GSH) or cellular proteins, covalently binding the prostaglandin to it (Straus and Glass, 2001).

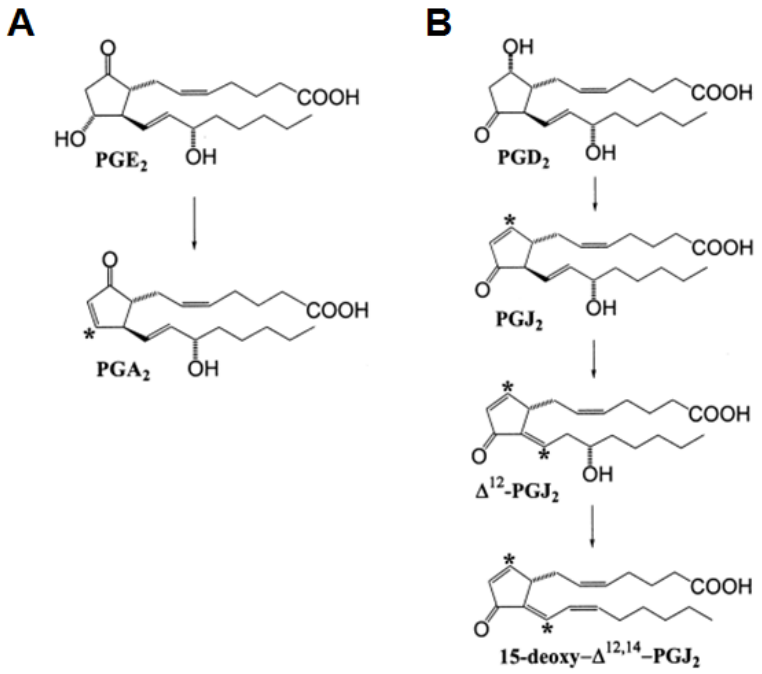

Figure 22 - Formation of cyclopentenone prostaglandins.

Formation of cyclopentenone prostaglandins via dehydration in the cyclopentane ring of PGE_2 (**A**) and PGD_2 (**B**) into PGA_2 and 15-deoxy-$\Delta^{12,14}$-PGJ_2 (15d-PGJ_2), respectively. Formation of 15d-PGJ_2 involves a sequence of non-enzymatic dehydration steps. Asterisks indicate the positions of the reactive electrophilic carbon atoms. Figure adapted from (Straus and Glass, 2001).

Intracellular generation of cyclopentenone prostaglandins affects important cellular pathways. GSH is a ubiquitous cellular molecule required for redox stability, correct protein folding and protection from cytotoxins. The cyclopentenone prostaglandin-GSH conjugate is excreted protecting the cell from the electrophilic carbons but can result in GSH depletion and induction of oxidative stress (Uchida and Shibata, 2008).

Recently it was found that PGA_2 binds to the ligand-binding domain of the nuclear orphan receptor 1 (NOR1), leading to its activation. Consistently, splenocytes from mice overexpressing NOR1 were more sensitive to PGA_2-induced apoptosis (Kagaya et al., 2005). However, these actions were only observed with high PGA_2 doses. The question still remains wheter PGA_2 is generated *in vivo* in quantities required to exert these effects.

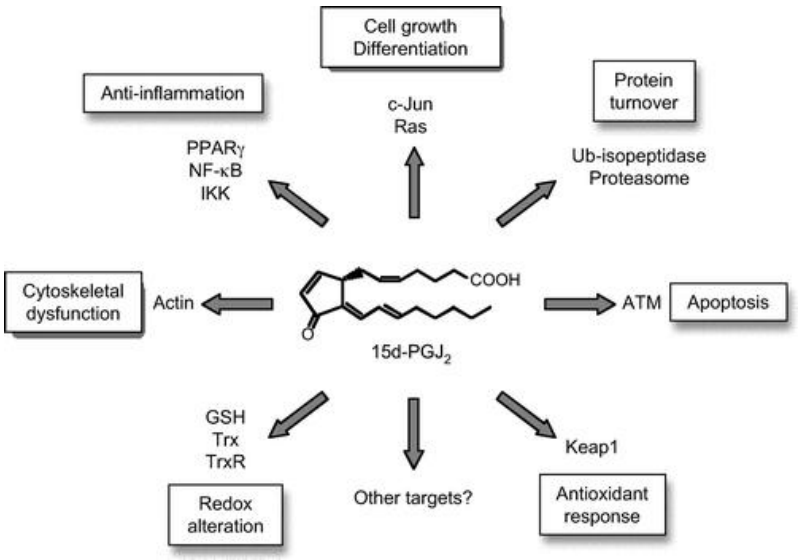

Figure 23 - Targets and biological functions of 15d-PGJ_2.

Figure from (Uchida and Shibata, 2008)

15d-PGJ_2 has several cellular targets

Unlike PGA_2, significant levels of 15d-PGJ_2 have been measured *in vivo*, particularly during inflammation (Giri et al., 2004, Rajakariar et al., 2007, Trivedi et al., 2006) and several biological targets have been identified (Figure 23). Intracellular accumulation of 15d-PGJ_2 affects important cellular pathways. GSH is a ubiquitous cellular molecule required for redox

stability, correct protein folding and protection from cytotoxins. The cyclopentenone prostaglandin-GSH conjugate is excreted protecting the cell from the electrophilic carbons but can result in GSH depletion and induction of oxidative stress (Uchida and Shibata, 2008). In addition, 15d-PGJ_2 also induces the expression of enzymes involved in antioxidant response (Uchida and Shibata, 2008). This is achieved by covalently binding to and activating redox sensitive transcription factors such as activator protein 1 (AP-1), NF-E2 related factors (Nrf2), hypoxia inducible factor (HIF) and signal transducers and activators of transcription (STAT) (Kim and Surh, 2006).

A major target of 15d-PGJ_2 conjugation is the cytoskeletal component β-actin (Gayarre et al., 2006). Disruption of cytoskeleton by 15d-PGJ_2 results in morphological changes and also induces cellular stress. Also, 15d-PGJ_2 was shown to inhibit the ubiquitin proteasome system, affecting the normal turn-over of cellular proteins (Uchida and Shibata, 2008). In addition, some pro-apoptotic and anti-proliferative effects of 15d-PGJ_2 are related to its ability to activate the tumours-suppresors ataxia telangiectasia mutated (ATM) and p53 (Uchida and Shibata, 2008).

In 1995 two groups independently reported that 15d-PGJ_2 is a high-affinity ligand and trans-activator of the nuclear receptor PPARγ, inducing adipocyte differentiation of mesenchymal stem cells (Kliewer et al., 1995, Forman et al., 1995). In leukocytes, activation of PPARγ also suppresses production of pro-inflammatory cytokines (Herlong and Scott, 2006). In the initiation phase of inflammation PGE_2 and PGD_2 are the prevalent COX products but levels of 15d-PGJ_2 increase during the resolution phase, suggests it may function as a feedback regulator of the inflammatory process (Gilroy et al., 1999). Indeed 15d-PGJ_2 represses pro-inflammatory gene expression in activated macrophages such as the inducible NO synthase (iNOS) and TNFα (Uchida and Shibata, 2008). These effects are only partially dependent on PPARγ activation suggesting 15d-PGJ_2 is interfering with other proteins.

The transcription factor nuclear factor-κB (NF-κB) is an important regulator of inflammation. In resting cells NF-κB is kept sequestered in the cytoplasm bound to its inhibitory protein IκB. Inflammatory stimuli activate the IκB kinase (IKK) which phosphorylates IκB and targets it for degradation. This releases NF-κB allowing it to translocate to the nucleus where it activates pro-inflammatory and pro-proliferative genes. Activation of NF-κB is inhibited by 15d-PGJ_2 in three crucial steps (Thomas et al., 2005, Straus et al., 2000). Firstly, 15d-PGJ_2

conjugates to IKK and inhibits its kinase activity over IκB, therefore silencing the pathway between stimuli and NF-κB activation. Secondly, 15d-PGJ_2 can conjugate to NF-κB directly preventing it from binding DNA and activating transcription. Finally, 15d-PGJ_2 activation of PPARγ leads to transrepression of NF-κB target genes (Straus et al., 2000). Since COX-2, the source of inflammatory prostaglandins, is an NF-κB target gene, 15d-PGJ_2 repression seems to work as a negative feedback signal to downregulate inflammatory prostaglandin production, such as PGE_2 and PGD_2. The anti-inflammatory properties of 15d-PGJ_2 contrast with the pro-inflammatory properties of PGD_2, mediated mainly by surface receptors (Herlong and Scott, 2006).

NF-κB activity is found augmented in many malignancies such as myeloid and lymphoid leukaemia leading to apoptosis resistance and increased proliferation (Cilloni et al., 2007). *In vitro* treatment of leukemic cells with 15d-PGJ_2 leads to differentiation and/or cell death partially by activation of PPARγ (pro-differenetiation) and NF-κB inactivation (anti-proliferative) (Giri et al., 2004, Thomas et al., 2005, Ray et al., 2006, Shin et al., 2009).

In summary, spontaneous dehydration of PGD_2 yields 15d-PGJ_2, a highly reactive prostaglandin with anti-proliferative, pro-differentiation, pro-apoptotic and oxidative properties. This cyclopentenone prostaglandin has been shown to have anti-tumour effects and inducing its accumulation in cancer cells is of therapeutical interest.

1.3.6.5 The isoprostane pathway

In the early 1990s a new non-enzymatic pathway was discovered for prostaglandin synthesis that circumvents the need for COXs. Isoprostanes (IsoP) are prostaglandin isomers that result from the free radical-mediated oxidation of arachidonic acid (Morrow et al., 1992). IsoPs with prostaglandin-like ring structures can be found *in vivo*. These are isomers of PGE_2 (E_2-IsoP), PGD_2 (D_2-IsoP) and $PGF_{2\alpha}$ ($F_{2\alpha}$-IsoP). Additionaly, D_2-IsoP and E_2-IsoP can give rise to cyclopentenone IsoPs, J_2-IsoP and A_2-IsoP, respectively (Figure 24). Importantly, IsoPs can be detected *in vivo* even in the presence of COX inhibitors, an observation that challenges the concept behind current anti-inflammatory drugs (Musiek et al., 2005).

Although $F_{2\alpha}/E_2/D_2$-IsoPs have been reported to interact with prostanoid receptors, conversion to prostaglandins is possible (Musiek et al., 2005). In a buffered solution at physiological pH, E_2-IsoP undergoes spontaneous time-dependent epimerization to form PGE_2. Because this is a non-enzymatic reaction the product is a racemic mixture of PGE_2 isomers (Gao et al., 2003). Similarly, racemic PGD_2 and PGE_2 mixtures have been identified in rat livers after oxidant injury, even in the presence of COX inhibitors. Since this alternative route for prostaglandin synthesis can bypass COXs and terminal synthases it is important to consider it when analysing the impact of enzyme inhibitors in any system (Musiek et al., 2005, Gao et al., 2003, Morrow et al., 1990).

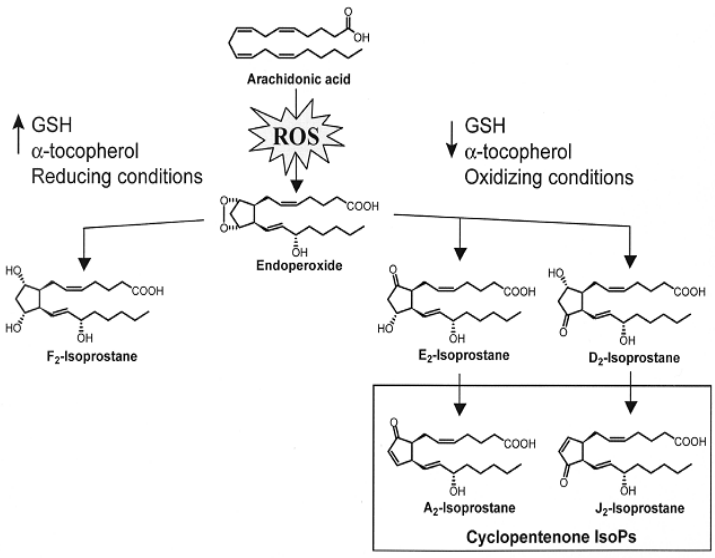

Figure 24 - Formation of cyclopentenone IsoP

The arachidonate endoperoxide intermediate can undergo reduction (facilitated by high local concentrations of GSH or α-tocopherol) to form stable F_2-IsoP. Alternatively,when the reducing conditions of the cell are depleted, the endoperoxide can undergo isomerization to form E_2- and D_2-IsoP, which spontaneously dehydrate to yield electrophilic A_2- and J_2-IsoP, also known as cyclopentenone IsoP. (Musiek et al., 2005)

.

1.3.7 Prostaglandin metabolism and leukaemia

Leukaemias (from Greek *leukos*- white, *-aema*, blood) are cancers of the blood, characterised by the abnormal accumulation of immature haemopoietic cells. In normal physiology, haemopoiesis is the process by which bone-marrow haemopoietic stem cells give rise to the different blood cell types (Figure 25). This is a tightly regulated and dynamic process that responds to physiological needs. For instance, more neutrophils will be generated during an infection and more red blood cells will be produced in low oxygen conditions. Haemopoiesis is regulated by a variety of internal and external signals, such as growth factors, hormones and cytokines (Figure 25). De-regulated proliferation of immature cells due to malignant transformation results in disrupted haemopoiesis, eventually leading to impaired blood functions and severe, often lethal, complications.

Leukaemias are classified as acute or chronic depending upon wheter the disease progresses rapidly (weeks or months) or slowly (several months or years). Leukaemias are further classified according to the lineage giving rise to the disease: lymphoblastic or myeloid. Therefore, the main types of leukaemia are acute myeloid leukaemia (AML), chronic myeloid leukaemia (CML), acute lymphoblastic leukaemia (ALL) and chronic lymphoblastic leukaemia (CLL) (Hoffbrand et al., 2006). In addition, solid tumours of lymphoid origin often arise in peripheral lymph nodes. These are termed lymphomas and include Hodgkin's lymphoma, B-cell lymphomas (such as Burkitt's lymphoma) and T-cell lymphomas, amongst other types (Hoffbrand et al., 2006).

Targeting leukaemia

Patients with leukaemia are normally submitted to a chemotherapy regimen and, in some cases, bone-marrow transplant is used to replace the malignant stem cells with normal haemopoietic stem cells. Some subtypes of leukaemia are characterised by the presence of recurrent lesions such as mutations or chromosome translocations that can be targeted as adjuvant therapies.

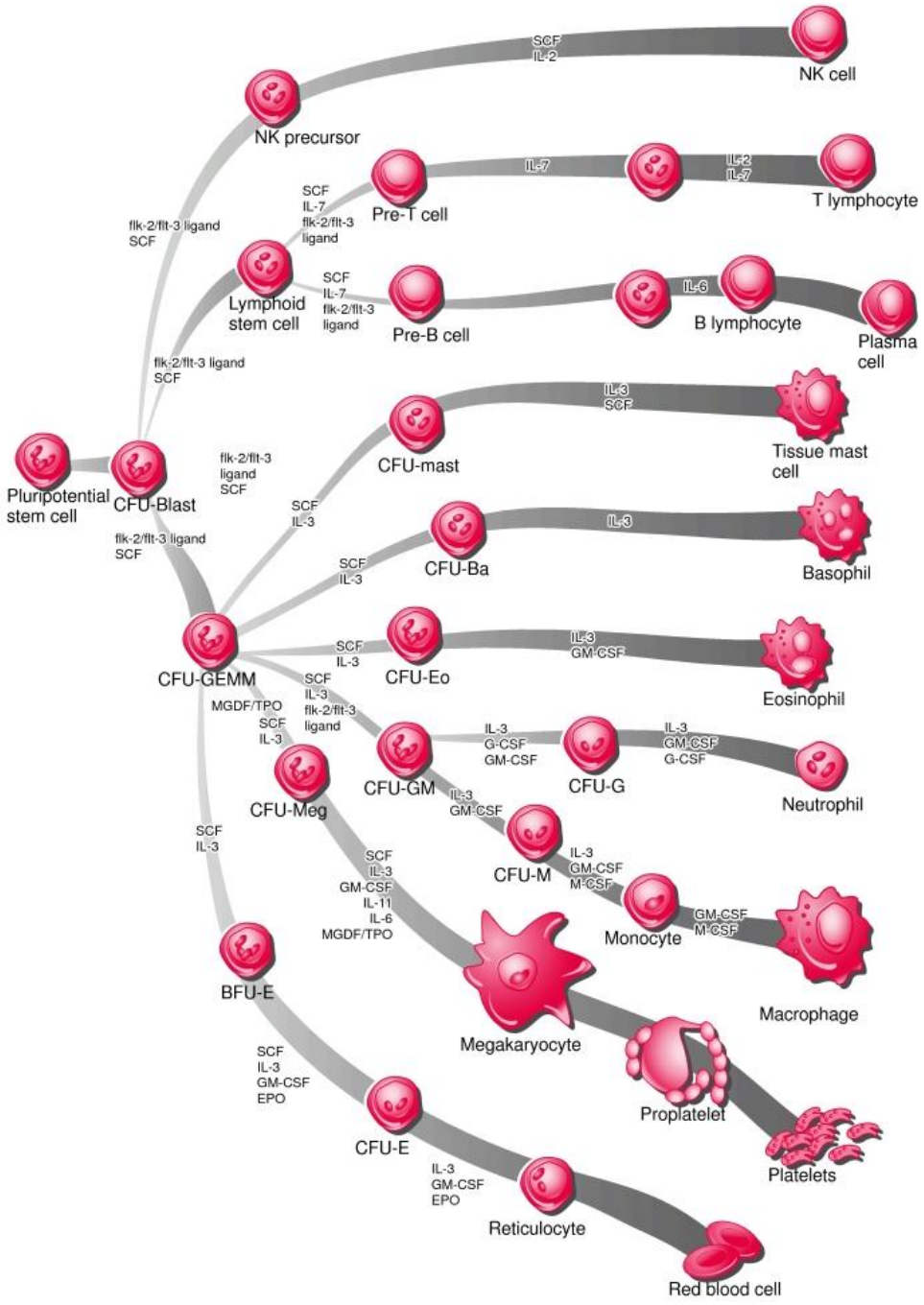

Figure 25 - Haemopoiesis and its growth factors

The bone-marrow pluripotent haemopoietic stem cell gives rise to a myeloid precursor (CFU-GEMM), a lymphoid stem cell or the natural killer (NK) cell precursor. The myeloid precursor gives rise to the erythroid (E) lineage for red blood cells, megakaryocytic (Meg) lineage for platelets, the granulocyte-monocyte (GM) lineage for macrophages and neutrophils, the eosinophil (Eo) and basophil (Ba) lineages. The lymphoid stem cell gives rise to B and T lymphocytes. Figure from (Kufe, 2003).

For instance, CML is characterised by the translocation t(9;22)(q34;q11), between chromosomes 9 and 22, yielding the Philadelphia chromosome. The translocation results in a gene fusion, conjoining the 5' exons of the *BCR* gene with the 3' exons of the *c-ABL* proto-oncogene. The resulting fusion protein has an increased tyrosine kinase activity relative to normal ABL that confers the cells with a proliferative advantage. The tyrosine kinase inhibitor Imatinib (Glivec) blocks BCR-ABL activity and, after 3 to 6 months of administration, causes a marked tumour decrease in the bone-marrow of nearly all CML patients. Imatinib is sufficient to keep the disease in check but eventually some patients develop mutations in the BCR-ABL protein rendering them resistant to the drug (Hoffbrand et al., 2006).

The translocation t(15;17)(q22;q21) also creates a fusion gene between the *PML* gene in chromosome 15 and the nuclear receptor *RARα* gene in chromosome 17. This lesion characterises a subtype of AML known as acute promyelocytic leukaemia (APL) (Koken et al., 1994). Wild-type RARα is activated by retinoic acid and heterodimerizes with RXR to promote cell differentiation. However, the PML-RAR fusion protein forms homodimers preventing association with RXR. The presence of this dominant-negative form of RARα results in the suppression of cell differentiation. Patients with PML-RAR fusion respond to high doses of all-*trans* retinoic acid (ATRA) which induces differentiation of the abnormal cells resulting in improved prognosis (Hoffbrand et al., 2006).

These are a few examples of molecular lesions being targeted in leukaemia. However, identification of new molecular targets that prevent proliferation and/or induce differentiation is essential for the development of new therapies.

AKR1C3 in leukaemia

Compounds such as NSAIDs (aspirin and indomethacin) and steroids (medroxyprogesterone acetate and 17β-estradiol) were shown to potentiate the ATRA-induced differentiation of HL-60, a model of AML (Bunce et al., 1996, Bunce et al., 1994). The pro-differentiation effect of NSAIDs and steroids was later attributed to the inhibition of AKR1C3 (Mills et al., 1998). In primary AML samples AKR1C3 is the most highly expressed isoform, with 100- and 1000-fold higher mRNA levels than AKR1C1 and -1C2, respectively (

Figure **26**) (Birtwistle et al., 2009). Predominant expression of AKR1C3 is also the case in commonly used AML immortalised cell lines KG1a, HL-60 and NB4 and in non-malignant proliferating $CD34^{+ve}$ cells, a population that includes the haemopoietic stem cells (Birtwistle et al., 2009).

In agreement with the inhibitor studies, artificial over-expression of AKR1C3 in HL-60 resulted in reduced sensitivity to ATRA-induced differentiation (Figure 27) (Desmond et al., 2003) while specific AKR1C3 knock-down in K562 cells using short hairpin RNA (shRNA) resulted in erythroid differentiation (Birtwistle et al., 2009) confirming the anti-differentiative role of AKR1C3 in leukaemic cells.

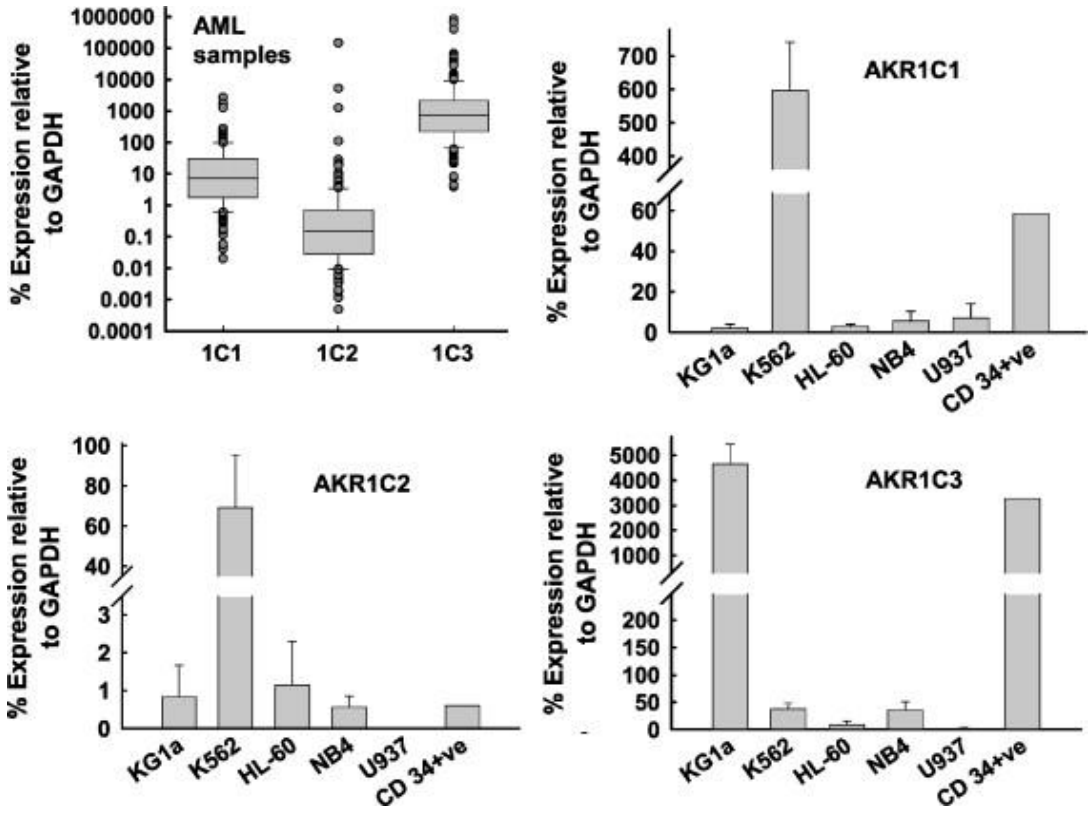

Figure 26 - Expression of AKR1C isoforms in leukemic cell lines and AML samples.

Expression of AKR1C1, -1C2 and -1C3 measured by Taqman QRT-PCR and is shown relative to GAPDH levels. Expression was measured in 213 primary AML samples, normal human $CD34^{+ve}$ cells and commonly used leukaemic cell lines: KG1a (AML), K562 (CML), HL-60 (AML), NB4 (APL) and U937 (histiocytic lymphoma) (Birtwistle et al., 2009).

Suppression of differentiation by AKR1C3 was not due to steroid hormone reduction as these substrates did not affect the ATRA-induced differentiation of HL-60 (Desmond et al., 2003). Instead, both PGD_2 and its dehydration product PGJ_2 mimicked the AKR1C3 inhibitors in promoting HL-60 differentiation (Desmond et al., 2003). These prostaglandins were also shown to have anti-neoplastic effects against a panel of leukemic cell lines (Tsao et al., 1986). In addition, the bone-marrow, which is the malignant stem cell niche, is a PGD_2-rich environment (Ujihara et al., 1988b) suggesting that AKR1C3 protects the cells from endogenously generated 15d-PGJ_2.

The anti-neoplastic activity of PGD_2 is in part conducted by PPARγ activation, suggesting that the spontaneous generation of the ligand 15d-PGJ_2 occurs inside the cells (Desmond et al., 2003). Indeed it was shown that in myeloid leukaemic cell lines PPARγ activation with synthetic ligands, such as rosiglitazone, suppresses cell growth (Asou et al., 1999). It is likely that 15d-PGJ_2 targets several other cellular processes that promote cell differentiation and suppress growth.

These findings have positioned AKR1C3 activity as a regulator of differentiation in myeloid leukaemia and, possibly, other forms of leukaemia (Figure 28). By converting PGD_2 to 11β-$PGF_{2\alpha}$, AKR1C3 prevents the spontaneous generation of 15d-PGJ_2, thus protecting the cells from an endgoneous anti-proliferative stimulus.

The identification of AKR1C3 as a molecular target has led to the development of therapies that inhibit the enzyme in order to induce differentiation or death of malignant cells. Combination of medroxyprogesterone acetate (MPA), an AKR1C inhibitor, and bezafibrate (BEZ), a lipid-lowering drug and PPAR agonist, showed anti-leukaemic activity against AML cell lines and primary samples by increasing endogenous 15d-PGJ_2 levels (Khanim et al., 2009). BEZ induced the generation of ROS and, consequently, the generation of PGD_2 via the isoprostane pathway while MPA prevented its conversion to 11β-$PGF_{2\alpha}$, resulting in accumulated 15d-PGJ_2. The combined actions of BEZ and MPA caused GSH-depletion, PPARγ activation and NF-κB inhibition resulting in growth arrest, apoptosis and differentiation of malignant cells but not of normal myeloid progenitors. Moreover, BEZ and MPA were shown to have a consistent impact on the metabolism of three AML cell lines (KG1a, K562 and HL-60) mediated by generation of ROS (Tiziani et al., 2009).

Theses studies led to the application of BEZ and MPA in a small-scale clinical trial with elderly AML sufferers who are too frail to undergo intense chemotherapy (Murray et al., 2010). The drug combination showed no haematological toxicity and 4 out of 15 patients who took the trial drugs for more than 4 weeks showed improved haemopoiesis. The results are promising since a non-toxic therapy was able to reestablish haemopoietic function in elderly AML patients and could be used as an alternative to chemotherapy. Dose-escalation of BEZ and MPA followed by randomized trials are the author's suggestions for the future.

Treatment of B-cell CLL (Hayden et al., 2009) and Burkitt's lymphoma (Fenton et al., 2003) with BEZ and MPA has also been shown to repress cell proliferation and induce apoptosis, suggesting the treatment can be applied to other types of leukaemia.

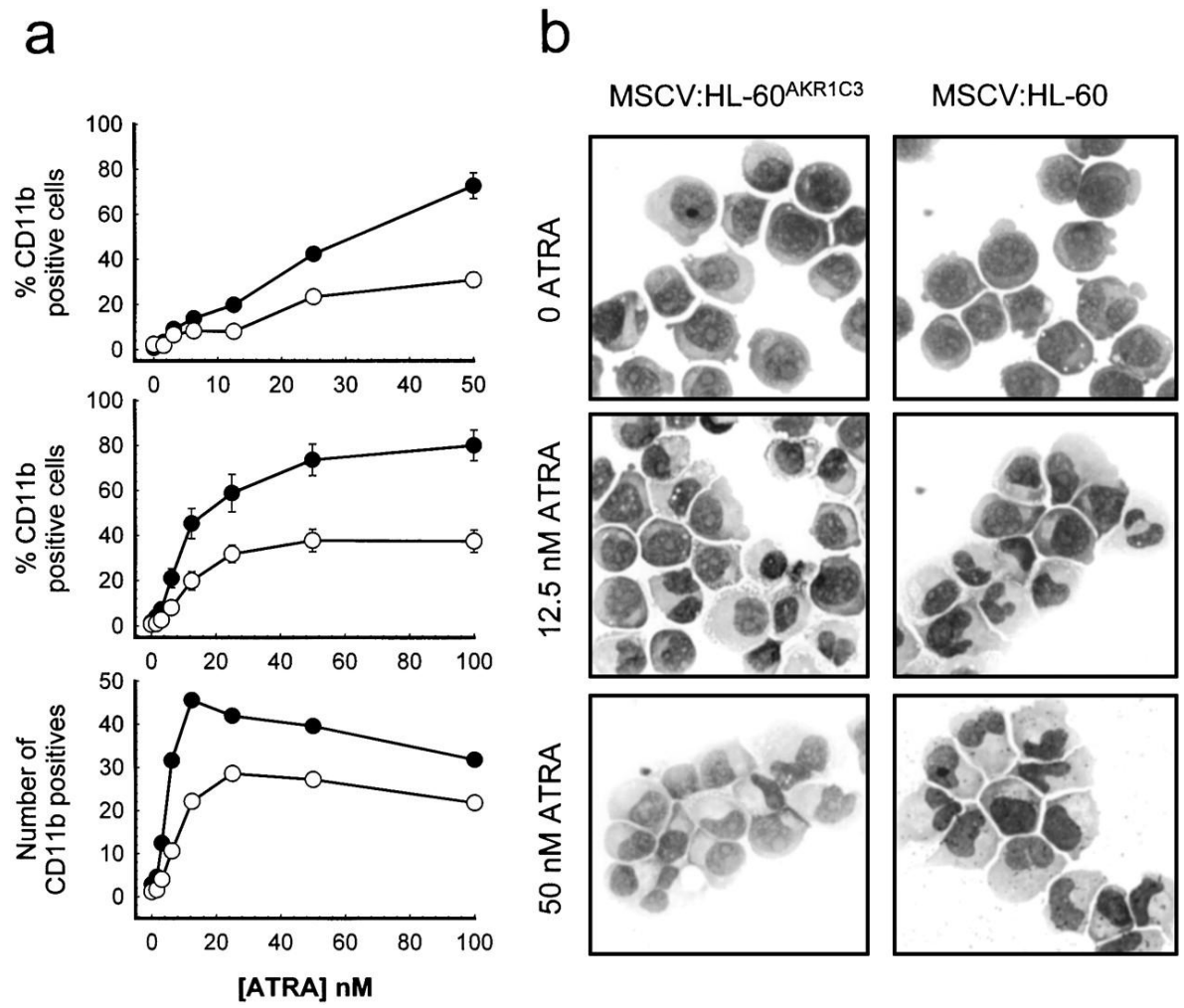

Figure 27 - AKR1C3 overexpression results in increased resistance to ATRA-induced cell differentiation.

A: analyses of CD11b expression. *Top panel*, wt-HL-60 (●) and pcDNA3.1:HL-60^{AKR1C3} cells (○) were treated for 5 days with the doses of ATRA shown and were analysed for expression of the differentiation-associated surface marker CD11b using FACS. Data are the mean ± SE of three experiments. *Middle panel*, MSCV:HL-60 (●) and MSCV:HL-60^{AKR1C3} cells (○) were treated for 5 days with the doses of ATRA shown and were analysed for expression of the differentiation-associated surface marker CD11b using FACS. Data are the mean ± SE of six experiments. *Bottom panel*, MSCV:HL-60 (●) and MSCV:HL-60^{AKR1C3} cells (○) were treated for 5 days with the doses of ATRA shown, and the actual numbers of cells expressing CD11b were determined from the data from the *middle panel* and the mean total numbers of cells/culture (x10^4) for the same six experiments. **B:** analyses of cell morphology. Jenner-Giemsa-stained cytospin preparations of MSCV:HL-60 and MSCV:HL-60^{AKR1C3} cells, treated in parallel for 5 days with the doses of ATRA shown. HL-60 neutrophil maturation is characterised by the development of pleiomorphic and, occasionally, fully lobed nuclei. The images show greater differentiation by ATRA-treated MSCV:HL-60 cells compared with MSCV:HL-60^{AKR1C3} cells (Desmond et al., 2003).

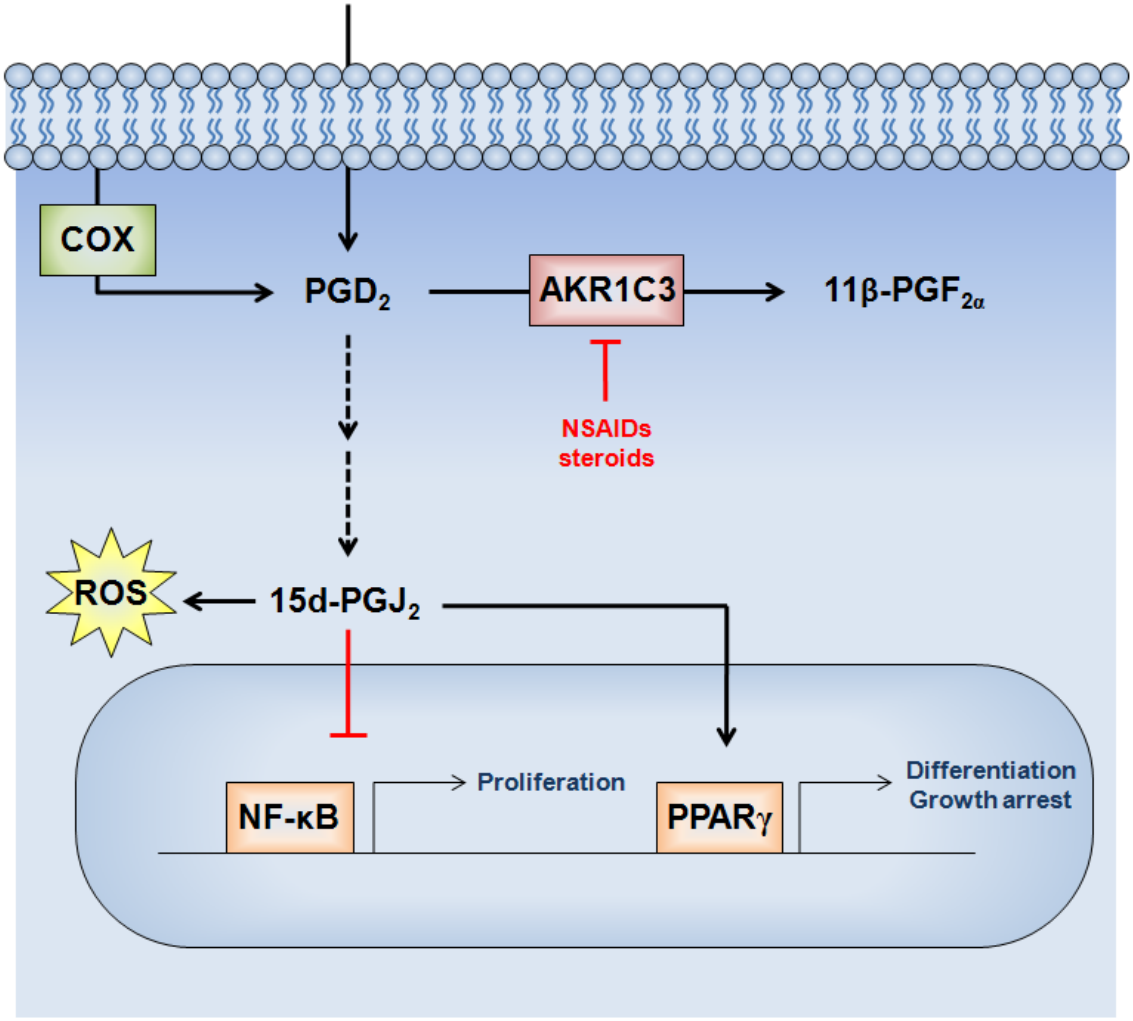

Figure 28 - Model for the role of AKR1C3 in preventing cell differentiation in leukaemia.

Prostaglandin D_2 (PGD_2) can be taken up from the extracellular medium or be produced intracellularly by the cyclooxygenase (COX) pathway. When accumulated in cells, PGD_2 suffers a series of spontaneous dehydration steps to generate 15d-PGJ_2, a reactive prostaglandin with anti-neoplastic properties. In cells, 15d-PGJ_2 interferes with several signaling pathways such as trans-activation of PPARγ, inhibition of NF-κB and generation of reactive oxygen species (ROS). Altogether, these effects promote cell differentiation and growth arrest. AKR1C3 prevents the generation of 15d-PGJ_2 by converting PGD_2 into 11β-$PGF_{2\alpha}$. This activity protects the cells from the anti-neoplastic effects of 15d-PGJ_2.

1.4 Mouse AKR1C enzymes

Despite impressive advancements, the understanding of how AKR1C enzymes function in normal physiology and carcinogenesis is limited to studies using isolated cells. This is in part due to the absence of animal models, particularly transgenic ones, which can inform about the role of AKR1C enzymes in a whole organism. In this aspect, mice are ideal models.

Mice are the most widely-used mammalian model to study the developmental and physiologic role of gene products. The generation of the first genetically modified mouse in 1982 sparked the development of techniques to alter the murine genome allowing researchers to study the function of genes and create models for human diseases. Mouse embryonic stem cells can be genetically manipulated so that a specific gene is ablated or over-expressed. The manipulated cells are injected into blastocysts and implanted in pseudo-pregnant mice where they develop into chimeric animals that can later be used to derive homozygously altered mouse strains.

Transgenic mice have been a powerful tool to assert the role of certain genes in cancer. For instance, mice over-expressing the fusion protein PML-RARα developed acute promyelocytic leukaemia (Wojiski et al., 2009) whilst mice lacking the tumour-suppressor p53 are more sensitive to carcinogens (Yamamoto et al., 2000). Therefore, we aimed to use a transgenic mouse model approach to study the role of AKR1C3 in leukaemia and other types of cancer.

1.4.1 The murine AKR1C locus

In 2002, a gene cluster harboring all murine AKR1C genes was described on mouse chromosome 13 (Figure 29) (Vergnes et al., 2003). The eight coded proteins share an average of 70% amino-acid sequence identity, though some enzymes, like AKR1C12 and AKR1C13, are 92% identical whilst others are relatively different, like AKR1C12 and AKR1C20 with merely 60% identity. Although part of the same subfamily, no murine AKR1C enzyme shares a particularly high sequence homology with a human enzyme. The average sequence identity between mouse and human isoforms is 70%. The most similar isoform to AKR1C3 is AKR1C6 with 74% identity.

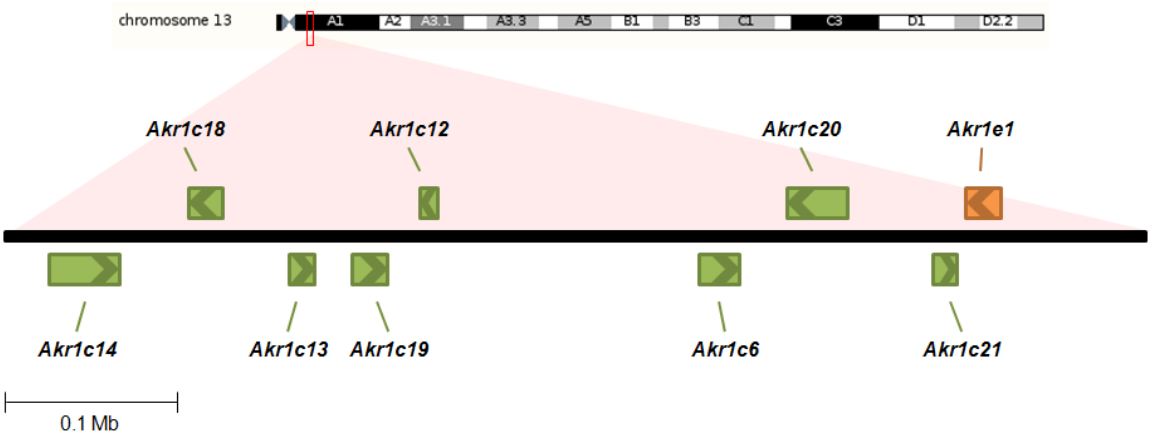

Figure 29 - Structure of the AKR1C locus on mouse chromosome 13.

Eight AKR1C-coding genes are located in the gene cluster on mouse chromosome 13. *Akr1c14, -1c13, -1c19, -1c6* and *-1c21* are coded in the plus orientation and *Akr1c18, -1c12* and *-1c20* are coded in the minus orientation. In addition, a gene coding for an enzyme of the AKR1E subfamily (*Akr1e1*) is present in the minus orientation. The eight AKR1C genes have identical number and size of exons. Diagram is drawn to scale and was based on the genomic map from the Ensembl database (Hubbard et al., 2009).

1.4.2 Known mouse AKR1C functions

AKR1C6

AKR1C6 was first cloned from mouse liver in 1995 and found to be active against steroid hormones and xenobiotic compounds (Deyashiki et al., 1995). Both 17β-HSD activity towards androgens and estrogens and 20α-HSD activity towards progesterone were described.

AKR1C12 and AKR1C13

When a murine haemopoietic progenitor cell line (EML) was induced to differentiate into the myeloid lineage by a combination of IL-3 and ATRA, AKR1C12 was identified as a highly upregulated gene (Du et al., 2000). High AKR1C12 expression was also found in murine promyelocytic cell lines, suggesting this AKR may be involved in myelopoiesis. AKR1C12, together with AKR1C13, was also cloned from a mouse stomach cDNA library (Ikeda et al., 1999). Both AKRs were predominantly expressed in the stomach, liver and ileum and the authors speculate about a possible role in dietary xenobiotic metabolism. Also, both enzymes were found to be inactive or poorly active towards prostaglandins and steroid hormones (Ikeda et al., 1999, Endo et al., 2006).

AKR1C14

The *Akr1c14* gene was identified when the mouse AKR1C cluster was described (Vergnes et al., 2003). Since then, no studies have attempted to elucidate its substrate preferences or physiological role. The known enzyme most similar to AKR1C14 is rat AKR1C9 (87% identity), a 3α-HSD active against androgens (Cooper et al., 2007).

AKR1C18

In rat, the inactivation of progesterone in the ovaries is mediated by a 20α-HSD later renamed AKR1C8 (Miura et al., 1994). In 1999, using a probe against AKR1C8, the murine homologue was cloned from a mouse ovary cDNA library and named AKR1C18 (Maho Ishida, 1999). AKR1C18 has 93% amino-acid sequence identity with its rat homologue and was found to be expressed in the ovaries, uterus and placenta during the late stages of gestation. Of all murine AKR1C isoforms, AKR1C18 is the only enzyme to have been targeted in a mouse transgenic model (Piekorz et al., 2005). Mice lacking AKR1C18

developed normally and had apparent normal adult physiology. However, during pregnancy, AKR1C18-deficient females sustained high levels of progesterone even at the end of gestation resulting in delayed parturition. This study strongly suggests an anti-progestin role for AKR1C18 important at the term of pregnancy.

AKR1C19 and AKR1C20

Like AKR1C14, both AKR1C19 and AKR1C20 were firstly described upon the discovery of the murine AKR1C locus (Vergnes et al., 2003). A later study using recombinant purified AKR1C19 showed that the enzyme was inactive towards prostaglandins and steroid hormones (Ishikura et al., 2005). Similarly, recombinant AKR1C20 showed poor 3α-HSD activity but the preference for prostaglandins was not measured (Matsumoto et al., 2006).

AKR1C21

While AKR1C21 was also described for the first time by Vergnes et al., the subsequent description of this enzyme has been much more extensive. AKR1C21 and a variant with 5 amino-acid substitutions were cloned from mouse kidney RNA (Ishikura et al., 2004). Both variants efficiently reduced 3- and 17-ketosteroids, including 5α-DHT. AKR1C21 was expressed almost exclusively in the kidney. Interestingly, the variant form was only detected in the kidney of female mice. A later study revealed that AKR1C21 has a rare 17α-HSD activity, converting androstenedione to epitestosterone (17α-Hydroxy-4-androsten-3-one) rather than testosterone (17β-Hydroxy-4-androsten-3-one) (Bellemare et al., 2005). This study also showed that AKR1C21 converts DHEA, androstanedione and androsterone to the respective 17α-hydroxyil forms and that the enzyme is highly expressed in mouse kidneys. Crystal structure and site-directed mutagenesis analysis revealed that the stereospecificity of AKR1C21 is attributed to the key residues Lys31 (Faucher et al., 2007), Gly225, Gly226 (Dhagat et al., 2009) and Tyr224 (Dhagat et al., 2010)

A murine AKR1C3 homologue?

Comparison of human and mouse AKR1C enzymes reveals no particularly conserved sequences that would suggest functional homology. In terms of sequence identity, the mouse isoforms more closely related to AKR1C3 are AKR1C6 (74%) and AKR1C18 (73%). However, at the beginning of this project it was not known if any of these enzymes catalyse

the 11β-ketoreduction of PGD_2 or have any other common substrates with AKR1C3. Interestingly, both AKR1C7 and AKR1C11 from bovine reduce PGD_2 to 11β-$PGF_{2\alpha}$ despite sharing merely 75% and 78% identity with AKR1C3, suggesting the activity may be present in the murine isoforms despite low sequence conservation. Therefore it was essential to address the question of whether any of the murine isoforms is a functional homologue of AKR1C3.

1.5 Prostaglandins and myogenesis

1.5.1 Introductory note

Although the role of AKR1C enzymes in cancer, especially the reduction of PGD_2 in haemopoietic tissues, is the main topic of this thesis, another project was developed that branched from the original theme. Chapter 6 of the results section is focused on how PGD_2 affects adult myogenesis, that is, the differentiation of muscle stem cells (myoblasts) into functional muscle fibers. The serendipitous origin of this side-project is explained at the beginning of chapter 6.

1.5.2 Origin of satellite cells

During early vertebrate embryogenesis the paraxial mesoderm is segmented into transient structures known as somites, from where the skeletal muscle originates. The somites are generated in an anterior-posterior orientation and signal extensively with the neighbouring structures (notochord, neural tube and ectoderm). As the somites mature the myogenic progenitors become confined to the ventral epithelium of the structure known as the dermomyotome. Myogenesis is initiated when the cells of the dermomyotome undergo epithelial-to-mesenchymal transition (EMT) and spread to the trunk and limbs where they differentiate into skeletal muscle. A small portion of the muscle progenitor cells are kept and settle in a satellite position relative to the muscle fibers. These satellite cells remain quiescent in a niche between the basal lamina of the extracellular matrix and the sarcolema (the cytoplasmic membrane of muscle fibers) (Le Grand and Rudnicki, 2007, Buckingham, 2006).

1.5.3 Satellite cells and adult myogenesis

Disruption of the muscle tissue, caused by injury or exercise, results in satellite cell activation. Activated satellite cells, known as myoblasts, enter cell cycle and transiently proliferate to generate a pool of myogenic progenitors. Afterwards, myoblasts exit cell cycle and become committed to terminal myogenic differentiation (myocytes). Eventually myocytes fuse with the damaged myofibers, repairing them. All myofibers result from myoblast fusion and are multinucleated. Some of the myoblasts revert to the quiescent satellite cell form thereby keeping the stem cell pool in the tissue (Le Grand and Rudnicki, 2007, Sabourin and Rudnicki, 2000).

Eventually, as age progresses, satellite cells become less frequent and muscle regeneration is impaired leading to sarcopenia, the degenerative loss of skeletal muscle mass and strength (Le Grand and Rudnicki, 2007, Sabourin and Rudnicki, 2000). The muscle microenvironment also seems to play an important role in regeneration as satellite cell transplanted from old animals are able to replenish the satellite cell pool in younger animals. This shows that an ageing microenvironment can affect stem cell renewal and that muscle stem cell potential is determined by both intrinsic and extrinsic factors (Collins et al., 2007).

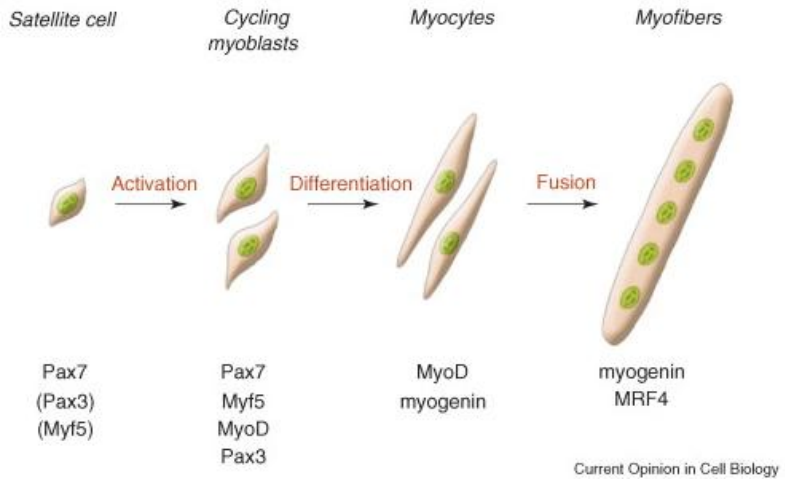

Figure 30 - Schematic representation of adult myogenesis.

Quiescent skeletal muscle satellite cell can become activated following stimuli originating from their associated fiber or from the micro-environment. Their proliferating progeny, the skeletal myoblasts, express the paired-box transcription factors Pax7 and Pax3, as well as the myogenic regulatory factors Myf5 and MyoD. Once committed to differentiation, myoblasts stop cycling and lose expression of Pax7, Pax3, and Myf5. Differentiating myogenin-positive myocytes will then align and fuse to form multinucleated myofibers. MRF4 is further required for hypertrophy of the new fibers. Figure from (Le Grand and Rudnicki, 2007).

1.5.4 Genetic regulation of myogenesis

The myogenic process is directed by two groups of transcription factors (Figure 30). The paired box (Pax) transcription factors Pax3 and Pax7 are important in the maintenance of muscle progenitor cells (Buckingham, 2007, Buckingham, 2006). Pax7 is highly expressed in

satellite cells where it prevents apoptosis. Mice lacking Pax7 have impaired muscle regeneration due to near absence of satellite cells. Pax3 is also expressed in satellite cells but at a lower level and does not prevent apoptosis. However, when cells become cycling myoblasts Pax3 expression is upregulated and, together with Pax7, promote the expression of myogenic target genes. As soon as the myogenic cascade of factors is initiated towards committed differentiation Pax3 and Pax7 are repressed. (Buckingham, 2007).

The second wave of myogenic transcription factors involves members of the basic helix-loop-helix (bHLH) superfamily. The myogenic regulatory factor (MRF) subfamily consists of myogenic differentiation 1 (MyoD), myogenic factor 5 (Myf-5), myogenin (Myog) and MRF4 (Buckingham, 2006, Bryson-Richardson and Currie, 2008). When overexpressed, all of these factors are able to convert non-muscle cell lines (like fibroblasts) into myogenic cells. However, MRFs work in a concerted manner to drive myogenesis *in vivo*. In activated satellite cells, Pax3 and Pax7 rapidly promote the upregulation of MyoD leading to cell cycle entry. Alternatively, some satellite cells upregulate Myf-5 to enter the proliferative state but eventually both MyoD and Myf-5 are co-expressed. After multiple rounds of division most myoblasts repress Pax3 and Pax7 expression. However, a fraction will retain Pax7, downregulate MRF expression and become quiescent satellite cells. Following proliferation, MRF4 and myogenin are upregulated in cells entering terminal differentiation. This leads to the formation of multinucleated fibers expressing contractile machinery proteins (myosin heavy chain, α-actin, desmin, etc.) and other markers of terminal muscle differentiation (such as creatine kinase) (Buckingham, 2006, Buckingham, 2007, Sabourin and Rudnicki, 2000).

In summary, adult myogenesis is a tightly regulated process where a series of transcription factors act in cascade to drive the myogenic fate. Nevertheless, external factors have the power to promote or inhibit the process.

1.5.5 Inflammation and muscle regeneration

Disruption of muscle fibers by injury or exdrcise also activates tissue-resident mast cells, causing them to release large amounts of pro-inflammatory factors such as histamine, PGD_2 and leukotriene C4 (Cote et al., 2008). These factors initiate a local inflammatory response by attracting circulating neutrophils and macrophages (Tidball, 2005, Tidball, 2008). Initially,

the inflammatory response aggravates the damage in the tissue but, on the long-term, the factors secreted by leukocytes are beneficial for healing.

Neutrophils are the first leukocytes to invade the injured muscle and their degranulation results in the secretion of oxygen radicals and proteases (Tidball, 2005). These reactive agents degrade the debris resulting from disrupted myofibers in order to facilitate their phagocytosis but also cause more damage. This is followed by the arrival of macrophages that remove the debris and secrete factors, such as IGF, TGF-β, LIF, IL-6 and CSF-1, that modulate myoblast proliferation and differentiation (Cantini et al., 2002, Massimino et al., 1997).

Despite the evidence suggesting the long-term benefit of inflammation in muscle healing, most clinicians recommend the use of NSAIDs to attenuate inflammation and pain (Jarvinen et al., 2007). Studies with human volunteers have shown that the intake of over-the-counter doses of ibuprofen (Trappe et al., 2001) or indomethacin (Mackey et al., 2007) reduce the gain of muscle function caused by exercise. Both COX-1 and COX-2 are up-regulated after muscle injury suggesting prostaglandins are important in regeneration (Weinheimer et al., 2007).

1.5.6 Prostaglandins and adult myogenesis

Many studies have attempted to determine the effect of COX inhibition during muscle regeneration using a wide variety of *in vitro* and *in vivo* models. Cyclical stretch increases proliferation of primary mouse myoblasts, accompanied by elevated PGE_2 and $PGF_{2\alpha}$ production. These effects are COX-2 dependent since myoblasts treated with SC-236 (COX-2 selective inhibitor) and myoblasts derived from COX-2 null mice show no response to stretching (Otis et al., 2005). Whilst informative, *in vitro* models do not address physiological scenarios such as the role of inflammatory cells and their interaction with myoblasts. Mishra et al. subjected rabbits to exercise-induced injury and monitored the recovery after treatment with flurbiprofen (non-selective NSAID). Treated animals had better short-term recovery but a long-term deficit in force generation when compared to controls (Mishra et al., 1995). This observation highlights the concept that inflammation can be both beneficial and detrimental. Bondesen et al. focused on the role of COX-2 in muscle healing after injury (Bondesen et al., 2004) and atrophy (Bondesen et al., 2006). The expression of COX-2 (but not COX-1) increased after these challenges and ablation of enzyme activity with SC-236 or in COX-2

null mice resulted in reduced myofiber diameter upon healing. Importantly, these COX-2 deficient systems showed reduced myoblast and macrophage count in the regenerating environment confirming the importance of COX metabolites in the healing process. Altogether, these studies indicate that COX activity promotes muscle healing. However, the type of prostaglandins produced downstream of COX depends on the type of terminal synthases expressed.

In the regenerating muscle the expression of prostaglandin synthases, receptors and its downstream signaling pathways has only recently begun to be described. In theory, modulating specific prostaglandin signaling in the healing muscle might be a more effective clinical approach than COX inhibition.

Proliferating myoblasts have consistently been shown to produce PGE_2 and $PGF_{2\alpha}$ (Rossi et al., 1989, Otis et al., 2005, Bondesen et al., 2004, McArdle et al., 1994, Rodemann and Goldberg, 1982, Palmer et al., 1983, McLennan, 1991). Early studies demonstrated that inhibition of myoblast fusion with indomethacin could be overcome by adding PGE_2 (Zalin, 1979, Zalin, 1977, Entwistle et al., 1986). However, the expression of PGE synthases (mPGES-1, mPGES-2 and cPGES) or receptors (EP1-EP4) has not been characterised in the homeostatic and regenerating muscle. Thus the exact role of PGE_2 in the healing context remains largely unknown. Interestingly, PGE_2 is abundantly produced by leukocytes in the early phase of inflammation (Shen et al., 2008) and could also affect myoblast differentiation (Figure 31).

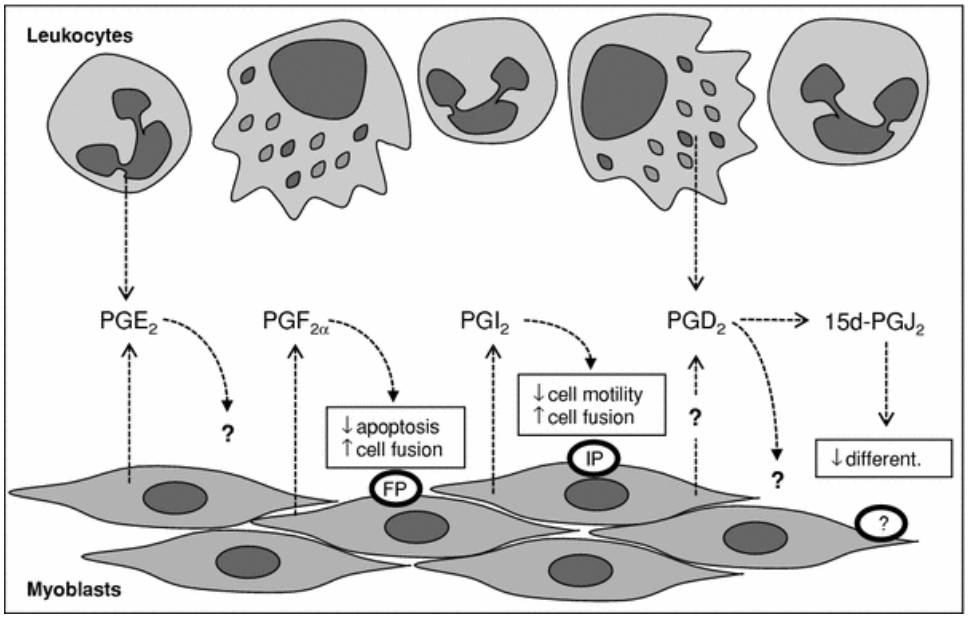

Figure 31 - Prostaglandin signaling in the regenerating muscle.

After muscle injury, satellite cells become proliferating myoblasts that later commit to differentiation and fuse to damaged myofibers. Simultaneously, leukocytes (mainly neutrophils and macrophages) invade the damaged tissue and initiate an inflammatory response. During this process both cell types secrete PGs that may influence myogenesis. Both myoblasts and leukocytes produce PGE_2 a promoter of myogenesis, but no PGE synthases or receptors have been shown to be expressed in myoblasts. $PGF_{2\alpha}$ is produced by myoblasts and signals via the PGF receptor (FP) to prevent apoptosis and promote cell fusion. Similarly, PGI_2 (prostacyclin) signals in autocrine fashion via the PGI receptor (IP) to restrain myoblast motility and enhance cell fusion. PGD_2 is produced by inflammatory leukocytes but its synthesis and signaling in myoblasts is unknown. However, 15d-PGJ_2, a PGD_2 dehydration metabolite, can inhibit myogenesis but the mechanism remains largely unknown. Figure from(Velica and Bunce, 2008).

In isolated muscles, $PGF_{2\alpha}$ was described as a promoter of protein synthesis and its production is increased upon exercise (Palmer et al., 1983, Trappe et al., 2001). Horsley et al. reported that primary mouse myoblasts treated with $PGF_{2\alpha}$ generated myotubes of increased size by stimulating fusion with nascent fibers (Horsley and Pavlath, 2003). This growth was FP-dependent and caused the activation of the calcium-regulated nuclear factor of activated T cells, isoform C2 (NFATC2). In a follow up study, the authors show that $PGF_{2\alpha}$ increases myotube size by preventing myoblast apoptosis, via the upregulation of BIR ubiquitin-conjugating enzyme (BRUCE), an inhibitor of caspases (Jansen and Pavlath, 2008). BRUCE was naturally expressed in the later phases of adult myogenesis and its upregulation was ablated in NFATC2 null myoblasts. Importantly, $PGF_{2\alpha}$ treated or BRUCE over-expressing myoblasts engraft more efficiently in a transplant model. These two studies characterised in

detail the autocrine signaling pathway of $PGF_{2\alpha}$ in myoblasts, confirming an important myogenic role of a COX product.

PGI_2 is the main COX metabolite produced by vascular endothelial cells where it promotes vasodilation. Primary mouse myoblasts were shown to express PGI synthase, PGI receptor (IP) and produce PGI_2 (Bondesen et al., 2007). IP null myoblasts had reduced fusion and differentiation but increased cell motility. The high motility rate of IP null myoblasts was blocked by Iloprost (stable PGI_2 analogue) resulting in increased cell fusion. The authors propose that myoblast motility is inversely correlated with differentiation and that PGI_2 plays a pivotal role in this balance.

1.5.7 Can inflammatory PGD_2 affect adult myogenesis?

Studies have shown that like PGE_2, synthesis and secretion of PGD_2 is strongly induced in the early phase of inflammation (Rajakariar et al., 2007, Trivedi et al., 2006, Gilroy et al., 1999) and can have both pro- and anti-inflammatory roles, depending on the cell-type context. Despite the importance of inflammation in muscle healing, PGD_2 synthesis and signaling has not been characterised in myoblasts. This could perhaps unravel a novel cross-talk pathway between inflammatory and muscle cells.

Like PGD_2, levels of 15d-PGJ_2 are increased during inflammation (Rajakariar et al., 2007, Gilroy et al., 1999) and might modulate myoblast behaviour. Although PPARγ expression seems to be important in C2C12 myoblast differentiation (Singh et al., 2007), it was observed that micromolar doses of 15d-PGJ_2 blocked myotube formation in a PPARγ-independent manner (Hunter et al., 2001). This differentiation block could be mediated by the other properties of 15d-PGJ_2 such as the generation of an oxidative environment which has also been shown to impair myogenesis (Ardite et al., 2004). However, due to its reactivity 15d-PGJ_2 rapidly binds to extracellular proteins such as albumin and it is unlikely that such high concentrations accumulate in the regenerating muscle.

The observations discussed here compile a scenario where activated myoblasts co-exist with an inflammatory environment where PGD_2 levels are high. Therefore, we analysed the impact of PGD_2 in adult myogenesis using the C2C12 myoblast model and the results are shown in chapter 6.

CHAPTER TWO: Materials and Methods

2.1 Sequence alignments

Genomic, mRNA and amino-acid sequences were obtained from the following databases: National Center for Biotechnology Information (http://www.ncbi.nlm.nih.gov/), Ensembl (http://www.ensembl.org/index.html) and the AKR homepage (http://www.med.upenn.edu/akr/). Amino-acid sequences were aligned using ClustalX2 (http://bips.u-strasbg.fr/fr/Documentation/ClustalX/). Phylogenetic tree was generated using TreeView X software (http://darwin.zoology.gla.ac.uk/~rpage/treeviewx) with random number generator of 111 and number of bootstrap trials of 1000.

2.2 Cell culture

2.2.1 HPC-7 (haemopoietic stem cell-like cell line)

The HPC-7 cell line was generated by transducing mouse embryonic stem cells with the transcription factor *LH2* (expressed in mouse fetal liver during haemopoiesis) (Pinto do et al., 2002, Pinto do et al., 1998). This resulted in a multipotent haemopoietic precursor cell line that requires stem cell factor (SCF) for growth and can be induced to differentiate into various mature myeloid lineages upon addition of other growth factors. The cell line was kindly supplied by Dr Carlsson (University of Umeå, Sweden)

2.2.1.1 Production of SCF using CHO-K3 cells

Chinese Hamster Ovarian (CHO) K3 cells stably transfected with mouse SCF were kindly supplied by the Frampton group (IBR, University of Birmingham, UK). Cells were expanded in DMEM supplemented with 10% FBS, 2 mM glutamine and antibiotics. For SCF production, CHO cells were seeded in 150 cm^2 tissue culture flasks (Costar) and allowed to reach confluence. After that, growth media was replaced with 30 ml Stem Pro medium (Invitrogen) with 0.5% FBS and antibiotics. The media was refreshed the following day and left for 2 days during which CHO cells secrete SCF into the supernatant. The media was harvested, sterile-filtered with a 0.45 µm filter and stored at -20 °C.

2.2.1.2 Culturing HPC-7 cells

HPC-7 cells were gently thawed from liquid nitrogen and resuspended in Stem Pro media supplemented with 2.6% Stem Pro serum replacement, 10% supernatant with SCF (see above), antibiotics and 2 mM glutamine. HPC-7 are non-adherent small cells and were kept between $1x10^6$ and 2.5 $x10^6$ cells per ml in 24-well plates or 25 cm^2 tissue cultures flasks (Costar). Medium was refreshed every 2 days.

2.2.1.3 Differentiation of HPC-7 cells

For differentiation, SCF was either replaced or used in combination with the following recombinant growth factors: 10 or 100 ng/ml murine IL-3 (with or without 100 nM ATRA), 4 U/ml human EPO and 20 ng/ml mouse TPO (all from R&D systems). Media was replaced every 2 days and cells counted daily using a haemocytometer. Cells were harvested for RNA extraction at identical intervals.

2.2.2 C2C12 and L6-C11 (myoblast cell lines)

C2C12 cell line was purchased from the American Type Culture Collection (ATCC). C2C12 is a subclone of the mouse myoblast cell line established by (Yaffe and Saxel, 1977). This cell line has a fibroblast-like appearance and can be driven to skeletal myogenic differentiation when at high confluence by reducing serum concentration, forming large multinucleated myotubes that result from cell fusion.

The L6 cell line was derived from adult rat muscle samples and behave like myoblasts, forming myotubes at high-density (Yaffe, 1968). L6-C11 cells were obtained from Dr R Harris (School of Biosciences, University of Birmingham)

2.2.2.1 Culture of C2C12 and L6-C11

C2C12 and L6-C11 were expanded in DMEM supplemented with 10% FBS, 2 mM glutamine and antibiotics (growth media) at 5% CO_2, 37°C. Cells were grown in 75 cm^2 tissue culture flasks (Corning) and split before reaching confluence (to avoid loosing myogenic potential). Media was changed every two or three days.

2.2.2.2 Myogenic differentiation of C2C12 and L6-C11

For differentiation, $5x10^4$ exponentially growing C2C12 cells were seeded per well in 6-well plates and kept in growth media for 2 days until reaching ~80% confluence. At this point, (day 0) growth media was replaced with DMEM supplemented with 5% Horse Serum (Gibco), 2 mM glutamine and antibiotics (differentiation media). Media was refreshed every 2 days. The differentiation process was monitored daily using an inverted microscope and was terminated between day 4 and day 6 (post-confluence/media change). Usually, cell fusion was observed from day 2 and became more evident on the following days.

For differentiation, L6 cells were seeded as above but always kept in growth media. In confluent cultures cells fuse to form long multinucleated myotubes.

2.2.2.3 Treatments of C2C12 cells

To assess the effect of certain molecules (prostaglandins, receptor agonists and antagonists) C2C12 were differentiated as detailed above. Treatments were initiated at day 0, upon replacement with differentiation media and were always done in biological triplicates. Control cultures were treated with equivalent amounts of solvent (ethanol, DMSO or water). Treatments were either added only at the beginning of the experiment or every two days until the end of the experiment. To determine the effect of these molecules on C2C12 differentiation, several methods were used as explained in section 2.6.

2.2.3 BA/F3

BA/F3 is a bone marrow-derived immortalized murine pro-B-cell line that requires IL-3 to survive and proliferate. BA/F3 was purchased from ATCC and grown in RPMI media supplemented with 10% FBS, 2 mM glutamine, 0.1% β-mercaptoethanol, 1% IL-3 conditioned media and antibiotics.

2.2.4 J774

J774 is a macrophage cell line derived from a solid tumor of a BALB/c mouse. J774 was a kind gift from the May lab (School of Biosciences, University of Birmingham) and was grown in DMEM supplemented with 10% FBS, 4 mM glutamine and antibiotics.

2.2.5 K562

K562 are an eryhtroleukemia cell line derived from a chronic myeloid leukemia patient in blast crisis. K562 were purchased from ATCC and were cultured in RPMI media supplemented with 10% FBS, 2 mM glutamine and antibiotics.

2.2.6 CHO

CHO (Chinese Hamster Ovary) cells were a kind gift from Dr. J Rappoport (School of Biosciences, University of Birmingham). Generation of stable recombinant CHO cells is relatively easy and these cells are commonly used to over-express secreted factors. CHO cells were grown in DMEM supplemented with 10% FBS and antibiotics.

2.3 General molecular biology techniques

2.3.1 RNA sourcing

Tissue culture cells ($2x10^6$ or less) were spun down, flash-frozen using liquid nitrogen and stored at -20 °C. For whole tissues, CD1 male and female (both pregnant and non-pregnant) mice were sacrificed for the dissection of spleen, liver, lung, stomach, small intestine, colon, kidney, prostate, testes, uterus and ovary (in triplicate). Each tissue was cut to a ~3 mm cube, stabilized in RNA*later* (RNA Stabilization Reagent; Qiagen) and stored at -80 °C.

2.3.2 RNA extraction

RNA was extracted using Qiagen's RNeasy Mini Kit according to manufacturer instructions. Homogenization of tissue culture samples was done by adding 350 µl RLT (lysis) buffer, mixing, pipetting directly into a QIAshredder spin column (Qiagen) and centrifuging for 2 minutes at 1200 rpm. Homogenization of stabilized mouse tissues was done by placing the tissue in liquid nitrogen and grinding it thoroughly with a mortar and pestle. Mortar and pestle were thoroughly washed with ethanol to avoid cross-contamination of tissue samples. Ground tissue was resuspended in 600 µl RLT buffer, transferred to a QIAshredder spin column and centrifuged for 2 minutes at 1200 rpm. After homogenization, RNA was bound to an RNeasy spin column, washed with Qiagen wash buffer and eluted with 30 – 50 µl of RNase-free water.

RNA was quantified by diluting the original sample 1/100 or 1/50 in water and measuring the absorbance at 260 nm. RNA concentration (in ng/µl) was calculated as follows: Abs_{260nm} x 40 x (dilution factor). RNA purity was assessed by the Abs260nm/Abs280nm ratio (should be between 1.9 and 2.1).

2.3.3 cDNA synthesis

Synthesis of cDNA from RNA used Super Script II Reverse Transcriptase (Invitrogen). Reaction mixtures were as follows:

- sample RNA…….... 0.35 – 2 µg
- 10 mM dNTPs…… 1.0 µl (0.5 mM)
- 3 µg/µl random hexamers……... 0.5 µl (75 ng/µl)
- RNase-free water…… up to 12 µl

Reactions were incubated at 65 °C for 6 minutes and then cooled on ice to promote annealing of random hexamers to RNA. After this, the following were added:

- 5X FS buffer……..... 4.0 µl (1X)
- 0.1 M DTT……... 2.0 µl (10 mM)
- 40 U/µl RNasin (RNAse inhibitor)….. 1.0 µl (2 U/µl)
- 200 U/µl SuperScript II RT…….. 1.0 µl (10 U/µl)

The final mixture was incubated at 25 °C for 10 minutes followed by 45° C for 90 minutes and finally 70 °C for 15 minutes. The synthesized cDNA was then diluted 1:2 or 1:4.

2.3.4 Standard PCR reaction

Quality of cDNA was assessed by RT-PCR for the control house-keeping gene *Gapdh* (primers 40 and 41, Table 6). The PCR mix was as follows:

- 10X buffer……. 2.0 µl (1X)
- 50 mM $MgCl_2$…… 0.6 µl (1.5 mM)
- 10 mM dNTPs……. 2.0 µl (1 mM)
- 9 µM forward primer……..… 2.0 µl (0.9 µM)
- 9 µM reverse primer…… 2.0 µl (0.9 µM)
- 1 U/µl BioTAQ Red DNA pol…… 1.0 µl (0.05 U/µl)
- Sample cDNA…….. 1.0 µl
- Water……..…. up to 20 µl

Reactions were incubated in an ABI9600 thermal cycler with the following cycling parameters: 96 °C for 5 minutes; (96 °C for 30 seconds; 65 °C for 30 seconds; 70 °C for 30

seconds) x 25; 70 °C for 7 minutes. The resulting amplified products were separated in 2% agarose gel stained with ethidium bromide and visualized on a UV transilluminator.

2.3.5 Taqman quantitative real-time (QRT)-PCR

In Taqman QRT-PCR two primers and one internal probe anneal in close proximity on the target sequence. The probe has a fluorochrome on its 5' end that is kept inactive by a quencher on the 3' end. During the elongation step of the PCR, as the polymerase amplifies the target sequence, it degrades the probe releasing the fluorochrome from the influence of the quencher, resulting in enhanced fluorescence. This allows the monitoring of product formation at the end of each cycle ("real-time"). By the end of the PCR cycles, an exponential curve followed by a plateau is obtained for each reaction. From the curves it is possible to define a fluorescence level ("threshold") at which all samples are in the exponential phase, thus determining a cycle number (C_T) that is proportional to the initial amount of target sequence. Given the exponential nature of PCR, C_T or ΔC_T values (the difference between two C_T values) have to be transformed using the formula $2^{(-C_T)}$ or $2^{(-\Delta C_T)}$.

Primers and probes were designed using the Primer Express software (Applied Biosystems). The oligonucleotides generated a product between 75 and 100 bp with optimal melting temperatures for QRT-PCR. The sequences were tested for specificity by using the BLAST algorithm (NCBI) against the mouse transcriptome. Primers were obtained from Sigma Genosys (Sigma) and are described in Table 6 (labeled "QRT F" or "QRT R"). Primers were tested using RT-PCR (as in page 74) before ordering the dual-labeled probes from Eurogentec. A list of all probes used with the respective 3'-quenchers and 5'-fluorochromes is presented on Table 7.

For each gene a "primers and probe" mix was prepared beforehand containing 9 μM of each primer and 1.25 μM of probe. A 2X QRT mastermix containing buffer, magnesium, polymerase and dNTPs was purchased from Eurogentec. The Taqman QRT-PCR reaction mix was prepared as follows:

- 2X QRT master mix ……. 10 μl
- Primers & Probe mix …… 2 μl
- Water…….……. 7 μl
- cDNA…… 1 μl

QRT-PCR for each sample was performed in triplicate 20 µl reactions in optical grade 96 well plates using standard cycle conditions for 44 cycles on an ABI Prism 7700 sequence detector (Applied Biosystems).

2.3.6 Western blotting

Sample protein concentrations were determined using the Protein Quantification kit (BioRad) and BSA standard curve. A fixed amount of protein was used (10 – 30 µg), mixed with gel loading buffer and boiled at 100 °C for 10 minutes. Proteins were separated by SDS-polyacrylamide gel electrophoresis (SDS-PAGE) using 10-12.5% gels depending on the size of the protein to be probed.

After electrophoresis, proteins were transferred to Immobilon-P membranes (Millipore Corp, Bedford, MA, USA), blocked with 5% milk in TBS-T for 1 hour (or overnight) and incubated with the primary antibody (diluted in blocking solution) for 1 hour at room temperature. Anti-LPGDS monoclonal antibody (rat, clone 10A5) was purchased from Cayman Chemicals and used at a 1/500 or 1/1000 dilution. Anti-6xHis polyclonal antibody (rabbit, H-15) was purchased from Santa Cruz Biotechnology and used at 1/1000 dilution. After incubation and washing with TBS-T, membranes were incubated with secondary antibodies at 1:1000 to 1:5000 dilutions. Rabbit polyclonal HRP-conjugated anti-rat IgG antibody was purchased from Abcam. Goat polyclonal HRP-conjugated anti-rabbit IgG antibody was purchased from Pierce. Detection was done using ECL Supersignal West Pico Chemiluminescent substrate (Pierce) and exposing the membrane to auto-radiography film.

2.3.7 Site-directed mutagenesis

Site-directed mutagenesis is a technique that allows for specific nucleotide changes in plasmid DNA using a PCR-based approach. The QuickChange XL Site-Directed Mutagenesis kit (Stratagene) was used according to manufacturer's instructions.

Mutagenic primers were designed using Stratagene's QuickChange Primer Design Program. Both complementary mutagenic primers contain the desired mutation and anneal to the same sequence on opposite strands of the plasmid.

Mutant strand synthesis reaction was performed in a thermal cycler using 10 or 50 ng original plasmid and the kit's *PfuTurbo* DNA polymerase (high-fidelity). Importantly, the original plasmid must have been grown in a bacterial strain that methylates DNA, such as DH5α. PCR reactions were prepared to a final volume of 50 µl as follows:

- 10X reaction buffer……...5 µl
- 10 ng/µl pcDNA-L-PGDS…….1 or 5 µl
- 125 ng/µl sense primer……..1 µl
- 125 ng/µl anti-sense primer……..1 µl
- 10 mM dNTP mix…….1 µl
- Stratagene Quick solution……3 µl

At the end of the PCR reaction, *Dpn*I was added and incubated for 1 hour at 37 °C. This enzyme digests the methylated DNA chains (original plasmid) leaving the un-methylated DNA (mutated) intact. The mutated single-strands were transformed into *E. coli* strain *XL10-Gold* (Stratagene). Success of mutation-reaction was confirmed by nucleotide sequencing.

2.3.8 PCR using proof-reading polymerase

The coding regions of murine AKRs were cloned using a reverse transcriptase (RT)-PCR strategy (Figure 32). The sequences of primers and the cDNA source used in the amplification are shown in Table 4. The forward primers were designed to introduce an *Nde*I restriction site coincident with the ATG start codon, and the reverse primer likewise incorporated an *Xho*I site (for PCR details, see below). The resulting PCR products were digested with *Xho*I and *Nde*I which were then ligated into the similarly digested pET28b(+) vector (Novagen). This expression plasmid incorporates an N-terminal histidine (6 × His) tag to aid purification. The constructs were then used to transform *E. coli* strains DH5α and subsequently BL21(DE3) (Novagen) for expression. The nucleotide sequence of the cDNA inserts were confirmed by sequencing.

PCR amplification of the AKR coding regions was performed using Bio-X-ACT (Bioline) high-fidelity DNA polymerase. These polymerases have slower synthesis rates than *Taq* polymerases but generate fewer errors. The BIO-X-ACT polymerase mix (Bioline) was used according to manufacturer instructions:

- 10X Optibuffer……..…… 5.0 µl (1X)
- 50 mM $MgCl_2$……..……. 2.5 µl (2.5 mM)
- 100 mM dNTPs……. 1.0 µl (2 mM)
- 100 µM forward primer……. 0.5 µl (1 µM)
- 100 µM reverse primer…….. 0.5 µl (1 µM)
- 4 U/µl BIO-X-ACT..…… 1.0 µl (0.08 U/µl)
- Source cDNA (Table 4)……. 1.0 - 5.0 µl
- Water…….. up to 50 µl

Samples were incubated in an ABI9600 Thermal Cycler with the following program. 96 °C for 5 minutes; 58 °C for 5 minutes (70 °C for 1 minute; 95 °C for 30 seconds; 56 °C for 1 minute) x 35; 70 °C for 10 minutes. The resulting amplified products were separated in 1% agarose gel stained with ethidium bromide and visualized in a UV transiluminator.

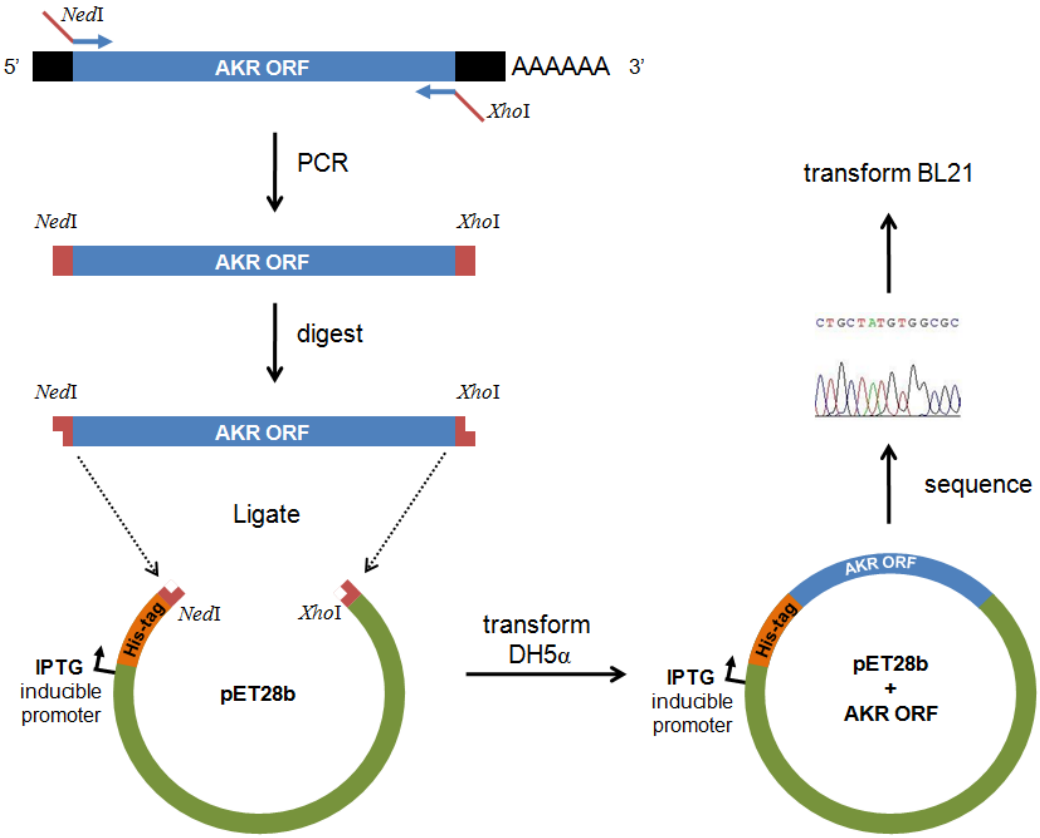

Figure 32 - Strategy for the cloning of AKR coding regions in pET-28b

The open reading frames (ORFs) of the AKR genes were amplified using primers that introduce a 5' *Nde*I site and a 3' *Xho*I site. These sites were later used to clone the coding regions in the bacterial expression vector pET-28b (Novagen). Correct amplification and cloning was confirmed by nucleotide sequencing before transforming the vector in the *E. coli* strain BL21(DE3).

Table 4 - Primers used for cloning the murine AKR coding regions.

Gene	Forward primer (5'-3') with *NdeI* site	Reverse primer (5'-3') with *XhoI* site	Product size (bp)	Source cDNA
Akr1c6	GCAGCAT**ATG**GATTCTAAGCAGCAGAC	CTGCCTCGAGTTAGTATTCATCCCAAAATG	989	Liver
Akr1c12	GCAGCAT**ATG**AGCTCCAAACAGCACTA	CTGCCTCGAGTTAATATTCCTCTGAAAATG	989	BA/F3
Akr1c13	GCAGCAT**ATG**AGCTCCAAACAGCACTG	CTGCCTCGAGTTAATATTCCTCCACAAATG	989	BA/F3
Akr1c14	GCAGCAT**ATG**AATTCTGTATCCCCACG	CTGCCTCGAGTTAATATTCATCAGTAAATG	989	C2C12
Akr1c18	GCAGCAT**ATG**AATTCCAAAATTCAGAA	CTGCCTCGAGTTAATATTCATCGAAGAAT	986	J-774
Akr1c19	GCAGCAT**ATG**AGTTCCAAACAGCAATG	CTGCCTCGAGCTAAAATTCATCAGAAAAG	986	BA/F3
Akr1c20	GCAGCAT**ATG**AATTCCAAGCAGCAGAC	CTGCCTCGAGTTAGTATTCATCCAAAAATG	989	Liver
Akr1c21	GCAGCAT**ATG**AACTCCAAATGTCATTG	CTGCCTCGAGCTAGTATTCATCCAAAAATG	986	Kidney

Primers were designed to introduce NdeI and XhoI sites at the 5' and 3' end of the coding region, respectively (sites are underlined)

starting codon (ATG) of each gene is highlighted in bold

2.3.9 DNA extraction from agarose gels

PCR products were electrophoresed in 1% agarose gel. The desired band was cut from the gel, the slice transferred to a microcentrifuge tube and weighed. For purification the QIAquick gel extraction kit (Qiagen) was used. Three volumes of QG buffer (relative to gel slice weight) were added to the slice followed by 10 minute incubation at 50^0C. When the gel was dissolved the solution was transferred to a QIAquick column and spun to bind DNA. DNA in column was washed with PE buffer and eluted with 30 µl of DNase-free water.

2.3.10 DNA digestion

The purified PCR product was digested with *Nde*I and *Xho*I. The primers were designed with 4 extra nucleotides after the restriction site in order to allow maximum digestion efficiency of the PCR product (some restriction enzymes can not cut sites very close to the DNA extremity). The purified PCR product was incubated with 1 U/µl *Nde*I (New England Biolabs), 1 U/µl *Xho*I (New England Biolabs) and 1X NEBuffer 2 (New England Biolabs) in a 50 µl volume at 37^0C, overnight. Approximately 1 µg of pET28b (Novagen) was digested under the same conditions. After digestion, 10% of each digestion was run in an analytical 1% agarose gel. If the band sizes were as expected the remain of the digestion mixes was run in a preparative 1% gel, the bands cut and purified as detailed in section 2.3.9.

2.3.11 DNA ligation

After purification both plasmid and insert (AKR ORF) had compatible cohesive termini. Ligation reactions were setup in a microcentrifuge tube as follows in a final volume of 10 µl:

- 1X ligase buffer (Promega)
- 0.3 U/µl T4 DNA Ligase (Promega)
- 2 µl plasmid
- 2 µl insert

The reaction was incubated either for 3 hours at room temperature or left at 4^0C overnight. Preferentially a smaller microcentrifuge tube was used to ensure the maximum interaction between the components of the reaction.

2.3.12 Transformation of competent DH5α bacteria

Freshly ligated DNA can be introduced in bacteria where it will be exponentially replicated within its host. Readily "competent" *E. coli* strains are available such as DH5α-T1^{R} (Invitrogen). For transformation 50 µl of competent DH5α were carefully transferred into a previously chilled microcentrifuge tube, placed on ice. Then, up to 5 µl of ligation mix was added to the bacteria and left on ice for 30 minutes. After this, bacteria were heat-shocked by placing the tube in a 42^{0}C water bath for exactly 30 seconds and then moved back to ice. The shock promotes the up-take of DNA by the permeated bacteria. After a few minutes, 250 to 950 µl of LB broth (Sigma) was added to the bacteria followed by 1 hour incubation at 37^{0}C. In the case of pET-28b the transformants will become resistant to kanamycin. After incubation, 20 to 100 µl of cell suspension were spread in 10 cm Petri dishes with agar-solidified LB supplemented with 50 µg/ml kanamycin. Only bacteria bearing the plasmid are able to survive and proliferate in the plate and because of the solid nature of the broth, bacteria grow as colonies. Importantly, these colonies arise from single cells and therefore are clonal.

Plates were left to incubate at 37^{0}C overnight with the lid facing down. The following day, for each ligation a few colonies were picked (usually between 6 and 20) with a wooden toothpick and placed in a 20 ml plastic tube with 5 ml of LB supplemented with 30 µg/ml kanamycin (standard concentration of kanamycin for bacterial selection). The cultures were incubated at 37^{0}C in a shaking incubator overnight.

2.3.13 Plasmid extraction from bacteria

Wizard *Plus* SV Miniprep DNA purification kists (Promega) were used to extract plasmid DNA. 1 to 5 ml of bacterial cultures was centrifuged and the cell pellets resuspended in 250 µl cell resuspension solution. Bacteria were lysed by the addition of 250 µl cell lysis solution and 10 µl alkaline protease solution and incubated for 5 minutes at room temperature. Addition of 350 µl neutralisation solution promotes the precipitation of proteins and genomic DNA. The solution was centrifuged for 10 minutes at 14000 rpm in order to separate the precipitated material from the supernatant containing the plasmid. The supernatant was transferred to a DNA-binding column. The column-bound plasmid DNA was washed with an ethanol based washing solution and finally eluted with 100 µl DNase-free water.

Also, at this point, 800 µl of bacterial overnight culture were added to 200 µl glycerol, mixed and frozen at -80 ºC. Later on, a new culture was started by simply picking the glycerol stock directly into liquid or solid LB broth.

2.3.14 Transformation of BL21 bacteria

The cloned plasmids were transformed into bacteria that are competent for large scale protein expression. BL21(DE3)pLysS (Novagen) is a commercially available strain of *E. coli* compatible with protein expression plasmids like pET-28b. The strain lacks the expression of bacterial proteases ensuring high quality protein recovery. Furthermore, these bacteria contain an isopropyl β-D-1-thiogalactopyranoside (IPTG)-inducible T7 RNA polymerase. This allows temporal control of protein expression since pET-28b depends on T7 RNA polymerase to express the cloned recombinant protein. The transformation protocol for BL21 was identical to the one described in section 2.3.12. After transformation, the bacteria were seeded in solid LB plates supplemented with kanamycin and incubated at 37^0C overnight. The next day three colonies were picked, expanded and glycerol stocks made.

2.3.15 Expression and purification of recombinant murine AKR enzymes

Overnight 5 ml cultures of the pET28b-AKR1C transformed BL21(DE3) cells were diluted 1:1000 in fresh LB broth (4 × 200 ml culture) containing 30 µg/ml kanamycin and incubated at 37 °C for 5 h (corresponding to an absorbance at 600 nm of ~ 1.0). Expression of recombinant protein was induced by adding IPTG to a final concentration of 1 mM and incubated at 37 °C overnight with shaking at 220 rpm. Cleared lysates were prepared by pelleting bacteria by centrifugation (15 min, 3000*g*, 4 °C) and disrupting cells in BugBuster reagent (Novagen) containing protease inhibitors [Mini-Complete ethylenediaminetetraacetic acid (EDTA)-free, Roche Molecular Biochemicals] and Benzonase DNase (Novagen), using 25 µl of lysis reagent per milliliter of original culture. After incubation at room temperature with shaking for 30 min, cell debris was pelleted by centrifugation (30 min, 38,000*g*, 4 °C). The cleared lysate (20 ml) was mixed with 1 ml of nickel-nitrilotriacetic acid (Ni-NTA) "His-bind" resin (Novagen) followed by gentle shaking on ice for 20–60 min. The mixture was loaded onto an empty minicolumn, and unbound protein was removed by washing with 15 ml of 50 mM $NaPO_4$ and 300 mM NaCl, pH 8.0. Bound protein was eluted in 1.5 column volumes of the same buffer containing 100 mM imidazole. Protein concentration was

estimated by Coomassie Blue binding, using a commercial reagent (Bio-Rad Laboratories). The imidazole fractions containing protein were subjected to further purification using gel filtration on a Superdex 200 HR 10/30 column (GE Healthcare) running in 10 mM potassium phosphate, 1 mM EDTA, and 1 mM DTT, pH 7.0. The purity of collected fractions was assessed by SDS-PAGE stained with Coomassie Brilliant Blue.

Activity of the purified recombinant proteins was confirmed by the reduction of phenanthrenequinone (PQ), measured as described in page 94.

2.4 Vector construction and cell transfections

2.4.1 Construction of a DP2 knockdown vector

The DP2 knock-down plasmid consists of a vector expressing a short-hairpin RNA (shRNA) targeting specifically DP2. The parent vector is a modified pcDNA3.1(+) in which the CMV promoter was replaced with the RNAse P H1 gene promoter (driven by RNA polymerase III) as described by (Kunath et al., 2003). The parent vector retains the bacterial selection marker (Ampicillin) and eukaryotic selection marker (Neomycin). The 5'-*Acc*65I site and the 3'-*Xba*I site of the vector is used for the ligation of targeted shRNA sequences (Figure 33).

The BIOPREDsi algorithm (Qiagen) was used to design a 19 bp sequence optimal for DP2 knockdown (see underlined sequence used for knockdown in Table 5). The selected sequence targets the 5' end of the coding region in the DP2 mRNA. BLAST analysis against the mouse transcriptome confirmed specificity against DP2. The targeting sequence was integrated into a shRNA context (Figure 33). Sense and anti-sense DP2 targeting sequences were separated by a 9 bp stem loop so that when expressed, the RNA molecule folds into a hairpin structure. The RNA polIII transcription of the sequence is initiated in adenosine +1 and terminated in a thymidine rich region. Two complementary oligonucleotides were ordered so that after annealing the sequence would have 5'- *Acc*65I and 3'- *Xba*I cohesive ends. A random non-targeting sequence with the same nucleotide composition as the DP2 targeting sequence was generated as a shRNA control. BLAST analysis showed the sequence did not target any known mRNA of the mouse transcriptome. This sequence was processed as for the DP2 targeting sequence

For insert generation, 4 μM of each complimentary oligonucleotide pair were mixed in Tris-EDTA buffer (pH 8.0) to a final volume of 50 μl and incubated at 70^0C for 10 minutes. After that, the oligonucleotides were left at room temperature for 40 – 60 minutes to promote annealing. The parent vector (pcDNA-H1) was digested with *Acc*65I and *Xba*I. The purified vector was ligated with the annealed insert. The ligation products were transformed into competent bacteria and seeded on LB plates supplemented with 30 μg/ml ampicillin. 6 colonies were picked and expanded for plasmid extraction. Cloning was confirmed by sequencing the plasmids with a primer binding in the BGH region (primer 56, Table 6). High quality plasmid DNA extraction was performed by using Plasmid Maxi Prep kit (Qiagen). The resulting plasmids were named pcDNA-shDP2 and pcDNA-shVC (vector control).

Table 5 - Oligonucleotides used to generate a DP2 silencing vector

Scrambled shRNA	Sense	5'-GTACCAAGCTTCGCATTGCACGTAGTTTCAAGAGAAACTACGTGCAATGCGAAGCTTTTTTTGGAAAT-3'
	Antisense	5'-CTAGATTTCCAAAAAAAGCTTCGCATTGCACGTAGTTCTCTTGAAACTACGTGCAATGCGAAGCTTG-3'
DP2 shRNA	Sense	5'-GTACCAAGGCGCTATCCGACTTGTTATTCAAGAGATAACAAGTCGGATAGCGCCTTTTTTTGGAAAT-3'
	Antisense	5'-CTAGATTTCCAAAAAAAGGCGCTATCCGACTTGTTATCTCTTGAATAACAAGTCGGATAGCGCCTTG-3'

Targeting sequences are underlined
Sense and antisense oligonucleotides are complimentary

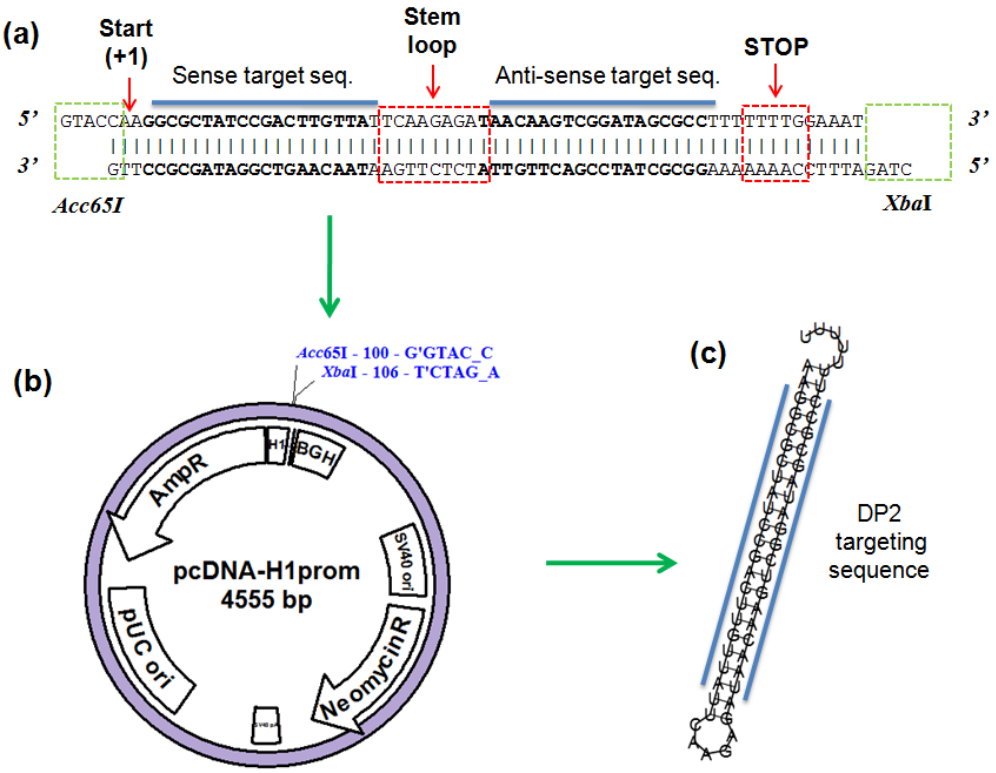

Figure 33 - Construction of a DP2 silencing construct

A DP2 specific targeting sequence was designed using the BIOPREDsi algorithm. **(a)** The sequence was integrated in a short-hairpin RNA context. Sense and anti-sense sequences are separated by a 9 bp stem loop. Transcription of the sequence is initiated at adenosine +1 and terminated in the thymidine rich region. Two complementary oligonucleotides have been designed so that, after annealing, *Acc*65I and *Xba*I cohesive ends are generated. **(b)** The annealed double-stranded sequence was then cloned in a modified pcDNA vector where the expression is driven by a RNA polymerase III promoter (H1 promoter). The resistance cassette for bacterial (ampicillin) and eukaryotic (neomycin) selection are retained. Digestion with *Sca*I linearizes the vector in the ampicillin resistance cassette. Vector map was drawn using the pDRAW software. **(c)** Once transfected in the cells, the vector will express the targeting sequence that folds into a short-hairpin RNA conformation. This RNA will be processed by the cellular RNA silencing machinery resulting in DP2 mRNA degradation.

2.4.2 Construction of an *Akr1c6* over-expression vector

The Akr1c6 coding region had been previously cloned into the MSCV-IRES-GFP vector by Dr Trong Luong. This vector has the cloned cDNA under regulation of the murine stem cell virus (MSCV) promoter. Transcription from this promoter generates a polycistronic mRNA in which the Akr1c6 coding region is followed by an internal ribosomal entry site (IRES) allowing the simultaneous translation of the green fluorescent protein (GFP). Therefore, Akr1c6 expressing cells can be identified by green fluorescence. A vector lacking the Akr1c6 coding region (but retaining all other components) was used as control.

2.4.3 Construction of a L-PGDS over-expression vector

The coding region of murine L-PGDS was cloned using the RT-PCR strategy described in page 77. Primers were designed to amplify L-PGDS coding region and introduce a 5'-*Bam*HI site (5'-CTAGGGATCCATGGCTGCTCTTCGCATGCTG-3') and a 3'- *Eco*RI site (5'-CATGGAATTCTTACTCTTGAATGCACTTATCCGGTTGGGGCAGG-3'). High-fidelity PCR was performed using cDNA from differentiated C2C12 as template.

The PCR product (590 bp) was initially cloned in pGEM-T Easy Vector (Invitrogen), a linearized vector with a single 3´-terminal thymidine at both ends. Since most polymerases leave a 5'-terminal adenine, this greatly facilitates ligation into pGEM-T. Also, ligation of insert interrupts the bacterial β-galactosidase (β-gal) gene thus allowing for blue/white selection of recombinants. After ligation, DH5α competent *E. coli* strains were transformed and plated on LB-agar plates supplemented with 30 μg/ml ampicillin and X-gal. The non-recombinant colonies growing on the plate will have an intact β-gal that breaks down X-gal and generate a blue compound (blue colonies). Colonies harbouring the pGEM-T vector with an insert do not have a functional β-gal enzyme and remain white. Six white colonies were picked, amplified and plasmid DNA extracted and sequenced using primers 72 and 73 (Table 6).

Correctly cloned pGEM-T+L-PGDS plasmids were digested with *BamH*I and *EcoR*I and the released fragment was ligated to pcDNA3.1(+) vector digested with the same enzymes. Ligation clones were sequenced using primers 27 and 56 (Table 6). This construct has the

murine L-PGDS coding region under regulation of the CMV promoter. Empty pcDNA was used as vector control.

2.4.4 PPARγ cloning

PPARγ was cloned from C2C12 cDNA using the RT-PCR strategy described on page 77. Primers used for cloning both PPARγ1 and PPARγ2 (γ2 is a splice variant lacking first 30 N-terminal residues relative to the γ1 amino-acid sequence) are 63, 67 and 65 (65 is common to both isoforms; Table 6). High-fidelity PCR was performed as described on page 76 and resulted in amplification only of PPARγ1 (1536 bp). The product was cloned into pGEM-T as described on page 87 and sequenced using primers 72 and 73 (Table 6).

2.4.5 Electroporation of cell lines

Plasmids were transfected into tissue culture cells using the Nucleofector I electroporator (Amaxa Biosystems). Plasmid DNA was previously linearised if the electroporation was intended to generate stably transfected cells as this greatly improves the chance of random integration in the genome (usually a *Sca*I digestion cuts on a single site, in the middle of the ampicillin resistance cassette). Variable amounts of plasmid were used (usually 1 – 10 μg). For each transfection reaction, 1 – $2x10^6$ cells were spun down, resuspended in 100 μl Cell Line Nucleofector Kit V (Amaxa Biosystems) mixed with plasmid DNA and transferred to an electroporation cuvette. Cells were electroporated in a Nucleofector I electroporator with the appropriate voltage program (B-32 for C2C12 and CHO; T-16 for J774 and K562). Electroporated cells were transferred to a well of a 6-well plate with 3 ml of warm media and left to recover for 24 hours.

2.4.6 G418 selection

Vectors derived from pcDNA3.1(+) have a neomycin-resistance cassette that confers resistance to G418 sulphate (Sigma). In order to produce stably transfected C2C12, selection with G418 was used after electroporation with linearised plasmids.

To determine the optimal G418 concentration for selection with C2C12 cells, a survival curve for an increasing concentration of the drug was made. C2C12 cells were seeded in wells of a 96-well plate (Corning) (1.7 x 10^3 cells per well) in 200 μl growth media. 24 hours later the

media was replaced with 100 µl growth media (see page 71) supplemented with G418 at 0-1600 µg/ml. Each condition was assayed in six wells. A no-cell control was used as control. Cells were cultured with G418 for 7 days with daily media replacement. Cell survival was measured with Cell Titre Blue (Promega), a solution containing resazurin (mentioned in page 96) a molecule that can be reduced by cellular mitochondrial activity generating a fluorescent dye (emits fluorescence at 590 nm after excitation at 530 nm). To each well, 10 µl of Cell Titre Blue were added and cells incubated at 37 °C for 4 hours. After that, fluorescence was measured in KC-4 96-well plate reader (Bio-Tek Instruments). The average fluorescence of the no-cell controls was subtracted from all wells. The relative fluorescence was normalised against the no-drug control wells (Figure 34). The optimal concentration for G418 selection was the lowest dose assayed that assured ~100% cell death (1200 µg/ml).

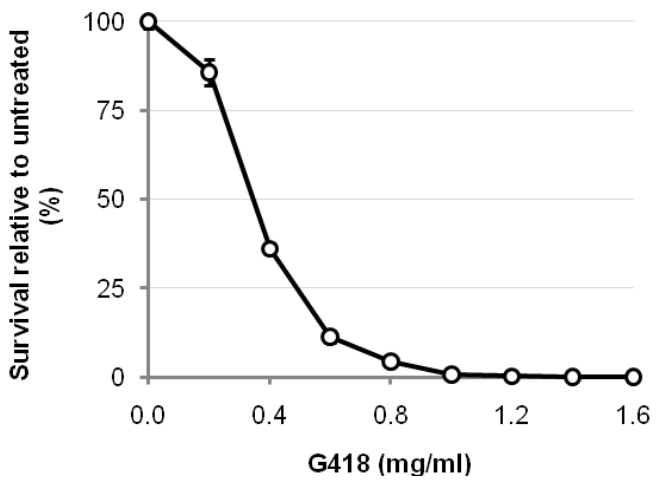

Figure 34 - G418 survival curve for C2C12 cells

C2C12 cells were grown for 7 days in the presence of increasing concentrations of G418. At day 7, cell viability was measured with Cell Titer Blue dye. Cell survival is shown in relation to untreated cells. Each circle represents the average survival of 6 replicate wells. Error bars represent standard deviation

.

Electroporated cells were left to recover for 24 hours before the addition of growth media with 1200 μg/ml G418. Cells were cultured in selective media for 9 days (until all mock-transfected cells had died) and individual colonies were visible. It is very likely that these colonies have a single-cell origin (monoclonal). After washing with PBS, sterilized plastic cylinders were placed over the colonies. The bottom of the cylinders was coated with vacuum grease allowing trypsin-EDTA to be put only on top of the colonies without spilling to the rest of the plate. Individually trypsinized colonies were moved to separate 25 cm^2 tissue culture flasks and expanded. Four pcDNA-shDP2 clones and two pcDNA-shVC clones were isolated. A fraction of the expanded cells were frozen as viable stocks in liquid nitrogen. The remaining cells were kept for RNA and protein analysis. In some experiments the G418-selected colonies were pooled together (polyclonal).

2.4.7 H-2Kk sorting

K562 were co-transfected with 8μg MSCV-Akr1c6-IRES-GFP (or control) and 4 μg H-2Kk plasmid (Amaxa). The latter encodes the mouse H-2Kk surface marker that is transiently expressed on the cell-surface and is used to positively select transfected cells. 24 hours after transfection, cells were pelleted by centrifugation at 263 x g for 10 minutes and washed with 1 ml cold PBE buffer (PBS with 2 mM EDTA), spun down, resuspended in 320 μl PBE with 80 μl MACSelect microbeads (Miltenyi Biotec) and incubated for 15 minutes at 4 °C. The ferrous microbeads are coated with an antibody against H-2Kk and bind transfected cells. After incubation, cold PBE was added to a final volume of 2 ml and the cell suspension transferred to a MS column (Miltenyi Biotec) and placed in a magnet. Beads bound to H-2Kk-positive cells were held by the magnetic field in the column while H-2Kk-negative cells were washed away using 4 X 500 μl cold PBE. Selected cells were eluted by removing the column from the magnetic field and flushing with more buffer, counted and plated in fresh media at the density of $4x10^5$ cells/ml in 24- or 12-well plates.

Efficiency and enrichment of transfection with MSCV-IRES-GFP plasmids was assessed by measuring GFP fluorescence by flow cytometry (detailed in page 91).

2.5 Assessing HPC-7 differentiation

2.5.1 Jenner-Giemsa staining

To analyse cell morphology during differentiation, 60 µl of cell suspension were spun against a microscope slide using a Cytopsin3 cytocentrifuge (Shandon), fixed with 100% methanol for 5 minutes and left to air dry for 10 minutes. Jenner staining solution (VWR) diluted 1/3 in 1 mM sodium phosphate buffer pH5.6 was incubated on the slides for 5mins and then washed off with distilled water. Slides were then incubated with Giemsa stain (VWR) diluted 1/20 in 1 mM sodium phosphate buffer pH5.6 for 10mins at room temperature before washing again with water. Slides were dried and then mounted onto coverslips using DePex (VWR, UK). Stained cytospins were photographed using an Olympus Camedia C-5050 Zoom Camera adapted for inverted microscopes.

2.5.2 Flow cytometry analysis of surface markers

To analyse the expression of surface markers during differentiation, 100 µl of cell suspension were transferred to flow cytometry tubes (BD Biosciences) and incubated for 15 minutes at room temperature with 1 – 3 µl fluorochrome-conjugated antibody. Anti-mouse FITC-CD34 and PE-Sca1 were kindly supplied by the group of Prof Frampton (IBR, University of Birmingham, UK). After incubation 3 ml of cold PBS were added and tubes centrifuged at 1500 rpm for 5 minutes. Stained cells were resuspended in 300 µl FACS-fix solution (PBS with 1% formaldehyde and 2% FBS) and kept in the dark at 4° C. Analysis was performed on a BD FACSCalibur flow cytometer (BD Biosciences) using Cell Quest Pro software (Becton Dickinson).

2.6 Assessing C2C12 differentiation

2.6.1 Fusion index measurement

A standard method for quantifying C2C12 differentiation is to measure the fusion index (FI), that is, the fraction of myoblasts that have fused to generate myotubes. To assess this, C2C12 cultures in 6-well plates were washed and fixed with 100% methanol for 5 minutes at the desired time points. After fixation, cells were stained using the Jenner-Giemsa protocol (see page 91). Each sample was photographed in 4 randomly selected regions using a digital

Olympus Camedia C-5050 Camera adapted to an inverted microscope. Protein-rich myotubes can be identified by a darker purple color while nuclei stain pink. For each field the number of nuclei incorporated in myotubes and the total number of nuclei was scored. FI was calculated as the percentage of total nuclei incorporated in myotubes.

2.6.2 Creatine kinase assay

Creatine kinase (also creatine phosphokinase, CK) is a dimeric enzyme that is highly expressed in differentiated muscle tissue. CK catalyzes the conversion of creatine to phosphocreatine, consuming ATP, as well as the reverse reaction. In tissues where ATP can be rapidly consumed (such as skeletal muscle) phosphocreatine serves as an energy reservoir for the rapid buffering and regeneration of ATP. Thus, CK plays a key role in maintaining ATP levels in this tissue.

The following protocol was adapted from (Khurana and Dey, 2002) and its principle is detailed in Figure 35. Cells growing in 6-well plates were washed twice with ice-cold PBS before adding 50 µl of 0.05 M glycilglycin, pH 6.75 (lysis buffer). Plates were left overnight with lysis buffer at -20 °C. After thawing, the wells were scraped and the contents centrifuged at 16000 x g for 10 minutes in a microcentrifuge at 4 °C. Finally, the supernatant containing the soluble internal proteins was collected and stored at 4° C (to avoid freezing and thawing). Protein content was determined with the Protein Assay kit (BioRad).

The assay solution was prepared in 0.1 M glycilglycin (pH 6.75) as follows:

- 10 mM glucose
- 2.5 mM magnesium acetate
- 0.5 mM ADP (Calbiochem)
- 5.0 mM AMP (Calbiochem)
- 0.4 mM NADP+ (Sigma)
- 10 mM Phosphocreatine (Calbiochem)
- 1.0 U/ml hexokinase (Roche) (added immediately before assaying)
- 0.5 U/ml glucose-6-p dehydrogenase (Roche) (added immediately before assaying)
- 1.54 mg/ml DTT (added immediately before assaying)

Both hexokinase and glucose-6-p dehydrogenase are supplied as a 2:1 enzyme mix. For the assay, 100 µl assay solution was transferred to a quartz cuvette and set as zero absorbance at 340 nm in a spectrophotometer. Then 5 µl of sample was added and the increase in absorbance per minute recorded. If the solutions are correctly prepared, addition of CK

positive samples will result in a linear increase of absorbance for at least the first 5 minutes. The rates are subsequently normalised to the amount of protein measured previously in each respective sample.

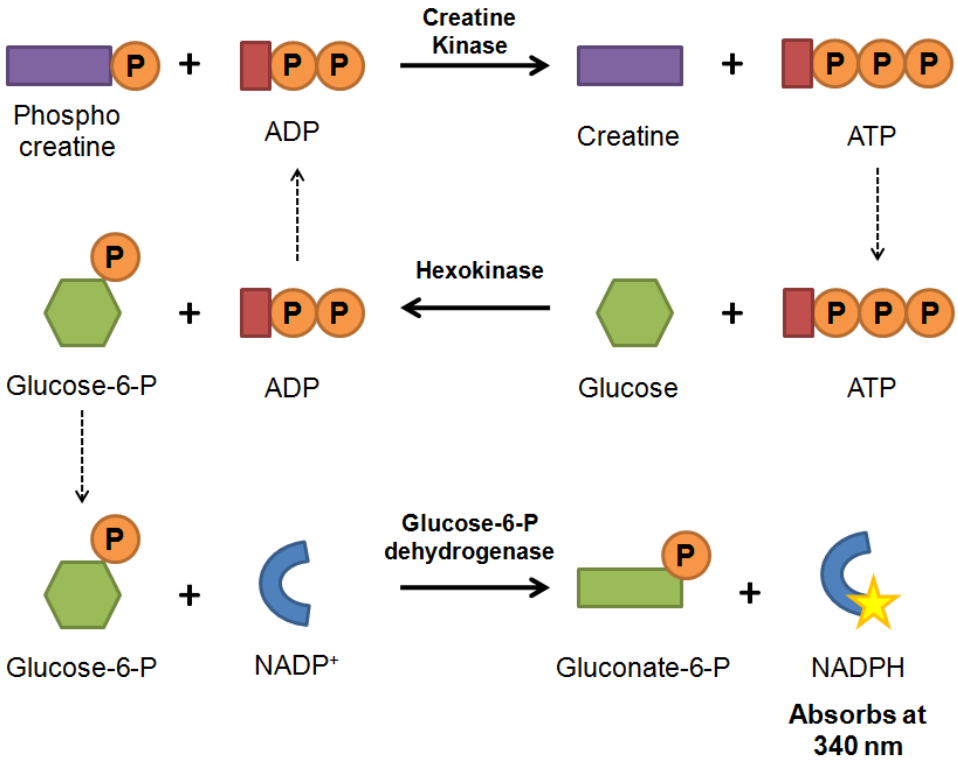

Figure 35 - Mechanism of creatine kinase assay.

The creatine kinase (CK) assay relies on three sequential reactions. First, the creatine kinase from the sample converts phosphocreatine and ADP to creatine and ATP, respectively. Secondly, the generated ATP is used to convert glucose to glucose-6-phosphate by hexokinase present in the assay solution. Lastly, glucose-6-phosphate-dehydrogenase uses glucose-6-phosphate to reduce $NADP^+$ to NADPH. The final product (NADPH) can be measured in a spectrophotometer at 340 nm and its production is proportional to the amount of CK added from the sample (all other reagents and enzymes exist at constant concentration).

2.6.3 Expression of myogenic markers

The expression of three myogenic markers was measured in C2C12, *MyoD*, *Myog* (myogenin) and *Acta1* (α-actin 1). At the desired time points, cells were released from the wells by adding trypsin-EDTA, washed and stored at -20 °C for later RNA extraction. RNA extraction, cDNA synthesis and Taqman QRT-PCR are described from page 73 onwards. Primers and probes used to quantify expression of these genes are present in Table 6 and Table 7, respectively.

2.7 Enzymatic assays

Several assays were used to determine AKR enzymatic activity. Reaction rates (v) were calculated as nanomoles of substrate turned over per minute per miligram of enzyme ($nmol.min^{-1}.mg^{-1}$) or as number of substrate molecules turned over by a molecule of enzyme per minute; k_{cat} (min^{-1}).

2.7.1 Spectrophotometric assay

In the spectrophotometric assay the reaction is monitored by measuring the consumption of co-factor in real time. NADPH absorbs at 340 nm (but not its oxidized form $NADP^+$) and its concentration can be calculated using the NADPH extinction coefficient ($\varepsilon = 6220\ M^{-1}.cm^{-1}$). Importantly, substrates that also absorb at 340 nm cannot be used in this assay as they interfere with the measurement of NADPH.

Reaction mixtures were prepared in a plastic cuvette to a final volume of 1 ml in 50 mM KH_2PO_4 (pH 6.5) buffer with 150 μM NADPH (Sigma), 0 – 100 μM substrate and 15 μg/ml recombinant enzyme. The cuvette was placed in a spectrophotometer kept at 37 °C and absorbance measured at 340 nm. Reaction was initiated by adding purified recombinant enzyme and NADPH consumption was monitored for 3 to 5 minutes in order to determine reaction rates. The intervals at which absorption was measured depended on the speed of the reaction. The rate of spontaneous NADPH reduction was also measured by preparing a mixture without substrate. This was the minimum measurable rate (background).

2.7.2 Radiometric assay

For the radiometric assay the obtained substrates were radioactively labeled with tritium (^3H) so that the reaction products could be visualized after separation in thin layer chromatography

(TLC). This method is useful for substrates that absorb in the same wavelength of NADPH (340 nm; see above) and informs about the type of products formed. It is also a more sensitive method able to detect slower activities.

For prostaglandin turn-over, reaction mixtures were prepared in borosilicate glass tubes (13 x 100 mm) (Corning) in a final volume of 0.2 ml in 50 mM KH_2PO_4 (pH 6.5) buffer with the following:

- 150 μM NADPH
- 0.2 μCi radio labeled substrate ([^{3}H]-PGD_2, [^{3}H]-PGE_2, [^{3}H]-PGH_2) (GE Healthcare)
- 0 – 250 μM "cold" substrate (PGD_2, PGE_2, PGH_2) (Cayman Chemical)

For 5α-dihydrotestosterone (5α-DHT) turn-over, a similar set-up was used but with the following mixture:

- 150 μM NADPH
- 25 μM 5α-DHT (Sigma)
- 1 μCi [^{3}H]-5α-DHT (GE Healthcare)
- 0 – 250 μM "cold" substrate (PGD_2, PGE_2, PGH_2) (Cayman Chemical)

Reactions were initiated by adding purified recombinant enzyme (35 μg/ml) and stopped after a desired time either by flash-freezing with liquid nitrogen or initiating the extraction protocol.

2.7.3 Extraction of prostanoids

For extraction, 500 μl methanol and 2.5 μl 10% formic acid (Sigma) were added to each sample and vortexed for 1 minute before the addition of 1 ml chloroform and 50 μl 4.2% KCl (Sigma). After vortexing for a further 3 minutes the reaction mixtures were spun down at 2500 rpm for 10 minutes and the resulting aqueous and proteinaceous layers removed by aspiration. The prostanoid containing chloroform fraction was evaporated to dryness at 35°C under a steam of nitrogen and and prostaglandins were resuspended in 40 μl chloroform.

2.7.4 Extraction of steroids

For extraction, 500 μl methanol and 2.5 μl 10% formic acid were added to each sample and vortexed for 1 minute before the addition of 1 ml dichloromethane. After vortexing for a further 3 minutes the reaction mixtures were incubated at room temperature for 2 hours. Samples where then spun down at 2500 rpm for 10 minutes and the resulting aqueous and

proteinaceous layers removed by aspiration. The steroid containing chloroform fraction was then evaporated to dryness under a steam of nitrogen and at 35°C and the steroids were resuspended in 40 µl chloroform.

2.7.5 Separation of prostanoids and steroids by thin layer chromatography (TLC)

Extracted prostaglandins and steroids were spotted on to TLC plates (Fluka), 2 cm above the bottom edge and each sample separated laterally by 1.5 cm. As a control, 0.2 µCi of radio-labeled substrate were also spotted along with cold standards. Prostaglandins were separated using chloroform/methanol/acetic acid/distilled water (90:8:1:0.8). Steroids were separated using chloroform/ethyl acetate (4:1). The solvents were placed in a chromatography tank for at least 2 hours for equilibration before inserting the TLC plates. Chromatography was run for 1 to 2 hours. After running, the plates were dried for 10 minutes at room temperature before being scanned in a Bioscan Plate Reader to detect the location of the radioactive label. Cold standards were visualized after a short incubation with iodine vapour. For optimal separation of 5α-DHT reduction products plates were run three times consecutively in the same solvent solution.

2.7.6 Resazurin/Diaphorase assay

The Resazurin/Diaphorase assay is a quick method to measure the consumption of NADPH at a certain timepoint in a reaction. The assay is based on two sequential reactions: first the normal reaction (enzyme, substrate and NADPH) followed by addition of resazurin (a blue non-fluorescent dye) and diaphorase (a cytochrome reductase). Upon addition, the diaphorase quickly consumes the remaining NADPH to catalyze the reduction of resazurin to resorufin (a pink dye that emits fluorescence at 590 nm after excitation at 530 nm). Fluorescence levels are proportional to the amount of NADPH remaining in the well. This assay can be performed in 96-well plate format allowing for large scale screens.

Reaction mixtures were prepared in 96-well plates (Costar) in a final volume of 0.2 ml in 50 mM KH_2PO_4 (pH 6.5) buffer with the following final concentrations:

- 150 µM NADPH
- 0 – 500 µM substrate
- 35 µg/ml recombinant enzyme

The reaction was left to incubate at 37 °C for the desired period of time followed by the addition of 5 µl of the second reaction mixture (concentration in mixture / final concentration):

- 1.1 mM / 26.8 µM resazurin (Sigma)
- 22.2 U/ml / 0.54 U/ml diaphorase (Sigma)

After pipette-mixing the second mixture, the reaction was left to incubate at 37 °C for further 10 minutes. Fluorescence in the 96-well plate was read using a KC 4 microplate reader with excitation at 530 nm, emission at 590 nm and sensitivity of 50. Because AKRs are also reductases, a control experiment without substrate was performed for all enzymes to check for diaphorase-independent conversion of resazurin to resorufin.

2.7.7 Determination of enzyme kinetic parameters

For determination of the enzyme kinetic parameters K_m and k_{cat}, the reaction velocity was measured using different substrate concentrations. The results were fitted to a Michaelis-Menten curve using the VisualEnzymics software (SoftZymics).

2.8 Prostanoid synthesis and turn-over by tissue culture cells

2.8.1 Prostaglandin turn-over by tissue culture cells

This assay was used to measure if intact live cells (from tissue culture cell lines) were able to metabolise prostaglandins. For adherent cells (like C2C12), cells were seeded in 6-well plates and grown to the desired confluence. Then, cells were washed with warm PBS and left in 1 ml PBS or serum-free DMEM with 0.2 µCi radio labeled prostaglandin ($[^3H]$-PGD_2, $[^3H]$-PGE_2) for 9 hours or overnight. For non-adherent cells (like HPC-7 or K562), 1 – $2x10^6$ cells were spun down and resuspended in 0.2 ml PBS with 0.2 µCi radio labeled prostaglandin for 9 hours or overnight at 37 °C, 5% CO_2. After incubation, PBS or serum-free DMEM were

collected after centrifugation and prostaglandins extracted, separated and detected as detailed in page 95.

2.8.2 Measuring prostaglandins in tissue culture supernatant

Levels of secreted prostaglandins were measured in the culture supernatant of C2C12 cells using kits from Cayman Chemical (PGD_2-MOX EIA kit and $PGF_{2\alpha}$ EIA kit) according to manufacturer's instructions. Media was harvested at different time points during C2C12 differentiation, flash-frozen with liquid nitrogen and stored at -80 °C. Both are Enzyme-linked Immunosorbent Assays (EIA) and are based on the competition between prostaglandin from the sample and a fixed amount of prostaglandin-acetylcholinesterase (AChE) conjugate for a limited number of prostaglandin-specific antiserum binding sites, coating the inside of a well (Figure 36). The more prostaglandin present in the sample, the less prostaglandin-AChE is retained in the well after the washings. In the end, a reagent is added containing a compound that is converted by AChE into a yellow substance that strongly absorbs at 412 nm. The assay is performed in a 96-well plate (each sample read in triplicate) alongside a calibration curve with known prostaglandin concentrations. The PGD_2-MOX EIA kit has one extra step, converting the unstable PGD_2 into the more stable PGD_2 methoxyme (PGD_2-MOX)

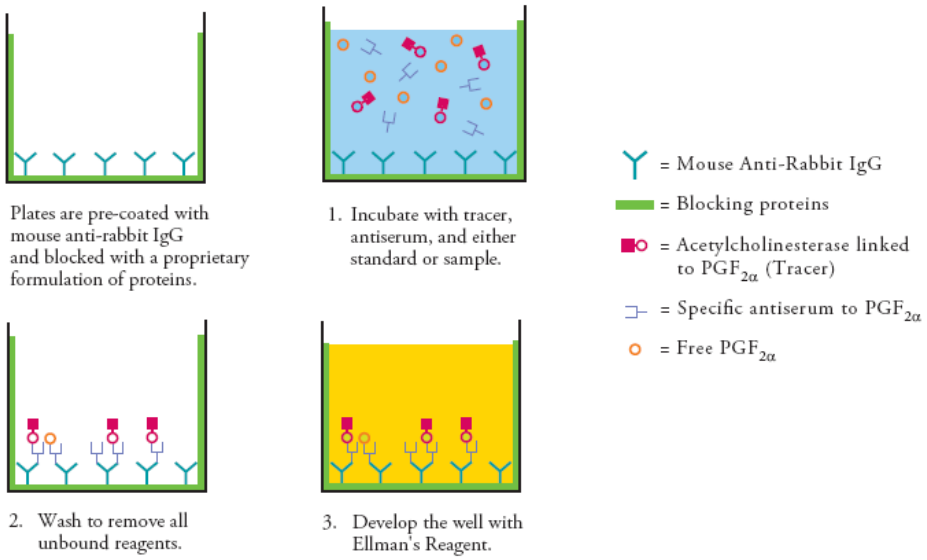

Figure 36 - Prostaglandin enzyme-linked immunosorbent assay

Diagram of the enzyme-linked immunosorbent assay (EIA) for the detection of prostaglandins in tissue culture supernatant. Taken from Cayman Chemical website.

2.8.3 Arachidonic acid metabolism by tissue culture cells

Arachidonic acid (AA) is the precursor of all eicosanoids and radio-labeled AA can be used to trace which prostanoids can be synthesized by a certain cell type. Also, this method can be used to detect changes or inhibition in synthesis of certain prostanoids. Tissue culture cells were exposed to 0.25 μCi [1-^{14}C] arachidonic acid (GE Healthcare), as detailed in page 97 and incubated overnight at 37 °C, 5% CO_2. Eicosanoids were extracted and separated as in page 95. For visualization of AA products, a light-sensitive film was exposed to the TLC plate for 3 days at -80 °C before being developed. Cold standards were run in the TLC as references.

2.9 Analysis of cell motility

C2C12 cells were seeded in 6-well plates (5 x10^4 per well) and left overnight to adhere. On the following day, 2 ml of fresh media with either 10 μM PGD_2 or vehicle was added to the cells. Each treatment was done in triplicate. The plates were placed on a microscope stage equipped with an incubator where they were kept at 37 °C and 5% CO_2. Time-lapse imaging began 20 minutes after addition of PGD_2 with a Nikon Eclipse TE200-U microscope with 20x phase contrast objective, capturing 1 frame every 2 minutes over a period of 3 hours.

Cell movement was tracked using the Manual Track software plug-in for ImageJ. For each condition, the movement of 30 cells (10 from each replicate) was tracked and used to generate a dispersion plot.

2.10 Measuring generation of mitochondrial superoxide

To measure the generation of mitochondrial superoxide, C2C12 cells were seeded in 6-well plates (5 x10^4 cells per well) and left to incubate for 48 hours in growth media. After this, growth media was replaced with differentiation media with either100 μM hydrogen peroxide (H_2O_2), 10 μM PGD_2, 10 μM 15d-PGJ_2 or vehicle (in triplicate) and incubated for 24 hours. After incubation, cells were washed twice with PBS and were incubated with 1 ml PBS with 5 μM MitoSOX red (Invitrogen). MitoSOX red exhibits red fluorescence when oxidized by mitochondrial superoxide (absorption/emission ~510/580 nm). Cells were incubated for 20 minutes with MitoSOX red before imaging.

For each well, three fields were photographed using a digital camera associated with an Axiovert 135 TV microscope (Zeiss). For each field a contrast-phase and a red-fluorescence picture was taken. For each field MitoSOX red fluorescence was quantified using ImageJ software and normalised to the cell number.

2.11 Murine embryonic stem cell (mESC) manipulation

2.11.1 Culture of G4 murine embryonic stem cells

The G4 embryonic stem cell line was derived from a male blastocyst originating from the natural mating of a 129S6/SvEvTac female with a C57BL/6Ncr male (Nagy et al., 1993). G4 ES cells are commonly used for *in vitro* manipulation (gene knock-out, over-expression, etc.) and can be used to derive transgenic mouse strains.

Embryonic stem cell growth is supported *in vitro* by a layer of mouse embryonic fibroblasts (feeder cells). These fibroblasts are obtained from 13.5 day old embryos and treated with 0.01 mg/ml mitomycin C for two hours. After treatment cells remain viable but are unable to proliferate, thus supporting stem cell growth without competing for nutrients.

Before culturing G4 cells, 60 mm plastic Petri dishes (Costar) were coated with 0.1% gelatin solution (Sigma) and a layer of mitomycin C treated feeder cells was seeded on top of it (1 x 10^6 per dish). Feeder cells were allowed to attach and form a monolayer overnight. G4 mESCs were then seeded on top of the feeder layer (1 – 3 x 10^6 cells per dish) and cultured with DMEM (Gibco) with 4500 mg/ml glucose (without sodium pyruvate) and supplemented with 15% mESC-tested fetal calf serum (FBS), 2 mM glutamine, 500 U/ml penicillin, 500 µg/ml streptomycin, 1% non-essential amino acids (Gibco), 100 µM β-mercaptoethanol (Sigma), 1% nucleosides and 100 U/ml murine Leukemia Inhibitory Factor (LIF) (Gibco) and kept at 5% CO_2 at 37°C. Media was changed daily and cells passaged every two or three days (before reaching confluence).

2.11.2 Electroporation and selection of G418-resistant colonies

For electroporation, 1 x 10^7 G4 cells were resuspended in 0.8 ml PBS and transferred to an electroporation cuvette (Gene Pulser Cuvette, Bio-Rad) with 25 µg of targeting construct (previously generated by M Scholze, Max Planck Institute for Molecular Genetics, Berlin,

Germany) and electroporated using a Gene Pulser electroporator (Bio-Rad) at 240 V and 500 µF. After electroporation cells were plated in four 60 mm plastic Petri dishes over neomycin-resistant feeder cells. Media was changed the following day to remove dead cells. Selection began 36 hours after electroporation by changing to selective media with 350 ng/ml G418 sulphate (Geneticin) (Sigma). Media was changed daily until colonies were clearly visible. Neomycin resistant colonies were picked using a stereomicroscope and plated in 96 well plates coated with gelatin and a layer of neomycin resistant feeder cells (1 x 10^4 cells per well). Cells were grown in selection media for 3 days and the colonies were replicated (keeping the relative position in the plate) into 2 other plates. After 2 more days of culture one of the plates was frozen (keeping cells viable) by adding to each well 140 µl of bicarbonate-free DMEM supplemented with 10mM Hepes, 20% mESC-tested FBS and 20% DMSO and storing at -80^{0}C. This was the master plate from where the clones would be propagated before generating chimeric mice. The remaining two replica plates were grown to confluence for DNA extraction (4 – 5 days).

2.11.3 DNA extraction for mESCs growing in 96-well plates

Cells growing in 96 well plates were washed with PBS and lysed overnight at 60°C with 50 µl lysis buffer (10 mM Tris•Cl, 10 mM EDTA, 10 mM NaCl, 0.5% sacrosyl and 1 mg/ml proteinase K) per well. DNA was precipitated by adding 150 µl NaCl and ethanol mix (150 µl 5 M NaCl in 10 ml cold absolute ethanol) and incubating for 30 minutes at room temperature. The DNA precipitated as a filamentous network attached to the bottom of the well. The solution was removed by carefully inverting the plate and the DNA washed 3 times with 150 µl 70% ethanol.

2.11.4 Colony screening by southern blotting

Genomic DNA in the 96 well plates was digested in a humid chamber at 37 ^{0}C overnight with 30 µl per well of 330 U/ml genomic tested *Eco*RV (Promega), 1X *Eco*RV digestion buffer (Promega), 1X bovine serum albumin (BSA) (Promega), 100 µg/ml RNase (Promega) and 1 mM spermidine (Sigma). The contents of the well were only mixed after 2 – 4 hours of digestion to avoid mechanical breakage of genomic DNA. Next day, loading buffer was added to the wells and digested DNA electrophoresed in a 0.7% TBA agarose (Invitrogen) gel with ethidium bromide (Sigma) at 4 V/cm. After 2 – 3 hours the gel was analysed under UV light.

A DNA smear was visible. DNA in the gel was depurinated for 10 minutes with 0.25 M HCl and then denatured with 0.5 N NaOH for a further 45 minutes. A Zetaprobe GT membrane (BioRad) was pre-wet with H_2O for 2 minutes and then soaked in 0.5 N NaOH for 2 minutes. DNA in the agarose gel was transferred onto the membrane by capillary blotting overnight. Next day, membrane and DNA were cross linked then neutralized with 2x SSC (0.3 M NaCl, 0.03 M sodium citrate, 0.1 mM EDTA) for 20 minutes. After that, the membrane was incubated with a specific ^{32}P dCTP labeled probe in hybridization solution (5X SSC, 5X Denhardt's solution, 40% formamide, 0.5% SDS) overnight at 60^0C. The following day, membranes were washed with 2x SSC + 1% SDS, exposed to Phospho Image plate (Fujifilm) and scanned with Phospho Image Scanner (Fujifilm).

Table 6 - Sequence of primers used for RT-PCR, QRT-PCR, cloning and sequencing

Primer Name	Sequence (5'-3')	#	Gene	Comment
18S QRT F	GCCGCTAGAGGTGAAATTCTTG	**1**	18S	For mouse and human (taqman)
18S QRT R	CATTCTTGGCAAATGCTTTCG	**2**	18S	For mouse and human (taqman)
AKR1C12 QRT F	TTTGTGATGTGGCCAAAAGG	**3**	Akr1c12	Designed for mouse gene (taqman)
AKR1C12 QRT R	GGCACAATCCCACGTTGAA	**4**	Akr1c12	Designed for mouse gene (taqman)
AKR1C13 QRT F	ATCATGGCTTCTGCCTGATGT	**5**	Akr1c13	Designed for mouse gene (taqman)
AKR1C13 QRT R	ACAAGTCCATCCAACAGTCCATCT	**6**	Akr1c13	Designed for mouse gene (taqman)
AKR1C14 QRT F	CTACGGATGATTGTGAATCACCAT	**7**	Akr1c14	Designed for mouse gene (taqman)
AKR1C14 QRT R	GGCACTTGCTGCTCTAACAGAA	**8**	Akr1c14	Designed for mouse gene (taqman)
AKR1C18 QRT F	GCCCTTGCCACGAGTTCTATTA	**9**	Akr1c18	Designed for mouse gene (taqman)
AKR1C18 QRT R	GGAGGCGGTGTGTCGAGTT	**10**	Akr1c18	Designed for mouse gene (taqman)
AKR1C19 QRT F	AGCAATGAGTTCCAAACAGCAA	**11**	Akr1c19	Designed for mouse gene (taqman)
AKR1C19 QRT R	CTGGTTTGTAGGTGCCAAAGC	**12**	Akr1c19	Designed for mouse gene (taqman)
AKR1C20 QRT F	AACGCCTGCGCTGATTG	**13**	Akr1c20	Designed for mouse gene (taqman)
AKR1C20 QRT R	GAAACTCTTGGCTAGGACCACAA	**14**	Akr1c20	Designed for mouse gene (taqman)
AKR1C21 QRT F	CCATGGCAAAAAAATATAATCGAACT	**15**	Akr1c21	Designed for mouse gene (taqman)
AKR1C21 QRT R	GACCACAATCCCACGCTGTA	**16**	Akr1c21	Designed for mouse gene (taqman)
AKR1C6 F	CGTCCAGAACTCGTACGG	**17**	Akr1c6	Designed for mouse gene (taqman)
AKR1C6 R	GAGGTACAGGTCCACATAGTCCAA	**18**	Akr1c6	Designed for mouse gene (taqman)
AKR1C6 QRT F	GATGACCTGAATAAAAATATCCGATACA	**19**	Akr1c6	Designed for mouse gene (taqman)
AKR1C6 QRT R	CCTCCAGTTAGTATTCATCCCAAAA	**20**	Akr1c6	Designed for mouse gene (taqman)
ACTA1 QRT F	CGACGGGCAGGTCATCA	**25**	α-actin1	Designed for mouse gene (taqman)
ACTA1 QRT R	CGATAAAGGAAGGCTGGAAGAG	**26**	α-actin1	Designed for mouse gene (taqman)
CMV FOR	CGCAAATGGGCGGTAGGCGTG	**27**	CMV promoter	For sequencing
COX1 QRT F	CCAGAACCAGGGTGTCTGTGT	**28**	Cox-1	Designed for mouse gene (taqman)
COX1 QRT R	GTAGCCCGTGCGAGTACAATC	**29**	Cox-1	Designed for mouse gene (taqman)
COX2 QRT F	TGACCCCCAAGGCTCAAATA	**30**	Cox-2	Designed for mouse gene (taqman)
COX2 QRT R	CCCAGGTCCTCGCTTATGATC	**31**	Cox-2	Designed for mouse gene (taqman)
DP1 QRT F	GTGGCCGCCTTCTGCTT	**32**	DP1	Designed for mouse gene (taqman)
DP1 QRT R	AGTACTGCACGAACTTCCCAAAA	**33**	DP1	Designed for mouse gene (taqman)
DP1 SCREEN F	GAAGTTCGTGCAGTACTGTCCAG	**34**	DP1	For DP1 receptor screening
DP1 SCREEN R	TCCACTATGGAAATCACAGAC	**35**	DP1	For DP1 receptor screening
DP1 RT F	TCTACCAAAGGCACGTCACCTT	**36**	DP1	For DP1 receptor screening
DP1 RT R	CGAACTTCCCAAAACCAGCA	**37**	DP1	For DP1 receptor screening

Primer Name	Sequence (5'-3')	#	Gene	Comment
DP2 QRT F	ATGCCCCGACATGTTGTACA	**38**	DP2	Designed for mouse gene (taqman)
DP2 QRT R	TCTTCTACCAGCACGCTTTCAA	**39**	DP2	Designed for mouse gene (taqman)
DP2 SCREEN F	CATGTGCTACTACAACTTGC	**40**	DP2	For DP2 receptor screening
DP2 SCREEN R	GCAGACTGAAGATGTGGTAGG	**41**	DP2	For DP2 receptor screening
GAPDH QRT F	GACGGCCGCATCTTCTTGT	**42**	Gapdh	Gapdh control (Taqman)
GAPDH QRT R	CACACCGACCTTCACCATTTT	**43**	Gapdh	Gapdh control (Taqman)
GAPDH FWD	TCAAGAAGGTGGTGAAGCAG	**44**	Gapdh / GAPDH	Gapdh control (human and mouse)
GAPDH REV	ACCACCCTGTTGCTGTAGCC	**45**	Gapdh / GAPDH	Gapdh control (human and mouse)
H PGDS QRT F	TTTAAAGCCTGGCTTGTTGGA	**46**	H-Pgds	Designed for mouse gene (taqman)
H PGDS QRT R	AATGGCAGGGATAGCTTGGA	**47**	H-Pgds	Designed for mouse gene (taqman)
L PGDS QRT F	CACTCGGGCAGCATCCA	**48**	L-Pgds	Designed for mouse gene (taqman)
L PGDS QRT R	TGAATAGCAGAGCGTACTCGTCAT	**49**	L-Pgds	Designed for mouse gene (taqman)
MYOD QRT F	TGGTTCTTCACGCCCAAAAG	**50**	MyoD	Designed for mouse gene (taqman)
MYOD QRT R	TCTGGAAGAACGGCTTCGAA	**51**	MyoD	Designed for mouse gene (taqman)
MYOG QRT F	GACCCTACAGACGCCCACAA	**52**	Myogenin	Designed for mouse gene (taqman)
MYOG QRT R	CATATCCTCCACCGTGATGCT	**53**	Myogenin	Designed for mouse gene (taqman)
POLYA R	GGGTCCATGGTGATACAAGG	**56**	PolyA seq.	For sequencing
PPARG QRT F	TGCCAGTTCGATCCGTAGAA	**61**	PPARγ	Designed for mouse gene (taqman)
PPARG QRT R	TCAAGGTTAATGAAACCAGGGATATT	**62**	PPARγ	Designed for mouse gene (taqman)
PPARG1 CL F	ATTACCATGGTTGACACAGAGATGCCATT	**63**	PPARγ	Designed for mouse gene (cloning)
PPARG1 SCR F	GGACCGAGTGTGACGACAAGAT	**64**	PPARγ1	Designed for mouse gene (screening)
PPARG CL R	TTTCCTGCTAATACAAGTCCTTGTAGATC	**65**	PPARγ1/2	Designed for mouse gene (cloning)
PPARG1/2 SCR R	AGCTGATTCCGAAGTTGGTGG	**66**	PPARγ 1/2	Designed for mouse gene (screening)
PPARG2 CL F	TTTATGCTGTTATGGGTGAAACTCTGGGA	**67**	PPARγ 2	Designed for mouse gene (cloning)
PPARG2 SCR F	TTCTCCTGTTGACCCAGAGCAT	**68**	PPARγ 2	Designed for mouse gene (screening)
SP6 PROMOTER	ATTTAGGTGACACTATAG	**71**	SP6 promoter	For sequencing
T7 PROMOTER	TAATACGACTCACTATAGGG	**72**	T7 promoter	For sequencing
T7 TERMINATOR	GCTAGTTATTGCTCAGCGG	**73**	T7 terminator	For sequencing

Table 7 - Sequence and modifications of probes used for Taqman QRT-PCR

Gene	Sequence	Mod 3' (quencher)	Mod 5' (fluorochrome)	Forward primer	Reverse Primer
18S	TCTGGTCCGTCTTGCGCCGG	5-TAMRA	VIC	1	2
Akr1c12	AAGCCCTGCCCTAATTGCACTTCGAT	5-TAMRA	6-FAM	3	4
Akr1c13	TGTGTGTGGACAGTGATGCTGGCAATATG	5-TAMRA	6-FAM	5	6
Akr1c14	TGGGCACTGGGAGCCAAACCTAAGT	5-TAMRA	6-FAM	7	8
Akr1c18	TTGTGTGATGCTGGACTCTCAGATGCC	5-TAMRA	6-FAM	9	10
Akr1c19	ATGGCAACTTCATCCCTGCGCTG	5-TAMRA	6-FAM	11	12
Akr1c20	CCTTCGCTACCAGGTGCAACGTGG	5-TAMRA	6-FAM	13	14
Akr1c21	CAGCCTTGATTGCCCTTCGCTACCA	5-TAMRA	6-FAM	15	16
Akr1c6	AAGTGGTTCTAGCTTTAAGGACCATCCTGATTTTCC	5-TAMRA	6-FAM	19	20
COX-2	TTGCCCAGCACTTCACCCATCAGTT	5-TAMRA	6-FAM	30	31
DP2	CGCTCGCTACGCGCGGTG	5-TAMRA	6-FAM	38	39
Gapdh	CAGTGCCAGCCTCGTCCCGTAGA	BHQ-1	6-JOE	42	43
H-PGDS	ATCTACCCCAAACTGGTGTCATTACGGAACAAA	5-TAMRA	6-FAM	46	47
L-PGDS	TCCGTGTCAGTGGTGGAGGCCA	5-TAMRA	6-FAM	48	49
MyoD	TGAAGCTTAAATGACACTCTTCCCAACTGTCC	5-TAMRA	6-FAM	50	51
Myogenin	CTGCACTCCCTTACGTCCATCGTGG	5-TAMRA	6-FAM	52	53
PPARγ	CCGTGCAAGAGATCACAGAGTATGCCAA	5-TAMRA	6-FAM	61	62
α-actin	AGCGTTTCCGTTGCCCGGAGA	5-TAMRA	6-FAM	25	26

5-TAMRA, 5-tetramethylrhodamine
6-FAM, carboxyfluorescein
BHQ-1, black hole quencher
6-JOE, 6-Carboxy-4',5'-dichloro-2',7'-dimethoxyfluorescein

CHAPTER THREE: Screening for PGD_2-reductase activity amongst the mouse AKR1C enzymes

In humans, AKR1C3 is the only isoform of the AKR1C subfamily capable of catalysing the 11β-ketoreduction of PGD_2 to 11β-$PGF_{2\alpha}$. In myeloid leukaemia cells, this activity promotes proliferation and resistance to differentiation making AKR1C3 a novel therapeutic target (see section 1.3.7). Mice however have eight AKR1C isoforms and it is not known which, if any, is the homologue of AKR1C3.

3.1 Phylogenetic analysis of the AKR1C subfamily

3.1.1 Comparison of human and murine AKR1C gene clusters

According to the AKR superfamily nomenclature system, members of the same subfamily, such as the AKR1C subfamily, share a minimum of 60% amino-acid sequence identity. All AKR1C isoforms from human and mouse are coded in gene clusters on chromosomes 10 and 13, respectively (scale comparison of both clusters is shown in Figure 38). In both clusters, all AKR1C genes have an identical exon-intron organization. However, the phylogenetic relationship between enzymes of both species can not be inferred by merely analysing the organization of the gene clusters.

3.1.2 Amino-acid sequence alignment of human and murine AKR1C enzymes

Higher conservation of amino-acid sequence often reflects a conserved function between two proteins. The loci syntenic to that of the human AKR1C gene cluster was analysed in the genomes of chimpanzee (*Pan troglodytes*), macaque (*Macaca fuscata*), bull (*Bos taurus*), horse (*Equus ferus*), dog (*Canis familiaris*), rat (*Rattus norvegicus*) and mouse (*Mus musculus*) using the Ensembl database (Hubbard et al., 2009). The amino-acid sequence of all known and predicted AKR proteins coded in the loci was obtained. The rabbit (*Oryctolagus cuniculus*) genome was not annotated in the Ensembl database but one AKR1C enzyme (-1C5) had been previously described and is listed on the AKR homepage database

(Wintergalen et al., 1995). A total of 62 sequences were obtained from which only 24 had been previously described at the AKR homepage (Table 8). The AKR amino-acid sequences were aligned using the ClustalW algorithm and a phylogram was generated from this alignment using the TreeView X software (Figure 37).

Interestingly, not all AKR sequences in these clusters belonged to AKR1C subfamily. All species have at least one gene in their cluster encoding an AKR1E member (less than 60% sequence identity with the remaining) from which only mouse AKR1E1 and human AKR1E2 had been previously reported (Sakuma and Kubota, 2008). Note that from the three AKR genes in the dog (*Cf*) cluster, two encode enzymes of the AKR1E subfamily (AKR1CL2 and AR1). On the other hand, the remaining species have only one AKR1E and several AKR1C enzymes.

Closely related to the AKR1E isoforms is a group of AKR1C enzymes that has been poorly described. This includes rat (*Rn*) AKR1C15, three horse (*Ef*) enzymes (XP_001500212.1, XP_001500201.2 and XP_001500793.2) and AKR1CL1 from human (*Hs*), chimpanzee (*Pt*) and macaque (*Mf*). Apart from the cloning of rat AKR1C15 (Qin and Cheng, 1994) no other reports have focused on these enzymes. Bull (*Bt*) and mouse (*Mm*) do not have any enzyme in this group. As mentioned previously, human *AKR1CL1* is labeled as a pseudogene in the NCBI database.

The four human isoforms (AKR1C1-1C4) have an average of 88% amino-acid sequence identity amongst them hence the proximity in the phylogram. In fact, AKR1C isoforms from human, chimpanzee and macaque are all closely related suggesting a recent common ancestor in the primate order. Chimpanzee and macaque have 3 AKR1C isoforms while humans have 4. This is most likely due to a gene duplication occurring in humans that gave rise to AKR1C1 and -1C2 (97% sequence similarity). For AKR1C3 and -1C4 there seems to be a closely related homologue in the three primate species.

In contrast to the close kinship of the human AKR1C enzymes, murine isoforms appear to be far more diverse. Rodent enzymes have high variability amongst them suggesting that their enlarged array of AKR1C proteins has multiple ancestral origins (Figure 37). In most cases, mouse enzymes have one-to-one homologues with rat isoforms, for example rat AKR1C8 and mouse AKR1C18, which are believed to be functional homologues (Miura et al., 1994, Maho

Ishida, 1999). Nevertheless, some mouse and rat-specific gene duplications are observed. Importantly, this analysis did not reveal any clear evolutionary homologues between individual human and murine AKR1C enzymes.

As in primates, all AKR1C isoforms found in bull and horse are closely related with isoforms of the same species. This suggests that duplication and diversification of AKR1C genes has occurred after radiation of the several mammalian orders.

Another interesting finding is that the positioning of the AKR1C genes in the human and mouse genomic cluster strikingly recapitulates the phylogeny of the coded enzymes (Figure 38). Genes coding for AKRs with higher sequence identity were found to sit in close proximity, a likely record of the gene duplication history in the origin of the clusters.

In conclusion, this analysis revealed high evolutionary divergence amongst mammalian AKR1C enzymes. Human enzymes appear to have arisen from gene duplication events occurring after the divergence between primates and rodents and thus, one-to-one homologies can not be identified.

Table 8 - List of AKR proteins encoded in the AKR1C gene cluster of several mammalian species.

Species	Designation in Ensembl	Alternative designations	Described in AKR homepage?	Subfamily
Bos taurus	AKR1C3		no	1C
Bos taurus	NP_001030444.1		no	1C
Bos taurus	DDBX_BOVIN	AKR1C11	yes	1C
Bos taurus	NP_001033673.1		no	1C
Bos taurus	PGFS2_BOVIN	AKR1C7	yes	1C
Bos taurus	IPI00903711.1		no	1C
Bos taurus	IPI00837681.2		no	1C
Bos taurus	Q8HZ63_BOVIN		no	1C
Bos taurus	LOC785996		no	1C
Bos taurus	IPI00697013.4		no	1E
Canis familiaris	AKR1C3		no	1C
Canis familiaris	AKR1CL2		no	1E
Canis familiaris	AR1		no	1E
Equus ferus	AK1CN_HORSE	AKR1C23	yes	1C
Equus ferus	XP_001500212.1		no	1C
Equus ferus	XP_001500201.2		no	1C
Equus ferus	XP_001500793.2		no	1C
Equus ferus	XP_001500932.2		no	1C
Equus ferus	XP_001916998.1		no	1C
Equus ferus	XP_001500971.1		no	1C
Equus ferus	XP_001500834.1		no	1C
Equus ferus	XP_001501068.1		no	1C
Equus ferus	XP_001501043.1		no	1C
Equus ferus	XP_001500336.1		no	1C
Equus ferus	AK1CO_HORSE		no	1C
Equus ferus	AKR1CL2		no	1E
Homo sapiens	AKR1C1		yes	1C
Homo sapiens	AKR1C2		yes	1C
Homo sapiens	AKR1C3		yes	1C
Homo sapiens	AKR1C4		yes	1C
Homo sapiens	AKR1CL1		no	1C
Homo sapiens	AKR1CL2	AKR1E2	yes	1E

| Species | Designation in Ensembl | Alternative designations | Described in AKR homepage? | Subfamily |

Macaca fuscata	AKR1C3		no	1C
Macaca fuscata	AKR1C4	AKR1C25	yes	1C
Macaca fuscata	AKR1CL1		no	1C
Macaca fuscata	AKR1CL2		no	1E
Mus musculus	AKR1C14		yes	1C
Mus musculus	AKR1C20		yes	1C
Mus musculus	AKR1C6		yes	1C
Mus musculus	AKR1C12		yes	1C
Mus musculus	AKR1C13		yes	1C
Mus musculus	AKR1C19		yes	1C
Mus musculus	AKR1C18		yes	1C
Mus musculus	AKR1C21		yes	1C
Mus musculus	AKR1E1		yes	1E
Oryctolagus cuniculus	n/a	AKR1C5	yes	1C
Pan troglodytes	XM_001143407.1		no	1C
Pan troglodytes	AKR1C3		no	1C
Pan troglodytes	AKR1C4		no	1C
Pan troglodytes	AKR1CL1		no	1C
Pan troglodytes	AKR1CL2		no	1E
Rattus norvegicus	NP_001103370.1	AKR1C15	yes	1C
Rattus norvegicus	NP_001028869.1	AKR1C1	no	1C
Rattus norvegicus	AKR1C12	AKR1C16	yes	1C
Rattus norvegicus	NP_001129216.1	AKR1C17	yes	1C
Rattus norvegicus	NP_001014262.3	AKR1C24	yes	1C
Rattus norvegicus	NP_001094046.1	AKR1C19	no	1C
Rattus norvegicus	AK1CH_RAT	AKR1C8	yes	1C
Rattus norvegicus	AK1CL_RAT	AKR1C21	no	1C
Rattus norvegicus	DIDH_RAT	AKR1C9	yes	1C
Rattus norvegicus	AKCL2_RAT	AKR1CL2	no	1E

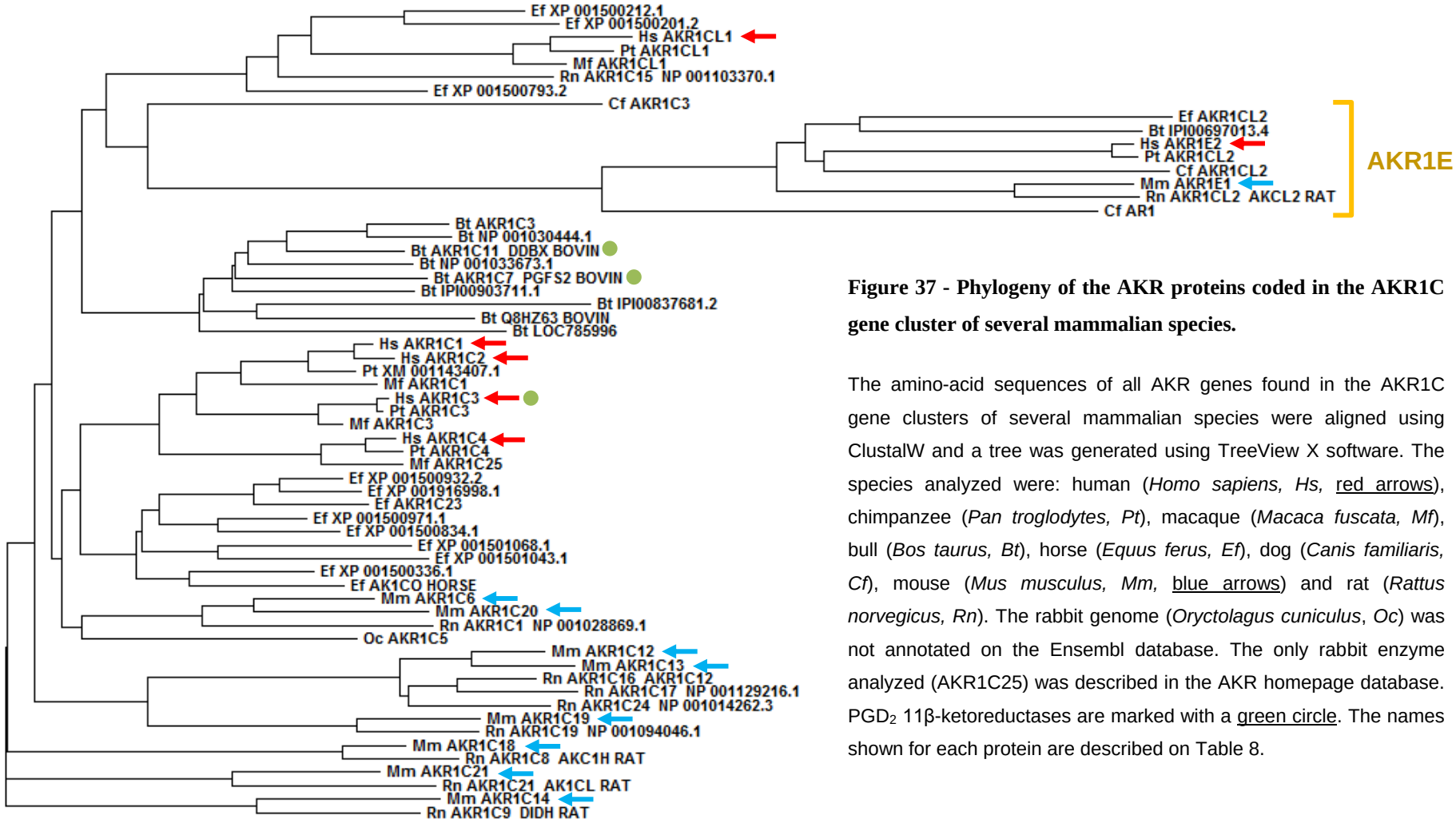

Figure 37 - Phylogeny of the AKR proteins coded in the AKR1C gene cluster of several mammalian species.

The amino-acid sequences of all AKR genes found in the AKR1C gene clusters of several mammalian species were aligned using ClustalW and a tree was generated using TreeView X software. The species analyzed were: human (*Homo sapiens, Hs,* red arrows), chimpanzee (*Pan troglodytes, Pt*), macaque (*Macaca fuscata, Mf*), bull (*Bos taurus, Bt*), horse (*Equus ferus, Ef*), dog (*Canis familiaris, Cf*), mouse (*Mus musculus, Mm,* blue arrows) and rat (*Rattus norvegicus, Rn*). The rabbit genome (*Oryctolagus cuniculus*, *Oc*) was not annotated on the Ensembl database. The only rabbit enzyme analyzed (AKR1C25) was described in the AKR homepage database. PGD_2 11β-ketoreductases are marked with a green circle. The names shown for each protein are described on Table 8.

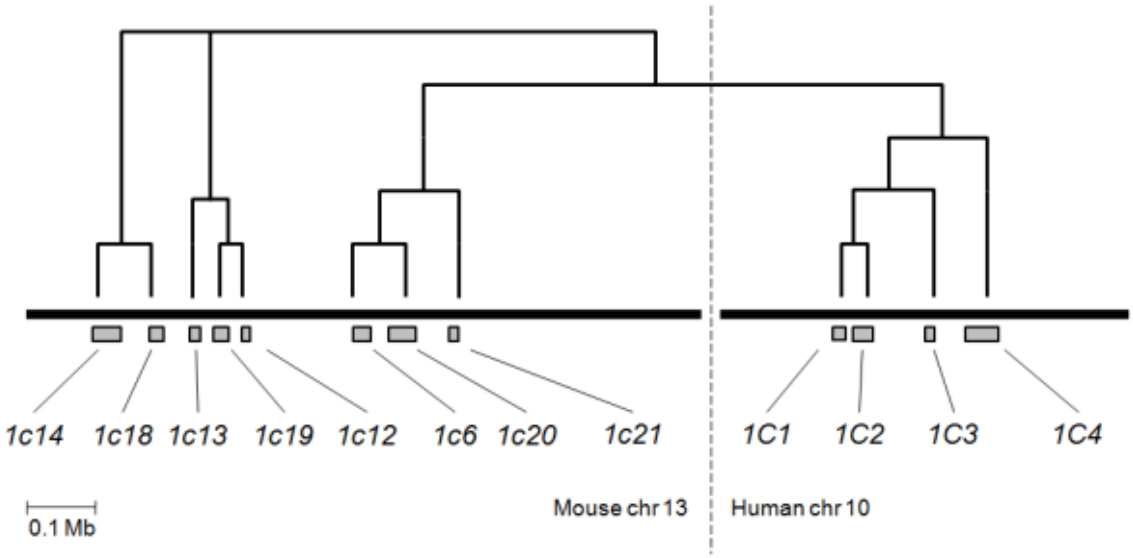

Figure 38 – Relationship between phylogeny and gene positioning of the human and mouse AKR1C cluster.

Position of AKR1C genes in chromosome reflects phylogenetic relationships. Scale representation of murine (chromosome 13) and human (chromosome 10) AKR1C gene clusters. Grey boxes represent individual genes.

3.2 Production of recombinant murine AKR1C proteins

The phylogenetic analysis of the AKR1C subfamily revealed high evolutionary divergence between human and murine isoforms. Nevertheless, this does not rule out the existence of a PGD_2 11β-ketoreductase amongst the murine enzymes since bovine isoforms AKR1C7 and -1C11 with low identity with AKR1C3 also have this activity. In order to test if the mouse AKR1C enzyme can reduce PGD_2, purified His-tagged recombinant proteins were generated for the eight mouse isoforms.

The open reading frames of the eight AKR1C isoforms were amplified from a panel of mouse tissues and cell line cDNAs (see Table 4). The amplified coding regions were cloned into the expression vector pET28b. Figure 39 shows the cloning process of *Akr1c14* and is representative of the remaining isoforms. Correct cloning was confirmed by nucleotide sequencing before over-expression of the protein in *E. coli* strain BL21. The expressed recombinant protein was isolated by affinity column purification taking advantage of a 6xHis tag introduced in the N-terminus of the protein. To achieve a greater level of purity, the protein was further purified by fast protein liquid chromatography (FPLC). Purity of the recombinant proteins was assessed by SDS-PAGE as shown in Figure 40. Cloning and production of human recombinant AKR1C proteins had been previously performed by Dr N Davies and Dr J Ride.

Amplification of the *Akr1c18* coding region resulted in two products: the expected product containing the full coding region and a product lacking exon 4 (as confirmed by nucleotide sequencing). The apparent splice variant lacking exon 4 did not yield any recombinant protein after over-expression suggesting it formed an unstable product. The complete coding region of *Akr1c18* resulted in production of reasonable levels of recombinant protein. However, the total amount of AKR1C18 produced was much what was obtained for the remaining recombinant AKRs for reasons that were not determined.

To test for activity, recombinant proteins were incubated with NADPH and phenanthrenequinone (PQ), a synthetic compound with two carbonyl groups, commonly used to detect AKR-mediated reduction (Penning et al., 2000, Byrns et al., 2008, Suzuki et al., 1999, Chen et al., 1992). Consumption of NADPH was monitored spectrophotometrically as

shown in Figure 41. All recombinant AKRs consumed NADPH in the presence of PQ. This assay was routinely used to assess the integrity of the recombinant enzymes.

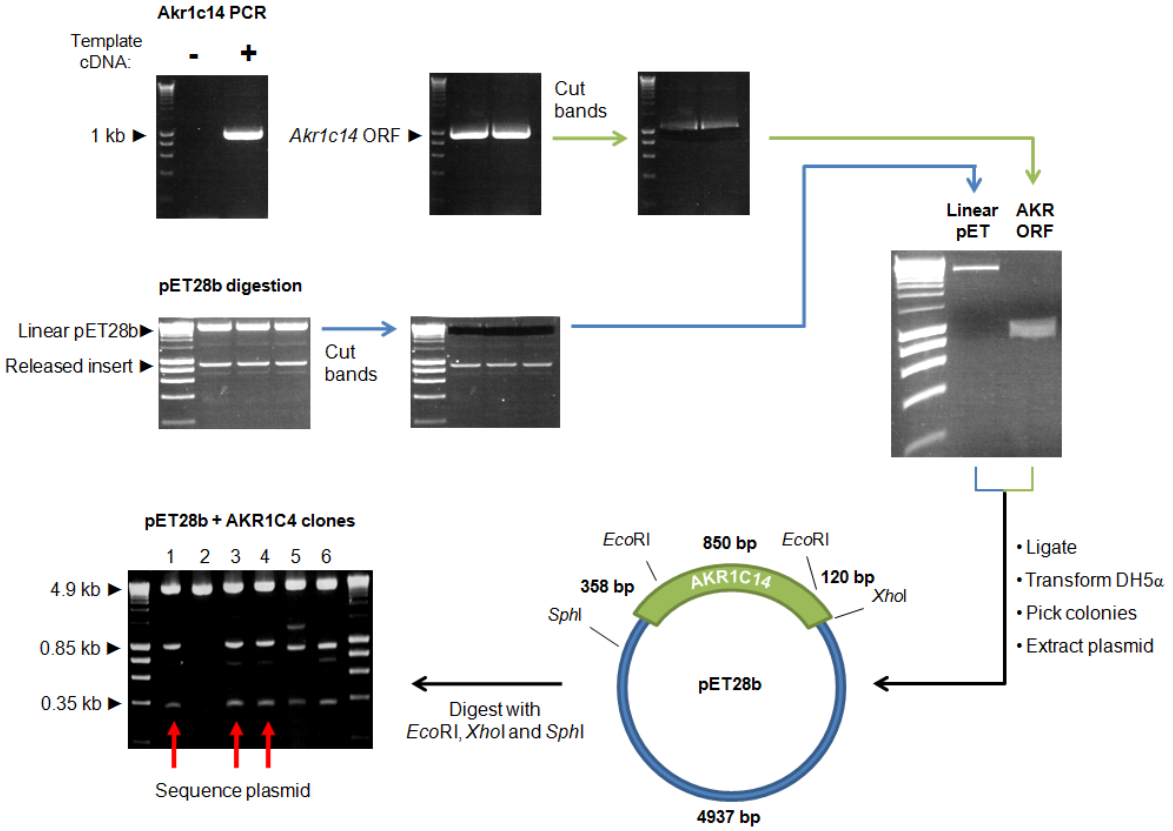

Figure 39 - Cloning AKR1C14 open reading frame into pET28b

This scheme is representative for the cloning of all AKRs. The open reading frame (ORF) of *Akr1c14* was amplified by PCR from total C2C12 cDNA. The ~1 kb product was purified, digested (*Nde*I, *Xho*I) and purified. The expression vector pET28-b was linearised (*Nde*I, *Xho*I) and gel purified. Purified vector and insert have compatible cohesive ends and were ligated. Ligation products were transformed into competent bacteria (DH5α), colonies were picked, expanded and plasmid DNA extracted. Correct cloning was firstly analysed by restriction pattern. In this example, digestion with *Sph*I, *Eco*RI and *Xho*I allowed the identification of three clones with the expected pattern (red arrows). The selected plasmids were sequenced to confirm correct cloning of the AKR ORF.

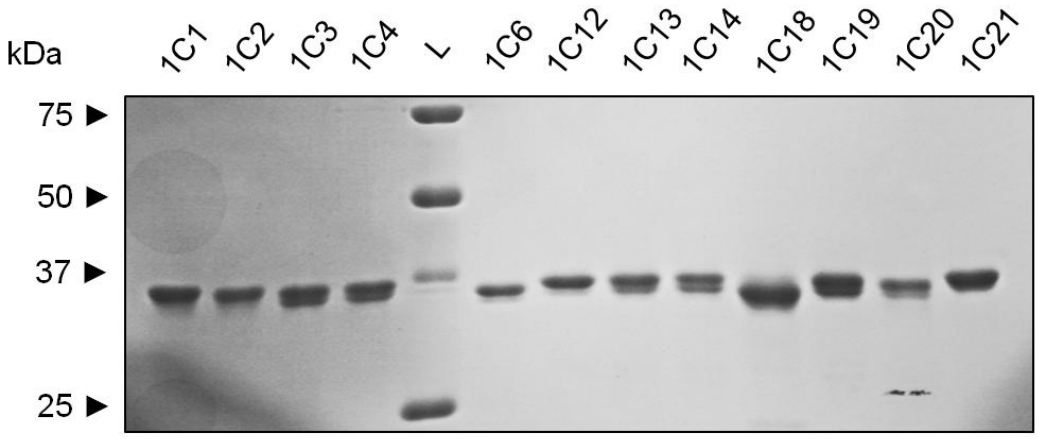

Figure 40 - SDS-PAGE of purified recombinant AKR1C proteins

Purity of recombinant AKR1C proteins was assessed by SDS-PAGE followed by Coomassie Blue staining. 3 µg of recombinant AKR was loaded in each lane before separation in a 12% SDS-polyacrylamide gel. L: ladder.

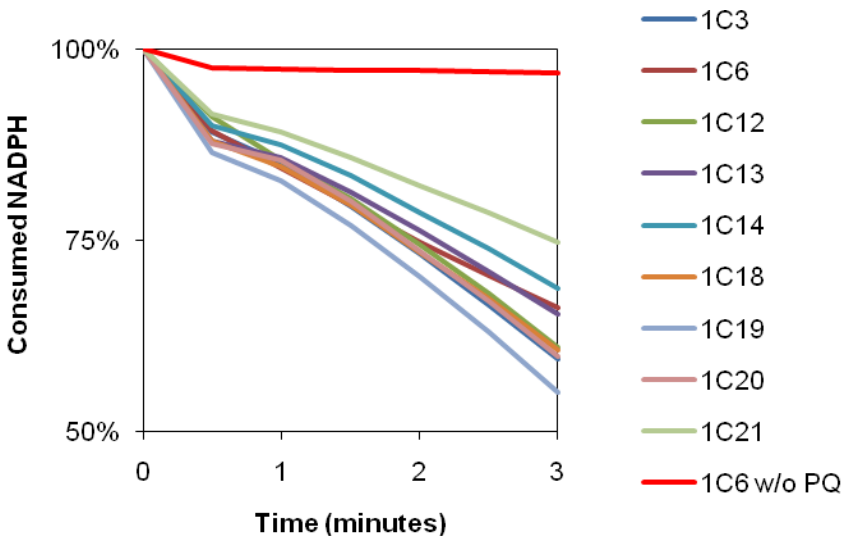

Figure 41 - Recombinant AKR1C enzymes have activity against phenanthrenequinone (PQ)

Purified recombinant AKR1C enzymes were incubated with NADPH and phenanthrenequinone (PQ), a synthetic compound with two carbonyl groups that is reduced by AKR enzymes. Reduction of PQ was assessed by monitoring the consumption of NADPH in a spectrophotometric assay. Absence of PQ resulted in no consumption of NADPH (red line).

3.3 Activity of murine AKR1C enzymes against PGD_2

The purified recombinant enzymes were then used to determine which of the murine isoforms, if any, has PGD_2 reductase activity. Recombinant AKRs were incubated with NADPH and [^{3}H]-PGD_2 at 37 ºC for four hours. The products were extracted and separated by thin layer chromatography (TLC) along with known standards for PGD_2, 15d-PGJ_2 and 11β-$PGF_{2\alpha}$ (as detailed on page 95). Each lane of the TLC plate was scanned to identify the position of the radio-labeled products. A representative set of traces is shown in Figure 42.

A trace of non-incubated radio-labeled substrate (hot standard) shows a major peak, co-migrating with PGD_2, and a smaller peak co-migrating with 15d-PGJ_2, which is the result of spontaneous dehydration. Incubation of PGD_2 in buffer without enzyme results in increased spontaneous generation of 15d-PGJ_2. Human AKR1C3 was used as positive control, as this enzyme was able to efficiently convert PGD_2 to a product co-migrating with 11β-$PGF_{2\alpha}$ and prevent further 15d-PGJ_2 generation. When PGD_2 was incubated with the murine AKR1C enzymes no 11β-ketoreduction or any other type of modification was observed. This result was obtained with different batches of recombinant enzymes. An alternative assay measuring the consumption of NADPH (detailed on page 96) also showed that, unlike AKR1C3, murine AKR1C enzymes do not use PGD_2 as a substrate (data not shown).

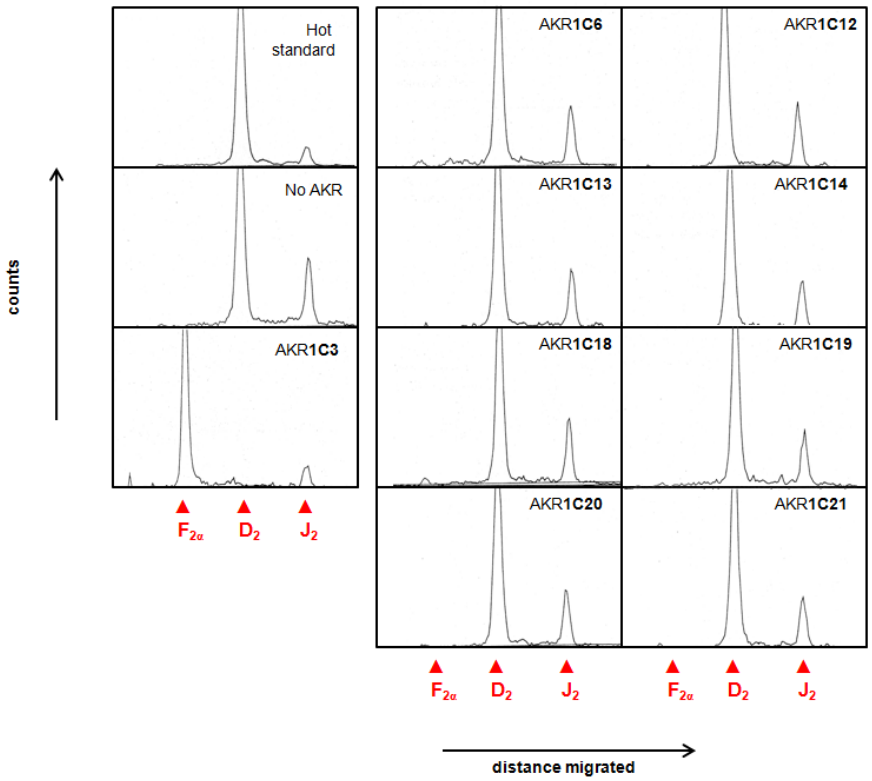

Figure 42 - Murine AKR1C enzymes do not reduce PGD_2

Human AKR1C3 and murine AKR1C6, -1C12, -1C13, -1C14, -1C18, -1C19, -1C20 and -1C21 were incubated with NADPH and [^{3}H]-PGD_2 at 37 °C for 4 hours. Reaction products were separated by thin layer chromatography and the lanes were scanned to detect radio-labeled species. The hot standard lane represents [^{3}H]-PGD_2 separated without incubation. Incubation of [^{3}H]-PGD_2 in the absence of AKR enzymes (no AKR) resulted in spontaneous dehydration into 15d-PGJ_2 (J_2). Human AKR1C3 converted PGD_2 (D_2) into 11β-$PGF_{2\alpha}$ ($F_{2\alpha}$) preventing the spontaneous generation of J_2. None of the murine AKR1C enzymes was able to reduce PGD_2 or modify it in any other way. This experiment was repeated several times with identical results.

3.4 Activity of murine AKR1C enzymes towards PGH_2 and PGE_2

Production of $PGF_{2\alpha}$ can be achieved by two other routes, the 9,11-endoperoxide reduction of PGH_2 and the 9-ketoreduction of PGE_2 (Figure 18). These two routes generate 11α-$PGF_{2\alpha}$ (simply denominated $PGF_{2\alpha}$), a stereoisomer of 11β-$PGF_{2\alpha}$ capable of activating the FP receptor with similar affinity. All these reductions are considered PGF synthase activities and are commonly performed by members of the AKR superfamily. Recently, the first three murine PGF synthases have been described. Two of the AKR1B subfamily (Kabututu et al., 2008) and one of the thioredoxin-like superfamily (Moriuchi et al., 2008). Because human AKR1C3, bovine AKR1C7 and AKR1C11 and rabbit AKR1C5 have PGF synthase activity the ability of murine AKR1C enzymes to reduce PGH_2 or PGE_2 was interrogated.

Incubation of murine enzymes with [^{3}H]-PGH_2 did not result in reduction or any other modification (data not shown). Incubation with [^{3}H]-PGE_2 revealed that only mouse AKR1C6 was able to perform the 9-ketoreduction to generate a product co-migrating with $PGF_{2\alpha}$ (Figure 43 A). These results were confirmed with the NADPH consumption assay (data not shown). This as yet undescribed PGF synthase activity of AKR1C6 occurred at a slow rate and was incomplete, as only ~ 40% of PGE_2 was reduced after 4 hours at which point the reaction reached equilibrium (Figure 43 B). This was not due to product inhibition since 0.05, 0.5, 5 and 50 μM $PGF_{2\alpha}$ did not impair AKR1C6-mediated reduction of PQ. Analysis of enzyme kinetics revealed that the AKR1C6-mediated reduction of PGE_2 was not only slow (k_{cat} = 0.24 ± 0.03 min^{-1}) but also occurred with low affinity (K_m = 73.1 ± 19.9 μM) (Figure 43 C). These parameters, however, are comparable to those described for another PGE_2 9-ketoreductase, rabbit AKR1C5 (Wintergalen et al., 1995).

3.4.1 K562 cells overexpressing AKR1C6 do not acquire PGE_2 reductase activity.

Given that AKR1C6 reduces PGE_2 with low efficiency *in vitro* it was interrogated if the artificial over-expression of AKR1C6 could confer PGE_2-reductase activity to cells. For over-expression an MSCV-IRES vector that produces a bicistronic mRNA with AKR1C6 and GFP was used (detailed on page 87). The co-expression of GFP with the gene of interest allows for the determination of transfection efficiency using flow cytometry. The cell line of choice was K562, since these cells are of human origin and therefore have no expression of AKR1C6, are easy to transfect and do not metabolise PGE_2 (Figure 44). Nevertheless, PGE_2 seems to be able to cross the membrane and enter the cytoplasm of K562 cells as radio-labelled product was identified inside cells (Figure 44, bottom pannel).

K562 cells were co-transfected with a vector coding for a truncated membrane protein H-2Kk and either MSCV-GFP (vector control) or MSCV-AKR1C6-GFP. Transient expression of H-2Kk allowed for the enrichment of transfected cells, as described on page 90. After enrichment, the proportion of GFP positive cells was 91% and 83% for MSCV-GFP and MSCV-AKR1C6-GFP, respectively (Figure 45 A). The over-expression of AKR1C6 was confirmed by RT-PCR, using mouse liver as a positive control (Figure 45 B). However, cells over-expressing AKR1C6 did not metabolise radio-labeled PGE_2 (Figure 45 C).

3.5 Discussion

In human AML cells AKR1C3 promotes cell proliferation and prevents differentiation by depleting PGD_2 from the cytosol. In order to produce an animal model to study the physiological role of AKR1C3 I have searched for a mouse AKR1C enzyme with PGD_2 11β-ketoreductase activity.

To date, 24 sequences are attributed to the AKR1C subfamily. In order to have a more comprehensive overview of the AKR1C phylogeny, all known and predicted AKR sequences coded in the human, chimpanzee, macaque, rat, horse and bull AKR1C gene clusters were aligned in order to generate a phylogenetic tree (Figure 37). The 38 additional AKR1Cs are predicted sequences that were obtained by screening the Ensembl database for AKR-coding genes in the loci homologous tho the human AKR1C gene cluster. The phylogenetic analysis revealed significant diversity amongst mammalian AKR1C enzymes. Isoforms were more

closely related to others of the same mammalian order (primate, rodent, etc.) suggesting the AKR1C enzymes have diversified later in mammalian evolution. Thus, this analysis failed to identify phylogenetic homologues between human and mouse AKR1C isoforms. Nevertheless, PGD_2 reductase activity seems to have evolved independently in at least two phylogenetic branches: the primate (AKR1C3) and the bovine (AKR1C7 and AKR1C11).

Therefore, the murine isoforms were screened for PGD_2 reductase activity using purified recombinant enzymes. Surprisingly, none of the murine AKR1C enzymes reduced PGD_2 suggesting this activity is absent in mice or is performed by an enzyme of another family (AKR or non-AKR). This result has strong implications in the modeling of AKR1C3 in mice since there is no apparent functional homologue that could be targeted for a knock-out. This also raises the question of how conserved are the remaining AKR1C functions, such as steroid metabolism and its implications in prostate, breast and endometrial tissues.

We have also identified that AKR1C6 has PGF synthase activity by catalysing the 9-ketoreduction of PGE_2. To date, the only AKR described as a PGE_2 reductase was AKR1C5, an enzyme expressed in the corpus luteum of rabbits (Wintergalen et al., 1995). Because AKR1C5 acted both as a PGF synthase and an inactivator of progesterone it was speculated that the enzyme plays a role in promoting the regression of the corpus luteum. In order to ascertain if AKR1C6 has a similar role in mouse physiology it is essential to determine its exact tissue expression pattern as well as its steroid metabolism properties.

The results so far have shown that human and murine AKR1C enzymes are highly divergent in sequence and prostaglandin metabolizing properties. The next stage was to fully characterize these enzymes for their steroid substrate preference and tissue expression.

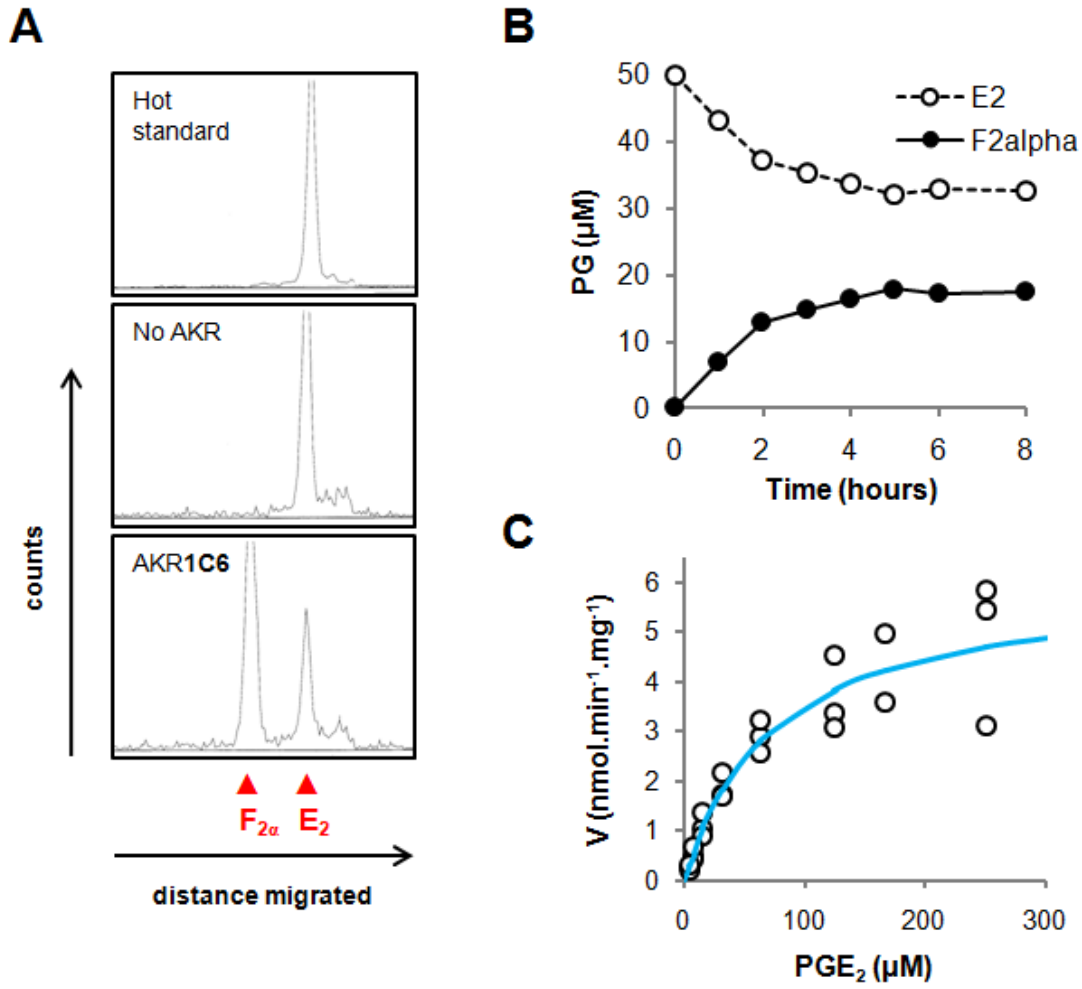

Figure 43 - Mouse AKR1C6 reduced PGE_2 to $PGF_{2\alpha}$

A: [^{3}H]-PGE_2 was incubated with NADPH for 6 hours at 37 ºC in the presence or absence of murine purified recombinant AKR1C enzymes. Products were extracted, separated by TLC and visualized as described on page 94. Non-incubated PGE_2 (hot standard) shows a peak co-migrating with PGE_2 (E_2). Incubation of PGE_2 without AKR does not result in spontaneous generation of other products. Incubation of PGE_2 with AKR1C6, but not other mouse or human AKR1C enzymes, resulted in generation of a product co-migrating with $PGF_{2\alpha}$ ($F_{2\alpha}$). **B:** Reduction of PGE_2 to $PGF_{2\alpha}$ by AKR1C6 was incomplete reaction with only 40% of conversion at equilibrium after 4 hours incubation. **C:** Michaelis-Menten curve for the reduction of PGE_2 by AKR1C6. Incubation with increasing concentrations of PGE_2 was stopped 1 hour after addition of enzyme and reaction rates were calculated. Data was fitted to a Michaelis-Menten curve using Visual Enzymics. Dots represent biological replicates for each concentration.

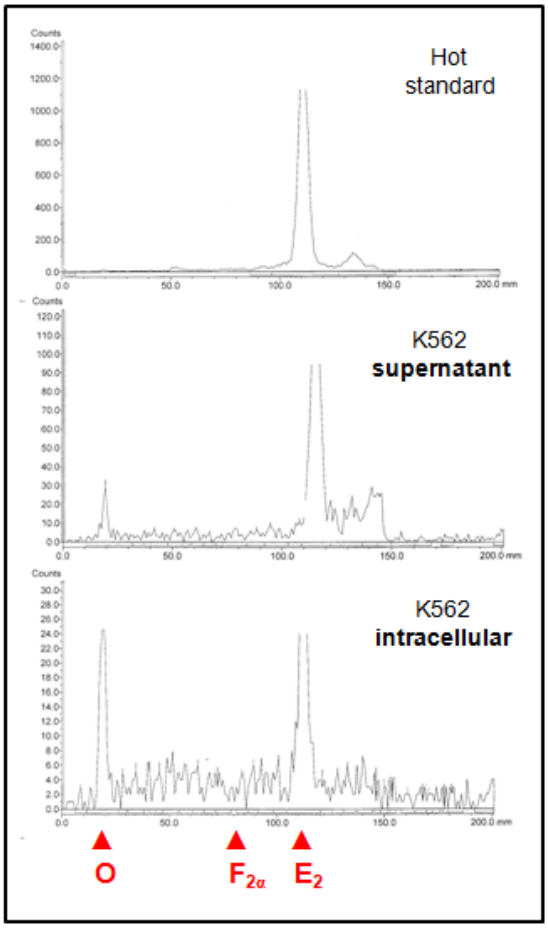

Figure 44 - K562 cells do not metabolise PGE_2

$5x10^6$ K562 cells were resuspended in 200 µl PBS with 5 µCi [^{3}H]-PGE_2 and incubated at 37 ºC overnight. Prostanoids were extracted from supernatant and cells and analysed by TLC. Although K562 did not metabolise PGE_2, the radio-label was found inside the cells suggesting PGE_2 can enter the cytoplasm of K562.

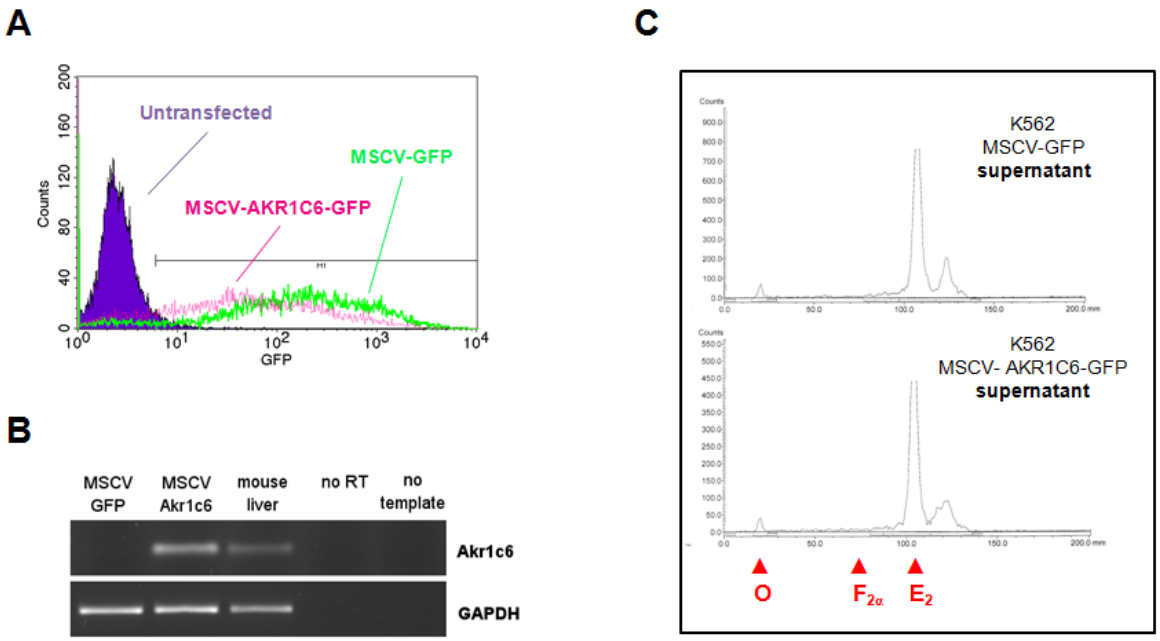

Figure 45 - Ectopic expression of AKR1C6 in K562 does not confer PGE_2 reductase activity

A: K562 cells were co-transfected with plasmids encoding for the membrane protein H-2Kk and with MSCV-GFP or MSCV-AKR1C6-GFP. Transfected cells were purified by affinity column taking advantage of the transient expression of the H-2Kk protein (detailed on page 90). Transfection efficiency was assessed by measuring GFP fluorescence in a flow cytometer. Purple filled curve: untransfected K562. Green line: MSCV-GFP (91% GFP^{+ve}). Pink line: MSCV-AKR1C6-GFP (83% GFP^{+ve}). **B:** Expression of AKR1C6 was measured by RT-PCR. Mouse liver cDNA was used as a positive control. **C:** Transfected K562 were incubated with radio-labeled PGE_2 overnight and analysed by TLC. Over-expression of AKR1C6 did not confer PGE_2 metabolizing activity to K562.

CHAPTER FOUR: Unveiling the differences between human and murine AKR1C enzymes

4.1 Activity of human and murine AKR1C enzymes towards steroids

Most AKR1C enzymes have hydroxysteroid dehydrogenase (HSD) activity, reducing carbonyl groups at position 3 (3α/β-HSD), 17 (17β-HSD) or 20 (20α-HSD). These enzymes are responsible for the tissue-specific activation or inactivation of steroids, thus regulating the transcriptional activity of steroid hormone receptors. In order to find functional homologies, human and murine AKR1C enzymes were characterised for their ability to reduce androstanedione, 5α-dihydrotestosterone (5α-DHT), estrone and progesterone.

4.1.1 Screen for steroid reducing activities

A spectrophotometric assay was used to measure the real-time consumption of NADPH (described on page 94), an indirect measure of the reduction reaction. However, using this assay, the reaction products can not be identified. The possible products for each reaction are shown in Figure 46. Androstanedione, a steroid precursor, has two carbonyl groups in positions 3 and 17. Reduction at position 3 yields androsterone, a weak androgen, whilst reduction at position 17 yields 5α-DHT, a potent androgen. Reduction at both sites results in androstanediol, a weak androgen or an estrogen depending upon wether the hydroxyl group is in the α or β orientation, respectively. Reduction of progesterone at position 20 to 20α-dihydroxyprogesterone results in its inactivation. Estrone when reduced at position 17 yields 17β-estradiol, a potent estrogen. These steroids were incubated with the human and murine recombinant AKR1C enzymes to detect reduction activity. Results are summarized in Table 9.

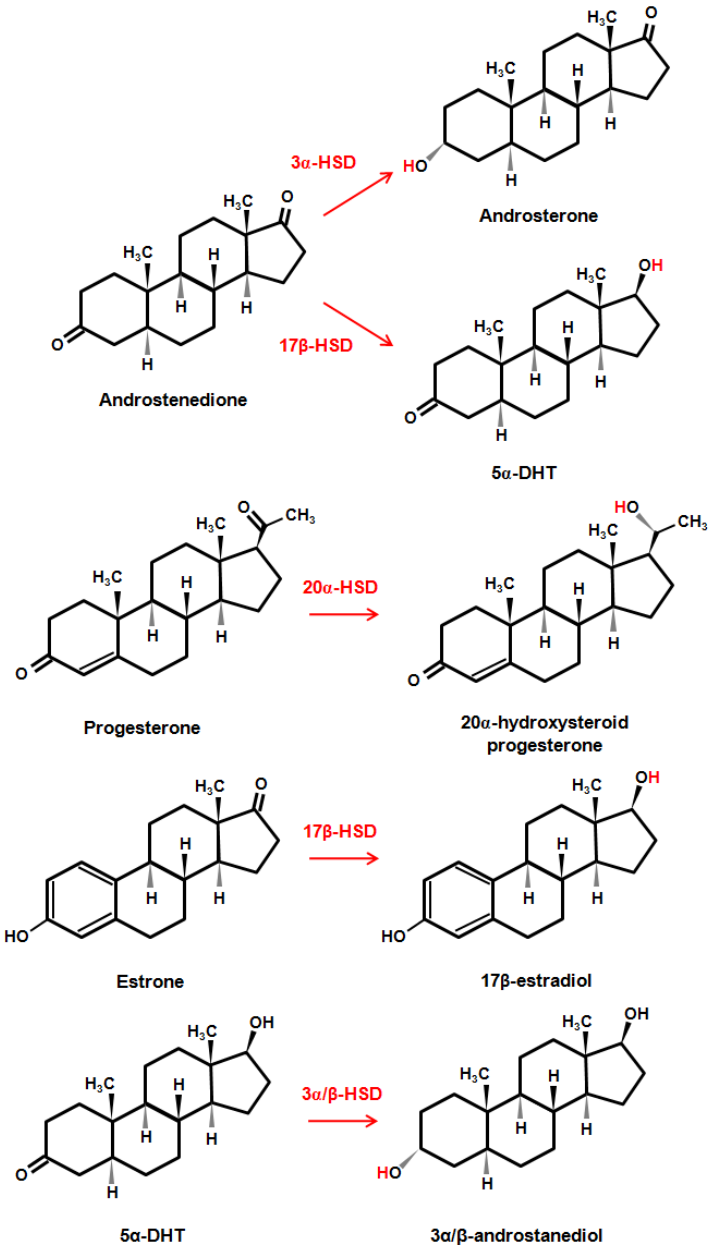

Figure 46 - Steroid reduction reactions.

A panel of steroids was used as test substrates for human and murine AKR1C enzymes. Androstanedione, an inactive steroid precursor, can be converted to the weak androgen androsterone (3α-HSD) or the potent androgen 5α-DHT (17β-HSD). Progesterone can be inactivated to 20α-dihydroxyprogesterone (20α-HSD). Estrone can be converted to the potent estrogen 17β-estradiol (17β-HSD). The potent androgen 5α-DHT can be inactivated to the weak androgen 3α-androstanediol or the estrogen 3β-androstanediol (3α/β-HSD).

Androstanedione (adione) was reduced by all human enzymes, with AKR1C2 and AKR1C4 being the most efficient (k_{cat}/K_m = 795 and 627 $min^{-1}.mM^{-1}$, respectively). Murine AKR1C6 and AKR1C21 were the only isoforms with detectable androstanedione reduction activity. However, the kinetic profile of AKR1C21 did not fit a Michaelis-Menten curve, with reaction velocities increasing until ~ 6 μM adrostanedione (~ 4 min^{-1}) followed by a decrease.

Reduction of estrone to 17β-estradiol was not detected amongst the human enzymes with this assay. However, murine AKR1C6 and AKR1C18 were able to reduce estrone with relatively high efficiency (k_{cat}/K_m = 452 and 652 $min^{-1}.mM^{-1}$, respectively).

Reduction of progesterone to its 20α-hydroxy form was detected with AKR1C4, -1C3 and -1C1, the latter being the most efficient (k_{cat}/K_m = 421 $min^{-1}.mM^{-1}$). Amongst the murine isoforms, AKR1C6, -1C18 and -1C20 were able to reduce progesterone with different efficiencies (k_{cat}/K_m = 192, 1080 and 138 $min^{-1}.mM^{-1}$, respectively). It should be noted that in spite of its relatively low affinity (K_m = 105.7 μM) AKR1C18 showed rapid turn over of progesterone (114.12 min^{-1}).

Reduction of 5α-DHT was detected for all human isoforms except AKR1C3. Efficiency was highest with AKR1C4, followed by -1C2 and -1C1 (k_{cat}/K_m = 1096, 472 and 146 $min^{-1}.mM^{-1}$, respectively). Murine AKR1C18 was capable of reducing 5α-DHT with extremely high efficiency (k_{cat}/K_m = 5746 $min^{-1}.mM^{-1}$). AKR1C6 and AKR1C21 also showed activity towards 5α-DHT but, once again, the kinetic profile of AKR1C21 did not fit a Michaelis-Menten curve with reaction velocity peaking at ~ 15 μM (~ 4 min^{-1}) followed by a decrease with higher substrate concentrations.

These results show that despite androstanedione, progesterone, estrone and 5α-DHT being used by human and murine enzymes there are no clear functional homologues in terms of substrate preference.

Table 9 - Kinetic parameters for the NADPH-dependent reduction of steroid hormones by purified recombinant murine AKR isoforms

Enzyme	K_m (μM)	k_{cat} (min^{-1})	k_{cat}/K_m ($min^{-1}.mM^{-1}$)	Enzyme	K_m (μM)	k_{cat} (min^{-1})	k_{cat}/K_m ($min^{-1}.mM^{-1}$)
Adione				**Estrone**			
AKR1C1	35.9 ± 4.4	5.24 ± 0.36	146	AKR1C1	na	na	na
AKR1C2	1.9 ± 0.7	1.51 ± 0.10	795	AKR1C2	na	na	na
AKR1C3	3.8 ± 1.0	0.79 ± 0.05	210	AKR1C3	na	na	na
AKR1C4	7.4 ± 2.1	4.64 ± 0.39	627	AKR1C4	na	na	na
AKR1C6	19.1 ± 4.5	10.33 ± 1.06	541	AKR1C6	11.4 ± 3.5	5.15 ± 0.58	452
AKR1C12	na	na	na	AKR1C12	na	na	na
AKR1C13	na	na	na	AKR1C13	na	na	na
AKR1C14	na	na	na	AKR1C14	na	na	na
AKR1C18	na	na	na	AKR1C18	8.9 ± 4.4	5.8 ± 0.95	652
AKR1C19	na	na	na	AKR1C19	na	na	na
AKR1C20	na	na	na	AKR1C20	na	na	na
AKR1C21	nmm	nmm	nmm	AKR1C21	na	na	na
Progesterone				**5α-DHT**			
AKR1C1	4.2 ± 1.0	1.77 ± 0.13	421	AKR1C1	46.9 ± 6.5	6.85 ± 0.45	146
AKR1C2	na	na	na	AKR1C2	4.3 ± 0.6	2.03 ± 0.08	472
AKR1C3	0.9 ± 0.3	0.14 ± 0.01	156	AKR1C3	na	na	na
AKR1C4	9.4 ± 3.5	0.74 ± 0.09	79	AKR1C4	6.7 ± 1.9	7.34 ± 0.66	1096
AKR1C6	25.1 ± 5.6	4.81 ± 0.87	192	AKR1C6	5.8 ± 2.2	0.93 ± 0.10	160
AKR1C12	na	na	na	AKR1C12	na	na	na
AKR1C13	na	na	na	AKR1C13	na	na	na
AKR1C14	na	na	na	AKR1C14	na	na	na
AKR1C18	105.7 ± 29.1	114.12 ± 19.2	1080	AKR1C18	3.9 ± 0.5	22.41 ± 0.82	5746
AKR1C19	na	na	na	AKR1C19	na	na	na
AKR1C20	3.7 ± 1.2	0.51 ± 0.05	138	AKR1C20	na	na	na
AKR1C21	na	na	na	AKR1C21	nnm	nnm	nnm

adione; androstanedione
5α-DHT; 5α-dihydrotestosterone
na; no detectable activity
nmm; data does not fit a Michaelis-Menten curve

4.1.2 Validation of 5α-DHT reduction using radio-labeled substrate

The spectrophotometric assay used to characterize the steroid preference of human and murine AKR1C enzymes is an easy and convenient method. However, its sensitivity is limited and slow enzymatic activities (with low K_m and k_{cat}) may not be detected. Therefore, a radiometric assay was used to measure the turn-over of 5α-DHT in order to compare the two methods.

Enzymes were incubated with 25 μM 5α-DHT for 30 and 90 minutes before extraction of reaction products and separation by TLC (Figure 47). All enzymes apart from AKR1C19 and -1C20 reduced 5α-DHT. The majority converted 5α-DHT to 3α-androstanediol (3α-adiol)

whilst AKR1C2 produced mainly 3β-androstanediol, AKR1C4 produced both stereoisomers and mouse AKR1C21 yielded a product that did not co-migrate with 3α- or 3β-androstanediol. The percentage of substrate reduced to product was determined at 30 and 90 minutes (Figure 48). In agreement with the spectrophotometric assay, AKR1C1, -1C2, -1C4, -1C18 and -1C21 were the most efficient in reducing 5α-DHT (between 50 and 100% substrate reduction at 30 minutes). AKR1C6 showed an intermediate efficiency whilst AKR1C3, -1C12, -1C13, -1C14 reduced 5α-DHT at a slow rate.

Both methods identified AKR1C1, -1C2, -1C4, -1C6, -1C18 and -1C21 as the most efficient in reducing 5α-DHT (Table 9 and Figure 48). However, the lower activities of AKR1C3, -1C12, -1C13 and -1C14 against 5α-DHT were only detected using the radiometric method. This result exposes the limitations of the spectrophotometric assay but does not contradict the results obtained in the previous section.

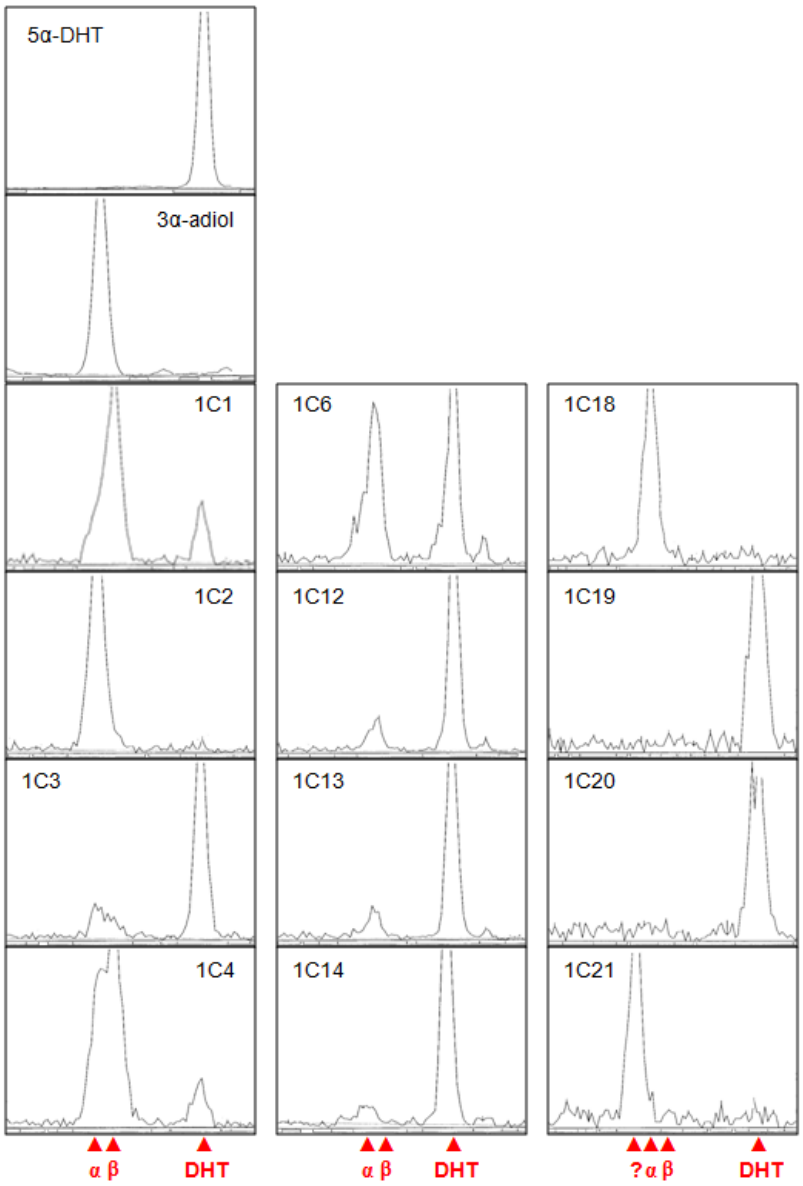

Figure 47 - Reduction of 5α-DHT by human and murine AKR1C enzymes.

Murine and human recombinant AKR1C enzymes were incubated with 25 μM 5α-DHT spiked with radio-labeled 5α-DHT and NADPH for 90 minutes. Steroids were extracted, separated by thin layer chromatography (TLC) and visualized by scanning the lanes for radioactive products. Hot standards for 5α-DHT and 3α-androstanediol (3α-adiol) ran as shown on top two panels of left column. Most enzymes that reduced 5α-DHT produced 3α-adiol (3α) except AKR1C1 that produced mainly 3β-adiol (3β), AKR1C4 produced a mixture of both stereoisomers and AKR1C21 that produced an unknown species (?). These are representative traces. Experiment was repeated thrice.

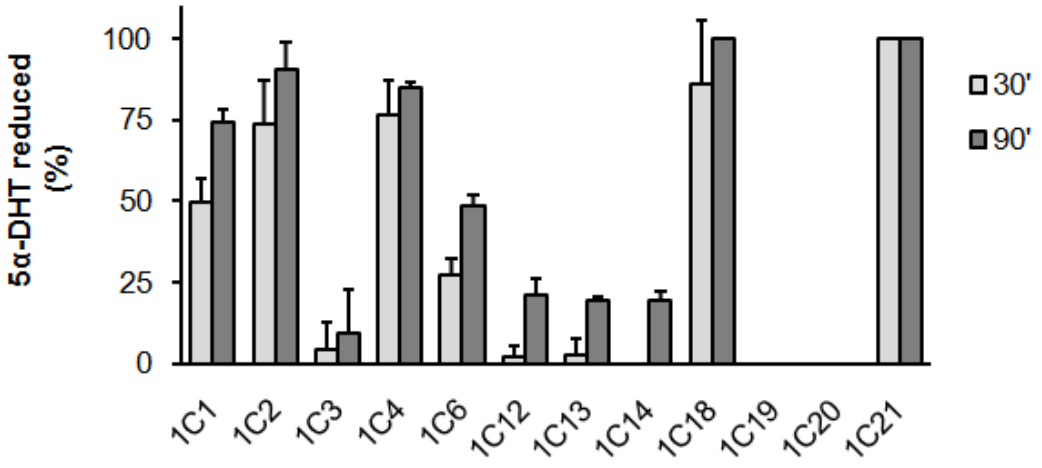

Figure 48 – Fraction of 5α-DHT reduced to 3α/β-androstanediol by human and murine AKR1C enzymes.

Human and murine AKR1C enzymes were incubated with radio-labeled 5α-DHT for 30 or 90 minutes and reaction products were analysed as shown in Figure 47. Bars represent the average percentage of 5α-DHT converted to 3α/β-androstanediol at those time points, obtained from three replicates. Errors bar represent standard deviation. Note that AKR1C21 quickly converted 5α-DHT to a product that did not co-migrate with either 3α- or 3β-androstanediol.

4.2 Tissue-expression pattern of murine AKR1C enzymes

The four human AKR1C enzymes have distinct tissue expression patterns (Penning et al., 2000) which correlate with their enzymatic preferences (androgens and estrogens in prostate and breast; PGD_2 in haemopoietic cells) and their implication in cancer (Figure 8). In order to assertain the relationship between enzymatic activity and tissue distribution the expression of the 8 murine AKR1C enzymes was measured in mouse spleen, liver, lung, stomach, small intestine, colon, kidney, prostate, testes, uterus (from pregnant animals) and ovary (from pregnant and non-pregnant animals).

For this analysis all tissues were obtained in triplicate (from three different animals) from our collaborators (Dr H. Schrewe and P. Rocha) at the Max Planck Institute for Molecular Biology in Berlin, Germany. RNA was extracted, cDNA prepared and gene expression measured using Taqman QRT-PCR (detailed in page 75). Sequences of primers and probes used are shown in Table 6 and Table 7, respectively. Two "housekeeping" genes were used as loading controls, *Gapdh* and *18S*. The expression levels of *18S* were more consistent between tissues than *Gapdh*. Therefore, expression of AKR1C genes in each sample was normalized to *18S* expression. Variability between tissue replicates was identical for *Gapdh* and *18S*.

Normalized expression of the 8 murine AKR1C genes and *Gapdh* is shown in Figure 49. Most AKR1C genes were found to be expressed in the liver, particularly *Akr1c6* and *-1c20* which were detected exclusively in this tissue. Tissue specificity was also observed for *Akr1c21* which was detected only in the kidney. Progesterone-inactivating *Akr1c18* was highly expressed in the ovaries of non-pregnant mice but was absent in ovaries of pregnant mice. The closely related *Akr1c12*, *-1c13* and *-1c19* showed a similar expression pattern, being detected mainly in gastrointestinal tissues (stomach, small intestine and colon). *Akr1c14* showed the broadest tissue distribution being detected in liver, lung, stomach, colon, kidney, uterus and ovary. Surprisingly, tissues that are highly responsive to sex-steroids (prostate, testes and uterus) showed very low or no expression of AKR1C isoforms. As mentioned previously, *Gapdh* was expressed in all tissues but at variable levels.

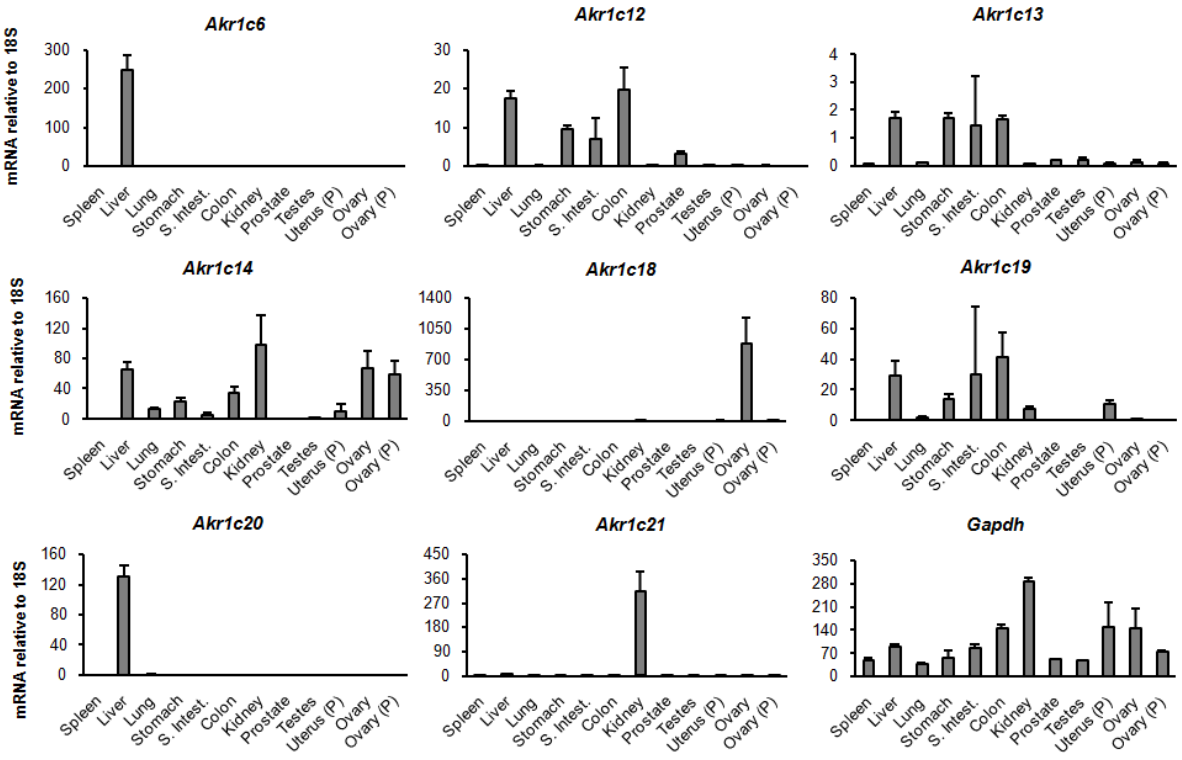

Figure 49 - Tissue expression of the eight murine AKR1C enzymes.

RNA was extracted from several tissues from CD1 mice (in triplicate), cDNA generated and gene expression quantified by Taqman QRT-PCR. Expression levels were normalized to *18S* expression using the following formula: ($2^{-(CT gene - CT 18S)}$) x10^6 and *Gapdh* expression was measured as control of cDNA quality. P; extracted from pregnant mice. Bars represent average expression of three biological replicates and error bars represent standard deviation.

4.3 Expression of AKR1C enzymes in a murine haemopoietic stem cell line (HPC-7)

Since AKR1C1, -1C2 and -1C3 are expressed in human haemopoietic stem cells we interrogated which AKR1C genes are similarly expressed in mouse. However, haemopoietic stem cells comprise a very small fraction of the bone marrow cell content (0.1 - 0.01%) and harvesting large amounts of these cells is difficult and requires the sacrifice of many animals. Therefore we used a mouse cell line with haemopoietic stem cell properties (HPC-7) to measure the expression of AKR1C genes in haemopoietic lineages.

4.3.1 Differentiation of HPC-7

The HPC-7 cell line was generated in 1998 by transducing mouse embryonic stem cells with the coding region of *LH2*, a transcription factor expressed in foetal liver at the time of active haemopoiesis (Pinto do et al., 2002, Pinto do et al., 1998). This resulted in the generation of a multipotent haemopoietic precursor cell line that requires stem cell factor (SCF) for growth and expresses appropriate haemopoietic progenitor markers. Furthermore, HPC-7 cells can be induced to differentiate into various mature myeloid lineages upon addition of other factors.

The SCF required for expansion of HPC-7 was obtained by harvesting the conditioned media from CHO cells over-expressing SCF (method detailed on page 70). HPC-7 cells were cultured with 10% SCF-conditioned media. The expression of AKR1C genes was measured in both differentiated and undifferentiated HPC-7.

When cultured in the presence of SCF, HPC-7 cells retained their blast morphology and grew at a steady rate (Figure 50). Removal of SCF resulted in a quick decrease in cell number with culture death occurring 2 days after factor-deprivation (Figure 50 B). Exposure to 4 U/ml human erythropoietin (hEPO) induced a notable increase in cell proliferation after 2 days followed by stabilization of cell number after 4 days (Figure 50 B). Treatment with hEPO also induced differentiation into the erythroid lineage, with red blood cells appearing after 4 days in culture (Figure 50 A). The cell pellets of hEPO-treated cultures, collected every two days, became increasingly red, probably due to the production of haemoglobin.

Previous reports using another mouse haemopoietic progenitor cell line (EML) showed that a combination of SCF, interleukin-3 (IL-3) and all-trans retinoic acid (ATRA) is able to induce

the initiation of promyelocytic differentiation (Tsai et al., 1994, Weiler et al., 1999, Du et al., 2000). HPC-7 cells were cultured in the presence of SCF, 100 ng/ml mouse IL-3 and 100 nM ATRA for 72 hours and changes in cell number, cell morphology and surface expression of the markers CD34 and Sca-1 monitored. After 72 hours no differences were observed in cell number and morphology between SCF-treated and SCF+IL3+ATRA-treated cultures. Surface expression of CD34 and Sca-1 was measured by flow cytometry and found to be significantly upregulated in cells cultured with SCF, IL-3 and ATRA relative to cells cultured with SCF only (Figure 51). The upregulation of these markers was interpreted as an initial commitment to differentiation. Cells from undifferentiated, hEPO and SCF + IL3 + ATRA treated cultures were harvested for RNA extraction and gene expression analysis.

4.3.2 AKR1C expression

Expression of murine AKR1C genes was measured in undifferentiated HPC-7 cells as well as in cells cultured with hEPO or the combination of SCF, IL-3 and ATRA. Gene expression was assessed by Taqman QRT-PCR using the primers and probes shown in Table 6 and Table 7. In undifferentiated HPC-7 cells only very low levels of *Akr1c13* mRNA but no other AKR1C genes were detected. Culture of HPC-7 cells with hEPO resulted in a small increase of *Akr1c13* expression but no other AKR1C gene. Similarly, culture with SCF, IL-3 and ATRA had no effect on *Akr1c13* expression nor did it cause the upregulation of other AKR1C genes.

Also, expression of the inducible cyclooxygenase isoform (COX-2), the enzyme responsible for prostaglandin production, was not detected in differentiated or factor-treated cells. In agreement with this, HPC-7 cells were unable to convert radio-labeled arachidonic acid into any prostanoid species (Figure 52).

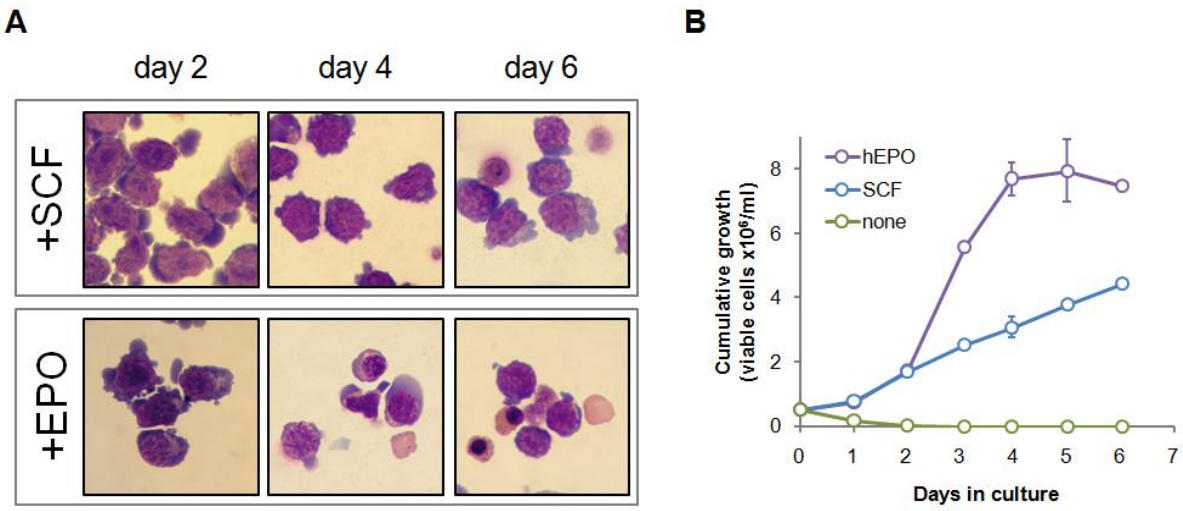

Figure 50 - Erythropoietin induces erythrocyte differentiation of HPC-7

HPC-7 cells were cultured in the presence of 10% conditioned medium with stem cell factor (SCF), 4U/ml human erythropoietin (hEPO) or no factor for seven days. **A:** Cells were harvested every two days, cytospun preparations fixed with methanol and stained with Jenner-Giemsa stain. Cells cultured with SCF retained the initial blast morphology while exposure to hEPO induced the differentiation of erythrocytes. Notice in day 6 the appearance of cells in different stages of erythropoiesis (with and without nuclei). **B:** Cells in culture were counted daily using a haemocytometer. SCF-treated cells showed a constant linear growth while hEPO induced cell proliferation. Absence of SCF resulted in death of all cells after 2 days in culture. Dots represent the average of two biological replicates and error bars represent the standard deviation.

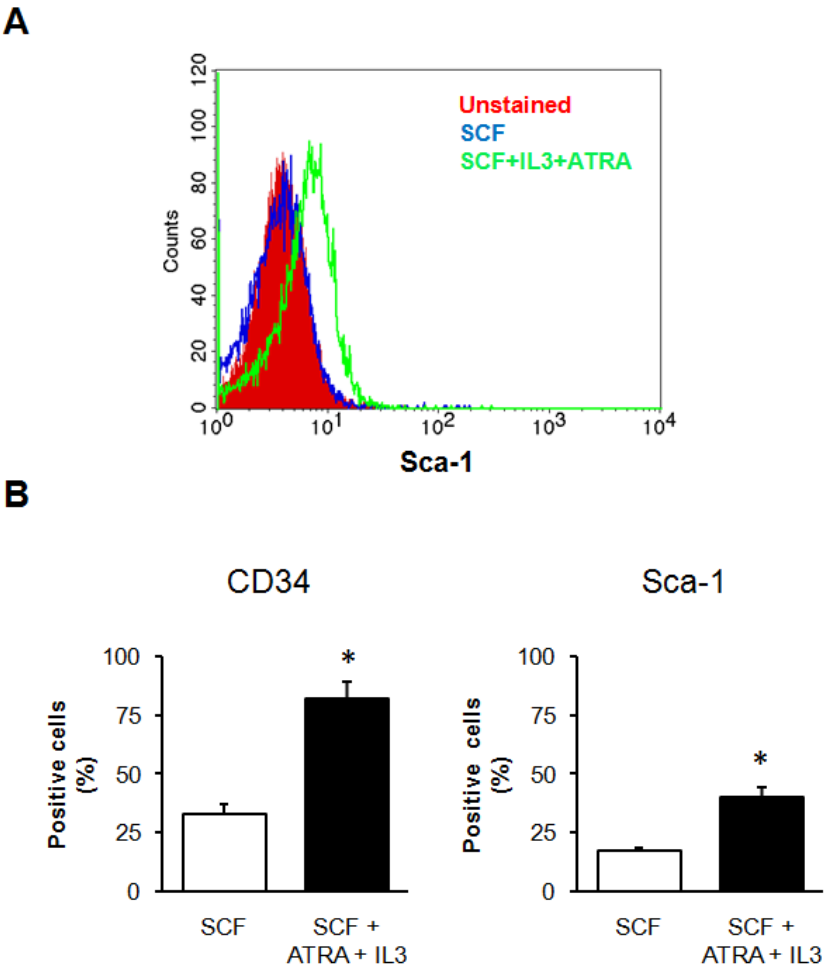

Figure 51 - Combination of ATRA, IL-3 and SCF causes upregulation of surface markers CD34 and Sca-1 in HPC-7 cells

HPC-7 cells were cultured in the presence of 10% conditioned medium with stem cell factor (SCF) alone or in combination with 100 nM all-trans retinoic acid (ATRA) and 100 ng/ml interleukin-3 (IL-3) for 72 hours. **A:** representative flow cytometry analysis histogram for the expression of the surface marker Sca-1. Red curve: unstained cells; blue line: SCF alone; green line: SCF + ATRA + IL-3. **B:** fraction of CD34 and Sca-1 positive cells were calculated. Bars represent the average of three biological replicates and error bars represent standard deviation. *; $P < 0.05$.

4.4 Discussion

Results in the previous chapter demonstrated that human and murine AKR1C enzyme amino acid sequences are divergent and that none of the murine enzymes had PGD_2 reductase activity. This discrepancy in phylogeny and function prompted further elucidation of the functional differences between human and mouse AKR1C enzymes.

Firstly, we compared the preference of human and mouse enzymes for steroid substrates. All four human AKR1C enzymes showed ample steroid reductase activity. Amongst the mouse isoforms, AKR1C6 and -1C18 were active towards the most steroid substrates, followed by -1C20 and -1C21. Interestingly, the remaining isoforms, AKR1C12, -1C13, -1C14 and -1C19, were unable to reduce any of the tested steroids. In addition to reducing PGE_2 (see page 120), AKR1C6 was active towards androstanedione, estrone, 5α-DHT and progesterone (3-, 17- and 20-HSD). Such substrate promiscuity suggests the catalytic pocket of AKR1C6 might accommodate a variety of molecules and could possibly relate to a function in xenobiotic detoxification. Previous reports had already shown that AKR1C18 is an efficient inactivator of progesterone, an activity related to the termination of pregnancy in mice (Miura et al., 1994, Maho Ishida, 1999, Piekorz et al., 2005). The present work showed that, in addition, AKR1C18 can inactivate 5α-DHT (anti-androgenic activity) and activate estrone to 17β-estradiol. This combination of activities implies that AKR1C18 acts in the ovary and uterus by promoting an estrogenic environment whilst inactivating androgenic and gestational steroids. Interestingly, AKR1C21 showed potent activities towards androstanedione and 5α-DHT but the respective enzyme kinetics did not fit a Michaelis-Menten curve. Also, AKR1C21 reduced 5α-DHT to a product other than 3α- or 3β-androstanediol. This different behavior of AKR1C21 may be related to its ability to bind steroids differently, as reported previously (Faucher et al., 2007). These results further expose the difference between human and mouse AKR1C enzymes, since no functional homologue in terms of steroid substrate preference could be identified.

Contrary to previous reports, estrone reductase activities amongst the human enzymes (Penning et al., 2000, Penning and Byrns, 2009) was not detected. In these reports radiometric assays were used that allow the detection of slower and less efficient AKR activities. The results obtained for the reduction of 5α-DHT with the spectrophotometric assay were

validated using a radiometric assay. Results from both methods were in agreement for the most efficient enzymes (AKR1C1, -1C2, -1C4, -1C6, -1C18 and -1C21) but exposed the lack of sensitivity of the spectrophotometric assay by revealing the slower activities of AKR1C3, -1C12, -1C13 and -1C14. This result should be taken into consideration when analysing the data shown on Table 9, where lower activities towards progesterone, estrone and androstanedione might have been undetected.

The eight mouse AKR1C genes were also characterised in their tissue expression profile. Tissues were harvested from male and female animals and gene expression measured by Taqman QRT-PCR. Although some of the murine isoforms show steroid metabolizing activities, expression of these enzymes in prostate, uterus, ovary and testes was very low or not detected. For instance, AKR1C6 reduced androstanedione, estrone, 5α-DHT and progesterone, yet its expression was restricted to the liver. Similarly, AKR1C20 was able to inactivate progesterone but was not detected outside the liver, further suggesting a hepatic detoxification role. The exception is perhaps AKR1C18, an efficient inactivator of progesterone and 5α-DHT and potentiator of estrone, expressed in the ovary of non-pregnant animals but repressed during pregnancy. As mentioned above, the progesterone-inactivating role of AKR1C18 has been previously linked to its expression in ovary and role in induction of parturition (Piekorz et al., 2005). The anti-androgenic and pro-estrogenic activities described here are in agreement with its expression in estrogen-sensitive tissues.

Conversely, AKR1C12, -1C13, -1C14 and -1C19 showed a broad tissue distribution but were unable to reduce any of the tested steroids. These AKRs, which have no close phylogenetic relation with the human isoforms, are found in gastrointestinal tissues (stomach, small intestine and colon) suggesting a possible function in metabolizing dietary compounds. This comparison revealed a discrepant tissue-expression pattern between human and murine AKR1C enzymes involved in estrogen and androgen metabolism.

Because three of the four human AKR1C isoforms are expressed in haemopoietic stem cells (Birtwistle et al., 2008) we used the mouse haemopoietic progenitor cell line HPC-7 to measure AKR1C expression. HPC-7 cells were induced to differentiate using EPO or a combination of SCF, IL-3 and ATRA. The differentiation was assessed by monitoring changes in cell morphology and surface marker expression, respectively. A more extensive characterisation of these lineage commitments would be necessary, such as expression of

lineage-specific transcription factors and other surface markers. Surprisingly, only very low levels of *Akr1c13*, but no other AKR1C gene, was detected. This pattern of expression was not altered by EPO or the SCF, IL-3 and ATRA combination. This lack of AKR1C expression in HPC-7 is further evidence of the functional divergence between human and mouse enzymes.

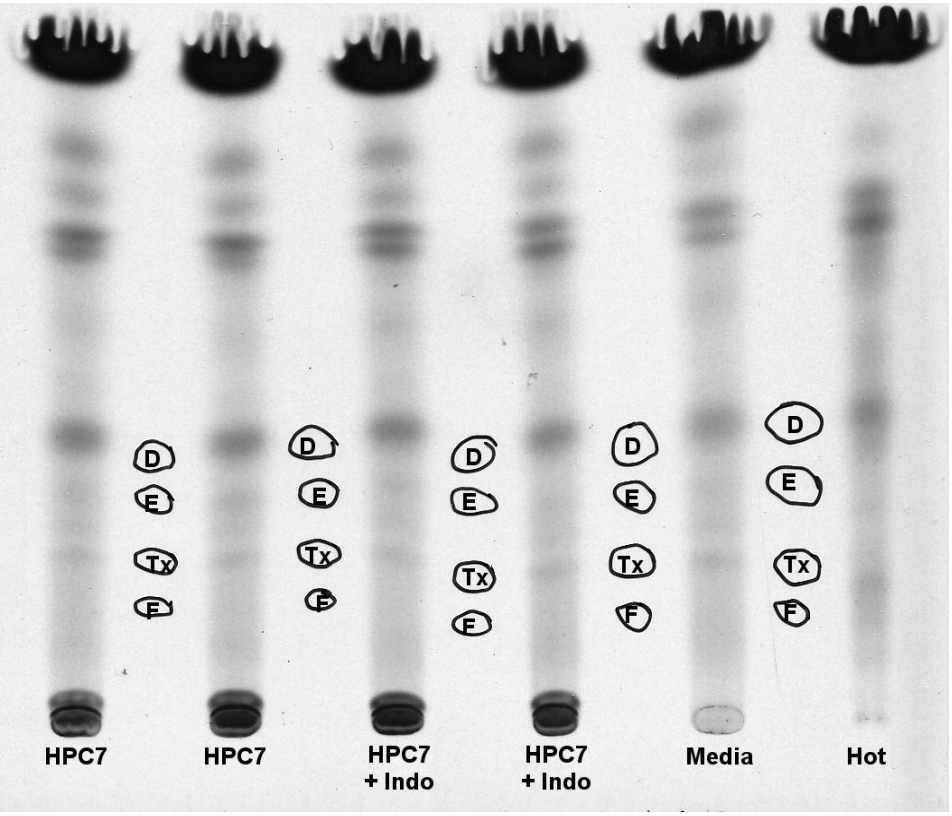

Figure 52 - HPC-7 cells do not convert arachidonic acid into prostanoids.

HPC-7 cells were resuspended in serum-free media supplemented with 0.25 µCi [1-^{12}C]-arachidonic acid with or without 20 µM indomethacin (COX inhibitor) and incubated at 37ºC for 3 hours. Cell-free incubation was used as control (Media). Prostanoids were extracted, separated by TLC and exposed to light-sensitive film. The following cold standards were run between sample lanes: PGD_2 (D), PGE_2 (E), TXA_2 (Tx) and $PGF_{2\alpha}$ (F). Top large band: arachidonic acid. Note that non-incubated arachidonic acid (Hot) is contaminated with products co-migrating with PGD_2 and other unidentified species.

CHAPTER FIVE: Targeting aldo-keto reductases in embryonic stem cells

Previous amino-acid sequence analysis had revealed higher sequence identity between murine AKR1C6 and human AKR1C3. Therefore, at the beginning of this project the *Akr1c6* gene was targeted in murine embryonic stem cells in order to generate a knock-out mouse strain. This work was performed before the lack of homology between human and mouse AKR1C enzymes was exposed.

5.1 Production of *Akr1c6* ^{floxed} murine embryonic stem cell line

Generation of a knock-out mouse strain requires specific targeting of the genomic locus of the gene of interest in embryonic stem cells. For this, specific DNA sequences known as LoxP sites are introduced in introns flanking one or more key exons of the gene. Introduction of these sites does not alter gene expression and the targeted cells behave normally. The manipulated stem cells are used to derive transgenic mice where the gene of interest is flanked by LoxP sites. The strain, which has wild type expression of the gene, is then crossed with mice expressing the Cre recombinase, a bacterial enzyme that recognizes LoxP sites. In the cells of the progeny, the Cre recombinase recognizes the LoxP sites in the gene of interest and promotes recombinantion between them. This results in excision of the key exons rendering the gene inactive (knock-out). Also, strains expressing Cre recombinase in a tissue-specific manner can be used to produce tissue-specific knock-out animals.

The procedure used to target the *Akr1c6* gene in murine embryonic stem cells is detailed in Figure 53. The *Akr1c6* gene is composed of 9 exons and 8 introns. A targeting construct for *Akr1c6* had been previously built by M Scholze and Dr H Schrewe (Max Planck Institute for Molecular Genetics, Berlin, Germany). The construct has a large region of homology with the *Akr1c6* genomic locus (spanning exons 1 to 3), a neomycin resistance cassette (conferring resistance to G418) and three LoxP sites (LoxP1-LoxP3).

After electroporation, the region of homology between the vector DNA and genomic DNA allows for homologous recombination and introduction of the Neomycin cassette and LoxP sites in the chromosome locus. Recombinant embryonic stem cell colonies were selected with

G418, clonally picked and expanded. Southern blotting was used to assess the correct integration of the construct. Genomic DNA was extracted from the amplified clones and digested with the restriction enzyme *Eco*RV. The digested DNA was separated by agarose gel electrophoresis, transferred onto a membrane and probed with a 5' probe (Figure 53, in red). Digestion of the wild-type *Akr1c6* locus results in a 6.2 kb fragment detected by the probe. On the other hand, correct integration of the targeting construct introduces an *Eco*RV site between exons 1 and 2, resulting in a 3.0 kb fragment. Therefore, clones in which the *Akr1c6* locus was correctly targeted yielded both a wild-type 6.2 kb fragment and a modified 3.0 kb fragment (usually only one of the chromosomes is successfully targeted) whilst clones with incorrect integration yielded the 6.2 kb fragment only. An example screening blot is presented in Figure 54, with two positive clones identified by red arrows.

The selected clones were expanded and correct integration re-confirmed by Southern blotting. These *Akr1c6* $^{\text{floxed-neo}}$ cells (exons flanked by LoxP sites) were stored at the Max Planck Institute but were never used to generate transgenic animals due to the results described in chapters 2 and 4 showing the lack of PGD_2 reductase activity of AKR1C6 and the remaining mouse isoforms. However, if used, these cells would generate animals expressing AKR1C6 at wild-type levels since no exon is disrupted. These animals could then be crossed with Cre-expressing strains to achieve total or tissue-specific knock-out.

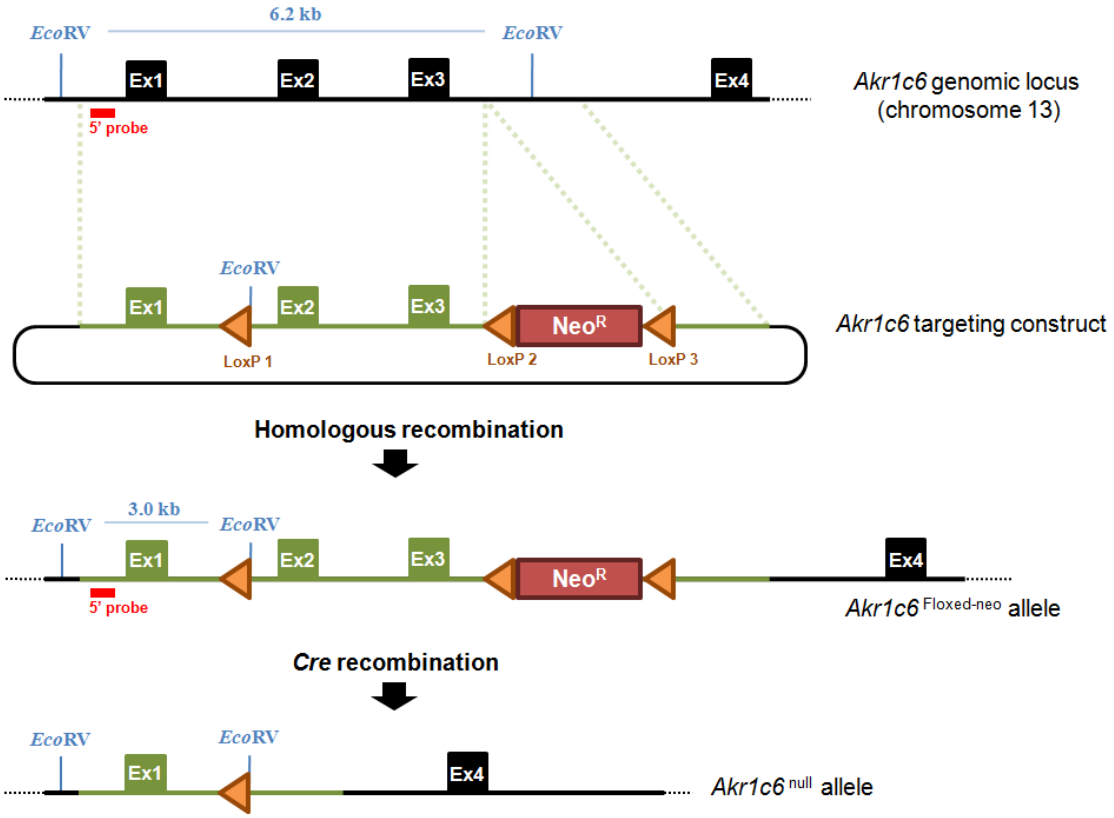

Figure 53 – Strategy for the generation of an *Akr1c6*$^{\text{floxed-neo}}$ mouse embryonic stem cell line.

The *Akr1c6* gene is located on mouse chromosome 13 and is composed of 9 exons, the first 4 of which are represented here (Ex1-Ex4). The targeting construct contains a large region of homology with the *Akr1c6* locus (in green) including exons 1 to 3, three LoxP sites (orange triangles) and a neomycin resistance cassette (red box). The vector is introduced in G4 murine embryonic stem cells by electroporation and integrates the locus via homologous recombination. Treatment with G418 selects colonies with an inserted neomycin^{R} cassette. To identify clones with homologous recombination, genomic DNA from G418-resistant colonies is screened by southern blotting with the 5' probe (in red) after digestion with *Eco*RV (sites in blue). A 3 kb fragment will be generated instead of the 6.2 kb (wild-type). These Akr1c6$^{\text{floxed-neo}}$ cells are expanded and used to generate transgenic animals (Akr1c6 expression is not affected as all exons are intact). Akr1c6$^{\text{floxed}}$ mice can later be crossed with animals expressing the bacterial Cre recombinase in a tissue-specific manner. In these tissues, Cre recombinase will act on the LoxP sites removing the DNA between. The resulting genomic locus lacks exons 2 and 3 and the respective mRNA leads to expression of a truncated non-functional protein (knock-out).

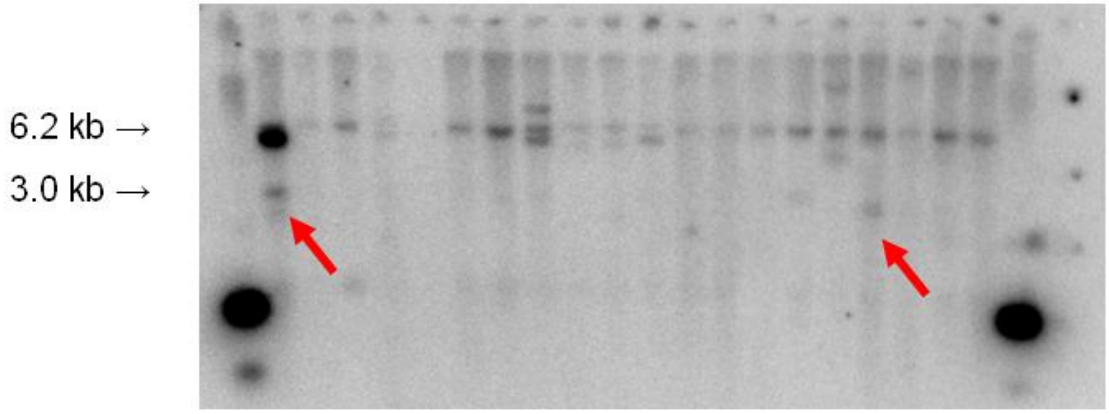

Figure 54 - Southern blot screen for homologous recombination in mESCs

Genomic DNA was extracted from G418-resistant mESC colonies, digested with *Eco*RV and analysed by southern blotting using a 5' probe (see Figure 53 for details). Colonies with correct insertion of targeting construct yield two bands: 6.2 kb (wild type allele) and 3.0 kb (modified allele). Red arrows point to clones with correct integration of target construct.

5.2 Production of a murine inducible knock-down system

Gene function can also be studied *in vivo* by over-expressing modified microRNAs (miRNAs) to silence gene expression in mouse tissues. Expression of these miRNAs can be regulated using inducible systems that enable temporal control of gene silencing. An inducible knock-down system was developed at the Max Planck Institute for Molecular Genetics (Berlin) as described in Figure 55. Because this system was of potential use for the study of AKR1C enzymes in mice, the collaboration effort was extended to the development of the pDONOR vector (Figure 55).

Previously, Dr M Morkel and co-workers had manipulated the ROSA26 locus in murine embryonic stem cells as shown in Figure 55. The murine ROSA26 locus is a constitutively open chromatin region in the mouse genome and, for this reason, is often used in transgene over-expression studies (Soriano, 1999). The locus was modified by inserting a gene encoding the tetracycline-responsive transcription silencer (tTS), two LoxP sites (with different sequence and orientation) and a promoterless gene conferring resistance to puromycine.

The pDONOR vector was designed to be compatible with the modified ROSA26 locus. The vector contains the enhanced GFP (eGFP) gene interrupted by an intron. The intron harbors the modified mir30 sequence (an endogenous miRNA) with the targeting sequence for the gene of interest. The *eGFP-mir30* gene is under regulation of a CMV or a tissue-specific promoter. Furthermore, the activity of this promoter is under influence of a tetracycline responsive element (TRE). A PGK promoter is located at the 3' end of the construct. All these elements are flanked by two LoxP sites compatible with the LoxP sites present in the ROSA26 locus. Importantly, the pDONOR vector was designed so that the CMV promoter and the mir30 targeting sequence can be quickly exchanged, allowing for quick customization of the system.

Upon co-transfection with a Cre-recombinase expressing vector, the pDONOR elements integrate the ROSA26 locus via homologous recombination of the LoxP sites. This brings the puromycin-resistance cassette under control of the PGK promoter, rendering the cells resistant to this antibiotic and allowing for positive selection. The specificity of the Cre-Lox recombination and the puromycin selection make the knock-in process highly efficient.

In the recombinant cells, the tTS protein binds to the TRE and silence the eGFP-mir30 gene. Exogenously added tetracycline binds the tTS releasing it from the TRE leading to expression of the *eGFP-mir30* gene. Upon translation the nascent *eGFP-mir30* mRNA is spliced releasing the mir30 sequence. This results in production of eGFP (green fluorescence can be used as reporter) and a miRNA specific against the target-gene that is processed by the cellular silencing machinery. These stem cells can be used to generate transgenic mice and, at the desired timepoint, silence expression of target gene by adding tetracycline to the animal's drinking water.

This inducible knock-down system is currently being optimized at the Max Planck Institute. However, and despite the contribution in building the pDONOR vector, the system was not used to study the role of AKR1C enzymes.

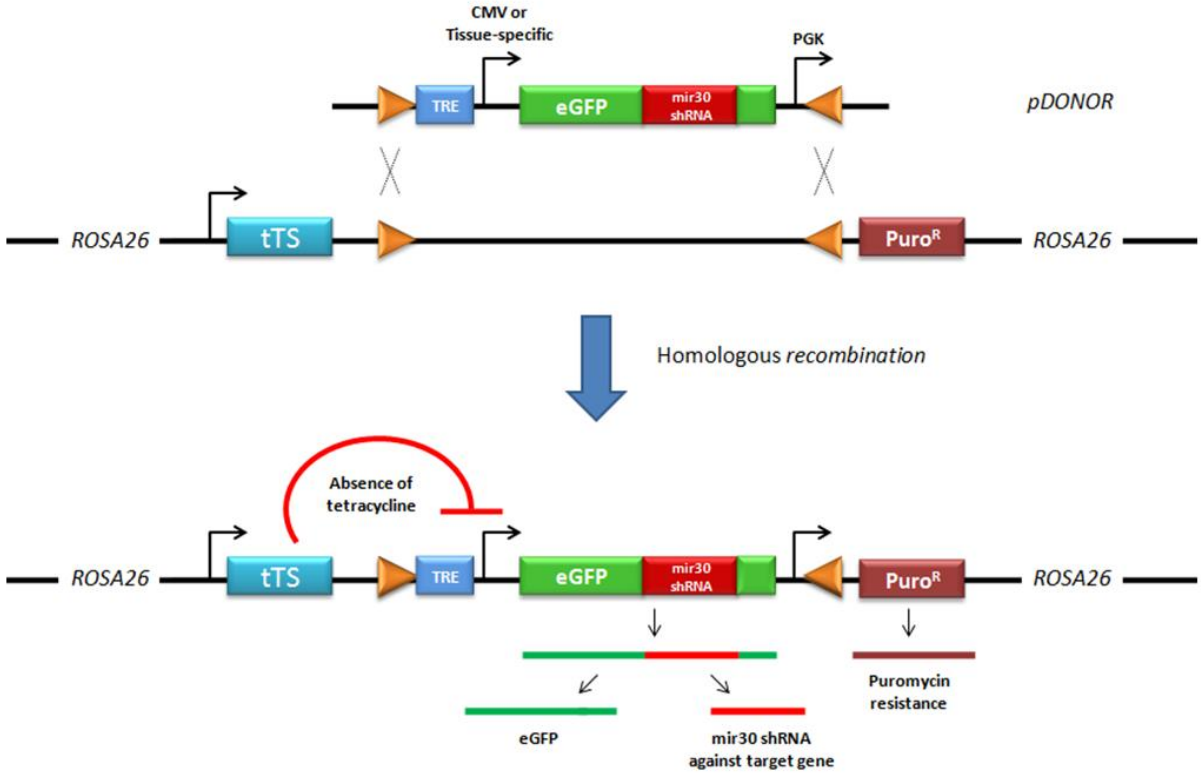

Figure 55 - Construction of an inducible knock down system.

The *ROSA26* locus is a constitutively open chromatin region of the mouse genome. Two loxP sites (orange triangles), the tetracycline-responsive transcription silencer (tTS) gene and a promoterless coding region for puromycine resistance (Puro^R) have been introduced in the *ROSA26* locus. The pDONOR construct has loxP sites homologous to those in *ROSA26* above flanking a Tet-responsive element (TRE) in the vicinity of a promoter (CMV or a tissue-specific promoter), the coding sequence of the enhanced green fluorescence protein (eGFP) interrupted by an intron coding for a modified *mir30* shRNA targeting a gene of interest and a PGK promoter. Upon transient Cre recombinase expression, the pDONOR construct is integrated in the *ROSA26* locus. The PGK promoter will drive puromycine resistance, facilitating the selection of homologous recombination events. The expression of the eGFP-shRNA gene depends on the promoter cloned upstream and on the tTS. In the absence of tetracycline the tTS recognizes the TRE and promotes chromatin condensation in the promoter region blocking eGFP-shRNA expression. Added tetracylin blocks tTS activity allowing gene expression. Under these conditions the RNA for eGFP-mir30 is transcribed and processed, generating GFP and a shRNA. The shRNA will be processed by the RNAi silencing machinery resulting in target gene repression while GFP is used as a marker of shRNA production.

CHAPTER SIX: Inhibition of myogenesis by PGD_2

6.1 Introduction to the myogenesis project

During the early stages of the project, whilst searching for the murine PGD_2 11β-ketoreductase, a panel of mouse cell lines was screened for AKR1C gene expression. These cell lines were later used as a source for cloning the open reading frames of the AKR1C genes (see Table 4). The C2C12 cell line, which was part of the panel, was derived from adult mouse myoblasts in 1977 (Yaffe and Saxel, 1977) and can undergo *in vitro* myogenesis generating long multinucleated myotubes (muscle fibers) and has become a widely used model for the study of adult myogenesis. A previous study had shown that C2C12 differentiation was sensitive to 15d-PGJ_2 (Hunter et al., 2001). This project was dedicated to elucidating the effect of PGD_2 in C2C12 differentiation, a widely used model for the study of adult myogenesis.

6.2 Differentiation of C2C12 myoblasts

If kept below confluence and in serum-supplemented media, C2C12 cells retain their myoblast properties and rapidly proliferate. In order to induce myogenic differentiation, C2C12 cells are allowed to reach confluence and, at that point, are changed to low-serum conditions to induce terminal myogenic differentiation (day 0). In most C2C12 protocols, differentiation is performed with media supplemented with low levels of horse rather than bovine serum (Hunter et al., 2001, Ardite et al., 2004). In this study C2C12 cells were differentiated with 5% horse serum (HS)-supplemented media and the process followed over the period of 4 days (Figure 56). The change was made after the cells reached 80 to 90% confluence. Twenty four hours after the addition of low-serum media, some cells detached from the plate suggesting cell death had occurred. At day 2 the first signs of cell fusion were observed, with large di- or polynucleated structures arising. These structures became larger over the remaining days and began to take on a fiber-like morphology. At day 4, long multinucleated myotubes could be observed (Figure 56).

Longer differentiation assays of up to 10 days were also performed. Myotubes continued to increase until day 6-7 after which cell fusion had largely ceased. A single addition of differentiation media at day 0 resulted in a slight increase in myotube formation when compared with cultures that hadthe media refreshed every two days.

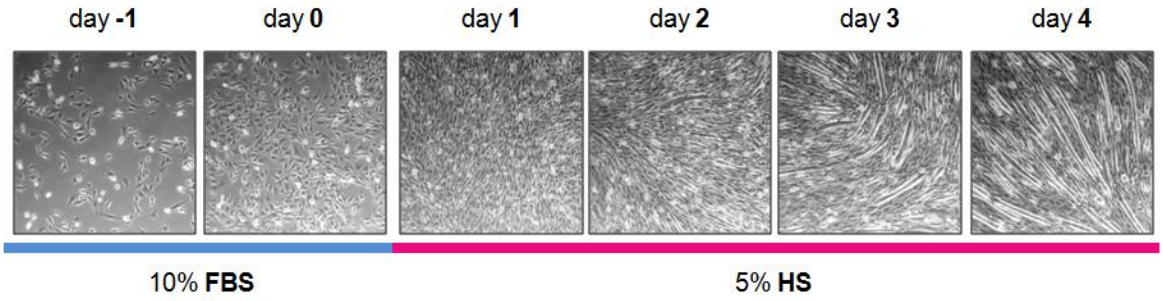

Figure 56 - Myogenic differentiation of C2C12.

C2C12 cells were seeded in six-well plates in DMEM supplemented with 10% foetal bovine serum (FBS). When cultures reached 80-90% confluence media was replaced with DMEM supplemented with 5% horse serum (HS). This is considered day 0. Media was refreshed every 2 days. Cultures were monitored daily using an inverted microscope. Cells begin to fuse around day 2 to form multinucleated structures, the myotubes. By day 4 the myotubes are multinucleated. Pictures taken at 20X amplification.

6.3 Development of an assay to measure myotube density

There are several methods to measure *in vitro* myogenic differentiation that can be applied to C2C12. The most widely used method consists of staining the cultures with antibodies against myotube-specific proteins (myogenin; myosin heavy chain), staining the nuclei (Hoechst; propidium iodide) and scoring the number of nuclei inside and outside myotubes. The fusion index, the proportion of myotube-integrated nuclei relative to the total nuclei count is calculated. Other dying methods, such as the Jenner-Giemsa stain, can also be used as long as nuclei and myotube structures are distinguishable. This method (detailed on page 91) is labour-intensive and is biased by the operator's decisions of whether a nucleus is inside or outside the myotube or whether a certain structure is indeed a myotube.

A less biased method is the measurement of creatine kinase (CK) activity (detailed on page 92). CK is an enzyme highly expressed in muscle tissue where, according to the energetic demands, it regulates ATP levels by transferring phosphate groups between ADP and creatine (phospho-kinase activity). For this method, cells are washed thoroughly with PBS to remove traces of CK that might have leaked from dead cells. Afterwards, the cells are lysed and the soluble cytoplasmic proteins purified by centrifugation. The protein extract is incubated with a reaction mix (Figure 35) and the activity measured is proportional to the amount of CK in the sample. The activity is normalized to the protein content of the sample. Despite being a quick and unbiased assay, measurement of CK activity does not inform about the overall aspect, protein content and myotube size of the cultures. Therefore this assay is often used as an additional method that complements the fusion index.

I have developed a simple and quick method that uses an unbiased analysis of stained cells to measure the density of the cultures *i. e.* the amount of protein-rich myotubes. C2C12 cells were differentiated over the period of 7 days and, at days -1, 0, 1, 3, 5 and 7, cultures were fixed and stained using Jenner-Giemsa dyes (staining detailed in page 91). The staining was done simultaneously for all samples in order to minimize technical variation between dyed samples. The Jenner-Giemsa dyes contain methylene blue and eosin. The former stains nuclei with a light pink color while the latter stains muscle fibers and collagen with a dark purple color. Therefore, with this staining it is possible to follow myotube formation during C2C12 differentiation, as show in Figure 57 A.

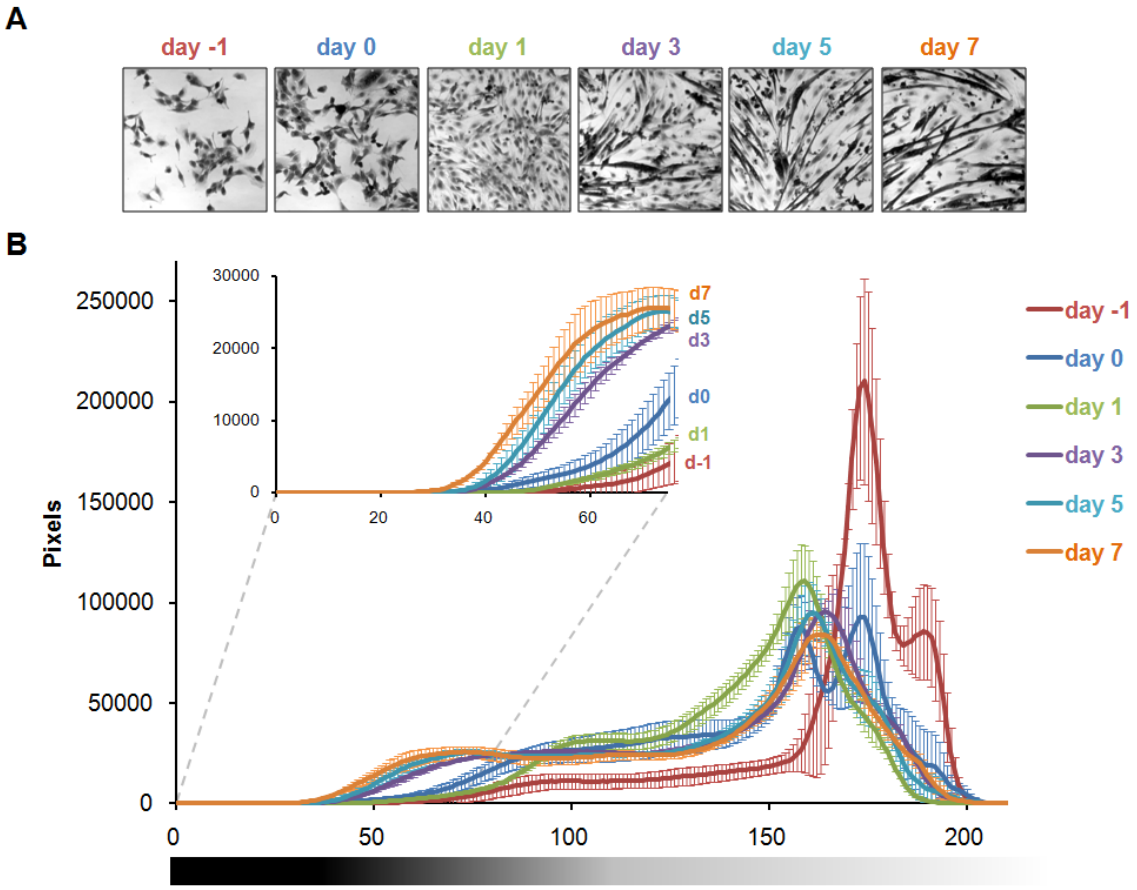

Figure 57 - Analysis of C2C12 differentiation using image histograms.

C2C12 cells were differentiated for a period of 7 days (day 0; change to differentiation media). At days -1, 0, 1, 3, 5 and 7 cells were fixed, stained with Jenner-Giemsa dyes and photographed (four fields per well). **A:** Representative pictures of stained cultures during differentiation (20X amplification). Note that protein-rich structures, such as the myotubes, are stained darker. **B:** Pictures of stained cultures were analysed with ImageJ. For each picture an image histogram was acquired. In the image histogram, the colour tones of the picture are divided into 255 units (0 being the darkest and 255 being the lightest) and the number of pixels attributed to each tone is shown (axis only up to 210). Lines represent the average pixel count of three biological replicates and error bars represent the standard deviation. Note that as cultures become myotube-rich more pixels are distributed to the darker tones.

For each time point, three biological replicates were fixed and four different fields photographed in each replicate well. Each picture was analysed with the ImageJ software and the respective image histograms were obtained. In an image histogram the spectrum of color tones is divided into 255 units with 0 being the darkest and 255 the lightest. The histogram shows how the pixels of the picture are distributed across the tone range. In Figure 57 B the average image histograms from cultures of the several time points are plotted. The error bars represent the standard deviation of the three biological replicates for each tone unit. The histogram for day -1 shows that most pixels have lighter tones as shown by the peak around tone 175. As cells reach confluence in day 0, the pixels become more distributed to the darker tones. At day 1 the amount of pixels in darker tones reduces slightly. At days 3, 5 and 7, a progressive increase in the amount of pixels allocated to the darker tones is observed, in agreement with the growth and maturation of myotubes.

This measurement of differentiation was then compared with the fusion index (FI). The same photographs of stained cultures were used to count the total number of nuclei and the fraction residing inside the myotubes (Figure 59 A). In this method, nuclei are considered inside myotubes irrespective of how dark those structures stain. The total number of nuclei per field increased steadily until day 1 and decreased slowly afterwards. However, the proportion of nuclei inside myotubes increased between days 1 and 3 and stabilized until the end of the experiment, implying that the fusion rate decreased after day 3. This also suggests that the decrease in total nuclei is related to death of un-fused cells. Therefore, the calculated fusion index showed a quick increase between day 1 and 3 that decelerated until day 7 (Figure 59 B).

For quantification of the culture density the sum of the pixels allocated to the darkest tones was compared (Figure 58). In this experiment, the number of pixels allocated to tones between 0 and 50 (darkest) was added and used as a measure of culture density. The choice of these values is arbitrary and depends on the histogram distribution, which varies depending on the magnification of the photograph, light exposure and staining process. As shown in Figure 59 C, the culture density remained low until day 1, from which point a rapid and constant increase occurred that lasted until day 7.

This analysis shows three events that occur in sequence during C2C12 differentiation. First the rapid increase of cell number (between days -1 and 1) followed by cell fusion (between days 1 and 3) and, finally, the increasing maturation of myotubes as these become more

protein-rich (between days 1 and 7). This newly developed method measures a phenomenon different to the one measured by the fusion index. Nevertheless, this measurement can also be used to quantify C2C12 differentiation. This assay was used in the following experiments as an unbiased complementary analysis to the fusion index.

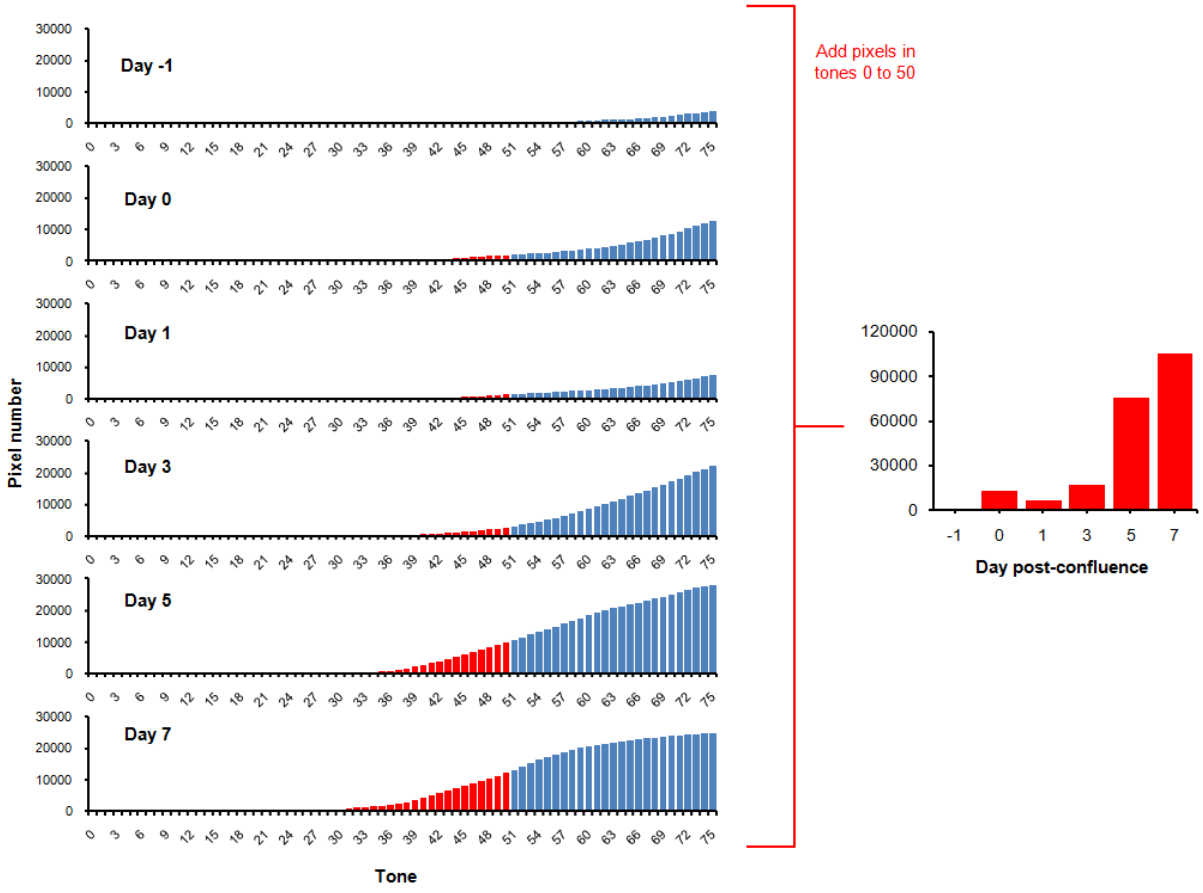

Figure 58 - Calculation of culture density from picture histograms.

In order to quantify the culture density, the pixels attributed to the darkest tones in the picture histogram are added. The threshold tone is chosen arbitrarily (in this experiment the tones 0 to 50 were added) depending on the distribution of the histogram.

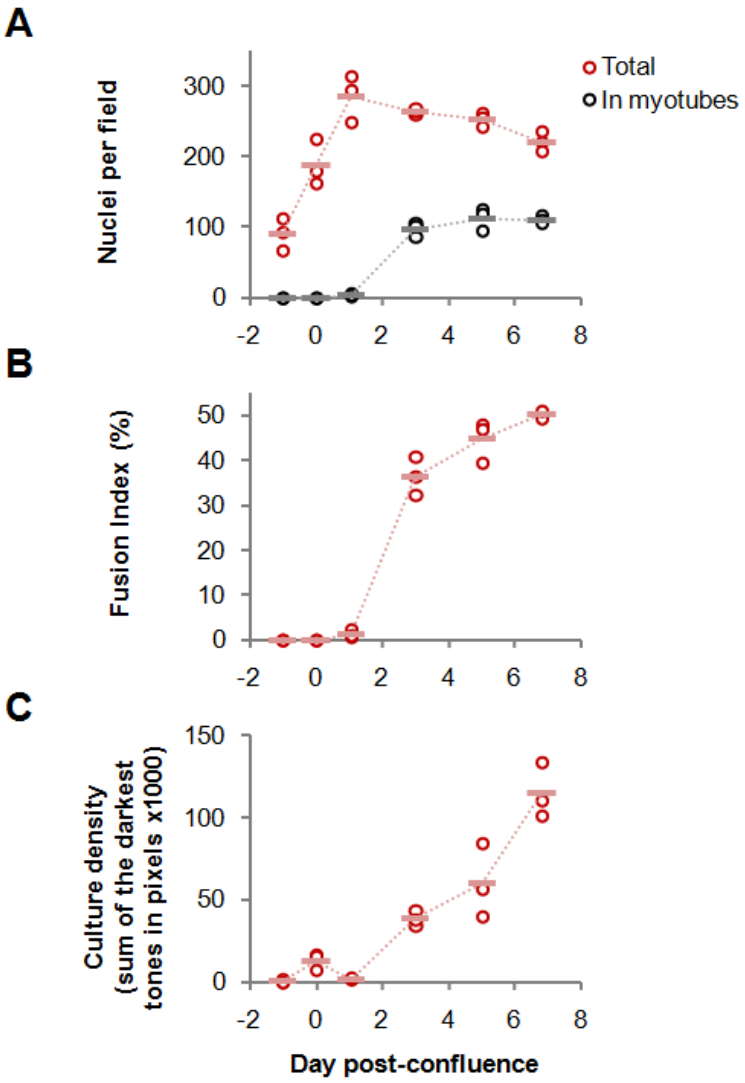

Figure 59 - Fusion index and culture density during C2C12 differentiation.

C2C12 cells were differentiated over a period of 7 days. At days -1, 0, 1, 3, 5 and 7 cells were fixed, stained with Jenner-Giemsa dyes and photographed (four fields per well). **A:** Number of total nuclei and nuclei inside myotubes per field. **B:** Fusion index, the fraction total nuclei inside myotubes. **C:** For each image histogram, the number of pixels attributed to tones 50 or less (darkest) was added. Each circle corresponds to one biological replicate and is the average measure of four pictures taken. Lines represent the average of the three biological replicates and are linked by the dotted line (trend over time).

6.4 PGD_2 inhibits C2C12 myogenesis

C2C12 cells were differentiated in the presence of 0.001, 0.01, 0.1, 1, 2.5, 5 and 10 μM PGD_2 or vehicle (Figure 60). Myotube formation was inhibited at micromolar doses (1-10 μM), as assessed by the fusion index and culture density. The effect was dose-dependent and had an IC50 of approximately 5 μM. Importantly, this effect was specific to PGD_2, since equimolar doses of PGE_2 and $PGF_{2\alpha}$ did not affect C2C12 myotube formation even at 10 μM (Figure 61), despite the structural similarity of these molecules. Inhibition of differentiation by PGD_2 was identical whether it was administered only once at the beginning of the experiment or every two days, suggesting the myogenic block occurs at an early stage.

The time-course of PGD_2 inhibition of myogenesis was also analysed (Figure 62). Reduced fusion index and creatine kinase activity relative to vehicle control were observed as early as day 2 post-confluence. Also, suppression of myotube formation was still evident at day 7 with no recovery occurring post day 4.

Because inhibition of myotube formation by PGD_2 could be due to a C2C12-specific artifact, the effect of PGD_2 was tested in another widely used *in vitro* model of myogenesis, the rat L6 cell line. Like C2C12, L6 were isolated from primary muscle samples and behave as myoblasts, fusing at high confluence to form long syncytial myotubes (Yaffe, 1968). When exposed to micromolar doses of PGD_2, the number and size of myotubes was reduced in L6 cells relative to controls (Figure 63 A). However, with L6 cells, the staining did not allow for clear distinction of nuclei and therefore the fusion index could not be calculated. Instead, CK activity was measured in these cultures and shown to be impaired in a dose-dependent manner (Figure 63 B).

These results show that PGD_2, but not PGE_2 or $PGF_{2\alpha}$, impairs *in vitro* myogenesis of two myoblast cell lines. The inhibition seems to occur in the early stages of differentiation and no recovery was observed after 7 days of culture.

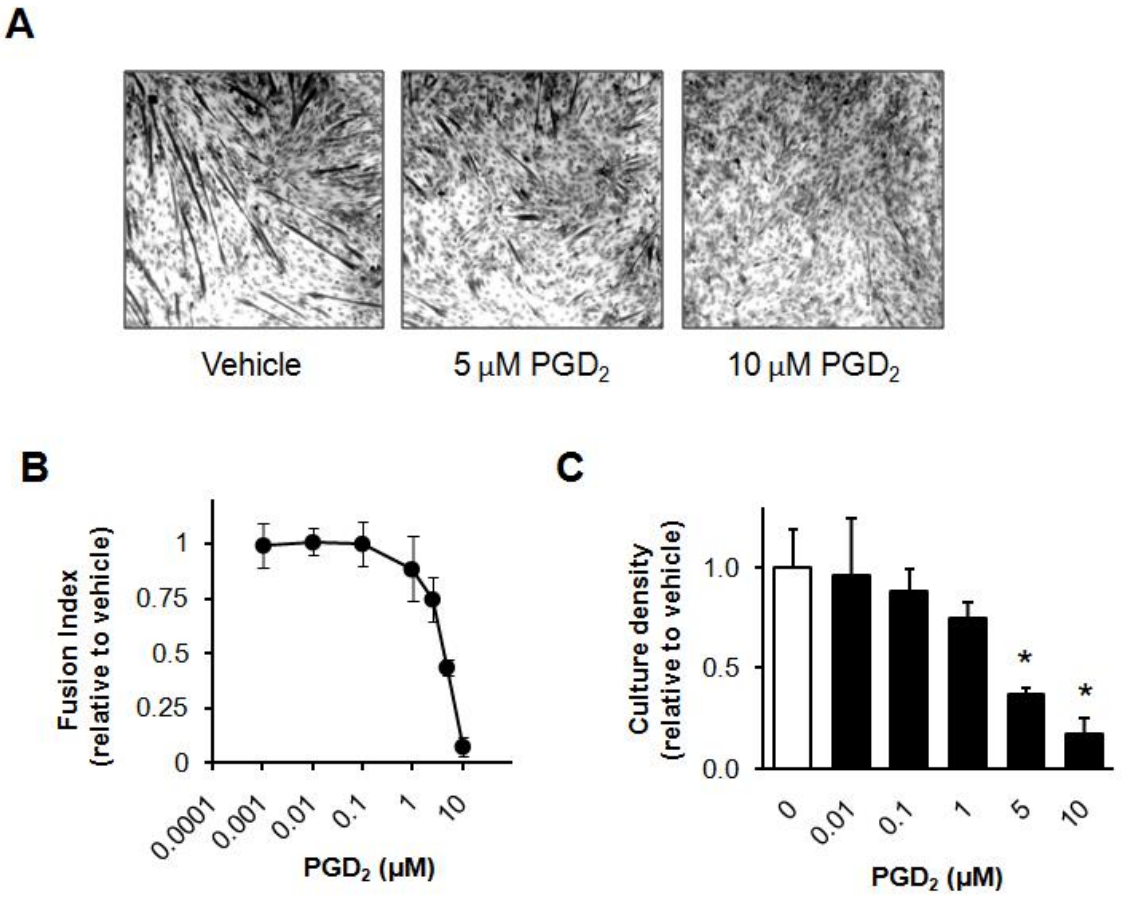

Figure 60 - PGD_2 inhibits C2C12 differentiation in a dose-dependent manner.

C2C12 cells were differentiated for 4 days in the presence of PGD_2 (0.001, 0.01, 0.1, 1, 2.5, 5 and 10 μM) or vehicle. **A:** representative staining of cultures treated with vehicle, 5 μM or 10 μM PGD_2 (amplification: 20X). **B:** myotube formation in PGD_2-treated cells was quantified by measuring the fusion index relative to vehicle-treated cells. PGD_2 inhibits the fusion index in a dose-dependent manner with an IC50 of ~5 μM. **C:** Culture densities of PGD_2-treated cultures. All measurements are the average of three biological replicates and error bars represent standard deviation. *; $P < 0.05$ relative to vehicle control.

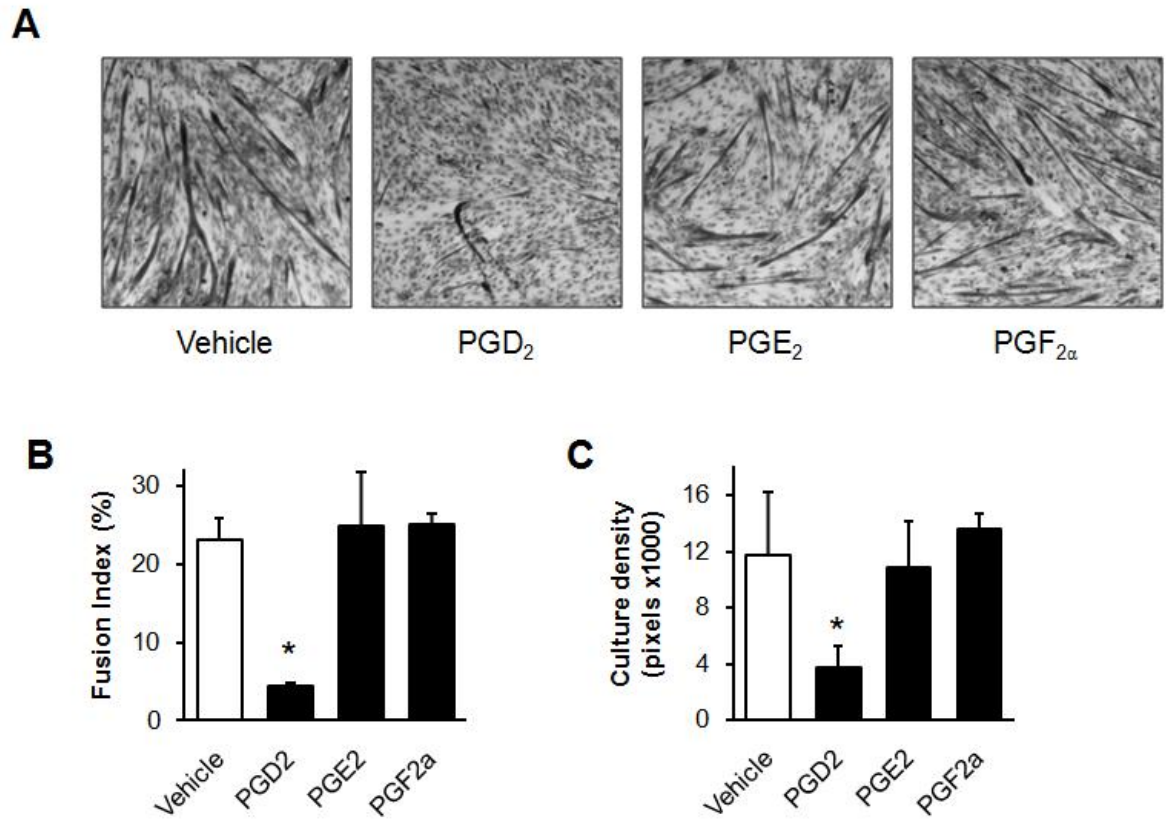

Figure 61 - PGD_2 but not PGE_2 and $PGF_{2\alpha}$ inhibit myotube formation.

C2C12 cells were differentiated for 4 days in the presence of 10µM PGD_2, PGE_2, $PGF_{2\alpha}$ or vehicle. **A:** representative pictures of Jenner-Giemsa stained cultures (amplification: 20X). Myotube formation is reduced in PGD_2-treated cultures only. **B:** myotube formation in PG-treated cells was quantified by measuring the fusion index relative to vehicle-treated cells. **C:** Culture densities of PG-treated cultures. All measurements are the average of three biological replicates and error bars represent standard deviation. *; $P < 0.05$ relative to vehicle control.

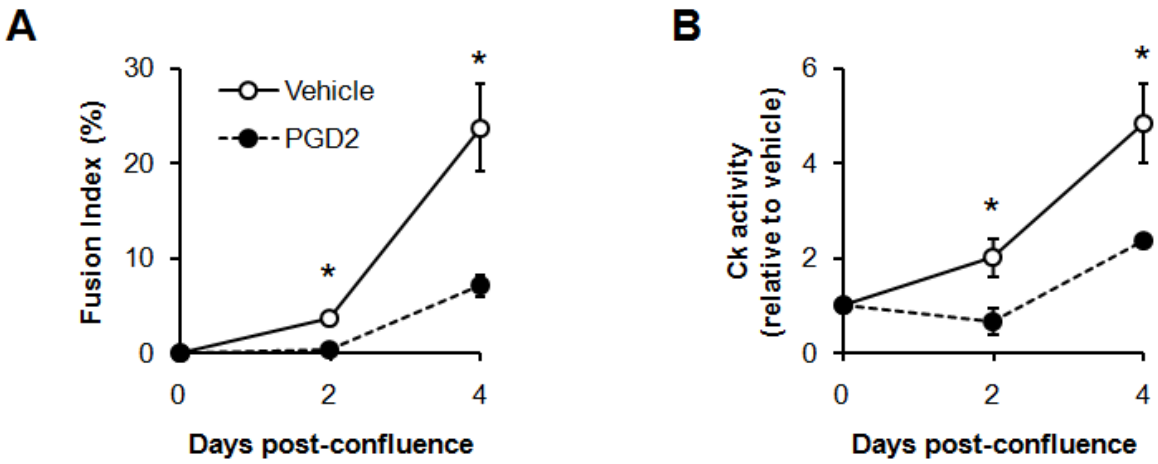

Figure 62 – Time course analysis of PGD_2-mediated inhibition of C2C12 differentiation.

C2C12 cells were differentiated for 4 days in the presence of 10μM PGD_2. Fusion index (**A**) and creatine kinase activity (**B**) were measured at days 0, 2 and 4. The inhibition caused by PGD2 is evident as early as day 2. All measurements are the average of three biological replicates and error bars represent standard deviation. *; $P < 0.05$ relative to respective vehicle control.

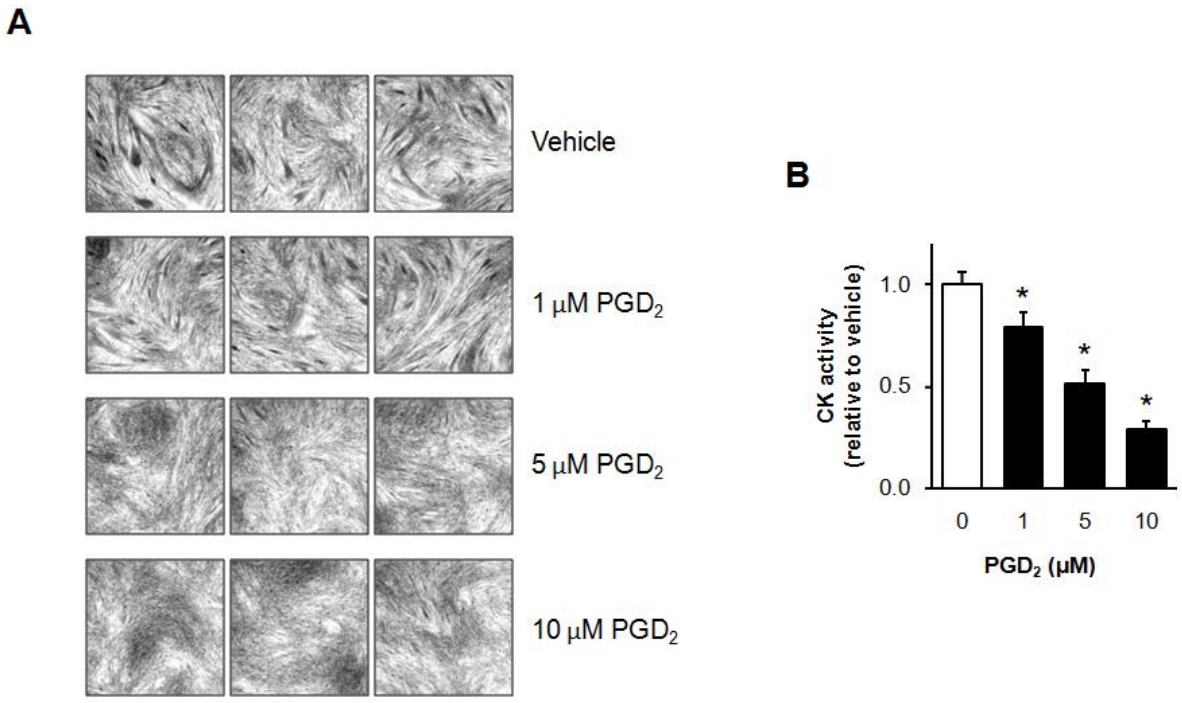

Figure 63 - PGD_2 inhibits differentiation of the rat L6 myoblast cell line.

L6 myoblasts were differentiated for 6 days in the presence of PGD_2 (1, 5 or 10 µM) or vehicle. **A:** Pictures of three biological replicates of Jenner-Giemsa stained L6 cultures (amplification: 10X). **B:** L6 differentiation was measured by creatine kinase activity. All measurements are the average of three biological replicates and error bars represent standard deviation. *; $P < 0.05$ relative to respective vehicle control.

6.5 PGD_2 alters gene expression during C2C12 myogenesis

Expression levels of the myogenic markers MyoD, myogenin and α-actin were measured using quantitative real-time PCR (QRT-PCR) during C2C12 differentiation in the presence or absence of 10 μM PGD_2. RNA was harvested at pre-confluence (day -1) and every 24 hours until day 4 post-confluence (Figure 64).

MyoD, a myogenic master regulator and a marker of activated satellite cells (Buckingham, 2006), was found to be expressed in pre-confluent C2C12, increased during differentiation until day 2 and decreased thereafter. In PGD_2-treated cultures the increase in MyoD expression was delayed reaching a maximum only at day 4. Myogenin is part of a second wave of regulators expressed in cells that have ceased dividing and committed to terminal differentiation (Buckingham, 2006). In control cultures, myogenin mRNA levels quickly increased after day 0 and remained high until day 4. However, this strong upregulation was markedly attenuated in cells exposed to PGD_2. Skeletal muscle α-actin is one of the most abundant proteins in mature myotubes as a key component of the contractile machinery. Expression of α-actin increased markedly during C2C12 differentiation and, as observed for myogenin, the upregulation was diminished in PGD_2-treated cells.

Altogether, these data demonstrate that PGD_2 disrupts normal transcriptional changes during myogenesis, even in early events such as MyoD upregulation.

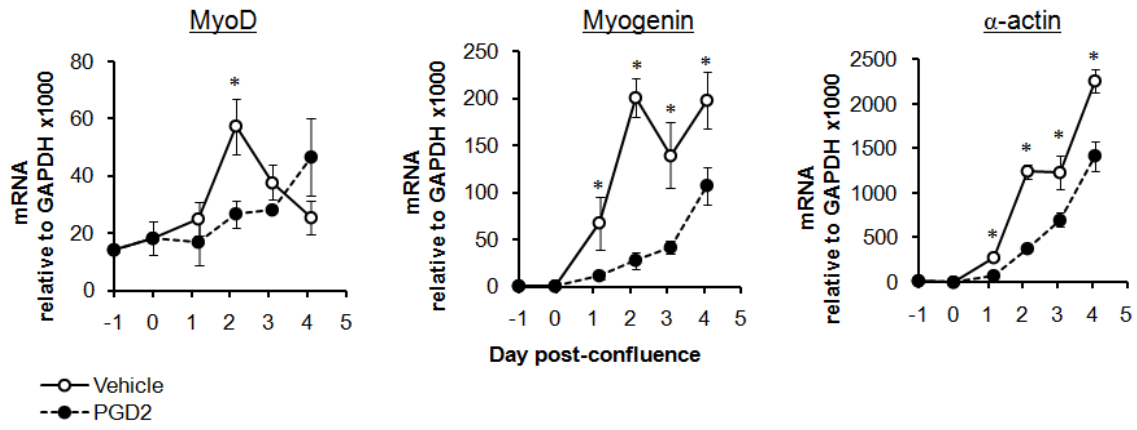

Figure 64 - PGD_2 disrupts transcriptional changes during C2C12 myogenesis.

Cells were differentiated in the presence of 10 μM PGD_2 or vehicle. Expression of MyoD, myogenin and α-actin was measured by Taqman QRT-PCR on RNA extracted every 24h from day -1 to day 4 post-confluence. Data are normalized to GAPDH expression and represent the average of three biological replicates ± standard deviation. *, *P* <0.05 versus equivalent vehicle timepoint.

6.6 PGD_2 alters C2C12 cell cycle resulting in increased cell number

Upon commitment to terminal differentiation, myoblasts cease to proliferate and initiate the process of cell fusion. Disrupting this withdrawal from cell cycle can affect the subsequent steps of myogenic differentiation. We exposed C2C12 to 10 μM PGD_2 and determined cell number and cell cycle profiles at 24 and 48 hours post treatment. PGD_2 treatment induced a ~30% increase in cell number relative to control (Figure 65 A). Cell counts did not change between 24 and 48 hours in either condition. Cell cycle analysis at 24 hours post addition of PGD_2 revealed a decrease in the proportion of cells in G1 phase relative to control (65.6% versus 75.8%, respectively) while, concomitantly, a higher proportion of cells in S and G2 phase was observed (Figure 65 B and Figure 65). At 48 hours, the proportion of cells in G1 phase increased in both treatments as expected in a cell population ceasing to proliferate (Figure 65 C and Figure 65). However, at this time point, no differences were observed between PGD_2-treated and control cultures.

Interestingly, PGD_2 induced an increase in cell number even in conditions of extreme serum deprivation as cultures incubated for 3 days in media with 0.5% serum and 10 μM PGD_2 had ~35% more cells than controls (Figure 67).

These results suggest that PGD_2 may affect C2C12 myogenesis by altering the cell cycle profile of the myoblast population at the onset of differentiation

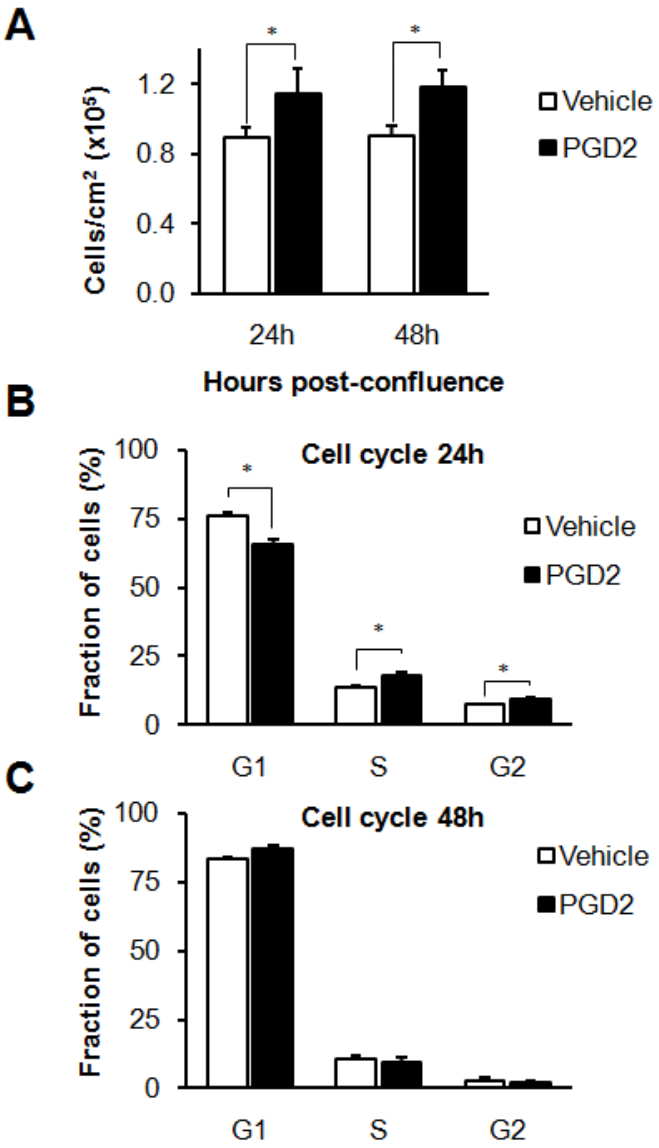

Figure 65 - PGD_2 causes an increase in cell number at the onset of C2C12 differentiation.

C2C12 cells were cultured in the presence or absence of 10 μM PGD_2. At 24 and 48 hours post-treatment, cells were trypsinized and counted (**A**) and stained with propidium iodide for cell cycle analysis with a flow cytometer (**B** and **C**). Flow cytometry histograms shown in Figure 66. Data are the average of three biological replicates ± standard deviation. *, *P* <0.05 versus equivalent vehicle control.

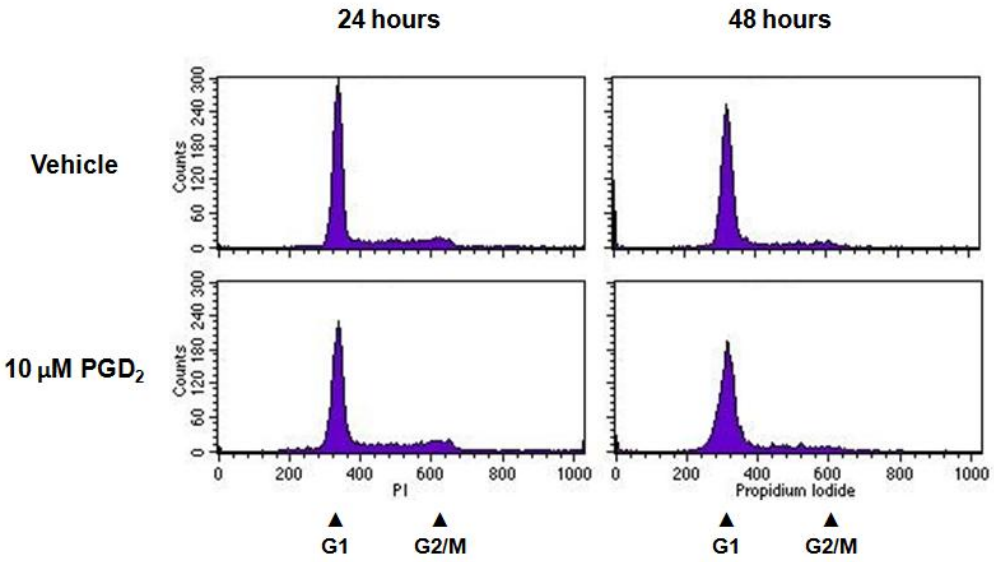

Figure 66 - Altered cell cycle of PGD_2-treated cells after 24 hours.

C2C12 cells were cultured in the presence or absence of 10 μM PGD_2. At 24 and 48 hours post-treatment, cells were trypsinized, stained with propidium iodide for cell cycle analysis with a flow cytometer. The histograms shown are representative of three biological replicates.

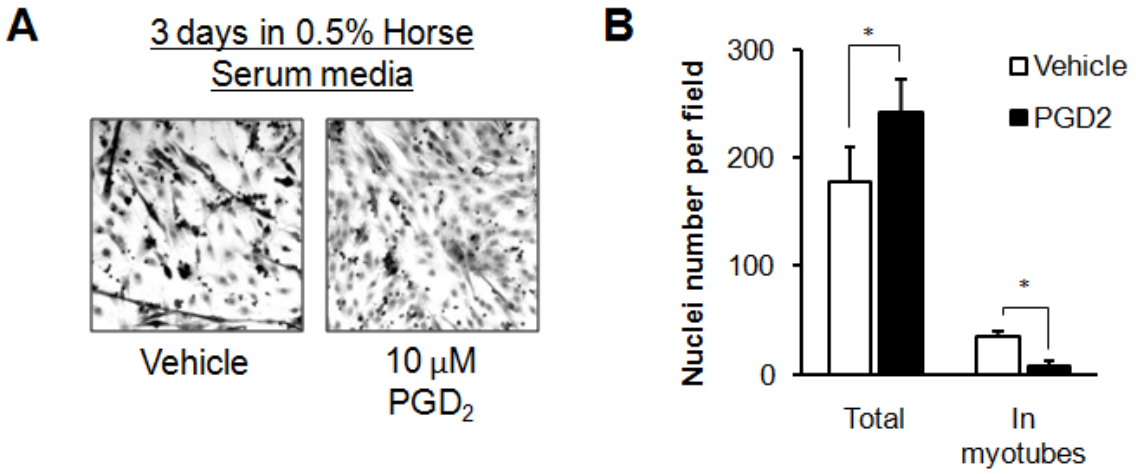

Figure 67 - PGD_2 induces an increase in cell number even in extreme low serum conditions.

C2C12 were differentiated for 3 days using media with 0.5% horse serum supplemented with either 10 µM PGD_2 or vehicle. Cultures were fixed and stained (**A**) and number of nuclei per field determined by counting (**B**; total and inside myotubes). Data are the average of three biological replicates ± standard deviation. *, $P < 0.05$ versus vehicle control.

6.7 Levels of exogenous PGD_2 in supernatant decrease after 24 hours

When in biological solutions, PGD_2 undergoes a series of spontaneous dehydration steps giving rise to the J-series prostaglandins (Straus and Glass, 2001). The end product of these non-enzymatic reactions is 15d-PGJ_2, also present in inflammatory tissues (Rajakariar et al., 2007). In order to measure the rate of conversion to J-series prostaglandins confluent C2C12 cultures were incubated with 10 μM PGD_2 spiked with radio-labeled PGD_2. After 3, 6 and 24 hours the media was harvested, prostaglandins extracted and separated in TLC. Levels of PGD_2 decreased to ~50% of the initial values in the first 6 hours of incubation (~30% after 24 hours). J-series intermediates and 15d-PGJ_2 were detected after 3 hours but remained unchanged during the time course. Instead, the total levels of radio-labeled PGs decreased in the supernatant as measured by total counts, suggesting an uptake by the cells. It is not clear whether it is PGD_2 or the dehydration products that are assimilated by the cells. Nevertheless, this data shows that PGD_2 has a transient presence in the supernatant and that J-series prostaglandins are generated and may have an effect on C2C12 myogenesis (data not shown).

6.8 PGD_2 treatment does not induce mitochondrial superoxide

A previous study demonstrated that high dose 15d-PGJ_2 can also inhibit C2C12 myogenesis (Hunter et al., 2001). However, even at the highest PGD_2 doses used in our assays (10 μM), it seems unlikely that the generated levels of 15d-PGJ_2 would be comparable to those used by Hunter et al. Nevertheless, 15d-PGJ_2 is a highly-reactive PG that is able to generate toxic reactive oxygen species and could affect myoblast behavior in low doses.

In order to measure if exposure to PGD_2, or its dehydration products, induces generation of reactive oxygen species in C2C12 the formation of mitochondrial superoxide was measured using the fluorescent Mitosox Red dye (Figure 68). Untreated C2C12 showed basal superoxide levels that were increased by approximately 2-fold after a 24h incubation with 100 μM H_2O_2 used as a positive control for the assay. Similarly and as expected, treatment with 15d-PGJ_2 generated mitochondrial superoxide. However in marked contrast, treatment with 10μM PGD_2 not only resulted in no increase in superoxide generation but lead to a small, yet significant, decrease. Interestingly, both 15d-PGJ_2 and H_2O_2 treatments resulted in a ~50% decrease in cell number relative to control.

These results suggest that the inhibition of myogenesis by PGD_2 is not mediated by conversion to high concentrations of 15d-PGJ_2 and subsequent mitochondrial superoxide generation.

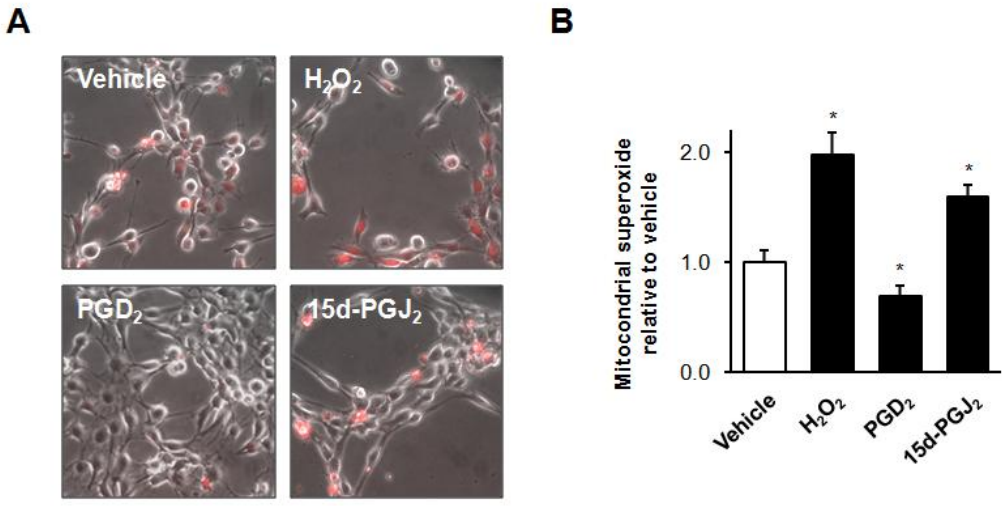

Figure 68 - Treatment with PGD_2 does not generate reactive oxygen species.

C2C12 were incubated with either 100 µM H_2O_2, 10 µM PGD_2 or 10 µM 15d-PGJ_2 for 24h. Generation of mitochondrial superoxide species was detected using Mitosox Red dye as described in page 99. **A**: Merged phase-contrast (grey) and Mitosox Red fluorescence (red) showing superoxide generation in cells. **B:** Mitosox Red fluorescence was normalized to cell number. Data are the average of three biological replicates ± standard deviation. *, *P* <0.05 versus equivalent vehicle control.

6.9 PPARγ is not required for PGD_2 inhibition of C2C12 myogenesis

Another mechanism of action attributed to 15d-PGJ_2 is the activation of the peroxisome proliferator-activated receptor (PPARγ), a member of the nuclear receptor family of transcription factors expressed in C2C12 and essential for myogenesis (Singh et al., 2007, Forman et al., 1995). Although an accumulation of 15d-PGJ_2 was not observed in culture media there was an overall decrease in the PGD_2 pool. Therefore it is possible that PGD_2 represses myogenesis via generation of 15d-PGJ_2 inside the cells resulting in activation of PPARγ.

We investigated whether PPARγ was involved in PGD_2-mediated inhibition of differentiation. Stimulation of PPARγ with the synthetic ligand ciglitazone did not affect myotube formation but these structures stained more lightly than controls, suggesting less accumulation of protein (Figure 69). Furthermore, pre-treatment with a PPARγ antagonist (GW9662) did not block the PGD_2 effect on myotube formation. Thus, PPARγ activation does not seem to be required for PGD_2 inhibition of C2C12 myogenesis. This observation further suggests that the suppression of myogenesis by PGD_2 is independent of 15d-PGJ_2.

Upon transition to differentiation media, PPARγ was found to be down-regulated and remained low until day 4 (

Figure 70). Interestingly, treatment with PGD_2 caused an up-regulation of PPARγ expression that remained high throughout differentiation. Given that activation or inhibition of PPARγ does not seem to affect C2C12 myogenesis we speculate this event is an effect of PGD_2 inhibition rather than an immediate cause.

Previous studies showed that upregulation or knockdown of PPARγ affects C2C12 differentiation (Singh et al., 2007). However, the present study shows that treatment with PPARγ specific agonist (ciglitazone) or antagonist (GW9662) does not alter myotube formation. This could be due to C2C12 expressing a mutated form of PPARγ that exerts ligand-independent effects. Therefore, PPARγ mRNA was cloned from C2C12 and sequenced (as described in page 88). The sequence obtained from 8 individual clones was that of wild-type PPARγ.

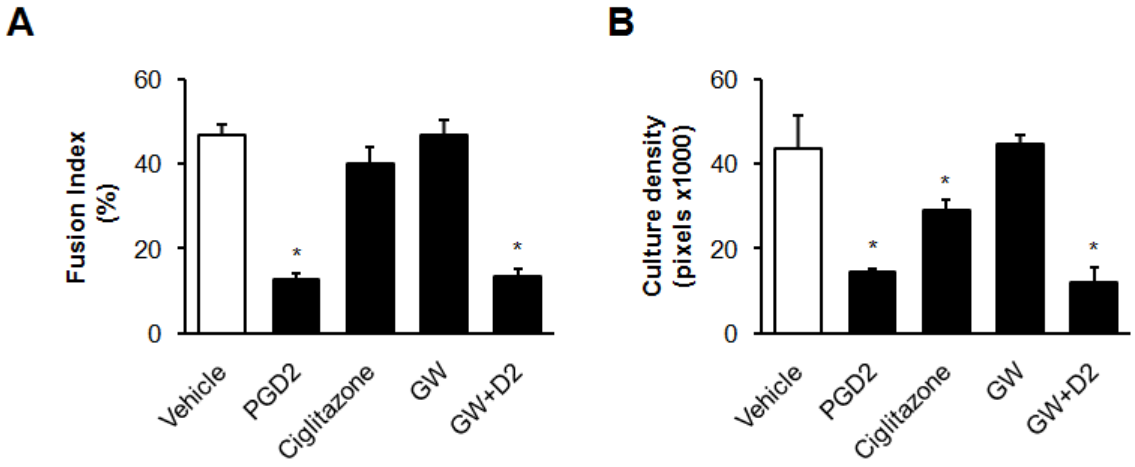

Figure 69 - PGD_2 inhibition of myogenesis does not require PPARγ activation.

C2C12 were differentiated for 4 days in the presence of 10 μM PGD_2, 10 μM Ciglitazone (synthetic PPARγ agonist), 1 μM GW9662 (PPARγ antagonist) and 1 μM GW9662 + 10 μM PGD_2. The PPARγ antagonist was added 30 minutes before PGD_2. Myotube formation was determined by fusion index (**A**) and culture density (**B**). Note that although ciglitazone did not affect fusion index it induced a small decrease in the culture density. Data are the average of three individual wells ± standard deviation. *, *P* <0.05 versus vehicle control.

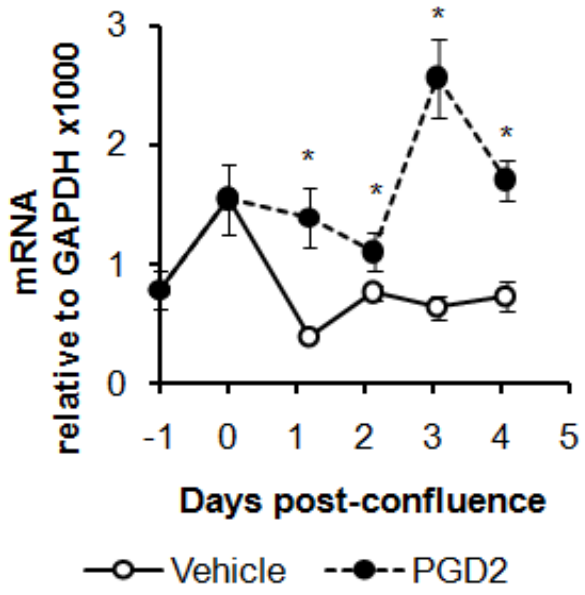

Figure 70 - PGD_2 induces upregulation of PPARγ during C2C12 differentiation.

Cells were differentiated in the presence of 10 μM PGD_2 or vehicle. Expression of PPARγ was measured by Taqman QRT-PCR on RNA extracted every 24h from day -1 to day 4 post-confluence. Data are normalized to GAPDH expression and represent the average of three biological replicates ± standard deviation. *, *P* <0.05 versus equivalent vehicle timepoint.

6.10 Altered cell motility in PGD_2-treated C2C12

During inflammation, PGD_2 acts as potent chemoattractant for leukocytes (Kostenis and Ulven, 2006). Also, migration of primary mouse myoblasts was shown to be modulated by PGI_2, resulting in enhanced cell fusion (Bondesen et al., 2007). Therefore, we speculated that PGD_2 may have an effect on C2C12 motility.

C2C12 cells were seeded in growth media which was replaced after 24 hours with differentiation media with 10 μM PGD_2 or vehicle. Cells were monitored using time-lapse imaging over the course of 3 hours and their motility was tracked (Figure 71). The dispersion plots shown in Figure 71 A represent the relative movement of 30 cells per treatment. It is noticeable that PGD_2-exposed cells are less mobile than untreated cells. The average velocity was reduced to ~60% in PGD_2-exposed cells relative to controls (Figure 71 B). The histogram in Figure 71 C shows the distribution of velocities of all monitored cells, with PGD_2-treated cells being clearly slower. This experiment was repeated twice with identical results.

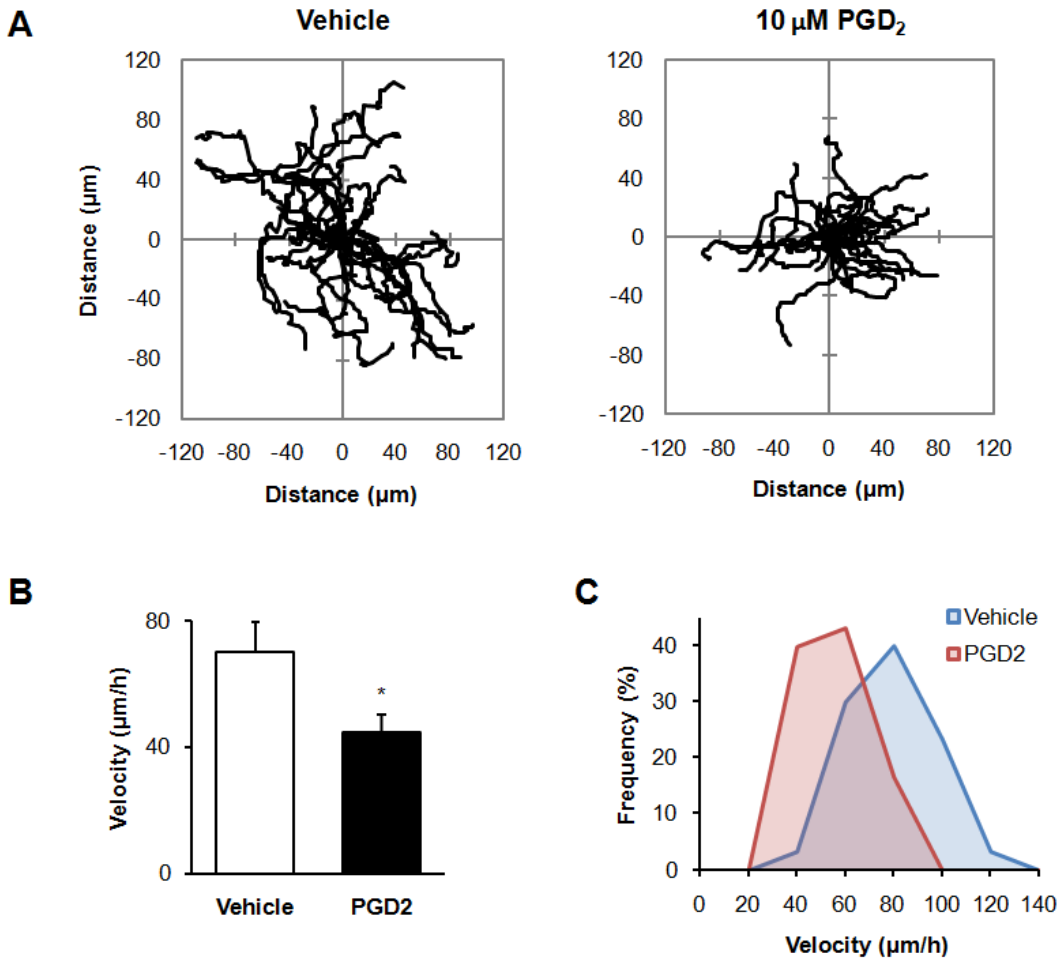

Figure 71 - PGD_2 reduces C2C12 cell motility.

C2C12 cells were seeded with growth media and, 24 hours later, changed to differentiation media with 10 µM PGD_2 or vehicle (three biological replicates per treatment). Cells were placed on a microscope stage equipped with an incubator and kept at 37 °C and 5% CO_2. Time-lapse imaging began 20 minutes after addition of PGD_2 capturing 1 frame every 2 minutes over a period of 3 hours. Cell movement was tracked using the Manual Track software plug-in for ImageJ. **A**: for each condition, the movement of 30 cells (10 from each replicate) was tracked and used to generate a dispersion plot. **B**: cell velocities of vehicle and PGD_2-treated cells. Data are the average of three individual wells ± standard deviation. *, *P* <0.05 versus vehicle control. **C:** histogram showing the velocity distribution of vehicle and PGD_2-treated cells.

6.11 PGD_2 inhibits C2C12 myogenesis in a DP1 and DP2-independent manner

Secreted prostanoids elicit many of their downstream effects on neighbouring cells via specific surface receptors of the G-protein coupled receptor (GPCR) superfamily. Extracellular PGD_2 can interact with two high-affinity receptors known as DP1 and DP2 (or CRTH2) (Kostenis and Ulven, 2006).

To test for DP receptor-mediated function, C2C12 myoblasts were differentiated in the presence of the DP1 and DP2 selective agonists BW245c and 15*R*-methyl- PGD_2, respectively. Both synthetic compounds selectively activate DP receptors with EC50 in the low nanomolar range (Monneret et al., 2003, Boie et al., 1995). As shown in Figure 72 A, 10 μM 15*R*-methyl- PGD_2, but not 10 μM BW245c, was able to mimic PGD_2 inhibition of culture density, cell fusion, creatine kinase activity and α-actin expression after 4 days of differentiation, suggesting a DP2-mediated effect. However, as observed for PGD_2, 15*R*-methyl- PGD_2 only exerted these effects at high micromolar doses (Figure 73), a concentration much higher than the described EC50 for DP2-mediated eosinophil activation (1.7 nM) (Monneret et al., 2003).

Expression of PGD_2 surface receptors was analysed by RT-PCR in pre-confluent undifferentiated and in differentiated C2C12 (Figure 74). Surprisingly, no mRNA was detected for DP1 or DP2 at either differentiation stage despite the DP2 agonist having mimicked PGD_2 in inhibiting myotube formation. Using Taqman QRT-PCR, very low levels of DP2 expression were detected (approximately 100 000x lower than GAPDH). Attempts, to knock-down DP2 expression in C2C12 using both transient and stable over-expression of a specific shRNA against this gene were unsuccessful (method detailed in pages 84 and 88).

To confirm if DP2 signaling is indeed absent, cells were pre-incubated with CAY10471 (DP2 selective antagonist) before addition of PGD_2 (Royer et al., 2007). CAY10471 failed to prevent the suppression of α-actin up-regulation at 0.5, 5 or 10 μM (Figure 72 C). Altogether, these data point to a non-DP mediated action of both PGD_2 and 15*R*-methyl- PGD_2.

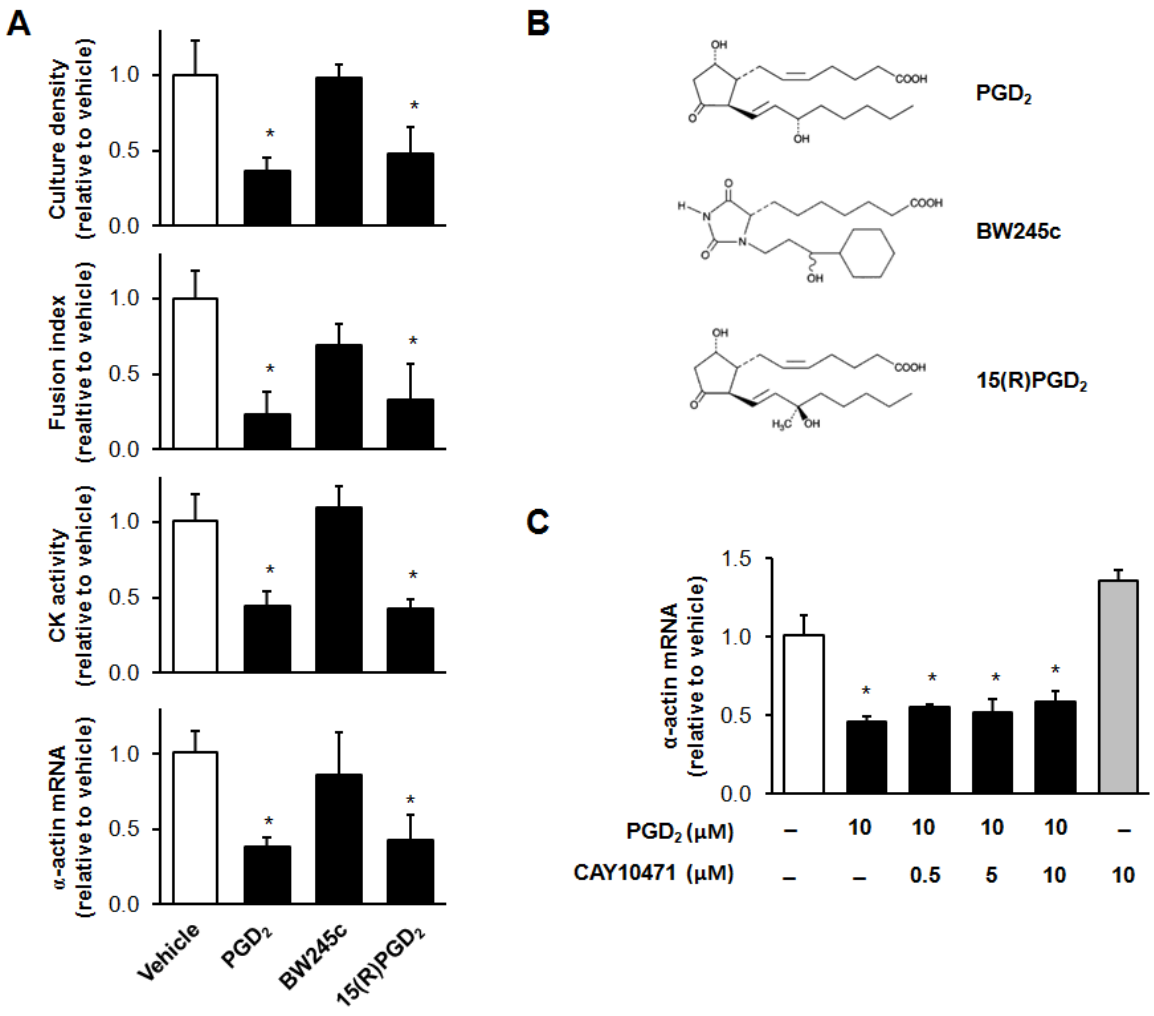

Figure 72 - Effects of DP1 and DP2 agonists and antagonists.

C2C12 were differentiated for 4 days in the presence of 10 μM PGD_2, 10μM BW245c (DP1 agonist), 10μM 15*R*-methyl-PGD_2 (DP2 agonist) or vehicle. **A:** Myogenic differentiation was measured by culture density, fusion index, creatine kinase activity and α-actin expression. **B:** Structures of PGD_2, BW245c and 15*R*-methyl-PGD_2 (15(R)-PGD_2). **C**: Cells were pre-incubated for 30 minutes with 0.5, 5 and 10 μM CAY10471 (DP2 antagonist) before the addition of 10 μM PGD_2. At day 4 post-confluence RNA was extracted and expression of skeletal α-actin 1 assessed by QRT-PCR. Data are the average of three biological replicates ± standard deviation. *, *P* <0.05 versus vehicle control.

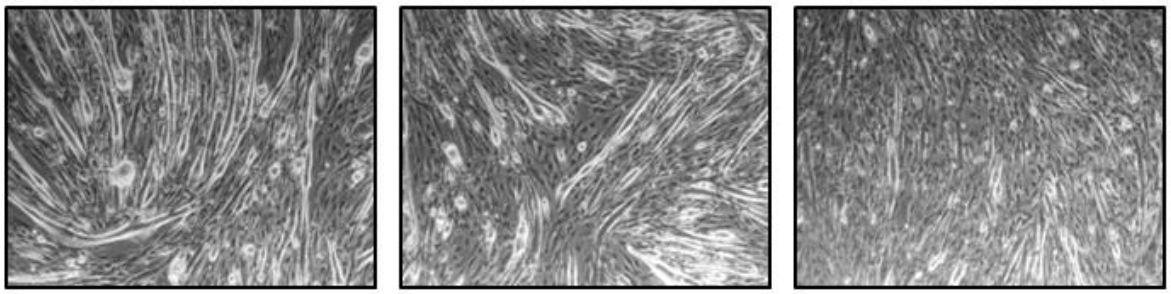

Figure 73 - DP2 agonist, 15R-methyl-PGD2, inhibits myogenesis at high micromolar doses.

C2C12 were differentiated in the presence of 1 and 10 μM 15*R*-methyl-PGD_2 or vehicle. Differentiation is shown by phase-contrast photography of cultures.

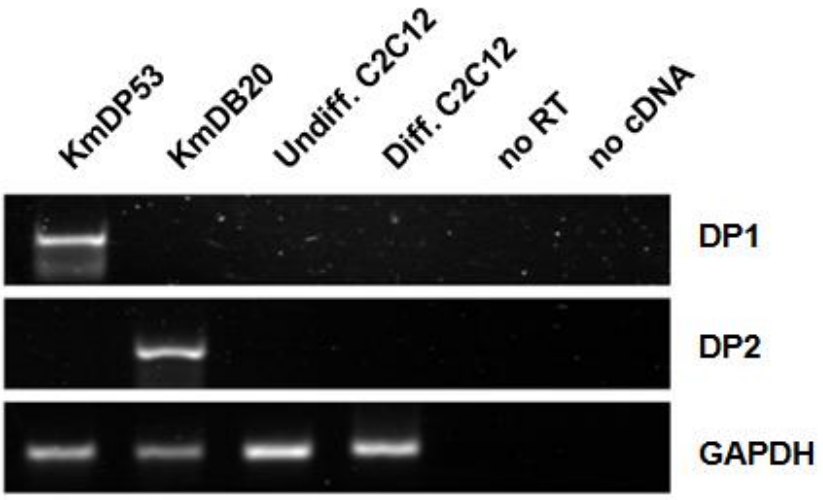

Figure 74 - C2C12 do not express DP1 or DP2.

Representative gel showing expression of DP1 and DP2 in differentiated and undifferentiated C2C12 using RT-PCR. As positive controls, cDNA from mouse DP1 (KmDP53) and DP2 (KmB20) transfected cells were used. Positive controls and GAPDH: 30 cycles. C2C12 samples and negative controls: 38 cycles.

6.12 Production of prostanoids by C2C12

Since PGD_2 has modulatory effects on C2C12 myogenesis we inquired if these cells are able to secrete endogenous PGD_2 as a form of autocrine and paracrine signalling. Firstly the expression of enzymes involved in the production of PGD_2 was analysed: COX-2 and the two PGD_2-synthases H-PGDS and L-PGDS (pathway in Figure 19). As shown in Figure 75, COX-2 mRNA levels were high in undifferentiated cells (day -1) but quickly dropped in the following days, suggesting PG production is reduced during myogenesis. Both PGDS enzymes were expressed at low levels in undifferentiated cells. However, L-PGDS was strongly upregulated during differentiation in a similar fashion to that observed for α-actin (Figure 64). Levels of H-PGDS remained unchanged.

In order to identify which PGs are produced by C2C12, undifferentiated (day 0) and differentiated (day 4) cultures were incubated with trace amounts of radio-labeled [^{14}C]-arachidonic acid (AA). Total prostanoids were extracted from culture supernatants and separated using thin layer chromatography. As shown in Figure 76 A, myoblasts produced several arachidonic acid-derived products, the most predominant of which co-migrated with PGE_2. Lower levels of products co-migrating with PGD_2 and $PGF_{2\alpha}$ were also detected. Inhibition of COX activity with 20 μM indomethacin blocked the formation of these products (Figure 76 A). In differentiated C2C12 cultures PG synthesis dramatically decreased (Figure 76 B) in agreement with COX-2 being downregulated at the onset of differentiation. PGE_2 was still detected in differentiated cultures but a large fraction of the radioactive label was retained in the origin, suggesting that arachidonic acid was being converted to more hydrophilic species. Production of an unidentified AA product was also reduced in differentiated C2C12.

Secretion of PGD_2 to culture media was also measured by an ELISA-based method. In agreement with the AA incubation assay, low levels of PGD_2 were detected in supernatant of undifferentiated cells which were further reduced to near undetectable levels in later stages of differentiation (Figure 76 C). These results show that, despite the upregulation of L-PGDS, the levels of PGD_2 secreted by C2C12 are unlikely to exert an autocrine or paracrine effect on differentiation.

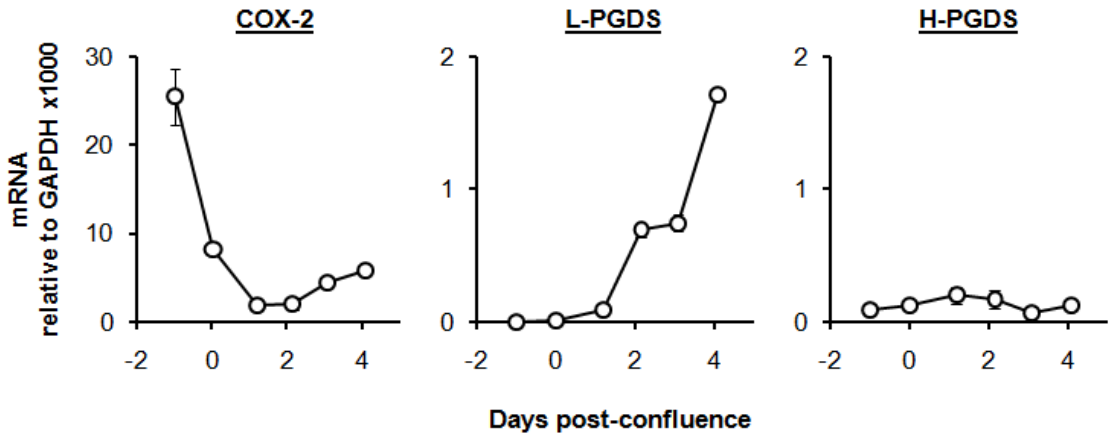

Figure 75 - Expression of COX-2, L-PGDS and H-PGDS during C2C12 differentiation.

C2C12 cells were differentiated for a period of 4 days. Expression of COX-2, L-PGDS and H-PGDS was measured by Taqman QRT-PCR on RNA extracted every 24h from day -1 to day 4 post-confluence. Note that L-PGDS and H-PGDS expression is presented at the same scale. Data are normalized to GAPDH expression and represent the average of three biological replicates ± standard deviation.

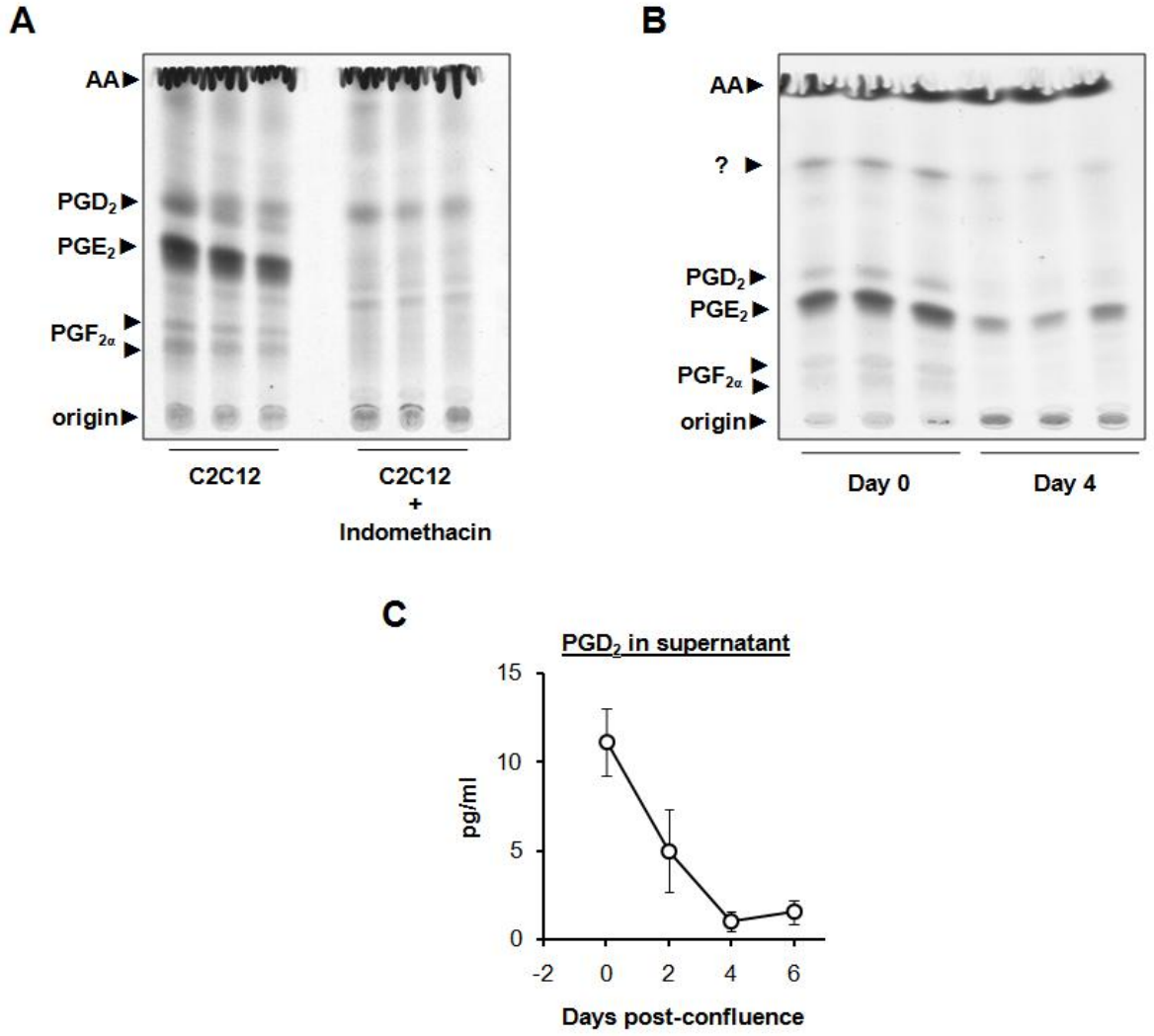

Figure 76 - Metabolism of arachidonic acid and production of PGD_2 by C2C12 cells.

A: Undifferentiated C2C12 were incubated with [^{14}C]-arachidonic acid (AA) for 3 hours in the presence or absence of 20 µM indomethacin. PGs were extracted from the supernatant and separated by thin layer chromatography (TLC) along with cold standards for PGD_2, PGE_2 and $PGF_{2\alpha}$. Three biological replicates are shown for each condition. **B**: Undifferentiated (day 0) and differentiated (day 4) cells were incubated with ^{1}C-arachidonic acid (AA) for 3 hours. PGs were extracted and separated as mentioned above. **C**: PGD_2 levels in the supernatant were measured during C2C12 differentiation using an ELISA-based assay as described in page 98. Dots represent average of six biological replicates and error bars represent standard deviation.

6.13 L-PGDS is upregulated during C2C12 myogenesis

The data in the previous section demonstrated that L-PGDS is markedly upregulated during C2C12 differentiation despite no increase in PGD_2 production being observed. This protein has a dual function, acting as a PGD_2 synthase in the cytoplasm and as a high affinity transporter for retinoids if secreted to the extra-cellular space (Urade and Hayaishi, 2000a).

Using a monoclonal antibody, the expression of L-PGDS protein was analysed during C2C12 differentiation in cells and in supernatant. L-PGDS protein was not detected inside cells at any time-point during myogenesis (data not shown). In contrast, L-PGDS was detected in the supernatant of cells from day 0 (addition of low-serum media) until day 4 (Figure 77). The two detected species migrated with a molecular weight of ~50 and ~60 kDa, much higher than the ~21 kDa predicted for the wild type protein. Such discrepancy in molecular weight might be due to post-translational modifications such as *N*-glycosylation, known to occur at two sites in L-PGDS (Ragolia et al., 2007). Pure recombinant GST-fused L-PGDS was used as a positive control and migrated according to the predicted molecular weight (~46 kDa).This result and the absence of PGD_2 production by C2C12 cells suggest that L-PGDS is not acting as a PGD_2 synthase.

I then tested if the change to differentiation media (5% serum) was sufficient to induce upregulation of L-PGDS. Also, because the regulatory region of the L-PGDS gene contains thyroid hormone responsive elements (TRE) and indeed thyroid hormone (T3) is able to induce L-PGDS expression in mouse neuronal cells (Garcia-Fernandez et al., 2000, Urade and Hayaishi, 2000b) the effect of 100 nM T3 on L-PGDS expression was examined. As shown in Figure 78, increased expression of L-PGDS, myogenin and α-actin were observed in cells incubated for 48h in differentiation media (5% HS) relative to cells kept in growth media (10% FBS). Addition of 100 nM T3 did not result in any change in expression of L-PGDS, myogenin or α-actin in any type of media. Like L-PGDS, the genes coding for myogenin and α-actin are flanked by thyroid hormone responsive elements and, in contrast to the results shown here, have been shown to be induced by T3 in C2C12 cells (Baumgartner et al., 2007). This suggests that the experimental conditions used in this experiment may not have been suitable.

In order to further elucidate the role of L-PGDS in C2C12 myogenesis the L-PGDS coding region was cloned and a pcDNA3.1-based over-expression plasmid was generated (see page 87). Using site-directed mutagenesis a C65A mutatation was introduced in the L-PGDS vector, thus coding for an enzymatically inactive protein (see page 76). Both plasmids were used to generate stably-transfected CHO cells that can be used to produce conditioned media with post-translationally modified L-PGDS protein. Unfortunately, due to time restriction these tools were not validated or used in experiments with C2C12. Therefore, the function and cause of L-PGDS upregulation in C2C12 remains unknown.

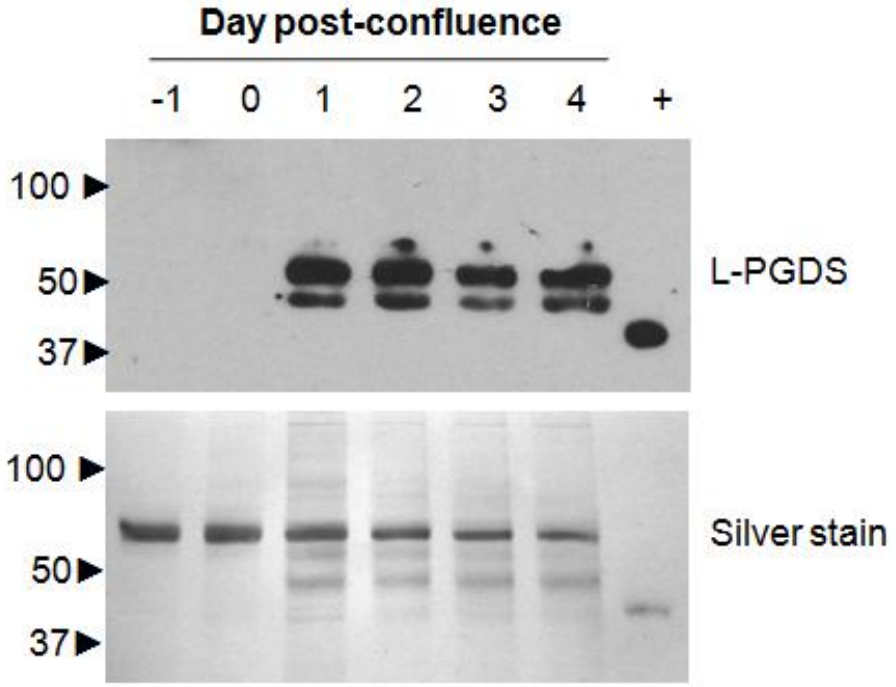

Figure 77 - C2C12 secrete L-PGDS into the supernatant after incubation with differentiation media.

C2C12 cells were differentiated for four days. At days -1, 0, 1, 2, 3 and 4, cells were washed, transferred to serum-free media and left to incubate for 24 hours. For each day, 30 µl of supernatant were separated in SDS-PAGE alongside purified recombinant mouse L-PGDS (+). Proteins were then transferred onto a membrane and probed with a monoclonal antibody against L-PGDS. Each lane contains proteins secreted by C2C12 over the period of 23 hours. Note that the recombinant L-PGDS used here as a positive control was produced in bacteria with a GST-tag and has a predicted molecular weight of 46 kDa. For visualization of total proteins, gels were silver stained. Values on the left correspond to the protein ladder (in kDa).

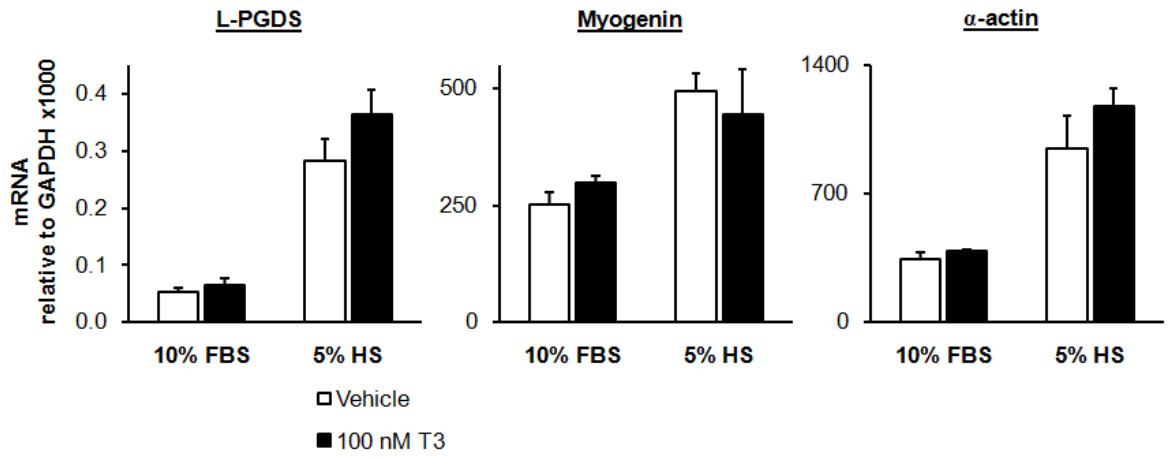

Figure 78 - Differentiation media induces upregulation of L-PGDS, myogenin and α-actin.

C2C12 were seeded in growth media and, after 24 hours changed to growth media (10% FBS) or differentiation media (5% HS) supplemented with 100 nM T3 or vehicle. Cells were harvested 48 hours later and used for RNA extraction. Expression of L-PGDS, myogenin and α-actin were measured using Taqman QRT-PCR. Bars represent the average of three biological replicates and error bars represent standard deviation.

6.14 Discussion

Disruption of myofibers, caused by either injury or exercise, activates two cellular processes essential for local tissue regeneration. Firstly, the transition of quiescent satellite cells to proliferating myoblasts and secondly the activation of resident mast cells followed by sequential infiltration of neutrophils and macrophages. Activated mast cells release large amounts of PGD_2 that is known to act as a chemoattractant for circulating leukocytes. Given that myoblasts share this pro-inflammatory microenvironment I questioned if high doses of PGD_2 can affect myoblast behaviour, particularly in their ability to form myotubes.

C2C12: tools of the trade

The C2C12 cell line, immortalised myoblasts derived from adult mice that retain the capability to undergo myogenic differentiation *in vitro*, were used as model for adult myogenesis. Although this system does not mimic all the aspects of the injured and inflamed muscle it offers the possibility of studying the myogenic process in isolation whilst adding the desired stimuli, like PGD_2, in a controlled fashion. C2C12 differentiation was induced by culturing confluent cultures in low-serum media (5% horse serum). This resulted in withdrawal from cell cycle, followed by cell fusion to form long syncytial myotubes. Differentiation was accompanied by increased expression of MyoD, myogenin and α-actin as well as increased creatine kinase activity.

A quick, cheap and easy method to quantify C2C12 myogenesis

I have also developed an unbiased and less labour-intensive method for quantifying C2C12 differentiation based on photographs of Jenner-Giemsa stained cultures. Protein-rich mature myotubes stain darker and this maturation can be assessed by obtaining the picture histograms and measuring the amount of pixels in the darkest tones. The method requires simultaneous staining using a single batch of dyes and simultaneous photography to minimize variability between pictures. The threshold of darkest tones is arbitrary and, in the experiment shown in Figure 59, the sum of tones 0 to 50 (tones range from 0 to 255) were chosen for comparison. In other experiments thresholds of 75 or even 100 were used, depending on the shape of the histograms. Nevertheless, for each individual experiment the same threshold was used. The data showed that the increase in culture density measured with this method is a different

phenomenon to that measured by the fusion index. In C2C12 *in vitro* differentiation, cells fuse quickly after serum-reduction to form long myotubes while accumulation of protein in these structures happens afterwards. The sequence of these two events, preceded by an increase in cell number, is shown in Figure 59. Measurement of fusion index, the most widely used method to assess *in vitro* myogenesis, requires the scoring of nuclei as inside or outside myotubes in a large number of photographs, increasing the chance of human error and biased assessment. The histogram method was used as an unbiased complement to the fusion index analysis for photographs of stained cultures.

PGD_2 inhibits C2C12 and L6 myogenesis

The experiments presented here show that micromolar doses of PGD_2 inhibit myotube formation in a dose dependent manner as measured by fusion index and culture density. The inhibition had an IC50 of ~ 5 μM, a level that is likely to occur in inflamed tissues according to previous studies (Rajakariar et al., 2007, Anhut et al., 1979, Irikura et al., 2009). These doses are however, far higher than those required to activate the surface receptors DP1 and DP2 (Ulven and Kostenis, 2006). Importantly, equimolar doses of PGE_2 and $PGF_{2\alpha}$ did not inhibit C2C12 differentiation despite being structurally very similar to PGD_2 (Figure 79). These molecules differ only in the configuration of the carbon ring: 9-hydroxyl, 11-keto for PGD_2; 9-keto, 11-hydroxyil for PGE_2 and 9,11-hydroxyl for $PGF_{2\alpha}$, suggesting this might be the moiety in PGD_2 responsible for inhibiting myotube formation.

Inhibition of cell fusion and creatine kinase activity could be observed as early as day 2 post-confluence. Also, one single administration of PGD_2 at day 0 exerted the same effect as refreshing PGD_2 every 2 days, suggesting the block occurs at an early stage in differentiation. Expression of myogenic markers during differentiation was deregulated by PGD_2 including the early upregulation of MyoD and the long-term upregulation of myogenin and α-actin. Altogether, these data suggest myogenesis is being blocked at an early stage by PGD_2.

Importantly, myogenic differentiation of the rat myoblast cell line, L6, was also inhibited by PGD_2 in an identical dose range. This strongly suggests that the PGD_2 effect is not a cell line-specific artifact. However, both cell lines are immortalised and of rodent origin, an important bias that should be taken into account. Future studies should therefore make use of isolated primary myoblasts to test the inhibitory effects of PGD_2. This, alongside *in vivo* studies with

regenerating muscle, would be the ultimate confirmation of the role of PGD_2 in adult myogenesis.

Exposure to PGD_2 caused an increase in cell number 24 hours after treatment accompanied by a higher proportion of cells in S and G2/M phase. Differences in cell cycle profile dissipated after 48 hours as cells in both treatments progressed almost exclusively to G1/G0 phase. Therefore, when myoblasts are induced to exit cell cycle in low-serum conditions, PGD_2 appears to keep cells in a proliferative state for longer, delaying the subsequent myogenic commitment. The increased cell number might be a consequence rather than the cause of the inhibition.

Previous reports had shown that micromolar doses of 15d-PGJ_2, the end product of PGD_2 spontaneous dehydration, were able to block C2C12 myogenesis (Hunter et al., 2001). We have observed that PGD_2 levels quickly decrease in culture media and dehydration products, including 15d-PGJ_2, are generated early on. However, the total levels of these dehydration products remained unchanged suggesting that either PGD_2 or the products themselves were being taken up by the cells. Nevertheless, generation of this reactive prostaglandin is specific to PGD_2 and does not occur with PGE_2 or $PGF_{2\alpha}$.

Treatment with PGD_2 did not induce mitochondrial superoxide levels instead bringing a small but significant decrease. In contrast, exogenous 15d-PGJ_2 caused a 1.5 fold increase in superoxide levels, comparable to the effect of H_2O_2, a known inducer of reactive oxygen species. Furthermore, cells treated with 15d-PGJ_2 appeared stressed and cell numbers decreased after 24 hours of treatment as opposed to the increase in cell numbers observed with PGD_2. Furthermore, inhibition of differentiation by PGD_2 did not seem to require PPARγ, a nuclear receptor activated by 15d-PGJ_2. Curiously, ciglitazone (PPARγ agonist) reduced culture density without affecting myotube formation suggesting activation of PPARγ may be involved in protein production during maturation. Also, whilst PPARγ was down-regulated during C2C12 differentiation, treatment with PGD_2 caused an upregulation instead. A previous study showed that over-expression or knock-down of PPARγ in C2C12 ablated myogenic differentiation. Therefore, the PGD_2-induced upregulation of PPARγ might be the downstream mechanism leading to the inhibition of myogenesis. These results imply that although PGD_2 generates 15d-PGJ_2 in culture, the inhibition is not likely to be mediated by the dehydration product.

Time-lapse imaging was also used to quantify changes in cell motility and found that PGD_2-treated cells are less motile than untreated cells. During inflammation, PGD_2 acts as a chemotractive signal for leukocytes and this phenomenon is mediated by DP2. However, the data shown here revealed that that C2C12 do not express DP2 (or DP1) at any time during differentiation. During myogenesis, myoblasts align with each other in parallel before fusion. This alteration in cell motility can therefore affect the process of fusion as cells fail to position themselves correctly.

As mentioned above, expression of the PGD_2 high-affinity surface receptors DP1 and DP2 was not detected using RT-PCR. Quantitative RT-PCR detected very low levels of DP2 but these measurements were too close to the detection limit of the method. Nevertheless a vector over-expresing a shRNA targeted against DP2 mRNA was built and used to attempt to knock-down gene expression. These attempts were without success as DP2 levels remained close to the detection limit of the QRT-PCR. It was concluded that DP2 expression is absent or too low to have any biological significance.

Despite the lack of DP2 expression, the selective agonist 15*R*-methyl- PGD_2 was able to mimic PGD_2 in blocking myogenesis. On the other hand, BW245c, a DP1 agonist, exerted no effect. Like PGD_2, 15*R*-methyl- PGD_2 only blocked differentiation at micromolar doses that are far higher than the published concentrations needed to activate DP2. This suggests that both PGD_2 and 15*R*-methyl- PGD_2 are acting independently of DP2 but hitting the same, yet unknown, biological target. Indeed, 15*R*-methyl- PGD_2 shares the same 9-hydroxyl, 11-keto configuration in the carbon ring as PGD_2 (Figure 79), further implying that this is the moiety responsible for the inhibition of differentiation. Also, it can not be ruled out that, like PGD_2, 15*R*-methyl- PGD_2 may suffer spontaneous dehydration and generate a reactive prostaglandin like 15d-PGJ_2.

COX-2 expression was markedly down-regulated at the onset of differentiation, therefore limiting the production of prostanoids. However, L-PGDS (but not H-PGDS) was strongly upregulated during differentiation, suggesting the PGD_2 production capability might be increased. Incubation of C2C12 with arachidonic acid revealed that undifferentiated cells produce several types of prostaglandins, mainly PGE_2 and to a lesser extend PGD_2 and $PGF_{2\alpha}$. In agreement with COX-2 down-regulation, differentiated (day 4) cells showed a marked decrease in prostaglandin production. Production of PGD_2 did not increase during

differentiation, despite L-PGDS up-regulation. Levels of PGD_2 were also measured with and ELISA-based assay yielding the same results. This suggests that C2C12 do not produce large enough amounts of PGD_2 to exert an autocrine or paracrine effect on differentiation.

L-PGDS: what role in myogenesis?

The scale of L-PGDS up-regulation mirrored that of α-actin suggesting that the expression of this protein to be important in terminal differentiation. L-PGDS is a bifunctional protein that can act as a PGD_2 synthase when retained in the cytosol or as a ligand-carrier protein for bile acids and retinoids when secreted (Urade and Hayaishi, 2000a). Because no increase in PGD_2 production was observed during differentiation and because L-PGDS protein was detected in the supernatant but not in cell lysates of differentiated cells it is reasonable to propose that it does not act as a synthase in C2C12 but has an extracellular function. L-PGDS expression and secretion was induced at the onset of differentiation and may induce myoblasts to exit the proliferative state as was previously observed in isolated vascular smooth muscle cells (Ragolia et al., 2004). L-PGDS may also be involved in muscle nutrient uptake as it has been shown to promote glucose transport in L6 cells (Ragolia et al., 2008) and L-PGDS knock-out mice develop glucose-intolerance (Ragolia et al., 2005). Culturing C2C12 cells in 5% horse serum caused a 5.5-fold increase in L-PGDS expression relative to cells cultured in 10% FBS. Despite previous reports showing that thyroid hormone induces L-PGDS expression, no change in mRNA levels after treatment with 100 nM T3 was observed. The reported myogenin and α-actin up-regulation in C2C12 after T3 exposure were also not observed perhaps suggesting the experimental conditions (e.g. T3 quality) were not ideal. CHO cell lines over-expressing wild type and C65A mutated L-PGDS were generated and will be used for future studies. However, due to time limitation I could not entirely explain the physiological relevance of L-PGDS in myogenic differentiation.

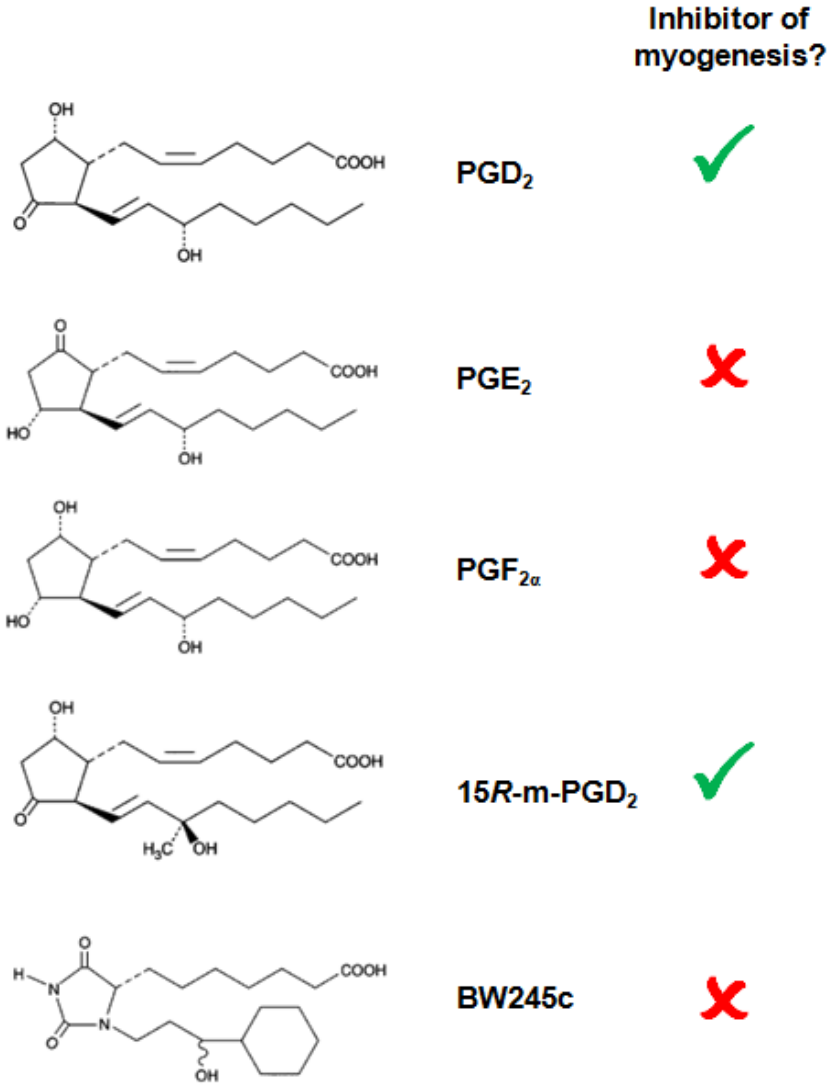

Figure 79 - Structure and inhibitory actions of PGs and PG-like molecules.

PGD_2 and 15*R*-mehtyl-PGD_2 (15*R*-m-PGD_2) blocked myotube formation in C2C12 at micromolar doses. However, structurally similar molecules PGE_2 and $PGF_{2\alpha}$ had no effect in differentiation at the same doses. Also, BW245c failed to block C2C12 myogenesis.

CHAPTER SEVEN: General discussion

7.1 Divergence between mouse and human AKR1C enzymes

7.1.1 Different phylogeny, substrate preference and tissue distribution

Enzymes of the AKR1C subfamily have been implicated in the progression of human prostate and breast carcinomas as well as leukaemias due to their steroid hormone and prostaglandin reductase activities. In this project I attempted to identify the homologue of AKR1C3 (PGD_2 11β-ketoreductase; 17β-HSD; 20α-HSD) amongst the eight murine AKR1C isoforms with the objective of generating a knock-out mouse strain and studying its role in leukaemogenesis.

A subfamily on the verge of a breakdown

When speciation occurs, the divergent copies of a given gene in the resulting species are said to be orthologous. Many human genes have a single corresponding orthologue ("one-to-one") in the mouse genome and their function is often conserved. In some cases, after speciation, the orthologues undergo gene duplication and a "one-to-one" comparison is no longer possible. This is the case for AKR1C genes of mice and humans.

Sequence alignment of known and predicted mammalian AKR1C amino-acid sequences revealed new aspects of the subfamily (Figure 37). Firstly, the number and sequence of AKR1C enzymes is highly variable across the different mammalian orders. Thus, AKR1C enzymes are only conserved in closely related species of the same order (primates, rodents, etc.). Human AKR1C enzymes have "one-to-one" orthology with isoforms from chimpanzee and macaque but not with isoforms of non-primate species. Similarly, bovine, equine and rodent enzymes have higher identity with enzymes of the same order. However, even in some species of the same order the number of AKR1C genes is not conserved. This is the case for AKR1C1 and -1C2, two genes existing in humans but not in chimpanzee or macaque. Likewise, rat and mouse have several species-specific duplications.

Nevertheless, previously described orthologues were identified such as human AKR1C4 and macaque AKR1C25, both liver-restricted enzymes with identical substrate preference and inhibitor sensitivity (Higaki et al., 2002). Also, murine AKR1C18 and rat AKR1C8 are

known homologues for their ability to inactivate progesterone in the ovary and uterus (Miura et al., 1994, Maho Ishida, 1999). Such parallelisms were not observed between human and mouse enzymes. Overall, this analysis implies that AKR1C enzymes have diverged significantly between mice and humans since their latest common ancestor. This analysis also suggests that the AKR1C isoforms have changed in number and sequence according to the evolutionary needs of each mammalian order, family or even genus.

Lack of a PGD_2 11β-ketoreductase amongst the mouse AKR1C enzymes

Surprisingly, none of the murine isoforms mimicked AKR1C3 in reducing PGD_2 (page 118) supporting the idea of a divergent function of the subfamily in the two species. The absence of a PGD_2 reductase also suggests that the roles of PGD_2 and 15d-PGJ_2 in mouse haemopoiesis may not be conserved and that their pro-differentiative effects are human or primate-specific. Murine haemopoietic progenitors may rely on a different molecule to regulate differentiation, such as PGE_2, recently shown to promote proliferation of haemopoietic stem cells in zebrafish and mouse (Lord et al., 2007, North et al., 2007). However, the bone-marrow of rodents, like that of humans, is a PGD_2-rich environment (Ujihara et al., 1988b). Alternatively, if the function of PGD_2 and 15d-PGJ_2 is conserved in mouse haemopoiesis, the reduction to 11β-$PGF_{2\alpha}$ may be performed by an enzyme of another AKR subfamily or a non-AKR enzyme (Figure 80). This hypothesis is further supported by the absence of AKR1C expression in the murine haemopoietic progenitor cell line HPC-7 (page 136). The absence of homology with the human isoforms reported here compromised the primary objective of this project, the creation of a mouse strain lacking the AKR1C3-homologue but, on the other hand, prompted further investigation on the divergence of AKR1C functions of mice and humans.

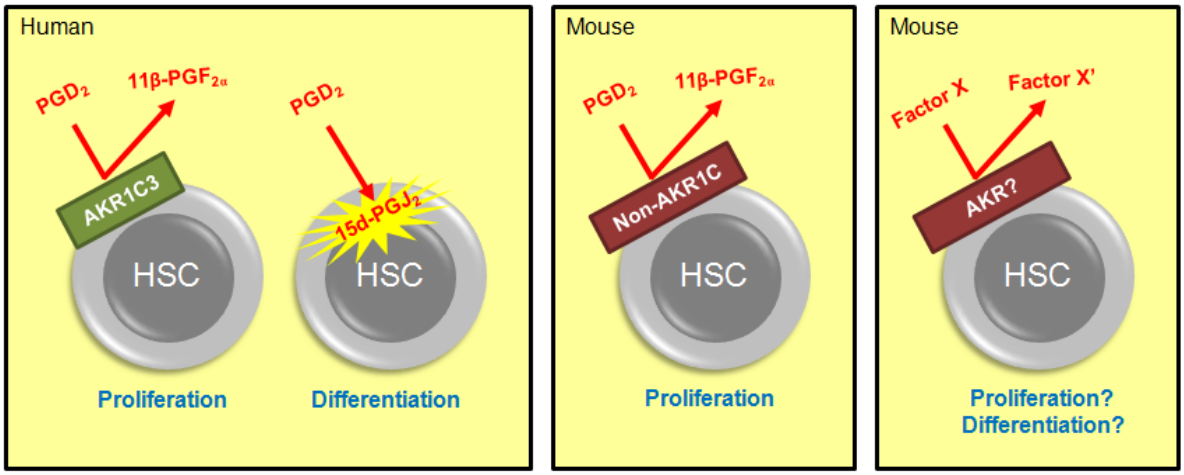

Figure 80 - Regulation of HSC proliferation by PGD_2 is not conserved between humans and mice.

In human haemopoietic stem cells (HSC) and leukaemic cells, AKR1C3 prevents differentiation by converting PGD_2 to 11β-$PGF_{2\alpha}$ and protecting from the generation of 15d-PGJ_2. However, mice lack an AKR1C with PGD_2 reductase activity suggesting an alternative mechanism. Either a non-AKR1C enzyme converts PGD_2 to 11β-$PGF_{2\alpha}$ or an alternative factor (X) regulates the balance proliferation and differentiation.

AKR1C6: a novel PGE_2 9-ketoreductase?

An as yet unreported PGE_2 reductase activity of mouse recombinant AKR1C6 was also shown here (page 120) similar to that observed with rabbit AKR1C5 (Wintergalen et al., 1995). AKR1C6 and -1C5 have high sequence identity (80%) and identical kinetic parameters towards PGE_2. In addition, both enzymes have 20α-HSD activity towards progesterone (page 130). These enzymatic activities are particularly important during female estrous cycle and parturition, where increased $PGF_{2\alpha}$ levels signaling via FP and inactivation of progesterone induce degeneration of the corpus luteum and uterine contraction, respectively (Unezaki et al., 1996). However, whilst AKR1C5 is expressed in the ovaries of rabbits, AKR1C6 was found to be expressed exclusively in the liver (Figure 49) suggesting these enzymes may not be functional homologues.

Steroid hormone metabolism and tissue expression

Despite some mouse enzymes being able to reduce androstanediol, 5α-DHT, estrone and progesterone, their expression was not detected in the usual sex steroid-sensitive tissues. For instance, AKR1C6 and AKR1C21 perform the pro-androgenic conversion of androstanediol to 5α-DHT and the anti-androgenic inactivation of 5α-DHT but their expression is restricted to liver and kidney, respectively. Conversely, only very low levels of AKR1C12 and -1C14 expression were detected in prostate ant testes, respectively, but these enzymes had no activity towards androgens (Figure 49). Similarly, AKR1C6 and AKR1C20 were able to reduce progesterone (20α-HSD activity) but no expression was detected in the ovary or uterus of mice. This discrepancy between enzymatic activity and tissue expression further accentuates the lack of homology between human and mouse AKR1C isoforms.

The only exception was AKR1C18, which is highly expressed in the mouse ovaries and inactivates progesterone. As reported previously (Piekorz et al., 2005), expression of AKR1C18 was found to be suppressed during pregnancy, when progesterone remains active in the serum to support the gestational tissues (Figure 49). The results shown here report for the first time two additional activities of AKR1C18 with possible relevance in female reproductive tissues: potentiation of estrone to 17β-estradiol (pro-estrogenic) and inactivation of 5α-DHT (anti-androgenic). AKR1C18 performed these three steroid reductase activities with efficiency several times higher than that observed with the human isoforms (Table 9). Judging by its distant phylogenetic relationship, enzymatic efficiency towards substrates and tissue expression it is reasonable to affirm that AKR1C18 has no functional homologue amongst the human isoforms.

Interestingly, very low or no steroid reductase activity was observed for AKR1C12, -1C13, -1C14 and -1C19. Given that steroids and prostaglandins are the substrate hallmarks of this subfamily, and possibly a characteristic of the AKR1C ancestor, it is likely that these enzymes have specialised in reducing other types of substrates. These AKR1C isoforms are mostly expressed in the gastro-intestinal tract and may be involved in metabolism of dietary compounds.

Overall, this analysis showed that despite some mouse AKR1C enzymes having ketosteroid reductase activities, the combination of these activities with their tissue-expression pattern does not resemble what occurs in humans.

7.1.2 Implications for modeling AKR1C enzymes in cancer

Due to the increasing range of tools available to manipulate it's genome, the mouse has become a powerful and commonly used tool to query gene function and model human disease (Jackson-Grusby, 2002). However, direct comparison between the two mammalian organisms requires conservation of orthologous genes. The results shown here have exposed a significant lack of phylogenetic and functional conservation between human and mouse AKR1C enzymes thus compromising the use of mice to model human AKR1C function in normal physiology and cancer. Other animal models should be considered and validated, particularly inside the primate order, in order to study the role of AKR1C enzymes in prostate and breast cancer and leukaemias and test novel anti-cancer drugs.

7.2 PGD_2 inhibits C2C12 myogenesis via an unknown mechanism

Disruption of muscle tissue occurring after injury or exercise triggers a series of physiological processes aimed to repair the damaged tissue. One process involves the activation of satellite cells into myoblasts that proliferate, commit to differentiation and finally fuse with and repair the damaged myofibers. In parallel, muscle damage also activates tissue-resident mast cells which initiate an inflammatory response by attracting neutrophils and macrophages from the blood stream. These two processes are known to cross-talk and coordinate tissue healing. A major signaling molecule secreted during early inflammation is PGD_2. Thus, despite proliferating myoblasts being exposed to high concentrations of PGD_2 during adult muscle regeneration, the effect of this eicosanoid in myogenesis had never been addressed.

I have shown here that C2C12 myoblast differentiation into myotubes is inhibited by PGD_2 in a dose-dependent manner with an IC50 of ~ 5 μM, a dose likely to occur in inflammatory fluids (Anhut et al., 1979). The block imposed by PGD_2 caused de-regulated expression of myogenic regulators MyoD and myogenin that could be observed already in the first 24 to 48 hours. Markers of terminal differentiation were also suppressed such as α-actin expression, creatine kinase activity and cell fusion. Inhibition of myogenesis did not occur when cells were exposed to equimolar doses of PGE_2 and $PGF_{2\alpha}$, despite their structural resemblance with PGD_2. Curiously, the synthetic molecule 15*R*-methyl-PGD_2, which has the same 9-hydroxyl, 11-keto configuration in the carbon ring as PGD_2, also inhibited myogenesis in the same range. Since this configuration is not present in PGE_2 or $PGF_{2\alpha}$ it is likely that this is the moiety responsible for inhibition.

The mechanism by which PGD_2 inhibits C2C12 myogenesis could not be uncovered in this study but some potential pathways were excluded. Firstly, the two surface receptors for PGD_2, DP1 and DP2, were not expressed in C2C12. A DP-mediated action was unlikely since these receptors are activated by nanomolar doses of PGD_2 rather than the micromolar doses required to exert effect. Alternatively, the spontaneous conversion of PGD_2 into the cyclopentenone prostaglandin 15d-PGJ_2 could account for the observed effects. Indeed, a significant proportion of PGD_2 was shown to spontaneously dehydrate in culture media. However, unlike 15d-PGJ_2, addition of PGD_2 to culture media did not result in generation of mitochondrial superoxide. Also, inhibition of myogenesis by PGD_2 did not require PPARγ

activation suggesting that spontaneous generation of 15d-PGJ_2 is not the mechanism of action. Therefore, the results shown here suggest an alternative form of PGD_2 signaling that responds to high concentrations, such as those observed at the onset of inflammation.

The findings presented here show that micromolar PGD_2 concentrations inhibit myogenesis in two commonly used myoblast models. Endogenous production of PGD_2 was found to be insufficient to bring about the block in myogenesis. Therefore I hypothesize that high levels of leukocyte-derived PGD_2 is the most likely signal for myoblasts to halt myogenic differentiation during the early noxious phases of inflammation in the wounded muscle. This mechanism would allow the local high PGD_2 levels to repress the onset of myogenesis while the diffused signaling from the same molecule would recruit inflammatory leucocytes via more conventional DP1 and DP2 signaling. Later in the process, when inflammation is resolved and PGD_2 is less prevalent, the myogenic block would be lifted and tissue regeneration could proceed. This coordinated process, involving cross talk between leucocytes and muscle cells, will be disrupted in the presence of COX inhibitory NSAIDs, resulting in reduced inflammation and deregulated myoblast function leading ultimately to improper healing.

7.3 L-PGDS up-regulation in C2C12 differentiation

L-PGDS was found to be markedly upregulated during C2C12 myogenesis, in a fashion similar to that of α-actin, a marker of terminal differentiation (Figure 81). Conversely, COX-2 expression was suppressed and, in agreement, prostanoid production (including PGD_2) decreased during differentiation. Thus, it was hypothesised that the increase in L-PGDS mRNA was related to its extracellular lipocalin functions rather than its cytosolic PGD_2-synthase activity. In agreement, L-PGDS protein was found to be efficiently exported to the culture supernatant after cells were cultured with differentiation medium (5% horse serum), further supporting a role of the protein in the extracellular space. The protein detected in the supernatant had a molecular weight higher than the predicted 21 kDa suggesting that L-PGDS is post-translationally modified, possibly by *N*-glycosylation (Ragolia et al., 2007).

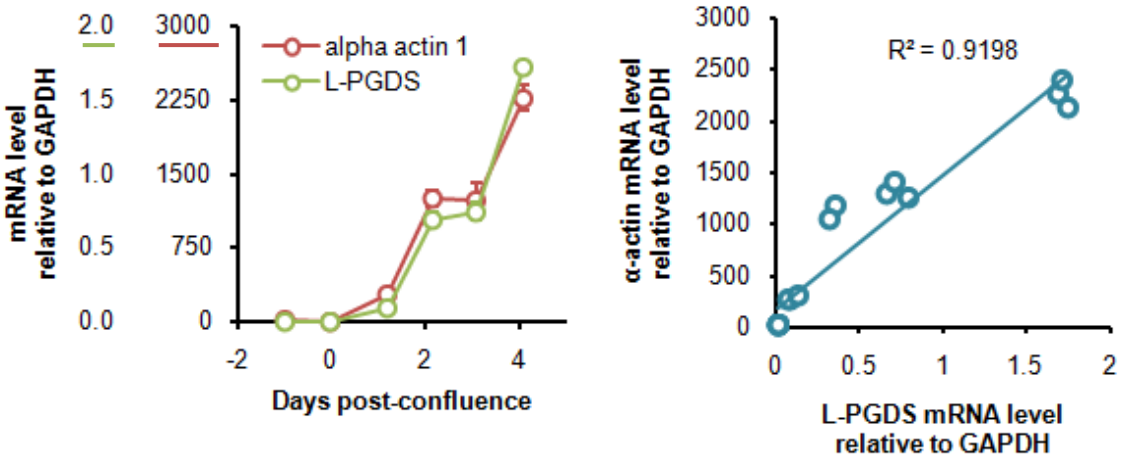

Figure 81 - Correlation between L-PGDS and α-actin mRNA levels during C2C12 differentiation

The physiological significance of L-PGDS upregulation and secretion in C2C12 myogenesis remains unclear. The promoter region of the L-PGDS gene contains thyroid hormone responsive elements, and its expression has been shown to be upregulated by T3 (Garcia-Fernandez et al., 2000). Myogenin and α-actin are also target genes of the thyroid hormone receptor (Baumgartner et al., 2007) further implying that L-PGDS upregulation is co-regulated with markers of terminal myogenic differentiation. However, we could not show a T3-mediated effect on either L-PGDS, myogenin of α-actin expression.

Several links between L-PGDS and muscle homeostasis have been previously made that can justify its expression in C2C12. L-PGDS induces glucose uptake in L6 myoblasts, an essential process for muscle function (Ragolia et al., 2008). Additionally, L-PGDS knock-out mice develop a glucose-intolerant phenotype very similar to that observed in diabetes type II (Ragolia et al., 2005). Thus, L-PGDS upregulation may be important in promoting the metabolic functions of the muscle tissue.

Future experiments such as knock-down and over-expression of L-PGDS in C2C12 will elucidate if its expression is essential during differentiation or only relevant in myotube function. Also, validation of L-PGDS expression in primary myoblast differentiation and *in vivo* muscle injury as well as studies with the L-PGDS null mice would be valuable.

LIST OF REFERENCES

Abe, H., Takeshita, T., Nagata, K., Arita, T., Endo, Y., Fujita, T., Takayama, H., Kubo, M. & Sugamura, K. (1999) Molecular cloning, chromosome mapping and characterisation of the mouse CRTH2 gene, a putative member of the leukocyte chemoattractant receptor family. *Gene,* 227**,** 71-77.

Abramovitz, M., Boie, Y., Nguyen, T., Rushmore, T. H., Bayne, M. A., Metters, K. M., Slipetz, D. M. & Grygorczyk, R. (1994) Cloning and expression of a cDNA for the human prostanoid FP receptor. *J Biol Chem,* 269**,** 2632-6.

Andreassen, T. K. (2006) The role of plasma-binding proteins in the cellular uptake of lipophilic vitamins and steroids. *Horm Metab Res,* 38**,** 279-90.

Anhut, H., Brune, K., Frolich, J. C. & Peskar, B. A. (1979) Prostaglandin D2 is the prevailing prostaglandin in the acute inflammatory exudate of urate arthritis in the chicken. *Br J Pharmacol,* 65**,** 357-9.

Aparicio Gallego, G., Diaz Prado, S., Jimenez Fonseca, P., Garcia Campelo, R., Cassinello Espinosa, J. & Anton Aparicio, L. M. (2007) Cyclooxygenase-2 (COX-2): a molecular target in prostate cancer. *Clin Transl Oncol,* 9**,** 694-702.

Ardite, E., Barbera, J. A., Roca, J. & Fernandez-Checa, J. C. (2004) Glutathione depletion impairs myogenic differentiation of murine skeletal muscle C2C12 cells through sustained NF-kappaB activation. *Am J Pathol,* 165**,** 719-28.

Asou, H., Verbeek, W., Williamson, E., Elstner, E., Kubota, T., Kamada, N. & Koeffler, H. P. (1999) Growth inhibition of myeloid leukemia cells by troglitazone, a ligand for peroxisome proliferator activated receptor gamma, and retinoids. *Int J Oncol,* 15**,** 1027-31.

Azzarello, J. T., Lin, H. K., Gherezghiher, A., Zakharov, V., Yu, Z., Kropp, B. P., Culkin, D. J., Penning, T. M. & Fung, K. M. (2009) Expression of AKR1C3 in renal cell carcinoma, papillary urothelial carcinoma, and Wilms' tumour. *Int J Clin Exp Pathol,* 3**,** 147-55.

Baker, M. E. (2004) Co-evolution of steroidogenic and steroid-inactivating enzymes and adrenal and sex steroid receptors. *Mol Cell Endocrinol,* 215**,** 55-62.

Baumgartner, B. G., Orpinell, M., Duran, J., Ribas, V., Burghardt, H. E., Bach, D., Villar, A. V., Paz, J. C., Gonzalez, M., Camps, M., Oriola, J., Rivera, F., Palacin, M. & Zorzano, A. (2007) Identification of a novel modulator of thyroid hormone receptor-mediated action. *PLoS One,* 2**,** e1183.

Bellemare, V., Faucher, F., Breton, R. & Luu-The, V. (2005) Characterisation of 17alpha-hydroxysteroid dehydrogenase activity (17alpha-HSD) and its involvement in the biosynthesis of epitestosterone. *BMC Biochem,* 6**,** 12.

Birtwistle, J., Hayden, R. E., Khanim, F. L., Green, R. M., Pearce, C., Davies, N. J., Wake, N., Schrewe, H., Ride, J. P., Chipman, J. K. & Bunce, C. M. (2008) The aldo-keto reductase AKR1C3 contributes to 7,12-dimethylbenz(a)anthracene-3,4-dihydrodiol mediated oxidative DNA damage in myeloid cells: Implications for leukemogenesis. *Mutat Res*.

Birtwistle, J., Hayden, R. E., Khanim, F. L., Green, R. M., Pearce, C., Davies, N. J., Wake, N., Schrewe, H., Ride, J. P., Chipman, J. K. & Bunce, C. M. (2009) The aldo-keto reductase AKR1C3 contributes to 7,12-dimethylbenz(a)anthracene-3,4-dihydrodiol mediated oxidative DNA damage in myeloid cells: implications for leukemogenesis. *Mutat Res,* 662**,** 67-74.

Blobaum, A. L. & Marnett, L. J. (2007) Structural and functional basis of cyclooxygenase inhibition. *J Med Chem,* 50**,** 1425-41.

Boie, Y., Sawyer, N., Slipetz, D. M., Metters, K. M. & Abramovitz, M. (1995) Molecular cloning and characterisation of the human prostanoid DP receptor. *J Biol Chem,* 270**,** 18910-6.

Bondesen, B. A., Jones, K. A., Glasgow, W. C. & Pavlath, G. K. (2007) Inhibition of myoblast migration by prostacyclin is associated with enhanced cell fusion. *FASEB J,* 21**,** 3338-45.

Bondesen, B. A., Mills, S. T., Kegley, K. M. & Pavlath, G. K. (2004) The COX-2 pathway is essential during early stages of skeletal muscle regeneration. *Am J Physiol Cell Physiol,* 287**,** C475-83.

Bondesen, B. A., Mills, S. T. & Pavlath, G. K. (2006) The COX-2 pathway regulates growth of atrophied muscle via multiple mechanisms. *Am J Physiol Cell Physiol,* 290**,** C1651-9.

Bos, C. L., Richel, D. J., Ritsema, T., Peppelenbosch, M. P. & Versteeg, H. H. (2004) Prostanoids and prostanoid receptors in signal transduction. *Int J Biochem Cell Biol,* 36**,** 1187-205.

Breinig, M., Schirmacher, P. & Kern, M. A. (2007) Cyclooxygenase-2 (COX-2)--a therapeutic target in liver cancer? *Curr Pharm Des,* 13**,** 3305-15.

Breyer, R. M., Bagdassarian, C. K., Myers, S. A. & Breyer, M. D. (2001) Prostanoid receptors: subtypes and signaling. *Annu Rev Pharmacol Toxicol,* 41**,** 661-90.

Bryson-Richardson, R. J. & Currie, P. D. (2008) The genetics of vertebrate myogenesis. *Nat Rev Genet,* 9**,** 632-46.

Buckingham, M. (2006) Myogenic progenitor cells and skeletal myogenesis in vertebrates. *Curr Opin Genet Dev,* 16**,** 525-32.

Buckingham, M. (2007) Skeletal muscle progenitor cells and the role of Pax genes. *C R Biol,* 330**,** 530-3.

Bunce, C. M., French, P. J., Durham, J., Stockley, R. A., Michell, R. H. & Brown, G. (1994) Indomethacin potentiates the induction of HL60 differentiation to neutrophils, by retinoic acid and granulocyte colony-stimulating factor, and to monocytes, by vitamin D3. *Leukemia,* 8**,** 595-604.

Bunce, C. M., Mountford, J. C., French, P. J., Mole, D. J., Durham, J., Michell, R. H. & Brown, G. (1996) Potentiation of myeloid differentiation by anti-inflammatory agents, by steroids and by retinoic acid involves a single intracellular target, probably an enzyme of the aldoketoreductase family. *Biochim Biophys Acta,* 1311**,** 189-98.

Byrns, M. C., Duan, L., Lee, S. H., Blair, I. A. & Penning, T. M. (2010) Aldo-keto reductase 1C3 expression in MCF-7 cells reveals roles in steroid hormone and prostaglandin metabolism that may explain its over-expression in breast cancer. *J Steroid Biochem Mol Biol,* 118**,** 177-87.

Byrns, M. C., Steckelbroeck, S. & Penning, T. M. (2008) An indomethacin analogue, N-(4-chlorobenzoyl)-melatonin, is a selective inhibitor of aldo-keto reductase 1C3 (type 2 3alpha-HSD, type 5 17beta-HSD, and prostaglandin F synthase), a potential target for the treatment of hormone dependent and hormone independent malignancies. *Biochem Pharmacol,* 75**,** 484-93.

Cantini, M., Giurisato, E., Radu, C., Tiozzo, S., Pampinella, F., Senigaglia, D., Zaniolo, G., Mazzoleni, F. & Vitiello, L. (2002) Macrophage-secreted myogenic factors: a promising tool for greatly enhancing the proliferative capacity of myoblasts in vitro and in vivo. *Neurol Sci,* 23**,** 189-94.

Capdevila, J. H., Falck, J. R. & Imig, J. D. (2007) Roles of the cytochrome P450 arachidonic acid monooxygenases in the control of systemic blood pressure and experimental hypertension. *Kidney Int,* 72**,** 683-9.

Chandrasekharan, N. V. & Simmons, D. L. (2004) The cyclooxygenases. *Genome Biol,* 5**,** 241.

Chen, L. Y., Watanabe, K. & Hayaishi, O. (1992) Purification and characterisation of prostaglandin F synthase from bovine liver. *Arch Biochem Biophys,* 296**,** 17-26.

Cilloni, D., Martinelli, G., Messa, F., Baccarani, M. & Saglio, G. (2007) Nuclear factor kB as a target for new drug development in myeloid malignancies. *Haematologica,* 92**,** 1224-9.

Clark, J. D., Schievella, A. R., Nalefski, E. A. & Lin, L. L. (1995) Cytosolic phospholipase A2. *J Lipid Mediat Cell Signal,* 12**,** 83-117.

Collins, C. A., Zammit, P. S., Ruiz, A. P., Morgan, J. E. & Partridge, T. A. (2007) A population of myogenic stem cells that survives skeletal muscle aging. *Stem Cells,* 25**,** 885-94.

Cooper, W. C., Jin, Y. & Penning, T. M. (2007) Elucidation of a complete kinetic mechanism for a mammalian hydroxysteroid dehydrogenase (HSD) and identification of all enzyme forms on the reaction coordinate: the example of rat liver 3alpha-HSD (AKR1C9). *J Biol Chem,* 282**,** 33484-93.

Cote, C. H., Tremblay, M. H., Duchesne, E. & Lapoite, B. M. (2008) Inflammation-induced leukocyte accumulation in injured skeletal muscle: role of mast cells. *Muscle Nerve,* 37**,** 754-63.

Desmond, J. C., Mountford, J. C., Drayson, M. T., Walker, E. A., Hewison, M., Ride, J. P., Luong, Q. T., Hayden, R. E., Vanin, E. F. & Bunce, C. M. (2003) The aldo-keto reductase AKR1C3 is a novel suppressor of cell differentiation that provides a plausible target for the non-cyclooxygenase-dependent antineoplastic actions of nonsteroidal anti-inflammatory drugs. *Cancer Res,* 63**,** 505-12.

Deyashiki, Y., Ohshima, K., Nakanishi, M., Sato, K., Matsuura, K. & Hara, A. (1995) Molecular cloning and characterisation of mouse estradiol 17 beta-dehydrogenase (A-specific), a member of the aldoketoreductase family. *J Biol Chem,* 270**,** 10461-7.

Dhagat, U., Endo, S., Mamiya, H., Hara, A. & El-Kabbani, O. (2009) Structure of the G225P/G226P mutant of mouse 3(17)alpha-hydroxysteroid dehydrogenase (AKR1C21) ternary complex: implications for the binding of inhibitor and substrate. *Acta Crystallogr D Biol Crystallogr,* 65**,** 257-65.

Dhagat, U., Endo, S., Mamiya, H., Hara, A. & El-Kabbani, O. (2010) Studies on a Tyr residue critical for the binding of coenzyme and substrate in mouse 3(17)alpha-hydroxysteroid dehydrogenase

(AKR1C21): structure of the Y224D mutant enzyme. *Acta Crystallogr D Biol Crystallogr,* 66**,** 198-204.

Du, Y., Tsai, S., Keller, J. R. & Williams, S. C. (2000) Identification of an interleukin-3-regulated aldoketo reductase gene in myeloid cells which may function in autocrine regulation of myelopoiesis. *J Biol Chem,* 275**,** 6724-32.

Dubois, R. N., Abramson, S. B., Crofford, L., Gupta, R. A., Simon, L. S., Van De Putte, L. B. & Lipsky, P. E. (1998) Cyclooxygenase in biology and disease. *FASEB J,* 12**,** 1063-73.

Eguchi, N., Minami, T., Shirafuji, N., Kanaoka, Y., Tanaka, T., Nagata, A., Yoshida, N., Urade, Y., Ito, S. & Hayaishi, O. (1999) Lack of tactile pain (allodynia) in lipocalin-type prostaglandin D synthase-deficient mice. *Proc Natl Acad Sci U S A,* 96**,** 726-30.

Eisinger, A. L., Prescott, S. M., Jones, D. A. & Stafforini, D. M. (2007) The role of cyclooxygenase-2 and prostaglandins in colon cancer. *Prostaglandins Other Lipid Mediat,* 82**,** 147-54.

Endo, S., Matsumoto, K., Matsunaga, T., Ishikura, S., Tajima, K., El-Kabbani, O. & Hara, A. (2006) Substrate specificity of a mouse aldo-keto reductase (AKR1C12). *Biol Pharm Bull,* 29**,** 2488-92.

Entwistle, A., Curtis, D. H. & Zalin, R. J. (1986) Myoblast fusion is regulated by a prostanoid of the one series independently of a rise in cyclic AMP. *J Cell Biol,* 103**,** 857-66.

Escriva, H., Bertrand, S. & Laudet, V. (2004) The evolution of the nuclear receptor superfamily. *Essays Biochem,* 40**,** 11-26.

Faucher, F., Cantin, L., Pereira de Jesus-Tran, K., Lemieux, M., Luu-The, V., Labrie, F. & Breton, R. (2007) Mouse 17[alpha]-Hydroxysteroid Dehydrogenase (AKR1C21) Binds Steroids Differently from other Aldo-keto Reductases: Identification and Characterisation of Amino Acid Residues Critical for Substrate Binding. *Journal of Molecular Biology,* 369**,** 525-540.

Fenton, S. L., Luong, Q. T., Sarafeim, A., Mustard, K. J., Pound, J., Desmond, J. C., Gordon, J., Drayson, M. T. & Bunce, C. M. (2003) Fibrates and medroxyprogesterone acetate induce apoptosis of primary Burkitt's lymphoma cells and cell lines: potential for applying old drugs to a new disease. *Leukemia,* 17**,** 568-75.

Forman, B. M., Tontonoz, P., Chen, J., Brun, R. P., Spiegelman, B. M. & Evans, R. M. (1995) 15-Deoxy-delta 12, 14-prostaglandin J2 is a ligand for the adipocyte determination factor PPAR gamma. *Cell,* 83**,** 803-12.

Funk, C. D. (2001) Prostaglandins and leukotrienes: advances in eicosanoid biology. *Science,* 294**,** 1871-5.

Gao, L., Zackert, W. E., Hasford, J. J., Danekis, M. E., Milne, G. L., Remmert, C., Reese, J., Yin, H., Tai, H. H., Dey, S. K., Porter, N. A. & Morrow, J. D. (2003) Formation of prostaglandins E2 and D2 via the isoprostane pathway: a mechanism for the generation of bioactive prostaglandins independent of cyclooxygenase. *J Biol Chem,* 278**,** 28479-89.

Garcia-Fernandez, L. F., Iniguez, M. A., Eguchi, N., Fresno, M., Urade, Y. & Munoz, A. (2000) Dexamethasone induces lipocalin-type prostaglandin D synthase gene expression in mouse neuronal cells. *J Neurochem,* 75**,** 460-70.

Gayarre, J., Sanchez, D., Sanchez-Gomez, F. J., Terron, M. C., Llorca, O. & Perez-Sala, D. (2006) Addition of electrophilic lipids to actin alters filament structure. *Biochem Biophys Res Commun,* 349**,** 1387-93.

Germain, P., Staels, B., Dacquet, C., Spedding, M. & Laudet, V. (2006) Overview of nomenclature of nuclear receptors. *Pharmacol Rev,* 58**,** 685-704.

Gilroy, D. W., Colville-Nash, P. R., Willis, D., Chivers, J., Paul-Clark, M. J. & Willoughby, D. A. (1999) Inducible cyclooxygenase may have anti-inflammatory properties. *Nat Med,* 5**,** 698-701.

Giri, S., Rattan, R., Singh, A. K. & Singh, I. (2004) The 15-deoxy-delta12,14-prostaglandin J2 inhibits the inflammatory response in primary rat astrocytes via down-regulating multiple steps in phosphatidylinositol 3-kinase-Akt-NF-kappaB-p300 pathway independent of peroxisome proliferator-activated receptor gamma. *J Immunol,* 173**,** 5196-208.

Glass, C. K. & Ogawa, S. (2006) Combinatorial roles of nuclear receptors in inflammation and immunity. *Nat Rev Immunol,* 6**,** 44-55.

Hayden, R. E., Pratt, G., Davies, N. J., Khanim, F. L., Birtwistle, J., Delgado, J., Pearce, C., Sant, T., Drayson, M. T. & Bunce, C. M. (2009) Treatment of primary CLL cells with bezafibrate and medroxyprogesterone acetate induces apoptosis and represses the pro-proliferative signal of CD40-ligand, in part through increased 15dDelta12,14,PGJ2. *Leukemia,* 23**,** 292-304.

Herlong, J. L. & Scott, T. R. (2006) Positioning prostanoids of the D and J series in the immunopathogenic scheme. *Immunol Lett,* 102**,** 121-31.

Higaki, Y., Kamiya, T., Usami, N., Shintani, S., Shiraishi, H., Ishikura, S., Yamamoto, I. & Hara, A. (2002) Molecular characterisation of two monkey dihydrodiol dehydrogenases. *Drug Metab Pharmacokinet,* 17**,** 348-56.

Hirabayashi, T., Murayama, T. & Shimizu, T. (2004) Regulatory mechanism and physiological role of cytosolic phospholipase A2. *Biol Pharm Bull,* 27**,** 1168-73.

Hirawa, N., Uehara, Y., Ikeda, T., Gomi, T., Hamano, K., Totsuka, Y., Yamakado, M., Takagi, M., Eguchi, N., Oda, H., Seiki, K., Nakajima, H. & Urade, Y. (2001) Urinary prostaglandin D synthase (beta-trace) excretion increases in the early stage of diabetes mellitus. *Nephron,* 87**,** 321-7.

Hoffbrand, A. V., Moss, P. A. H. & Pettit, J. E. (2006) *Essential Haematology,* Oxford, Blackwell Publishing.

Horsley, V. & Pavlath, G. K. (2003) Prostaglandin F2(alpha) stimulates growth of skeletal muscle cells via an NFATC2-dependent pathway. *J Cell Biol,* 161**,** 111-8.

Hubbard, T. J., Aken, B. L., Ayling, S., Ballester, B., Beal, K., Bragin, E., Brent, S., Chen, Y., Clapham, P., Clarke, L., Coates, G., Fairley, S., Fitzgerald, S., Fernandez-Banet, J., Gordon, L., Graf, S., Haider, S., Hammond, M., Holland, R., Howe, K., Jenkinson, A., Johnson, N., Kahari, A., Keefe, D., Keenan, S., Kinsella, R., Kokocinski, F., Kulesha, E., Lawson, D., Longden, I., Megy, K., Meidl, P., Overduin, B., Parker, A., Pritchard, B., Rios, D., Schuster, M., Slater, G., Smedley, D., Spooner, W., Spudich, G., Trevanion, S., Vilella, A., Vogel, J., White, S., Wilder, S., Zadissa, A., Birney, E., Cunningham, F., Curwen, V., Durbin, R.,

Fernandez-Suarez, X. M., Herrero, J., Kasprzyk, A., Proctor, G., Smith, J., Searle, S. & Flicek, P. (2009) Ensembl 2009. *Nucleic Acids Res,* 37**,** D690-7.

Hunter, J. G., van Delft, M. F., Rachubinski, R. A. & Capone, J. P. (2001) Peroxisome Proliferator-activated Receptor gamma Ligands Differentially Modulate Muscle Cell Differentiation and MyoD Gene Expression via Peroxisome Proliferator-activated Receptor gamma -dependent and -independent Pathways. *J Biol Chem,* 276**,** 38297-38306.

Hyndman, D., Bauman, D. R., Heredia, V. V. & Penning, T. M. (2003) The aldo-keto reductase superfamily homepage. *Chem Biol Interact,* 143-144**,** 621-31.

Ikeda, S., Okuda-Ashitaka, E., Masu, Y., Suzuki, T., Watanabe, K., Nakao, M., Shingu, K. & Ito, S. (1999) Cloning and characterisation of two novel aldo-keto reductases (AKR1C12 and AKR1C13) from mouse stomach. *FEBS Lett,* 459**,** 433-7.

Irikura, D., Aritake, K., Nagata, N., Maruyama, T., Shimamoto, S. & Urade, Y. (2009) Biochemical, functional, and pharmacological characterisation of AT-56, an orally active and selective inhibitor of lipocalin-type prostaglandin D synthase. *J Biol Chem,* 284**,** 7623-30.

Ishikura, S., Horie, K., Sanai, M., Matsumoto, K. & Hara, A. (2005) Enzymatic properties of a member (AKR1C19) of the aldo-keto reductase family. *Biol Pharm Bull,* 28**,** 1075-8.

Ishikura, S., Usami, N., Nakajima, S., Kameyama, A., Shiraishi, H., Carbone, V., El-Kabbani, O. & Hara, A. (2004) Characterisation of two isoforms of mouse 3(17)alpha-hydroxysteroid dehydrogenases of the aldo-keto reductase family. *Biol Pharm Bull,* 27**,** 1939-45.

Jackson-Grusby, L. (2002) Modeling cancer in mice. *Oncogene,* 21**,** 5504-14.

Jansen, K. M. & Pavlath, G. K. (2008) Prostaglandin F2alpha promotes muscle cell survival and growth through upregulation of the inhibitor of apoptosis protein BRUCE. *Cell Death Differ*.

Jarvinen, T. A., Jarvinen, T. L., Kaariainen, M., Aarimaa, V., Vaittinen, S., Kalimo, H. & Jarvinen, M. (2007) Muscle injuries: optimising recovery. *Best Pract Res Clin Rheumatol,* 21**,** 317-31.

Jez, J. M., Bennett, M. J., Schlegel, B. P., Lewis, M. & Penning, T. M. (1997a) Comparative anatomy of the aldo-keto reductase superfamily. *Biochem J,* 326 (Pt 3)**,** 625-36.

Jez, J. M., Flynn, T. G. & Penning, T. M. (1997b) A new nomenclature for the aldo-keto reductase superfamily. *Biochem Pharmacol,* 54**,** 639-47.

Jin, Y. & Penning, T. M. (2007) Aldo-keto reductases and bioactivation/detoxication. *Annu Rev Pharmacol Toxicol,* 47**,** 263-92.

Kabututu, Z., Manin, M., Pointud, J. C., Maruyama, T., Nagata, N., Lambert, S., Lefrancois-Martinez, A. M., Martinez, A. & Urade, Y. (2008) Prostaglandin F2{alpha} synthase activities of aldo-keto reductase 1B1, 1B3 and 1B7. *J Biochem.*

Kabututu, Z., Manin, M., Pointud, J. C., Maruyama, T., Nagata, N., Lambert, S., Lefrancois-Martinez, A. M., Martinez, A. & Urade, Y. (2009) Prostaglandin F2alpha synthase activities of aldo-keto reductase 1B1, 1B3 and 1B7. *J Biochem,* 145**,** 161-8.

Kagaya, S., Ohkura, N., Tsukada, T., Miyagawa, M., Sugita, Y., Tsujimoto, G., Matsumoto, K., Saito, H. & Hashida, R. (2005) Prostaglandin A2 acts as a transactivator for NOR1 (NR4A3) within the nuclear receptor superfamily. *Biol Pharm Bull,* 28**,** 1603-7.

Kanai, N., Lu, R., Satriano, J. A., Bao, Y., Wolkoff, A. W. & Schuster, V. L. (1995) Identification and characterisation of a prostaglandin transporter. *Science,* 268**,** 866-9.

Kanaoka, Y. & Urade, Y. (2003) Hematopoietic prostaglandin D synthase. *Prostaglandins Leukot Essent Fatty Acids,* 69**,** 163-7.

Khanim, F. L., Hayden, R. E., Birtwistle, J., Lodi, A., Tiziani, S., Davies, N. J., Ride, J. P., Viant, M. R., Gunther, U. L., Mountford, J. C., Schrewe, H., Green, R. M., Murray, J. A., Drayson, M. T. & Bunce, C. M. (2009) Combined bezafibrate and medroxyprogesterone acetate: potential novel therapy for acute myeloid leukaemia. *PLoS One,* 4**,** e8147.

Khurana, A. & Dey, C. S. (2002) Subtype specific roles of mitogen activated protein kinases in L6E9 skeletal muscle cell differentiation. *Mol Cell Biochem,* 238**,** 27-39.

Kim, E. H. & Surh, Y. J. (2006) 15-deoxy-Delta12,14-prostaglandin J2 as a potential endogenous regulator of redox-sensitive transcription factors. *Biochem Pharmacol,* 72**,** 1516-28.

Kliewer, S. A., Lenhard, J. M., Willson, T. M., Patel, I., Morris, D. C. & Lehmann, J. M. (1995) A prostaglandin J2 metabolite binds peroxisome proliferator-activated receptor gamma and promotes adipocyte differentiation. *Cell,* 83**,** 813-9.

Knight, L. P., Primiano, T., Groopman, J. D., Kensler, T. W. & Sutter, T. R. (1999) cDNA cloning, expression and activity of a second human aflatoxin B1-metabolizing member of the aldo-keto reductase superfamily, AKR7A3. *Carcinogenesis,* 20**,** 1215-23.

Koken, M. H., Puvion-Dutilleul, F., Guillemin, M. C., Viron, A., Linares-Cruz, G., Stuurman, N., de Jong, L., Szostecki, C., Calvo, F., Chomienne, C. & et al. (1994) The t(15;17) translocation alters a nuclear body in a retinoic acid-reversible fashion. *EMBO J,* 13**,** 1073-83.

Kostenis, E. & Ulven, T. (2006) Emerging roles of DP and CRTH2 in allergic inflammation. *Trends Mol Med,* 12**,** 148-58.

Kubata, B. K., Duszenko, M., Kabututu, Z., Rawer, M., Szallies, A., Fujimori, K., Inui, T., Nozaki, T., Yamashita, K., Horii, T., Urade, Y. & Hayaishi, O. (2000) Identification of a Novel Prostaglandin F2{alpha} Synthase in Trypanosoma brucei.

Kufe, D. W. (2003) *Cancer Medicine 6,* London, BC Decker Inc

Kunath, T., Gish, G., Lickert, H., Jones, N., Pawson, T. & Rossant, J. (2003) Transgenic RNA interference in ES cell-derived embryos recapitulates a genetic null phenotype. *Nat Biotechnol,* 21**,** 559-61.

Kurebayashi, J., Otsuki, T., Kunisue, H., Tanaka, K., Yamamoto, S. & Sonoo, H. (2000) Expression levels of estrogen receptor-alpha, estrogen receptor-beta, coactivators, and corepressors in breast cancer. *Clin Cancer Res,* 6**,** 512-8.

Le Grand, F. & Rudnicki, M. A. (2007) Skeletal muscle satellite cells and adult myogenesis. *Current Opinion in Cell Biology,* 19**,** 628-633.

Leone, M. G., Haq, H. A. & Saso, L. (2002) Lipocalin type prostaglandin D-synthase: which role in male fertility? *Contraception,* 65**,** 293-5.

Levin, E. R. (2009) Membrane oestrogen receptor alpha signalling to cell functions. *J Physiol,* 587**,** 5019-23.

Lord, A. M., North, T. E. & Zon, L. I. (2007) Prostaglandin E2: making more of your marrow. *Cell Cycle,* 6**,** 3054-7.

Lu, R., Kanai, N., Bao, Y. & Schuster, V. L. (1996) Cloning, in vitro expression, and tissue distribution of a human prostaglandin transporter cDNA(hPGT). *J Clin Invest,* 98**,** 1142-9.

Luu-The, V. (2001) Analysis and characteristics of multiple types of human 17beta-hydroxysteroid dehydrogenase. *J Steroid Biochem Mol Biol,* 76**,** 143-51.

Mackey, A. L., Kjaer, M., Dandanell, S., Mikkelsen, K. H., Holm, L., Dossing, S., Kadi, F., Koskinen, S. O., Jensen, C. H., Schroder, H. D. & Langberg, H. (2007) The influence of anti-inflammatory medication on exercise-induced myogenic precursor cell responses in humans. *J Appl Physiol,* 103**,** 425-31.

Maho Ishida, K.-T. C., Keiji Hirabayashi, Masugi Nishihara and Michio Takahashi (1999) Cloning of Mouse 20α-Hydroxysteroid Dehydrogenase cDNA and Its mRNA Localization during Pregnancy. *Journal of Reproduction and Development*.

Massimino, M. L., Rapizzi, E., Cantini, M., Libera, L. D., Mazzoleni, F., Arslan, P. & Carraro, U. (1997) ED2+ macrophages increase selectively myoblast proliferation in muscle cultures. *Biochem Biophys Res Commun,* 235**,** 754-9.

Matsumoto, K., Endo, S., Ishikura, S., Matsunaga, T., Tajima, K., El-Kabbani, O. & Hara, A. (2006) Enzymatic properties of a member (AKR1C20) of the aldo-keto reductase family. *Biol Pharm Bull,* 29**,** 539-42.

Matsuoka, T., Hirata, M., Tanaka, H., Takahashi, Y., Murata, T., Kabashima, K., Sugimoto, Y., Kobayashi, T., Ushikubi, F., Aze, Y., Eguchi, N., Urade, Y., Yoshida, N., Kimura, K., Mizoguchi, A., Honda, Y., Nagai, H. & Narumiya, S. (2000) Prostaglandin D2 as a mediator of allergic asthma. *Science,* 287**,** 2013-7.

McArdle, A., Edwards, R. H. & Jackson, M. J. (1994) Release of creatine kinase and prostaglandin E2 from regenerating skeletal muscle fibers. *J Appl Physiol,* 76**,** 1274-8.

McLennan, I. S. (1991) E and F alpha series prostaglandins in developing muscles. *Prostaglandins Leukot Essent Fatty Acids,* 43**,** 77-82.

Mellado, B., Codony, J., Ribal, M. J., Visa, L. & Gascon, P. (2009) Molecular biology of androgen-independent prostate cancer: the role of the androgen receptor pathway. *Clin Transl Oncol,* 11**,** 5-10.

Mills, K. I., Gilkes, A. F., Sweeney, M., Choudhry, M. A., Woodgate, L. J., Bunce, C. M., Brown, G. & Burnett, A. K. (1998) Identification of a retinoic acid responsive aldoketoreductase expressed in HL60 leukaemic cells. *FEBS Lett,* 440**,** 158-62.

Mishra, D. K., Friden, J., Schmitz, M. C. & Lieber, R. L. (1995) Anti-inflammatory medication after muscle injury. A treatment resulting in short-term improvement but subsequent loss of muscle function. *J Bone Joint Surg Am,* 77**,** 1510-9.

Miura, R., Shiota, K., Noda, K., Yagi, S., Ogawa, T. & Takahashi, M. (1994) Molecular cloning of cDNA for rat ovarian 20 alpha-hydroxysteroid dehydrogenase (HSD1). *Biochem J,* 299 (Pt 2)**,** 561-7.

Mizrachi, D. & Auchus, R. J. (2009) Androgens, estrogens, and hydroxysteroid dehydrogenases. *Mol Cell Endocrinol,* 301**,** 37-42.

Monneret, G., Cossette, C., Gravel, S., Rokach, J. & Powell, W. S. (2003) 15R-methyl-prostaglandin D2 is a potent and selective CRTH2/DP2 receptor agonist in human eosinophils. *J Pharmacol Exp Ther,* 304**,** 349-55.

Morita, I. (2002) Distinct functions of COX-1 and COX-2. *Prostaglandins & Other Lipid Mediators,* 68-69**,** 165-175.

Moriuchi, H., Koda, N., Okuda-Ashitaka, E., Daiyasu, H., Ogasawara, K., Toh, H., Ito, S., Woodward, D. F. & Watanabe, K. (2008) Molecular characterisation of a novel type of prostamide/prostaglandin F synthase, belonging to the thioredoxin-like superfamily. *J Biol Chem,* 283**,** 792-801.

Morrow, J. D., Hill, K. E., Burk, R. F., Nammour, T. M., Badr, K. F. & Roberts, L. J., 2nd (1990) A series of prostaglandin F2-like compounds are produced in vivo in humans by a non-cyclooxygenase, free radical-catalysed mechanism. *Proc Natl Acad Sci U S A,* 87**,** 9383-7.

Morrow, J. D., Minton, T. A. & Roberts, L. J., 2nd (1992) The F2-isoprostane, 8-epi-prostaglandin F2 alpha, a potent agonist of the vascular thromboxane/endoperoxide receptor, is a platelet thromboxane/endoperoxide receptor antagonist. *Prostaglandins,* 44**,** 155-63.

Murray, J. A., Khanim, F. L., Hayden, R. E., Craddock, C. F., Holyoake, T. L., Jackson, N., Lumley, M., Bunce, C. M. & Drayson, M. T. (2010) Combined bezafibrate and medroxyprogesterone acetate have efficacy without haematological toxicity in elderly and relapsed acute myeloid leukaemia (AML). *Br J Haematol*.

Musiek, E. S., Yin, H., Milne, G. L. & Morrow, J. D. (2005) Recent advances in the biochemistry and clinical relevance of the isoprostane pathway. *Lipids,* 40**,** 987-94.

Nagata, K. & Hirai, H. (2003) The second PGD2 receptor CRTH2: structure, properties, and functions in leukocytes. *Prostaglandins, Leukotrienes and Essential Fatty Acids,* 69**,** 169-177.

Nagy, A., Rossant, J., Nagy, R., Abramow-Newerly, W. & Roder, J. C. (1993) Derivation of completely cell culture-derived mice from early-passage embryonic stem cells. *Proc Natl Acad Sci U S A,* 90**,** 8424-8.

Nakahata, N. (2008) Thromboxane A2: physiology/pathophysiology, cellular signal transduction and pharmacology. *Pharmacol Ther,* 118**,** 18-35.

North, T. E., Goessling, W., Walkley, C. R., Lengerke, C., Kopani, K. R., Lord, A. M., Weber, G. J., Bowman, T. V., Jang, I.-H., Grosser, T., FitzGerald, G. A., Daley, G. Q., Orkin, S. H. & Zon, L. I. (2007) Prostaglandin E2 regulates vertebrate haematopoietic stem cell homeostasis. *Nature,* 447**,** 1007-1011.

Oguma, T., Palmer, L. J., Birben, E., Sonna, L. A., Asano, K. & Lilly, C. M. (2004) Role of prostanoid DP receptor variants in susceptibility to asthma. *N Engl J Med,* 351**,** 1752-63.

Olson, D. M., Zaragoza, D. B., Shallow, M. C., Cook, J. L., Mitchell, B. F., Grigsby, P. & Hirst, J. (2003) Myometrial activation and preterm labour: evidence supporting a role for the prostaglandin F receptor--a review. *Placenta,* 24 Suppl A**,** S47-54.

Otis, J. S., Burkholder, T. J. & Pavlath, G. K. (2005) Stretch-induced myoblast proliferation is dependent on the COX2 pathway. *Exp Cell Res,* 310**,** 417-25.

Palmer, R. M., Reeds, P. J., Atkinson, T. & Smith, R. H. (1983) The influence of changes in tension on protein synthesis and prostaglandin release in isolated rabbit muscles. *Biochem J,* 214**,** 1011-4.

Park, J. M., Kanaoka, Y., Eguchi, N., Aritake, K., Grujic, S., Materi, A. M., Buslon, V. S., Tippin, B. L., Kwong, A. M., Salido, E., French, S. W., Urade, Y. & Lin, H. J. (2007) Hematopoietic prostaglandin D synthase suppresses intestinal adenomas in ApcMin/+ mice. *Cancer Res,* 67**,** 881-9.

Park, J. Y., Pillinger, M. H. & Abramson, S. B. (2006) Prostaglandin E2 synthesis and secretion: the role of PGE2 synthases. *Clin Immunol,* 119**,** 229-40.

Patel, S. & Chiplunkar, S. (2007) Role of cyclooxygenase-2 in tumour progression and immune regulation in lung cancer. *Indian J Biochem Biophys,* 44**,** 419-28.

Penning, T. M., Burczynski, M. E., Jez, J. M., Hung, C. F., Lin, H. K., Ma, H., Moore, M., Palackal, N. & Ratnam, K. (2000) Human 3alpha-hydroxysteroid dehydrogenase isoforms (AKR1C1-AKR1C4) of the aldo-keto reductase superfamily: functional plasticity and tissue distribution reveals roles in the inactivation and formation of male and female sex hormones. *Biochem J,* 351**,** 67-77.

Penning, T. M. & Byrns, M. C. (2009) Steroid hormone transforming aldo-keto reductases and cancer. *Ann N Y Acad Sci,* 1155**,** 33-42.

Peters-Golden, M. & Henderson, W. R., Jr. (2007) Leukotrienes. *N Engl J Med,* 357**,** 1841-54.

Petrash, J. M., Tarle, I., Wilson, D. K. & Quiocho, F. A. (1994) Aldose reductase catalysis and crystallography. Insights from recent advances in enzyme structure and function. *Diabetes,* 43**,** 955-9.

Piekorz, R. P., Gingras, S., Hoffmeyer, A., Ihle, J. N. & Weinstein, Y. (2005) Regulation of progesterone levels during pregnancy and parturition by signal transducer and activator of transcription 5 and 20alpha-hydroxysteroid dehydrogenase. *Mol Endocrinol,* 19**,** 431-40.

Pinto do, O. P., Kolterud, A. & Carlsson, L. (1998) Expression of the LIM-homeobox gene LH2 generates immortalised steel factor-dependent multipotent hematopoietic precursors. *EMBO J,* 17**,** 5744-56.

Pinto do, O. P., Richter, K. & Carlsson, L. (2002) Hematopoietic progenitor/stem cells immortalised by Lhx2 generate functional hematopoietic cells in vivo. *Blood,* 99**,** 3939-46.

Pucci, M. L., Bao, Y., Chan, B., Itoh, S., Lu, R., Copeland, N. G., Gilbert, D. J., Jenkins, N. A. & Schuster, V. L. (1999) Cloning of mouse prostaglandin transporter PGT cDNA: species-specific substrate affinities. *Am J Physiol,* 277**,** R734-41.

Purmonen, S., Manninen, T., Pennanen, P. & Ylikomi, T. (2008) Progestins regulate genes that can elicit both proliferative and antiproliferative effects in breast cancer cells. *Oncol Rep,* 19**,** 1627-34.

Qin, K. N. & Cheng, K. C. (1994) Structure and tissue-specific expression of the aldo-keto reductase superfamily. *Biochemistry,* 33**,** 3223-8.

Ragolia, L., Hall, C. E. & Palaia, T. (2007) Post-translational modification regulates prostaglandin D2 synthase apoptotic activity: characterisation by site-directed mutagenesis. *Prostaglandins Other Lipid Mediat,* 83**,** 25-32.

Ragolia, L., Hall, C. E. & Palaia, T. (2008) Lipocalin-type prostaglandin D(2) synthase stimulates glucose transport via enhanced GLUT4 translocation. *Prostaglandins Other Lipid Mediat,* 87**,** 34-41.

Ragolia, L., Palaia, T., Hall, C. E., Maesaka, J. K., Eguchi, N. & Urade, Y. (2005) Accelerated glucose intolerance, nephropathy, and atherosclerosis in prostaglandin D2 synthase knock-out mice. *J Biol Chem,* 280**,** 29946-55.

Ragolia, L., Palaia, T., Koutrouby, T. B. & Maesaka, J. K. (2004) Inhibition of cell cycle progression and migration of vascular smooth muscle cells by prostaglandin D2 synthase: resistance in diabetic Goto-Kakizaki rats. *Am J Physiol Cell Physiol,* 287**,** C1273-81.

Ragolia, L., Palaia, T., Paric, E. & Maesaka, J. K. (2003) Prostaglandin D2 synthase inhibits the exaggerated growth phenotype of spontaneously hypertensive rat vascular smooth muscle cells. *J Biol Chem,* 278**,** 22175-81.

Rajakariar, R., Hilliard, M., Lawrence, T., Trivedi, S., Colville-Nash, P., Bellingan, G., Fitzgerald, D., Yaqoob, M. M. & Gilroy, D. W. (2007) Hematopoietic prostaglandin D2 synthase controls the onset and resolution of acute inflammation through PGD2 and 15-deoxyDelta12 14 PGJ2. *Proc Natl Acad Sci U S A,* 104**,** 20979-84.

Ray, D. M., Akbiyik, F. & Phipps, R. P. (2006) The peroxisome proliferator-activated receptor gamma (PPARgamma) ligands 15-deoxy-Delta12,14-prostaglandin J2 and ciglitazone induce human B lymphocyte and B cell lymphoma apoptosis by PPARgamma-independent mechanisms. *J Immunol,* 177**,** 5068-76.

Risbridger, G. P., Davis, I. D., Birrell, S. N. & Tilley, W. D. (2010) Breast and prostate cancer: more similar than different. *Nat Rev Cancer*.

Rizner, T. L., Smuc, T., Rupreht, R., Sinkovec, J. & Penning, T. M. (2006) AKR1C1 and AKR1C3 may determine progesterone and estrogen ratios in endometrial cancer. *Mol Cell Endocrinol,* 248**,** 126-35.

Rodemann, H. P. & Goldberg, A. L. (1982) Arachidonic acid, prostaglandin E2 and F2 alpha influence rates of protein turnover in skeletal and cardiac muscle. *J Biol Chem,* 257**,** 1632-8.

Rossi, M. J., Clark, M. A. & Steiner, S. M. (1989) Possible role of prostaglandins in the regulation of mouse myoblasts. *J Cell Physiol,* 141**,** 142-7.

Royer, J. F., Schratl, P., Lorenz, S., Kostenis, E., Ulven, T., Schuligoi, R., Peskar, B. A. & Heinemann, A. (2007) A novel antagonist of CRTH2 blocks eosinophil release from bone marrow, chemotaxis and respiratory burst. *Allergy,* 62**,** 1401-9.

Sabourin, L. A. & Rudnicki, M. A. (2000) The molecular regulation of myogenesis. *Clin Genet,* 57**,** 16-25.

Sakuma, M. & Kubota, S. (2008) Mouse AKR1E1 is an ortholog of pig liver NADPH dependent 1,5-anhydro-D-fructose reductase. *Biosci Biotechnol Biochem,* 72**,** 872-6.

Sanderson, J. T. (2006) The steroid hormone biosynthesis pathway as a target for endocrine-disrupting chemicals. *Toxicol Sci,* 94**,** 3-21.

Satoh, T., Moroi, R., Aritake, K., Urade, Y., Kanai, Y., Sumi, K., Yokozeki, H., Hirai, H., Nagata, K., Hara, T., Utsuyama, M., Hirokawa, K., Sugamura, K., Nishioka, K. & Nakamura, M. (2006) Prostaglandin D2 plays an essential role in chronic allergic inflammation of the skin via CRTH2 receptor. *J Immunol,* 177**,** 2621-9.

Schaloske, R. H. & Dennis, E. A. (2006) The phospholipase A2 superfamily and its group numbering system. *Biochim Biophys Acta,* 1761**,** 1246-59.

Schratl, P., Royer, J. F., Kostenis, E., Ulven, T., Sturm, E. M., Waldhoer, M., Hoefler, G., Schuligoi, R., Lippe, I. T., Peskar, B. A. & Heinemann, A. (2007) The role of the prostaglandin D2 receptor, DP, in eosinophil trafficking. *J Immunol,* 179**,** 4792-9.

Schuster, V. L. (2002) Prostaglandin transport. *Prostaglandins Other Lipid Mediat,* 68-69**,** 633-47.

Seibert, K., Sheller, J. R. & Roberts, L. J., 2nd (1987) (5Z,13E)-(15S)-9 alpha,11 beta,15-trihydroxyprosta-5,13-dien-1-oic acid (9 alpha,11 beta-prostaglandin F2): formation and metabolism by human lung and contractile effects on human bronchial smooth muscle. *Proc Natl Acad Sci U S A,* 84**,** 256-60.

Sharma, K. K., Lindqvist, A., Zhou, X. J., Auchus, R. J., Penning, T. M. & Andersson, S. (2006) Deoxycorticosterone inactivation by AKR1C3 in human mineralocorticoid target tissues. *Mol Cell Endocrinol,* 248**,** 79-86.

Shen, R. F. & Tai, H. H. (1998) Thromboxanes: synthase and receptors. *J Biomed Sci,* 5**,** 153-72.

Shen, W., Li, Y., Zhu, J., Schwendener, R. & Huard, J. (2008) Interaction between macrophages, TGF-beta1, and the COX-2 pathway during the inflammatory phase of skeletal muscle healing after injury. *J Cell Physiol,* 214**,** 405-12.

Shin, S. W., Seo, C. Y., Han, H., Han, J. Y., Jeong, J. S., Kwak, J. Y. & Park, J. I. (2009) 15d-PGJ2 induces apoptosis by reactive oxygen species-mediated inactivation of Akt in leukemia and colorectal cancer cells and shows in vivo antitumour activity. *Clin Cancer Res,* 15**,** 5414-25.

Simmons, D. L., Botting, R. M. & Hla, T. (2004) Cyclooxygenase isozymes: the biology of prostaglandin synthesis and inhibition. *Pharmacol Rev,* 56**,** 387-437.

Simon, L. S. (1999) Role and regulation of cyclooxygenase-2 during inflammation. *Am J Med,* 106**,** 37S-42S.

Singh, J., Verma, N. K., Kansagra, S. M., Kate, B. N. & Dey, C. S. (2007) Altered PPARgamma expression inhibits myogenic differentiation in C2C12 skeletal muscle cells. *Mol Cell Biochem,* 294**,** 163-71.

Smuc, T., Hevir, N., Ribic-Pucelj, M., Husen, B., Thole, H. & Rizner, T. L. (2009) Disturbed estrogen and progesterone action in ovarian endometriosis. *Mol Cell Endocrinol,* 301**,** 59-64.

Soriano, P. (1999) Generalized lacZ expression with the ROSA26 Cre reporter strain. *Nat Genet,* 21**,** 70-1.

Stanbrough, M., Bubley, G. J., Ross, K., Golub, T. R., Rubin, M. A., Penning, T. M., Febbo, P. G. & Balk, S. P. (2006) Increased expression of genes converting adrenal androgens to testosterone in androgen-independent prostate cancer. *Cancer Res,* 66**,** 2815-25.

Straus, D. S. & Glass, C. K. (2001) Cyclopentenone prostaglandins: new insights on biological activities and cellular targets. *Med Res Rev,* 21**,** 185-210.

Straus, D. S., Pascual, G., Li, M., Welch, J. S., Ricote, M., Hsiang, C. H., Sengchanthalangsy, L. L., Ghosh, G. & Glass, C. K. (2000) 15-deoxy-delta 12,14-prostaglandin J2 inhibits multiple steps in the NF-kappa B signaling pathway. *Proc Natl Acad Sci U S A,* 97**,** 4844-9.

Sugimoto, Y., Yamasaki, A., Segi, E., Tsuboi, K., Aze, Y., Nishimura, T., Oida, H., Yoshida, N., Tanaka, T., Katsuyama, M., Hasumoto, K., Murata, T., Hirata, M., Ushikubi, F., Negishi, M., Ichikawa, A. & Narumiya, S. (1997) Failure of parturition in mice lacking the prostaglandin F receptor. *Science,* 277**,** 681-3.

Suleyman, H., Demircan, B. & Karagoz, Y. (2007) Anti-inflammatory and side effects of cyclooxygenase inhibitors. *Pharmacol Rep,* 59**,** 247-58.

Suzuki-Yamamoto, T., Nishizawa, M., Fukui, M., Okuda-Ashitaka, E., Nakajima, T., Ito, S. & Watanabe, K. (1999) cDNA cloning, expression and characterisation of human prostaglandin F synthase. *FEBS Letters,* 462**,** 335-340.

Suzuki, T., Fujii, Y., Miyano, M., Chen, L. Y., Takahashi, T. & Watanabe, K. (1999) cDNA cloning, expression, and mutagenesis study of liver-type prostaglandin F synthase. *J Biol Chem,* 274**,** 241-8.

Tanabe, T. & Tohnai, N. (2002) Cyclooxygenase isozymes and their gene structures and expression. *Prostaglandins Other Lipid Mediat,* 68-69**,** 95-114.

Thomas, R. K., Sos, M. L., Zander, T., Mani, O., Popov, A., Berenbrinker, D., Smola-Hess, S., Schultze, J. L. & Wolf, J. (2005) Inhibition of nuclear translocation of nuclear factor-kappaB despite lack of functional IkappaBalpha protein overcomes multiple defects in apoptosis signaling in human B-cell malignancies. *Clin Cancer Res,* 11**,** 8186-94.

Tidball, J. G. (2005) Inflammatory processes in muscle injury and repair. *Am J Physiol Regul Integr Comp Physiol,* 288**,** R345-53.

Tidball, J. G. (2008) Inflammation in skeletal muscle regeneration. IN SCHIAFFINO, A. & PARTRIDGE, T. A. (Eds.) *Skeletal muscle repair and regeneration.* Springer.

Tiziani, S., Lodi, A., Khanim, F. L., Viant, M. R., Bunce, C. M. & Gunther, U. L. (2009) Metabolomic profiling of drug responses in acute myeloid leukaemia cell lines. *PLoS ONE,* 4**,** e4251.

Trappe, T. A., Fluckey, J. D., White, F., Lambert, C. P. & Evans, W. J. (2001) Skeletal muscle PGF(2)(alpha) and PGE(2) in response to eccentric resistance exercise: influence of ibuprofen acetaminophen. *J Clin Endocrinol Metab,* 86**,** 5067-70.

Trivedi, S. G., Newson, J., Rajakariar, R., Jacques, T. S., Hannon, R., Kanaoka, Y., Eguchi, N., Colville-Nash, P. & Gilroy, D. W. (2006) Essential role for hematopoietic prostaglandin D2 synthase in the control of delayed type hypersensitivity. *Proc Natl Acad Sci U S A,* 103**,** 5179-84.

Tsai, S., Bartelmez, S., Sitnicka, E. & Collins, S. (1994) Lymphohematopoietic progenitors immortalised by a retroviral vector harboring a dominant-negative retinoic acid receptor can recapitulate lymphoid, myeloid, and erythroid development. *Genes Dev,* 8**,** 2831-41.

Tsao, C. J., Ozawa, K., Hosoi, T., Urabe, A. & Takaku, F. (1986) In-vitro effects of antineoplastic prostaglandins on human leukemic cell growth and normal myelopoiesis. *Leuk Res,* 10**,** 527-32.

Uchida, K. & Shibata, T. (2008) 15-Deoxy-Delta(12,14)-prostaglandin J2: an electrophilic trigger of cellular responses. *Chem Res Toxicol,* 21**,** 138-44.

Ujihara, M., Tsuchida, S., Satoh, K., Sato, K. & Urade, Y. (1988a) Biochemical and immunological demonstration of prostaglandin D2, E2, and F2 alpha formation from prostaglandin H2 by various rat glutathione S-transferase isozymes. *Arch Biochem Biophys,* 264**,** 428-37.

Ujihara, M., Urade, Y., Eguchi, N., Hayashi, H., Ikai, K. & Hayaishi, O. (1988b) Prostaglandin D2 formation and characterisation of its synthetases in various tissues of adult rats. *Arch Biochem Biophys,* 260**,** 521-31.

Ulven, T. & Kostenis, E. (2006) Targeting the prostaglandin D2 receptors DP and CRTH2 for treatment of inflammation. *Curr Top Med Chem,* 6**,** 1427-44.

Unezaki, S., Sugatani, J., Masu, Y., Watanabe, K. & Ito, S. (1996) Characterisation of prostaglandin F2 alpha production in pregnant and cycling mice. *Biol Reprod,* 55**,** 889-94.

Urade, Y. & Eguchi, N. (2002) Lipocalin-type and hematopoietic prostaglandin D synthases as a novel example of functional convergence. *Prostaglandins & Other Lipid Mediators,* 68-69**,** 375-382.

Urade, Y. & Hayaishi, O. (2000a) Biochemical, structural, genetic, physiological, and pathophysiological features of lipocalin-type prostaglandin D synthase. *Biochimica et Biophysica Acta (BBA) - Protein Structure and Molecular Enzymology,* 1482**,** 259-271.

Urade, Y. & Hayaishi, O. (2000b) Prostaglandin D synthase: structure and function. *Vitam Horm,* 58**,** 89-120.

Velica, P. & Bunce, C. M. (2008) Prostaglandins in muscle regeneration. *J Muscle Res Cell Motil*.

Vergnes, L., Phan, J., Stolz, A. & Reue, K. (2003) A cluster of eight hydroxysteroid dehydrogenase genes belonging to the aldo-keto reductase supergene family on mouse chromosome 13. *J Lipid Res,* 44**,** 503-11.

Wang, L. H. & Kulmacz, R. J. (2002) Thromboxane synthase: structure and function of protein and gene. *Prostaglandins Other Lipid Mediat,* 68-69**,** 409-22.

Watanabe, K. (2002) Prostaglandin F synthase. *Prostaglandins & Other Lipid Mediators,* 68-69**,** 401-407.

Watanabe, K., Yoshida, R., Shimizu, T. & Hayaishi, O. (1985) Enzymatic formation of prostaglandin F2 alpha from prostaglandin H2 and D2. Purification and properties of prostaglandin F synthetase from bovine lung. *J Biol Chem,* 260**,** 7035-41.

Weiler, S. R., Gooya, J. M., Ortiz, M., Tsai, S., Collins, S. J. & Keller, J. R. (1999) D3: a gene induced during myeloid cell differentiation of Linlo c-Kit+ Sca-1(+) progenitor cells. *Blood,* 93**,** 527-36.

Weinheimer, E. M., Jemiolo, B., Carroll, C. C., Harber, M. P., Haus, J. M., Burd, N. A., LeMoine, J. K., Trappe, S. W. & Trappe, T. A. (2007) Resistance exercise and cyclooxygenase (COX) expression in human skeletal muscle: implications for COX-inhibiting drugs and protein synthesis. *Am J Physiol Regul Integr Comp Physiol,* 292**,** R2241-8.

Wintergalen, N., Thole, H. H., Galla, H. J. & Schlegel, W. (1995) Prostaglandin-E2 9-reductase from corpus luteum of pseudopregnant rabbit is a member of the aldo-keto reductase superfamily featuring 20 alpha-hydroxysteroid dehydrogenase activity. *Eur J Biochem,* 234**,** 264-70.

Wojiski, S., Guibal, F. C., Kindler, T., Lee, B. H., Jesneck, J. L., Fabian, A., Tenen, D. G. & Gilliland, D. G. (2009) PML-RARalpha initiates leukemia by conferring properties of self-renewal to committed promyelocytic progenitors. *Leukemia,* 23**,** 1462-71.

Wu, K. K. (1996) Cyclooxygenase 2 induction: molecular mechanism and pathophysiologic roles. *J Lab Clin Med,* 128**,** 242-5.

Wu, K. K. & Liou, J. Y. (2005) Cellular and molecular biology of prostacyclin synthase. *Biochem Biophys Res Commun,* 338**,** 45-52.

Xue, L., Gyles, S. L., Wettey, F. R., Gazi, L., Townsend, E., Hunter, M. G. & Pettipher, R. (2005) Prostaglandin D2 causes preferential induction of proinflammatory Th2 cytokine production through an action on chemoattractant receptor-like molecule expressed on Th2 cells. *J Immunol,* 175**,** 6531-6.

Yaffe, D. (1968) Retention of differentiation potentialities during prolonged cultivation of myogenic cells. *Proc Natl Acad Sci U S A,* 61**,** 477-83.

Yaffe, D. & Saxel, O. (1977) A myogenic cell line with altered serum requirements for differentiation. *Differentiation,* 7**,** 159-66.

Yamamoto, M., Tsukamoto, T., Sakai, H., Shirai, N., Ohgaki, H., Furihata, C., Donehower, L. A., Yoshida, K. & Tatematsu, M. (2000) p53 knockout mice (-/-) are more susceptible than (+/-) or (+/+) mice to N-methyl-N-nitrosourea stomach carcinogenesis. *Carcinogenesis,* 21**,** 1891-7.

Yokoyama, C., Yabuki, T., Shimonishi, M., Wada, M., Hatae, T., Ohkawara, S., Takeda, J., Kinoshita, T., Okabe, M. & Tanabe, T. (2002) Prostacyclin-deficient mice develop ischemic renal disorders, including nephrosclerosis and renal infarction. *Circulation,* 106**,** 2397-403.

Young, J. L., Jazaeri, A. A., Darus, C. J. & Modesitt, S. C. (2008) Cyclooxygenase-2 in cervical neoplasia: a review. *Gynecol Oncol,* 109**,** 140-5.

Yu, I. S., Lin, S. R., Huang, C. C., Tseng, H. Y., Huang, P. H., Shi, G. Y., Wu, H. L., Tang, C. L., Chu, P. H., Wang, L. H., Wu, K. K. & Lin, S. W. (2004) TXAS-deleted mice exhibit normal thrombopoiesis, defective hemostasis, and resistance to arachidonate-induced death. *Blood,* 104**,** 135-42.

Zalin, R. (1979) The cell cycle, myoblast differentiation and prostaglandin as a developmental signal. *Dev Biol,* 71**,** 274-88.

Zalin, R. J. (1977) Prostaglandins and myoblast fusion. *Dev Biol,* 59**,** 241-8.